VOLUME 81 FEBRUARY 10, 1977 NUMBER 3

JPCHAx

THE JOURNAL OF PHYSICAL CHEMISTRY

PUBLISHED BIWEEKLY BY THE AMERICAN CHEMICAL SOCIETY

THE JOURNAL OF

PHYSICAL CHEMISTRY

Published by the
AMERICAN CHEMICAL SOCIETY
BOOKS AND JOURNALS DIVISION

D. H. Michael Bowen, Director
Marjorie Laflin, Assistant to the Director

Editorial Department: Charles R. Bertsch, Head; Marianne C. Brogan, Associate Head; Celia B. McFarland, Joseph E. Yurvati, Assistant Editors
Magazine and Production Department: Bacil Guiley, Head
Research and Development Department: Seldon W. Terrant, Head

Advertising Office: Centcom, Ltd., 50 W. State St., Westport, Conn. 06880.

Published biweekly by the American Chemical Society at 20th and Northampton Sts., Easton, Pennsylvania 18042. Second class postage paid at Washington, D.C. and at additional mailing offices.

Editorial Information

Instructions for authors are printed in the first issue of each volume. Please conform to these instructions when submitting manuscripts.

Manuscripts for publication should be submitted to *The Journal of Physical Chemistry*, Department of Chemistry, University of Minnesota, Minneapolis, Minn. 55455. Correspondence regarding **accepted papers and proofs** should be directed to the Editorial Department at the ACS Easton address.

Page charges of $60.00 per page are assessed for papers published in this journal. Ability to pay does not affect acceptance or scheduling of papers.

Bulk reprints or photocopies of individual articles are available. For information write to Business Operations, Books and Journals Division at the ACS Washington address.

Requests for **permission to reprint** should be directed to Permissions, Books and Journals Division at the ACS Washington address. The American Chemical Society and its Editors assume no responsibility for the statements and opinions advanced by contributors.

Subscription and Business Information

1977 Subscription rates—including surface postage

	U.S.	PUAS	Canada, Foreign
Member	$24.00	$33.00	$34.00
Nonmember	96.00	105.00	106.00
Supplementary material	15.00	19.00	20.00

Air mail and air freight rates are available from Membership & Subscription Services, at the ACS Columbus address.

New and renewal subscriptions should be sent with payment to the Office of the Controller at the ACS Washington address. **Changes of address** must include both old and new addresses with ZIP code and a recent mailing label. Send all address changes to the ACS Columbus address. Please allow six weeks for change to become effective. **Claims for missing numbers** will not be allowed if loss was due to failure of notice of change of address to be received in the time specified: if claim is dated (a) North America—more than 90 days beyond issue date, (b) all other foreign—more than 1 year beyond issue date; or if the reason given is "missing from files". Hard copy claims are handled at the ACS Columbus address.

Microfiche subscriptions are available at the same rates but are mailed first class to U.S. subscribers, air mail to the rest of the world. Direct all inquiries to Special Issues Sales, at the ACS Washington address or call (202) 872-4554. **Single issues** in hard copy and/or microfiche are available from Special Issues Sales at the ACS Washington address. Current year $4.75. Back issue rates available from Special Issues Sales. **Back volumes** are available in hard copy and/or microform. Write to Special Issues Sales at the ACS Washington address for further information. **Microfilm** editions of ACS periodical publications are available from volume 1 to the present. For further information, contact Special Issues Sales at the ACS Washington address. **Supplementary material** mentioned in the journal appears in the microfilm edition. Single copies may be ordered directly from Business Operations, Books and Journals Division, at the ACS Washington address.

	U.S.	PUAS, Canada	Other Foreign
Microfiche	$2.50	$3.00	$3.50
Photocopy			
1–7 pages	4.00	5.50	7.00
8–20 pages	5.00	6.50	8.00

Orders over 20 pages are available only on microfiche, 4 × 6 in., 24X, negative, silver halide. Orders must state photocopy or microfiche if both are available. Full bibliographic citation including names of all authors and prepayment are required. Prices are subject to change.

American Chemical Society
1155 16th Street, N.W.
Washington, D.C. 20036
(202) 872-4600

Member & Subscription Services
American Chemical Society
P.O. Box 3337
Columbus, Ohio 43210
(614) 421-7230

Editorial Department
American Chemical Society
20th and Northampton Sts.
Easton, Pennsylvania 18042
(215) 258-9111

Notice to Authors last printed in the issue of January 13, 1977

THE JOURNAL OF

PHYSICAL CHEMISTRY

Volume 81, Number 3 February 10, 1977

JPCHAx 81(3) 187–280 (1977)

ISSN 0022-3654

COMMUNICATIONS TO THE EDITOR

■ Supplementary and/or miniprint material for this paper is available separately (consult the masthead page for ordering information); it will also appear following the paper in the microfilm edition of this journal.

* In papers with more than one author, the asterisk indicates the name of the author to whom inquiries about the paper should be addressed.

AUTHOR INDEX

THE JOURNAL OF
PHYSICAL CHEMISTRY

VOLUME 81, NUMBER 3 FEBRUARY 10, 1977

Measurement of the Rate Constant of the Reaction of Nitrous Acid with Nitric Acid

E. W. Kaiser* and C. H. Wu

Chemistry Department, Engineering and Research Staff, Ford Motor Company, Dearborn, Michigan 48121 *(Received July 6, 1976)*

Publication costs assisted by the Ford Motor Company

The rate constant of the reaction of nitrous acid with nitric acid, HONO + HNO_3 = $2NO_2$ + H_2O (k_1), has been measured in the gas phase in a Pyrex reactor at 300 K using a mass spectrometer detector. A reactant stoichiometry of unity was confirmed during these experiments, and the observed rate constant was k_1 = 1.55(0.3) × 10^{-17} cm^3/molecule s. Evidence was also obtained that this reaction can under certain conditions be sensitive to the reactor surface condition. Thus, the above value of k_1 must rigorously be regarded as an upper limit to the homogeneous rate constant.

I. Introduction

We have directly measured the rate of the gas phase reaction of nitrous acid (HONO) with nitric acid (HNO_3) at 300 K. To our knowledge, this is the first direct observation of the reaction

$$HONO + HNO_3 \underset{k_{-1}}{\overset{k_1}{\rightleftharpoons}} 2NO_2 + H_2O \qquad (1)$$

although an indirect estimate of the rate constant has been published previously.[1] These molecules are present in the polluted atmosphere, and a measurement of this rate constant is, therefore, important in the modeling of atmospheric chemistry.[2]

In our experiments, both HONO and HNO_3 were unambiguously monitored by a quadrupole mass spectrometer, and the rate constant of the reaction was deduced from concentration–time profiles of both species. The stoichiometry of the reaction was also determined during the course of the study.

II. Experimental Section

These experiments were performed in a static-cylindrical Pyrex reactor having a total volume of 750 cm^3 and a surface-to-volume ratio of 0.63 cm^{-1}. Samples were injected through a 2.54-cm diameter Pyrex sphere with 50 holes in its surface located at the center of the reactor. The total dead volume in this injection system was 12 cm^3. This type of injection produces a well-mixed sample immediately after introduction of the reactants. The contents of the reactor were continuously sampled through a 0.0025-cm diameter nozzle located at the apex of a cone which penetrated approximately 2 cm into one end of the reactor. This continuous sampling from the vessel resulted in a steady pressure drop of 0.3%/min within the reactor.

The detector was located in a differentially pumped chamber separate from the chamber containing the reactor. The detector consisted of an Extranuclear Laboratories quadrupole mass filter (Model 324-9 with D_2 high Q head) with a Type II high efficiency electron impact ion source. This ion source was operated at 70-eV electron-bombardment energy during the experiments.

The HONO and HNO_3 concentrations were monitored at the parent mass peaks of each species (47 and 63 amu, respectively). The parent mass of HONO contributed more than 19% of the total ion current from all HONO fragments and, therefore, provided a sensitive technique for monitoring the HONO concentration. The observed relative ion intensities in the fragmentation pattern of pure HONO are: I(47 amu) = 1.0; I(46 amu) ≤ 0.23; I(30 amu) ≤ 4.0. Only upper limits can be placed on the values for 46 and 30 amu because of unavoidable contamination of the sample by NO and NO_2. The parent mass of HNO_3 contributed only 1.6% to the total HNO_3 ion current, however, and the sensitivity for HNO_3 detection was substantially lower than that for HONO.

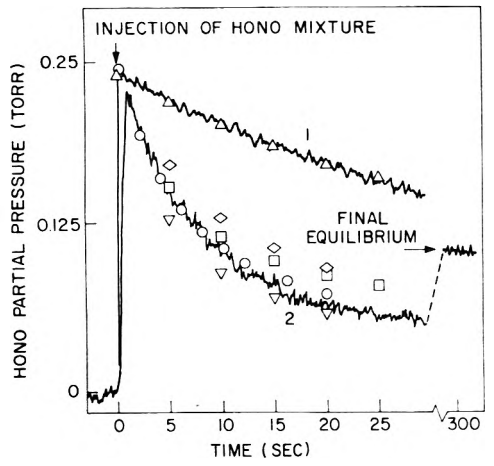

Figure 1. Experimental data obtained while monitoring the HONO concentration at 47 amu. (a) Curve 1 shows the HONO decay rate in the absence of HNO_3. The individual points (Δ) represent the best computer fit to the data obtained using $k_2 = 1.4 \times 10^{-18}$ cm^3/molecule s. (b) Curve 2 shows the decay curve of HONO in the presence of HNO_3 under the conditions of sample 5 in Table I. Computer fits to the data are shown as individual points: (O) best fit using the parameters given in Table I; (▽) same except $k_1 = 1.95 \times 10^{-17}$; (◇) same except $k_1 = 0.87 \times 10^{-17}$; (□) same except $k_3 = 3.0 \times 10^{-20}$.

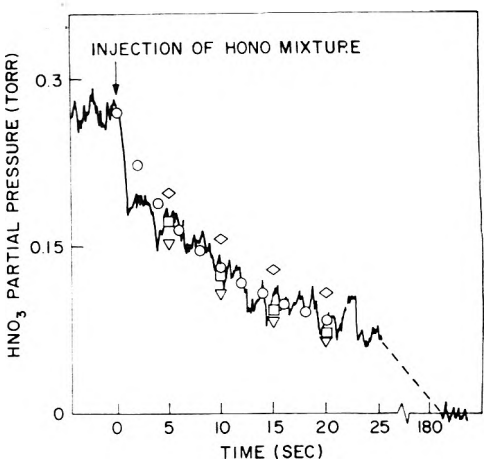

Figure 2. Experimental data obtained while monitoring the HNO_3 concentration at 63 amu under the conditions of sample 6 in Table I. Computer fits to the data are shown as individual points: (O) best fit using parameters given in Table I; (▽) same except $k_1 = 1.95 \times 10^{-17}$; (◇) same except $k_1 = 0.87 \times 10^{-17}$; (□) same except $k_3 = 3.0 \times 10^{-20}$.

Equilibrium samples of HONO were prepared by mixing measured amounts of NO, NO_2, and H_2O in a 2-l Pyrex storage bulb at a total pressure of approximately 1 atm. The equilibrium HONO concentration in the mixture at 300 K was calculated from the following equilibria using the indicated equilibrium constants:[1,3]

$$NO + NO_2 + H_2O = 2HONO \qquad K_{eq} = 1.42 \times 10^{-3}\ \text{Torr}^{-1}$$

$$NO + NO_2 = N_2O_3 \qquad K_{eq} = 6.43 \times 10^{-4}\ \text{Torr}^{-1}$$

$$NO_2 + NO_2 = N_2O_4 \qquad K_{eq} = 7.39 \times 10^{-1}\ \text{Torr}^{-1}$$

The HONO concentration in these mixtures was varied between 9 and 19 Torr by changing the initial NO, NO_2, and H_2O concentrations in the bulb. HNO_3 (purity >90%) was freshly prepared in vacuo prior to each experiment by the addition of KNO_3 (Reagent ACS) to concentrated H_2SO_4 (Reagent ACS) as described by Forsythe and Giauque.[4] The HNO_3 was injected into the reactor immediately after formation to avoid decomposition.

The experiments were performed using the following procedure. A measured amount of HNO_3 was first introduced into the reactor. The initial HNO_3 concentration was varied between 0.05 and 2 Torr as measured by a pressure transducer at the higher concentrations and by the calibrated mass spectrometer at the lower. A 12–28-cm^3 volume of the equilibrium NO, NO_2, H_2O, HONO mixture was then injected producing a total pressure of from 3 to 30 Torr in the vessel. The reaction between HONO and HNO_3 was observed by monitoring either the HONO or the HNO_3 ion current at the appropriate parent mass.

III. Results

Pure HNO_3 was stable in the reactor for time periods greater than 10 min. However, when a sample of the HONO mixture in the absence of HNO_3 was introduced into the reactor, the superequilibrium HONO concentration, which is a result of the decrease in mixture pressure from 1 atm to a few Torr after sample injection, decayed at a measureable rate to the new equilibrium value determined by the reaction

$$HONO + HONO \underset{k_{-2}}{\overset{k_2}{\rightleftharpoons}} NO + NO_2 + H_2O \qquad (2)$$

Curve 1 in Figure 1 shows a typical concentration–time profile of HONO in such an experiment. The HONO signal rises rapidly immediately after injection of the mixture and then decays by a reaction mechanism which we have determined to be heterogeneous and very sensitive to the condition of the surface. The decay curve of HONO in the absence of HNO_3 was frequently measured during the course of the experiments to obtain the best value of k_2 for each determination of k_1 using a rate law based on a simple interpretation of the mechanism represented by eq 2. The true rate law is not fully understood but is more complicated than this approximation.[5]

A typical HONO decay curve in the presence of HNO_3 is presented in curve 2 of Figure 1. Note that the initial decay rate is increased by approximately a factor of 5 in comparison to the self-decay rate, demonstrating that a reaction does occur between HONO and HNO_3.

Figure 2 presents the results obtained while monitoring the HNO_3 ion signal using initial concentrations which are virtually identical with those used in generating curve 2 of Figure 1. As discussed in section II, the signal-to-noise ratio is substantially lower when HNO_3 is monitored because of the unfavorable fragmentation pattern. In addition, the HNO_3 signal is disturbed for a period of approximately 2–3 s after injection of the HONO sample mixture because of the sudden pressure rise in the reactor. We have established that this is only a temporary effect and that the ion signal returns to near its original value after the 2–3-s interval if pure nitrogen is injected into the reactor at 12 Torr. This effect produces the sharp drop in the ion signal observed during the first second in this figure.

Figure 3 shows the decay observed when a portion of the HONO mixture is injected into a sample of HNO_3 whose concentration is a factor of 4 greater than the HONO concentration. The sharp initial drop in HNO_3 signal is again the result of the pressure disturbance. Injection of 13 Torr of N_2 into 1.2 Torr of HNO_3 confirms that the HNO_3 signal returns to its original value within 3–4 s after the N_2 is injected. Therefore, the net drop observed in Figure 3 after approximately 6 s have elapsed is primarily a result of the HONO–HNO_3 reaction. We have determined that the HONO is almost totally consumed during this period. The presence of the slower decrease in HNO_3 concentration after 10 s suggests that HNO_3 also reacts with one or more other components in the mixture but at a much slower rate. Modeling calculations to be described

TABLE I: Measured Rate Constants for the Reaction of HONO with HNO_3

Sample no.	Initial reactant concn, Torr		Total reactor pressure, Torr	Rate constants used to fit the data, cm^3/molecule s × 10^{17}		Species monitored	Measd stoichiometry (ΔHNO_3/$\Delta HONO$)
	HONO	HNO_3		k_1	k_2		
1	0.24[a]	0.14	12.3	1.50	0.092	HONO	
2	0.24	0.13	12.3	1.40	0.092	HNO_3	
3	0.12[b]	0.068	3.1	2.20	0.190	HONO	
4	0.24	0.17	12.3	1.40	0.140	HONO	
5	0.24	0.28	12.5	1.30	0.140	HONO	
6	0.24	0.27	12.3	1.30	0.140	HNO_3	
7	0.46[c]	0.50	22.1	1.50	0.145	HONO	
8	0.46[c]	0.50	22.1	1.80	0.145	HNO_3	
9	0.30	1.20	14.1	[e]	0.120	HNO_3	1.0
10	0.71[d]	2.00	33.0	[e]	0.100	HNO_3	1.0

[a] The HONO was injected into the reactor at known concentration from an an equilibrium mixture of NO, NO_2, H_2O, and HONO prepared as described in the text. Unless otherwise noted, the initial concentrations of NO, NO_2, and H_2O in the samples were: NO = 10.9 Torr; NO_2 = 0.75 Torr; H_2O = 0.15 Torr. The value of k_3 in all cases was 1.5×10^{-20} cm^3/molecule s. [b] Initial concentrations: NO = 2.0 Torr; NO_2 = 0.8 Torr; H_2O = 0.15 Torr. [c] Initial concentrations: NO = 19.5 Torr; NO_2 = 1.36 Torr; H_2O = 0.28 Torr. [d] Initial concentrations: NO = 28 Torr; NO_2 = 1.9 Torr; H_2O = 0.38 Torr. [e] At these high initial concentrations, the reaction proceeds too quickly to permit an accurate determination of k_1. However, the decay curves were compatible with the rate constant determined at lower concentrations.

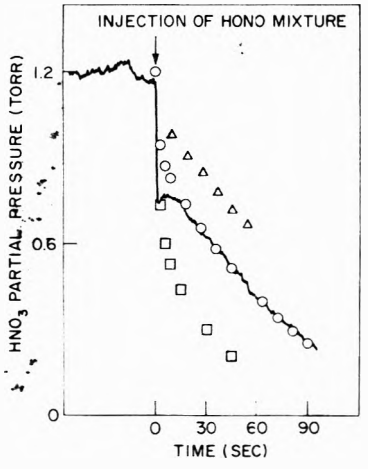

Figure 3. Experimental data obtained while monitoring the HNO_3 concentration at 63 amu under conditions of sample 9 in Table I. The best computer fit to the data using unit reactant stoichiometry is shown as individual points (O) in the figure ($k_1 = 1.5 \times 10^{-17}$, $k_2 = 1.00 \times 10^{-18}$, $k_3 = 1.5 \times 10^{-20}$). The points, (□), were obtained using a HNO_3/HONO stoichiometry of 2.0, while the points, (Δ), were obtained using a stoichiometry of 0.5.

later show that the steady-state HONO concentration formed by reactions 1 and 2 is 10 times smaller than would be necessary to account for this latter decay. These data confirm that a reaction does occur between HONO and HNO_3 which is faster than any of the competing reactions in the system. In fact the rate is sufficiently fast to drive the HONO concentration below the final equilibrium value as demonstrated in curve 2 of Figure 1. After the HNO_3 is consumed, the HONO equilibrium is reestablished by the formation of HONO via the much slower reaction −2. No such subequilibrium HONO concentration is observed when the self-decay of HONO in the absence of HNO_3 is measured.

We have established that HNO_3 does not react significantly with either NO_2 or H_2O in our reactor at the concentrations and time scales used in these experiments. However, a reaction does occur between HNO_3 and NO possibly by a mechanism involving reaction 3 followed by

$$HNO_3 + NO \underset{k_{-3}}{\overset{k_3}{\rightleftharpoons}} HONO + NO_2 \qquad (3)$$

reaction 1. This reaction was determined in separate experiments to be approximately first order with respect to both NO and HNO_3 concentrations. The reaction was heterogeneous in our reactor, and the true rate law was more complicated than that represented by a simple interpretation of the above reaction mechanism. A value of k_3 was obtained from these measurements which fitted the data reasonably well under the experimental conditions present in the reactor during the measurements of k_1. This measured value was $k_3 = 1.5 \times 10^{-20}$ cm^3/molecule s. The initial consumption of HNO_3 by this reaction is a factor of 20 smaller than the observed HONO or HNO_3 decay rates during the HNO_3 + HONO reaction. The HNO_3 + NO reaction does satisfactorily account for the slower decay in HNO_3 concentration which is observed to occur in Figure 3 after the rapid reaction between HONO and HNO_3 nears completion.

The rate constant k_1 was determined for each set of data by integrating the following rate expressions:

$$d(HONO)/dt = k_{-1}(NO_2)^2(H_2O) + 2k_{-2}(NO)(NO_2)(H_2O) + k_3(HNO_3)(NO) - k_1(HONO)(HNO_3) - 2k_2(HONO)^2 - k_{-3}(NO_2)(HONO)$$

$$d(HNO_3)/dt = k_{-1}(NO_2)^2(H_2O) + k_{-3}(NO_2)(HONO) - k_1(HONO)(HNO_3) - k_3(HNO_3)(NO)$$

The independently measured values of k_2, k_3, and the initial reactant concentrations were used as input to the integration program, which generated concentration–time profiles for comparison with experimental data. The reverse rate constants were calculated from the known equilibrium constants,[1,3] $K_1 = 1960.8$ Torr, $K_2 = 704.2$ Torr, $K_3 = 2.78$, and the measured forward rate constants. These reverse reactions are unimportant at the beginning of an experiment but control the final equilibria.

In the above kinetic expressions, we have assumed that the simplified mechanisms for reactions 2 and 3 are correct. As was previously stated, both of these reactions have more complicated true rate laws which are not fully understood. However, because reaction 2 contributes only 20–25% and reaction 3 only 5% to the initial decay rates observed during the HONO + HNO_3 reaction, use of the simplified mechanism produces negligible error in the data analysis and is fully justified.

In Figures 1–3, the best computer fits to the observed experimental data are plotted as individual points. Also included in Figures 1 and 2 are concentration–time profiles

calculated with different values of k_1 and k_3 in order to show the sensitivity of the data to these rate constants.

The stoichiometry of reaction 1 was verified to be unity (HNO_3/HONO) within experimental error by three methods. First, as presented in Table I, the calculated values of k_1 obtained while monitoring HNO_3 are identical with those obtained when HONO is monitored. Such a result is possible only if the stoichiometry is unity. Second, model calculations were carried out using stoichiometries different from unity. Figure 3 presents the results of the calculations carried out on sample 9. It is evident that only unit stoichiometry fits the observed data. Finally, the amount of HNO_3 and HONO consumed during a number of experiments was directly measured by following the HONO concentration and immediately measuring the HNO_3 concentration when the initial fast reaction was over. These experiments were carried out using a variety of initial HONO and HNO_3 concentrations. In all cases, the stoichiometry was 1.0 ± 0.2 after suitable small corrections were made for reactions 2 and 3. Thus, we believe that the reactant stoichiometry is well established.

The results in Table I show that the reaction is first order in HONO and HNO_3 concentrations with a rate constant at 300 K of $k_1 = 1.55(0.3) \times 10^{-17}$ cm^3/molecule s. The number in parentheses represents one standard deviation from the arithmetic mean of the eight sets of data presented in Table I. This value is in fair agreement with the value of $k_1 = 0.97(0.05) \times 10^{-17}$ cm^3/molecule s determined indirectly by England and Corcoran[1] under different experimental conditions. This agreement suggests that these values could represent measurements of the homogeneous rate constant of the reaction. However, in later experiments using a new reactor whose surface had not been well passivated, we observed rate constants for reaction 1 which were up to a factor of 3.5 greater than those presented in Table I. This proves that reaction 1 can be surface catalyzed. Adding between 0.3 and 5.0 Torr of water vapor to the reacting mixture slowed this catalyzed rate. The observed value of k_1 was reduced gradually to 1.4×10^{-17} cm^3/molecule s as the water vapor concentration was increased from 0.1 to 1.0 Torr. No furthur reduction was observed at water concentrations between 1.0 and 5.0 Torr. The existence of this plateau in the water vapor effect proves that the observed rate constant reduction is not a result of an increase in the reverse reaction rate. The most probable explanation for the effect is that the reactor surface is passivated by addition of water vapor. The ultimate rate constant observed when the effect reaches a plateau is identical with that presented in Table I, which was obtained at low water concentrations. This lends support to the suggestion that the value of k_1 reported in Table I could be a measurement of the homogeneous rate constant. However, we have not varied the surface-to-volume ratio of the reactor to verify the homogeneity of the reaction. Thus while the reaction could be homogeneous under the conditions in which the data of Table I were obtained, the value of k_1 determined in these experiments must rigorously be regarded as an upper limit to the homogeneous rate constant.

References and Notes

(1) C. England and W. H. Corcoran, *Ind. Eng. Chem., Fundam.*, **13**, 373 (1974).
(2) B. J. Finlayson and J. N. Pitts, Jr., *Science*, **192**, 111 (1976).
(3) P. G. Ashmore and B. J. Tyler, *J. Chem. Soc.*, 1017 (1961).
(4) W. R. Forsythe and W. F. Giauque, *J. Am. Chem. Soc.*, **64**, 48 (1942).
(5) E. W. Kaiser and C. H. Wu, manuscript in preparation.

Rate Constant for Formation of Chlorine Nitrate by the Reaction ClO + NO_2 + M†

M. T. Leu,* C. L. Lin, and W. B. DeMore

Jet Propulsion Laboratory, California Institute of Technology, Pasadena, California 91103 *(Received August 11, 1976)*

Publication costs assisted by Jet Propulsion Laboratory

A discharge flow/mass spectrometer apparatus has been used to measure rate constants for the reaction ClO + NO_2 + M. The results are: (cm^6 molecule^{-1} s^{-1}) k(M = He) = (2.66 ± 0.35) × 10^{-33} exp[(1140 ± 40)/T] (248–417 K, 1–9 Torr); k(M = N_2) = (3.69 ± 0.24) × 10^{-33} exp[(1150 ± 20)/T] (298–417 K, 1–6 Torr); k(M = Ar) = (1.15 ± 0.10) × 10^{-31} (298 K, 1–4 Torr). The results are compared with other current measurements of this reaction rate.

Introduction

Chlorine nitrate ($ClONO_2$) is currently thought to play a significant role in stratospheric chemistry related to the destruction of ozone.[1] Association of ClO and NO_2 by the process

$$ClO + NO_2 + M \rightarrow ClONO_2 + M \quad (1)$$

has been found to affect the rate of ozone depletion in model calculations.[2-5] In the present study we have undertaken the measurement of the rate constant for reaction 1 for M = He, Ar, and N_2 in the temperature range 248–417 K by monitoring the pseudo-first-order decay of ClO in a large excess of NO_2 in a discharge flow/mass spectrometer apparatus.

Experimental Section

The apparatus used for this research has been described in a previous publication.[6] Briefly, all rate constant measurements were made by observing the pseudo-first-order decay of ClO (m/e = 51) in a large excess of NO_2 in a Pyrex flow tube of 50 cm length and 2.5 cm i.d. (Figure 1). In the side arm of the flow tube, chlorine atoms were generated by passing a trace of molecular chlorine (~0.01%) in a helium carrier (~10% of total flow) through a microwave discharge with approximately 20 W of mi-

† This paper presents the results of one phase of research carried out at the Jet Propulsion Laboratory, California Institute of Technology, under Contract No. NAS7-100, sponsored by the National Aeronautics and Space Administration.

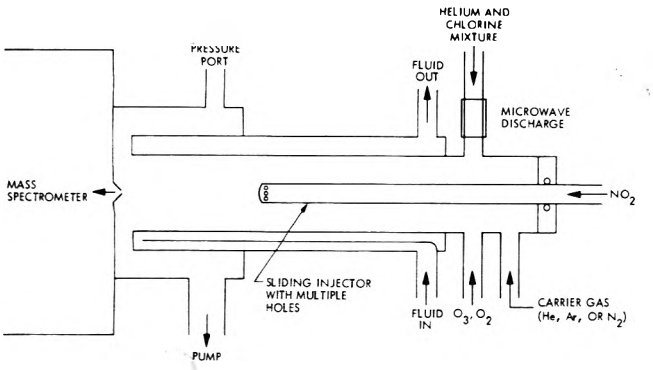

Figure 1. Schematic diagram of discharge flow/mass spectrometer apparatus.

crowave power. The ClO radicals were produced by admitting ozone into the flow tube, leading to the reaction

$$Cl + O_3 \rightarrow ClO + O_2 \quad (2)$$

The rate constant for reaction 2 has been measured previously in our laboratory and elsewhere.[7] The ozone concentration was monitored at $m/e = 48$, and the Cl concentration was adjusted to maintain about a tenfold excess of O_3. The bulk of the He flow entered by way of the carrier gas inlet, thereby minimizing the possible production of impurity radicals such as atomic oxygen. There was in fact no evidence that atomic oxygen was present in significant concentration, since rate constants were found to be unchanged when all the carrier gas was flowed through the discharge region. The reactant NO_2 was admitted into the flow tube through a sliding Pyrex injector (0.6 cm i.d.). Both the inside surface of the flow tube and the outside surface of the injector were coated with phosphoric acid, aged under vacuum conditions, to inhibit surface reactions.

Flow rates of gases (except NO_2) were measured by linear mass flowmeters (Teledyne Hastings-Raydist.). Flowmeters were calibrated by a Hastings bubble-type calibrator (Model HBM-1). The flow rate of NO_2 was measured by the method of pressure drop at a constant volume and temperature. A Haake circulator was used to regulate the temperature. The effect of dimer N_2O_4 was accounted for by using the equilibrium constant measured previously.[8,9] The total pressure (1–9 Torr) in the reaction tube was monitored with a calibrated MKS Baratron pressure meter (Model 310 AHS-1000).

The temperature of the flow tube was controlled by a high-capacity Haake circulator with fluids flowing through the jacket (see Figure 1) and measured by a chromel–constantan thermocouple dipped inside the circulator bath. The fluids used for the temperature ranges 220–300, 300–370, and 370–430 K were ethyl alcohol–dry ice, distilled water, and ethylene glycol, respectively. The temperature inside the flow tube, with flowing He, was checked by inserting a small thermocouple with radiation shield into the reaction tube through the injector. Both measurements agreed within about 1 K.

Most of the gases used for this research were supplied by Matheson Gas Products, including helium, argon, oxygen (UHP), nitrogen (HP), chlorine (research grade), and NO_2 (99.5%). All samples except NO_2 were used without further purification. Ozone was prepared in an oxygen carrier by means of a small laboratory ozonizer. To remove NO from the NO_2, the gaseous sample was treated with approximately 200 Torr of oxygen in the constant volume gas holder over a period of 16 h, and subsequently purified by vacuum distillation at 77 and 196 K. After treatment with O_2, the frozen sample was a white solid powder without colored impurity, indicating the absence of NO. Chlorine nitrate, used in mass spectrometric checks described later, was prepared from Cl_2O and N_2O_5, as described in the literature.[10]

Concentrations in the reaction tube were adjusted such that $10^{11} \leq [ClO] \leq 5 \times 10^{12}$, $4 \times 10^{14} \leq [NO_2] \leq 6 \times 10^{15}$, and $4 \times 10^{16} \leq [M] \leq 4 \times 10^{17}$ (cm^{-3}). The interference of side reactions such as

$$ClO + ClO \rightarrow ClO_2 + Cl$$
$$\rightarrow Cl_2 + O_2 \quad (3)$$

and

$$ClO + O_3 \rightarrow OClO + O_2 \quad (4)$$

was negligible, based on reported rate data for these reactions.[7] In unpublished experiments, we have confirmed that no ClO loss due to reaction 4 is observed at O_3 concentrations even one order of magnitude higher than in the present experiments.

The NO_2 concentration was calculated from the relationship

$$[NO_2] = [\text{total concn}] \times \frac{NO_2 \text{ flow rate}}{\text{total flow rate}} \quad (5)$$

The validity of this method was checked by a photometric method, as follows. An evacuated 10-cm quartz cell was used to sample the helium–NO_2 mixture at the downstream end of the flow tube. The sample was then analyzed by a Cary 15 spectrophotometer using an absorption cross section of 6.8×10^{-19} cm^2 at 4000 Å.[11] The measured NO_2 concentrations were in good agreement (±10%) with the calculated values.

Throughout this experiment, except for M = Ar, the electron gun was operated at 20 eV to ionize the gases in the molecular beam. The measured rate constants were found to be independent of the electron energy from 20 to 100 eV. For M = Ar, 40 eV was used in order to reduce spurious signals due to background modulation, which is a phenomenon observed with Ar but not with He.

Possible interference of ClO^+ from fragmentation of $ClONO_2$ by electron impact was checked at 20 eV. The sensitivity for ClO^+ from $ClONO_2$ was found to be about 1/30 the sensitivity for ClO^+ production from ClO itself. Calculations showed that this effect would cause the measured rate constant to be approximately 7% too low, for ClO decay over one order of magnitude. Such an effect was actually observed by admitting a large amount of NO_2, which gave a large fractional decay of ClO. The decay was found to be not exponential and to curve upward, consistent with interference from chlorine nitrate fragmentation. For this reason, all data were taken with ClO decay less than one order of magnitude. No attempt was made to correct for this effect.

Results and Discussion

A. *M = He.* Plots of ClO decay expressed in terms of the sliding injector position (measured from the injector tip to the mass spectrometer sampling hole) are shown in Figure 2. The linearity of the logarithmic decay profiles verifies the pseudo-first-order nature of the process. Without NO_2, the profile of ClO concentration remained constant, indicating that the effect of injector surface is negligible. A series of experiments was taken by varying NO_2 concentrations at the same conditions. The first-order rate constant (k_I) vs. NO_2 concentration was approximately linear with zero intercept

$$k_I = k_{II}[NO_2] \quad (6)$$

Plots of k_I vs. NO_2 concentration are shown in Figure 3.

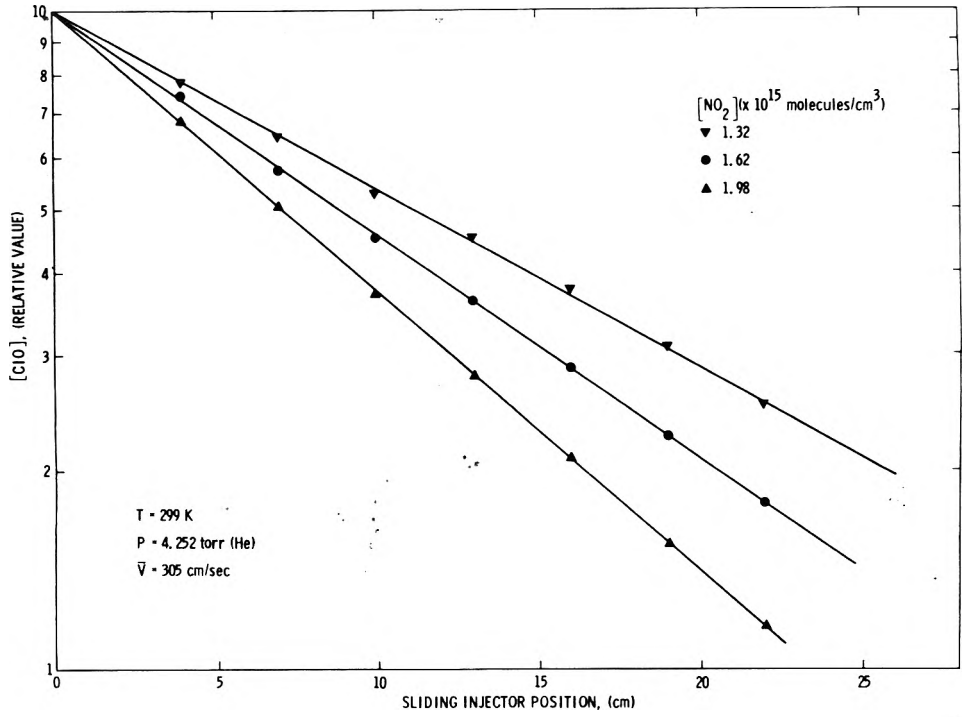

Figure 2. ClO decay resulting from the reaction ClO + NO_2 + He.

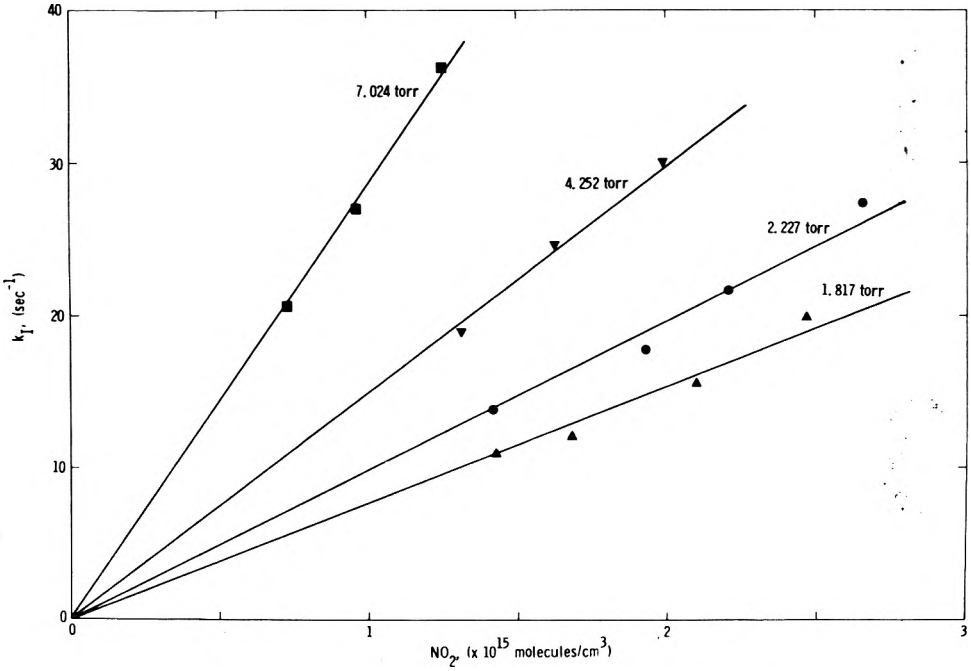

Figure 3. Plots of k_1 vs. NO_2 concentration for M = He and T = 299 K.

The second-order rate constant, k_{II}, could be expressed as

$$k_{II} = k_{III}[M] + k_{IIW} \quad (7)$$

where k_{III} is the homogeneous third-order reaction rate constant, [M] is the total concentration in the reaction zone, and k_{IIW} is the rate constant for heterogeneous reaction of ClO with NO_2 at the flow tube wall.

A plot of k_{II} vs. total pressure for M = He over the temperature range 248–417 K is shown in Figure 4. The slopes of k_{II} vs. P are constant at each temperature, which indicates that the reaction is purely third-order over the range P = 1–9 Torr. Rate constants k_{III} at 248, 299, 360, and 417 K are ($cm^6\ s^{-1}$): $(2.64 \pm 0.28) \times 10^{-31}$, $(1.20 \pm 0.05) \times 10^{-31}$, $(6.85 \pm 0.66) \times 10^{-32}$, and $(3.72 \pm 0.47) \times 10^{-32}$, respectively. The second-order heterogeneous reaction was found to be significant at 248 K, with $k_{IIW} = 1.16 \times 10^{-14}$ $cm^3\ s^{-1}$ but essentially negligible from 299 to 417 K. A weighted least-squares fitting program was used to calculate the following Arrhenius expression, with standard deviations:

$$k = (2.66 \pm 0.33) \times 10^{-33} \exp\left(\frac{1140 \pm 40}{T}\right) cm^6\ s^{-1}$$

over T = 248–417 K, for M = He.

At pressures above 9 Torr the logarithmic ClO decay was nonlinear, with downward curvature. This effect was attributed to poor radial mixing, and the data were not considered suitable for calculation of rate constants.

Measurements at low temperature were complicated by dimerization of NO_2 in the injector tube. This effect was

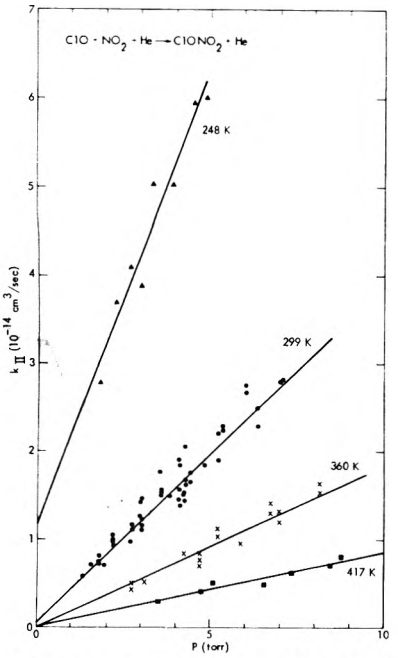

Figure 4. Plot of k_{II} vs. pressure for M = He at T = 248–417 K.

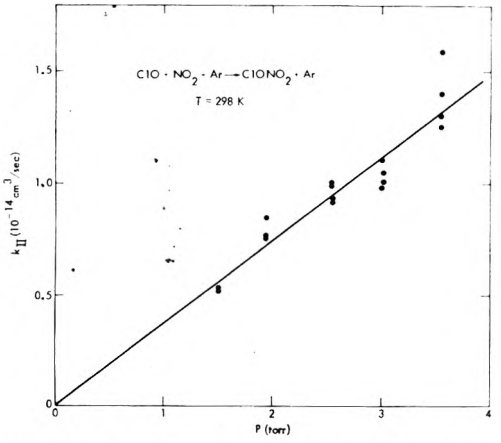

Figure 5. Plot of k_{II} vs. pressure for M = Ar at T = 298 K.

made evident at 248 K by downward curvature in the decay plots (arising from different extents of dimerization as a function of injector tube length exposed to the cold region), and by the fact that initial decay rates corresponded to rate constants which were anomalously low compared to extrapolated values from higher temperatures. These observations suggest that the reaction of ClO with N_2O_4 is relatively slow. To minimize the effect of dimerization, the residence time of NO_2 in the injector tube was decreased by admitting a flow of He sufficient to increase the flow velocity to 1300 cm/s or greater. This gave a residence time in the injector tube of less than 17 ms, which may be compared with an estimated $1/e$ time of about 500 ms for the dimerization reaction. Under these conditions linear decay plots were obtained.

B. M = *Ar*. A similar approach was used to measure the rate constant for M = Ar at 298 K. The data are shown in Figure 5. The slope of the plot of k_{II} vs. P yields the rate constant k_{III} = (1.15 ± 0.10) × 10^{-31} cm^6/s at 298 K, which is essentially identical with the value obtained for He at that temperature. Attempts to measure the rate constant between 4 and 10 Torr were not successful because of flow problems similar to those encountered at high pressures of He.

C. $M = N_2$. Two methods were used to study k_{III} for M = N_2. In both cases N_2 entered through the carrier gas

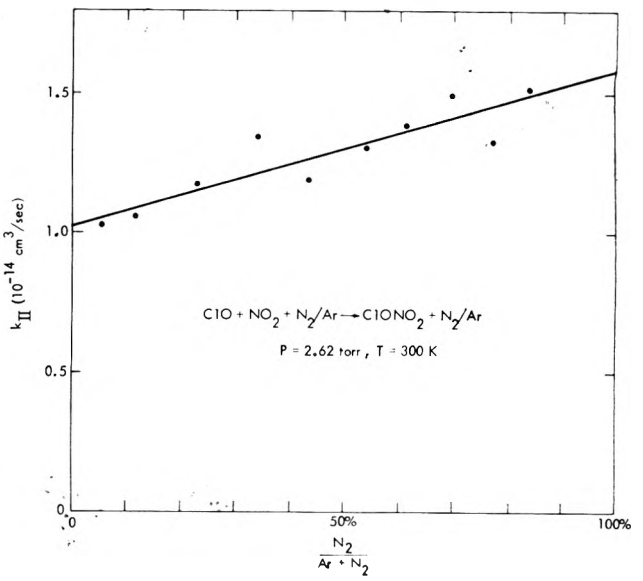

Figure 6. Plot of k_{II} vs. $N_2/(Ar + N_2)$ at a fixed pressure of 2.62 Torr and T = 300 K.

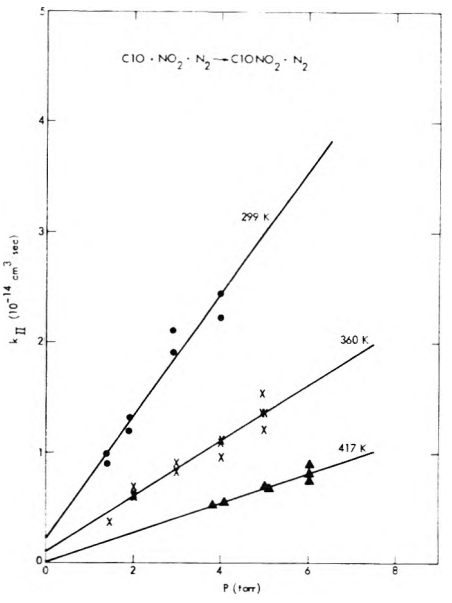

Figure 7. Plot of k_{II} vs. pressure for M = N_2 at T = 299–417 K.

port, and the discharge mixture was either Cl_2/Ar or Cl_2/He. This was done to avoid production of atomic nitrogen in the discharge. In the first method, k_{II} was measured as a function of the N_2 mole fraction in Ar/N_2 mixtures at a fixed total pressure of 2.62 Torr at 300 K. The results are shown in Figure 6. A least-squares determination of the slope of k_{II} vs. $N_2/(N_2 + Ar)$ gave k_{III}(M = N_2) = (1.80 ± 0.12) × 10^{-31}. In the second method, k_{II} was measured in the pressure range 1–6 Torr for carrier gas mixtures consisting of approximately 90% N_2 and 10% He. From the slopes of k_{II} vs. P (Figure 7), the rate constants (k_{III}) obtained at 299, 360, and 417 K were (1.72 ± 0.17) × 10^{-31}, (9.25 ± 0.73) × 10^{-32}, and (5.78 ± 0.93) × 10^{-32}, respectively. A weighted least-squares fitting of all data from both methods gave

$$k_{III}(M = N_2) = (3.69 \pm 0.24) \times 10^{-33} \exp\left(\frac{1150 \pm 20}{T}\right) cm^6/s \quad (8)$$

These results indicate a relative efficiency of 1.47 for N_2 compared to He as a third body.

TABLE I: Summary of Results for ClO + NO_2 + M

Ref	Rate constant, cm^6/s	M	Press, Torr	Temp, K	Technique
This work	$(1.20 \pm 0.05) \times 10^{-31}$	He	1-7	299	Discharge flow/MS
	$(2.66 \pm 0.35) \times 10^{-33} \exp[(1140 \pm 40)/T]$	He	1-9	248-417	
	$(1.15 \pm 0.10) \times 10^{-31}$	Ar	1-4	298	
	$(1.76 \pm 0.12) \times 10^{-31}$	N_2	1-5	299	
	$(3.69 \pm 0.24) \times 10^{-33} \exp[(1150 \pm 20)/T]$	N_2	1-6	298-417	
14	0.82×10^{-31}	He	1-5	297	Discharge flow/MS
	$(1.54 \pm 0.14) \times 10^{-31}$	N_2		297	
	$(4.0 \pm 0.8) \times 10^{-33} \exp[(1066 \pm 66)/T]$	N_2		250-356	
15	$(0.83 \pm 0.03) \times 10^{-31}$	He	1-6	300	Discharge flow/resonance fluorescence
	$(3.54 \pm 0.10) \times 10^{-33} \exp[(950 \pm 10)/T]$	He	1-6	250-365	(Detection of Cl from ClO by NO addition)
	$(1.52 \pm 0.08) \times 10^{-31}$	N_2	2-4	300	
16	2.3×10^{-31}	Ar	5-20	300	Discharge flow/resonance fluorescence (Detection of Cl from ClO by NO addition)

Possible backstreaming of N_2 into the discharge region, which would result in production of atomic nitrogen, is believed to have been negligible, based on the observation that the color of the discharge did not change upon admission of N_2 to the flow tube. Also, the absence of atomic nitrogen was verified by adding a small flow of NO and observing that the NO concentration did not change when the discharge was turned on or off.

D. *Estimation of Systematic Errors.* The systematic errors in all experiments are estimated as ±1% in absolute pressure measurement and ±2% in NO_2 and carrier gas flow rate measurements. Axial and radial diffusion errors[12,13] were less than +5%. The correction for fragmentation of chlorine nitrate is believed to be less than +5%. Combined with uncertainties associated with the geometry of the flow tube, pressure gradients, and temperature measurement, we assign a systematic uncertainty of 15% for all rate constants.

E. *The Reaction Product.* Direct mass spectrometric detection of $ClONO_2$ as a product of the reaction was not possible, owing to the near absence of a suitable peak (such as the parent peak) in the mass spectrum of $ClONO_2$. Tests with authentic $ClONO_2$ showed that the dominant fragment (20 eV) is NO_2^+, with the relative sensitivity for production of $ClONO_2^+$ being less than 1% of that for NO_2^+.

Nevertheless, there is little doubt that the observed disappearance of ClO corresponds to formation of $ClONO_2$, based on the observed first-order dependences on NO_2 and total pressure.

Also, we have conducted experiments (unpublished) on the photolysis of ClO_2 in the presence of NO_2, at total pressures in the range 6–10 Torr, which tend to confirm that $ClONO_2$ is a product of the ClO + NO_2 reaction. Although the overall mechanism is complex, the observed formation of $ClONO_2$ in yields greater than 70% (based on ClO_2 removed) can be attributed to the following steps:

$$ClO_2 + h\nu \rightarrow ClO + O \quad (9)$$

$$ClO + NO_2 + M \rightarrow ClONO_2 + M \quad (10)$$

F. *Comparison with Other Work.* Current measurements of the rate constant for ClO + NO_2 + M are summarized in Table I, and shown graphically in Figure 8. In general, the agreement is excellent, particularly for M = N_2. At a temperature of 220 K, which is typical of the stratosphere, the following results are obtained: this work, $k = 7.0 \times 10^{-31}$ (M = N_2) $cm^6\ s^{-1}$; Birks et al.,[14] $k = 5.1 \times 10^{-31}$ (M = N_2); Zahniser and Kaufman,[15] $k = 4.9 \times 10^{-31}$ (M = N_2). The latter expression was calculated by assuming the same temperature dependence as reported by these workers for M = He.

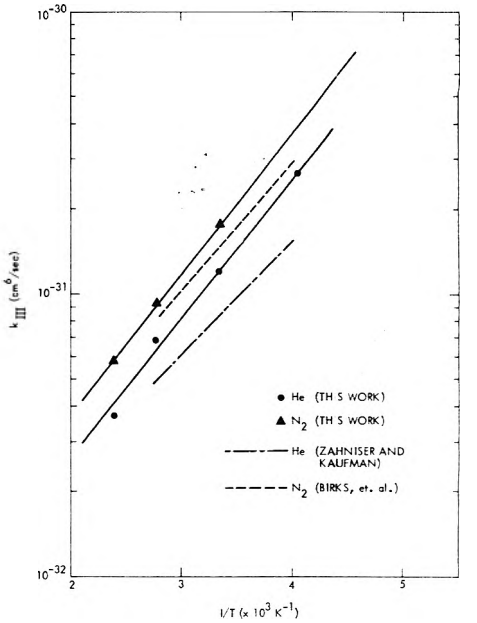

Figure 8. Arrhenius plot of k_{III} vs. $1/T$ of our data and data of Birks et al. and Zahniser and Kaufman.

Acknowledgment. The authors are grateful to J. Birks, M. Zahniser, F. Kaufman, and R. Young for disclosure of unpublished results from their laboratories, and for helpful discussions concerning the present rate constant measurement. We also wish to acknowledge very useful discussions with R. Watson throughout the course of this work.

References and Notes

(1) F. S. Rowland, J. E. Spencer, and M. J. Molina, *J. Phys. Chem.*, **80**, 2710 (1976).
(2) F. S. Rowland, J. E. Spencer, and M. J. Molina, *J. Phys. Chem.*, **80**, 2711 (1976).
(3) J. McAfee and P. J. Crutzen, The 12th Informal Conference on Photochemistry, National Bureau of Standards, Gaithersburg, Md., June 28–July 1, 1976.
(4) R. J. Cicerone, private communication.
(5) S. C. Wofsy, private communication.
(6) M. T. Leu and W. B. DeMore, *Chem. Phys. Lett.*, **41**, 121 (1976).
(7) (a) R. T. Watson, *J. Phys. Chem. Ref. Data Ser.*, accepted for publication; (b) M. A. A. Clyne and R. T. Watson, *J. Chem. Soc., Faraday Trans. 1*, **70**, 2250 (1974); (c) M. A. A. Clyne and W. S. Nip, *J. Chem. Soc., Faraday Trans. 2*, **72**, 838 (1976); (d) M. S. Zahniser, F. Kaufman, and J. G. Anderson, *Chem. Phys. Lett.*, **37**, 226 (1976); (e) M. Kurylo and W. Braun, *Chem. Phys. Lett.*, **37**, 232 (1976); (f) R. T. Watson, E. Machado, S. Fischer, and D. D. Davis, *J. Chem. Phys.*, **65**, 2126 (1976).
(8) H. Blend, *J. Chem. Phys.*, **53**, 4497 (1970).

(9) R. J. Nordstrom and W. H. Chan, *J. Phys. Chem.*, **80**, 847 (1976).
(10) M. Schmeisser, *Inorg. Syn.*, **9**, 127 (1967).
(11) A. M. Bass, A. E. Ledford, Jr., and A. H. Laufer, to be published.
(12) F. Kaufman, *Prog. React. Kinet.*, **1**, 1 (1961).
(13) R. V. Poirier and R. W. Carr, Jr., *J. Phys. Chem.*, **75**, 1593 (1971).
(14) J. Birks, private communication.
(15) M. S. Zahniser and F. Kaufman, private communication.
(16) R. A. Young, private communications.

Reaction of N_2H^+ with Methanol. Internal Energy Effects in Proton Transfer Reactions

Richard D. Smith*

Chemistry Division, Naval Research Laboratory, Washington, D.C. 20375

and Jean H. Futrell

Department of Chemistry, University of Utah, Salt Lake City, Utah 84112 *(Received June 21, 1976)*

The reactions of N_2H^+ with CH_3OH and CD_3OH have been examined as a function of the average number of collisions N_2H^+ undergoes with H_2 prior to reaction. The experiments used a tandem mass spectrometer, consisting of a Dempster 180° mass spectrometer first stage and an ion cyclotron resonance (ICR) second stage. The reactions were studied at average translational energies of ≤0.1 eV and at low pressures (single collision conditions in the ICR cell). Branching ratios (product distributions) support earlier suggestions concerning reaction mechanism for the H_3^+ and CH_3OH reaction. The QET treatment of $CH_3OH_2^+$ decomposition is discussed and it is concluded that a barrier of ~33 kcal/mol in excess of the thermodynamic requirements impedes the H_2 elimination process.

Introduction

Proton transfer reactions are of continuing interest for both applied and fundamental reasons. The establishment of gas phase proton affinities[1-3] is of enormous practical significance to chemical ionization techniques[4] where proton transfer reactions are often utilized for analytical purposes. In addition to proton affinities and related thermodynamic values, details of the precise proton transfer mechanism as well as the characteristics of typical competing reactions (such as hydride ion abstraction and charge transfer) are also of interest. Intimately related are details concerning equilibration of internal energy in the initial proton transfer product[5] and energy partitioning between translational and internal modes.[5-10] Once (and if) energy randomization is attained, subsequent fragmentation processes should be described adequately by quasi-equilibrium theory (QET)[11] or RRKM[12] calculations.

In this work we report the results of a tandem Dempster-ion cyclotron resonance (ICR) study of the reactions of N_2H^+ with CH_3OH and CD_3OH. Huntress and Bowers[13] and Fiaux, Smith, and Futrell[14] have used ICR and tandem Dempster–ICR mass spectrometers previously to study $H_3^+(D_3^+)$ reactions with CH_3OH (and CD_3OH in the former study). In these studies the average H_3^+ reactant ion internal energy was altered by varying the average number of H_3^+–H_2 (or D_3^+–D_2) collisions prior to reaction. Since the tandem Dempster–ICR instrument utilized a separate chamber for preparation of H_3^+ reactant ions, these studies are characterized by a narrower distribution of internal energies.[15] Such an experimental configuration allows one to execute studies at constant ICR cell pressures at the single-collision limit (~10^{-6} Torr). Aside from these minor differences, the experimental results were in essential agreement. The following reactions were observed:

$$H_3^+ + CH_3OH \rightarrow CH_3OH_2^+ + H_2 \quad (1)$$
$$\rightarrow CH_3OH^+ + H + H_2 \quad (2)$$
$$\rightarrow CH_2OH^+ + 2H_2 \quad (3)$$
$$\rightarrow CHO^+ + 3H_2 \quad (4)$$
$$\rightarrow CH_3^+ + H_2O + H_2 \quad (5)$$

The CHO^+ and CH_3OH^+ products are not observed for reaction of H_3^+ ions which have undergone several collisions with H_2 prior to reaction; for relaxed H_3^+ reactant ions only reactions 1, 3, and 5 occur.

In a later study, Bowers, Chesnavich, and Huntress[16] applied the quasi-equilibrium theory (QET) to compare calculated and experimental branching ratios for the decomposition of $CH_3OH_2^+$ ions formed in the initial proton transfer reaction

$$CH_3OH_2^+ \begin{cases} \rightarrow CH_2OH^+ + H_2 & (6) \\ \rightarrow CH_3^+ + H_2O & (7) \end{cases}$$

Adequate agreement between calculation and experiment was achieved by assigning an activation energy of 1.1 ± 0.1 eV to reaction 6 and no activation energy above reaction endothermicity for reaction 7.

The reaction of N_2H^+ with CH_3OH and CD_3OH provides additional information on the decomposition of protonated methanol. Since recent work[1] has established a proton affinity of N_2 at 0.55 ± 0.02 eV (12.7 ± 0.5 kcal) greater than H_2, the present results allow the examination of analogous reactions of collisionally relaxed N_2H^+ ions where the reaction enthalpies are approximately 12.7 kcal/mol lower.

Experimental Section

The tandem mass spectrometer used in this work has been described in detail elsewhere.[15] The first stage of the

* NRC-NRL Resident Research Associate 1975-1976. Present address: Radiological Sciences Department, Battelle-Northwest, Richland, Wash. 99352.

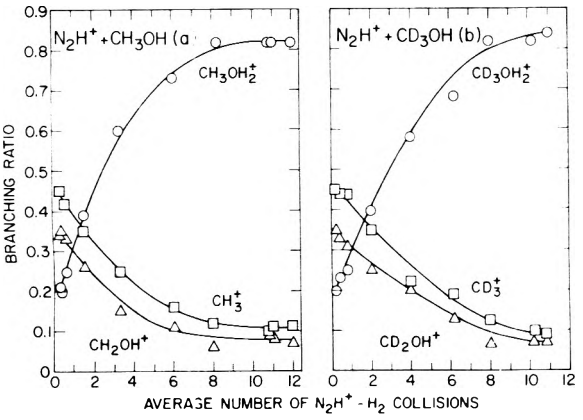

Figure 1. Branching ratios (product distributions) as a function of the average number of N_2H^+–H_2 collisions in the Dempster source prior to reaction in the ICR cell for (a) the N_2H^+ + CH_3OH and (b) N_2H^+ + CD_3OH reactions.

instrument is a 180°, 5.7-cm radius mass spectrometer equipped with a source capable of efficient operation at pressures up to approximately 10^{-2} Torr. By choosing specific repeller fields and source pressures, the average number of ion–neutral collisions ($\bar{n}$) in the source[5] may be varied from 0 to a maximum of approximately 25. Following mass analysis, ions are decelerated to less than 0.1 eV and are injected into the cavity of an ICR mass spectrometer. Relative ion intensities are determined using a conventional marginal oscillator detector which has been calibrated at each frequency. The reaction time is determined by the time the reactant ions spend in the ICR cell and is measured directly.

N_2H^+ reactant ions are prepared in the source from a 20 to 1 mixture of hydrogen to nitrogen. Rate constants and product distributions were determined as described previously.[5,7] All ICR experiments were carried out under low-conversion, single-collision conditions, utilizing ICR cell conditions state previously.[5,7]

Results

A total rate constant of 1.7 ± 0.3 cm^3 $molecule^{-1}$ s^{-1} was determined for the reaction of N_2H^+ with methanol. A small decrease was noted on progression from excited to collisionally relaxed N_2H^+ reactant ions, however, this decrease did not exceed our estimated experimental error limits. The rate constant is considerably larger than the orbiting (Langevin) collision rate constant of 1.1×10^{-9} cm^3 $molecule^{-1}$ s^{-1} calculated from the ion-induced-dipole theory of Gioumousis and Stevenson.[17] However, the average dipole orientation (ADO) theory of Bowers et al.[18,19] predicts a collision rate constant of 1.9×10^{-9} cm^3 $molecule^{-1}$ s^{-1}, in good agreement with the present results.

Figure 1 shows the product distributions obtained for the reactions of N_2H^+ with CH_3OH (a) and CD_3OH (b) as a function of the average number of N_2H^+–H_2 source collisions. Each point represents the average of no less than three determinations. The results were obtained at a number of pressures near the zero collision limit, and extrapolation to zero pressure was used to check for contributions of secondary processes.

In addition to the usual correction for naturally occurring $^{13}CD_3OH$, it was necessary to correct the product distributions for two isotopic impurities. One correction was required for a contribution (~5%) of CD_3OD and a second for CD_2HOH (2–4%). These isotopic impurities give rise to small ion intensities at m/e 17, 32, 34, 35, and 37 which have been subtracted out in the data presented in Figure 1.

Discussion

Reactions responsible for generating the N_2H^+ reactant ions have been described previously[5] and, hence, only a brief discussion will be presented here. In the low pressure limit (a low average number of collisions, $\bar{n}$) N_2H^+ ions are generated primarily by

$$H_2^+ + N_2 \rightarrow N_2H^+ + H \qquad \Delta H = -56 \text{ kcal/mol} \qquad (8)$$

At higher pressures, and in a large excess of H_2, H_2^+ is rapidly converted to H_3^+ by

$$H_2^+ + H_2 \rightarrow H_3^+ + H \qquad \Delta H = -43 \text{ kcal/mol} \qquad (9)$$

Thus, at high pressure N_2H^+ ions are formed primarily by

$$H_3^+ + N_2 \rightarrow N_2H^+ + H_2 \qquad \Delta H = -12.7 \text{ kcal/mol} \qquad (10)$$

Reactions 8, 9, and 10 are known to occur at approximately their collision rate constant.[20-24] The only other reactions of importance involve the collisional relaxation of N_2H^+ species prior to leaving the source. At high pressures the average reactant ion will undergo at least 10 collisions; previous results[5-10] suggest that many diatomic and triatomic ions are nearly completely relaxed after approximately 5–10 collisions.

From the similarity of reactions 8 and 9, one may assume that the distribution of initial N_2H^+ internal energies (at a low average number of collisions) parallels that determined previously for H_3^+. From the greater exothermicity of reaction 8, one would expect a shift toward the population of higher vibrational levels, resulting in an average N_2H^+ internal energy in excess of 45 kcal/mol. Since the initial H_2^+ distribution of internal energies is quite broad,[25] the maximum N_2H^+ internal energy will be limited to about 5 eV by the dissociation reaction

$$N_2H^+ \rightarrow H^+ + N_2 \qquad \Delta H = 112 \text{ kcal/mol} \qquad (11)$$

On the basis of previous studies of the $H_3^+ + CH_3OH$ reaction, one might expect to observe the following reaction channels for the N_2H^+–CH_3OH system:

$$N_2H^+ + CH_3OH \rightarrow \begin{cases} CH_3OH_2^+ + N_2 & \Delta H = \sim -62 \text{ kcal/mol} \quad (12) \\ CH_3OH^+ + H + N_2 & \Delta H = +54 \text{ kcal/mol} \quad (13) \\ CH_2OH^+ + H_2 + N_2 & \Delta H = -31 \text{ kcal/mol} \quad (14) \\ CHO^+ + 2H_2 + N_2 & \Delta H = -3.5 \text{ kcal/mol} \quad (15) \\ CH_3^+ + H_2O + N_2 & \Delta H = +2.2 \text{ kcal/mol} \quad (16) \end{cases}$$

Reaction 12 corresponds to proton transfer, reaction 13 to charge transfer, reaction 14 to dissociative proton transfer (or hydride ion abstration), reaction 15 to H_2 elimination from the ionic product of reaction 14, and reaction 16 to H_2O elimination from the proton transfer product. Reactions 13 and 15 are not observed experimentally, which is consistent with results for the reaction of collisionally relaxed H_3^+ with CH_3OH in which these products are also not observed.[13,14]

A detailed discussion of these reactions requires knowledge of the enthalpies of the competing reactions 12–16. Table I presents a list of the standard heats of formation used in this work. While most of these values are known with considerable precision from various photoionization studies, the heats of formation of protonated species (H_3^+, N_2H^+, and $CH_3OH_2^+$) are less well established. However, Bohme and co-workers[1] have recently established quite accurate limits on the relative proton affinities (PA) of several species relevant to this work, including H_3^+, N_2H^+, and COH^+. Using the value suggested by Bohme,[1b] $PA(H_2)$ = 104 kcal/mol, heats of formation of 262, 250, and 198 kcal/mol are obtained for

TABLE I: Standard Heats of Formation Used in This Work

Species	ΔH_f, kcal/mol[a]	Ref
H_3^+	260, 262	*a*
N_2H^+	248, 250	*a*
$CH_3OH_2^+$	138	*b*
CH_3OH^+	202	*c*
CH_2OH^+	169	*d*
HCO^+	196.5, 198.4	*a*
CH_3^+	260	*c*
CH_3OH	−48	*c*
H_2O	−57.8	*c*
N_2H_2	48.7	*c*

[a] Where two values are given for the heat of formation, the first (used in this work) corresponds to the values obtained using ΔH_f of COH^+ obtained in the photoionization study of Guyon et al.[27] The second corresponds to the use of $\Delta H_f(H_3^+) = 262$ kcal/mol, suggested by Bohme (ref 1). The relative proton affinities established by Bohme are used in both cases. [b] References 28 and 29. [c] Reference 26. [d] Obtained from photoionization data of Refaey and Chupka, ref 34.

TABLE II: Heats of Reaction (ΔH_R) for the H_3^+ + CH_3OH Reaction Used in This Work and Previous Studies

	ΔH_R, kcal/mol		
Ionic product	Ref 13,16	Ref 14	This work[a]
$CH_3OH_2^+$	−72	−74	−75
CH_2OH^+	−37	−32	−43
CHO^+		−18.4	−16.2
CH_3^+	−8	−16	−10

[a] Using ΔH_f values given in Table I.

H_3^+, N_2H^+, and COH^+, respectively. However, recently Guyon, Chupka, and Berkowitz[27] used photoionization techniques to determine a heat of formation of 196.5 ± 0.5 kcal/mol for CHO^+. If one uses this value to adjust the proton affinity scale, the heats of formation of H_3^+ and N_2H^+ are lowered by several kilocalories per mole, increasing the enthalpies of reactions 12–16 by an equivalent amount. The first-listed values given in Table I for the heats of formation of H_3^+, N_2H^+, and COH^+ are based on the new value for $\Delta H_f(HCO^+)$; subsequent discussion is based on these revised PA values.

While there is still doubt concerning the absolute PA of methanol,[28,29] we estimate an uncertainty of ≤6 kcal/mol. In Table II we compare the calculated exothermicities for the reactions of H_3^+ with CH_3OH used in discussing the previous ICR studies. The implication of these revised thermodynamic data for QET calculations of $CH_3OH_2^+$ decomposition will be discussed after we have considered the reaction mechanism and energy partitioning in more detail.

The principal reaction channels observed for the N_2H^+ + CH_3OH reaction are reactions 12, 14 and 16. Figure 1 shows that the stable proton transfer channel accounts for 20% of the products for excited (unrelaxed) N_2H^+ reactant ions and greater than 80% of the products for collisionally relaxed ions. In contrast, for the reaction of relaxed H_3^+ ions with methanol the following product distribution was observed: CH_3^+, 46%; CH_2OH^+, 28%; and $CH_3OH_2^+$, 26%.[14]

The CH_2OH^+ product may result from proton transfer followed by H_2 elimination from $CH_3OH_2^+$ or from a direct hydride ion (H^-) abstraction mechanism. A detailed discussion of these mechanisms is presented elsewhere.[5] Both previous studies of the more energetic reaction of H_3^+ with methanol show that this alternate mechanism becomes less likely as H_3^+ is collisionally relaxed and is negligible for reactant ions having undergone 5–10 collisions.[13,14] It has been suggested[5] that the equivalent process for the analogous reaction of N_2H^+ with ethane is better described as proton transfer followed by prompt H_2 elimination from a species which has not undergone energy equilibration. According to this mechanism, hydrogen molecule loss from the transient species always involves the transferred proton, making this mechanism isotopically indistinguishable from hydride ion abstractions.[5] While both mechanisms may contribute to the reactions of excited N_2H^+ ions, the higher energy H_3^+ results[13,14] suggest that dissociative proton transfer is the only mechanism which generates CH_2OH^+ from collisionally relaxed N_2H^+ reactant ions.

It is of interest to note that N_2H_2 may result from the hydride abstraction reaction, e.g.

$$N_2H^+ + CH_3OH \rightarrow CH_2OH^+ + N_2H_2 \qquad (17)$$
$$\Delta H = +17.7 \text{ kcal/mol}$$

This reaction may rationalize the apparent endothermicity of the hydride abstraction channel for the present system. However, the analogous stable H_4 product is unavailable for H_3^+ reaction with CH_3OH. Thus, while we cannot dismiss the possibility that the endothermicity of reaction 17 is a controlling factor, comparison with similar systems suggests the relevant mechanism is dissociative proton transfer.

The isotopic study indicates that CH_2OH^+ is formed by vicinal elimination of H_2 across the C–O bond from the $CH_3OH_2^+$ proton transfer product. For example, Figure 1b shows that decomposition of the $CD_3OH_2^+$ species occurs by

$$CD_3OH_2^+ \rightarrow CD_2OH^+ + HD \qquad \Delta H = +31 \text{ kcal/mol} \qquad (18)$$

Neither CDH_2O^+ nor CD_3O^+ were detected in this study. These results are consistent with the previous H_3^+ studies of Huntress and Bowers[13] and Fiaux, et al.[14]

The only other product observed in this study also corresponds to a dissociative proton transfer reaction via reaction 7. The results for the N_2H^+ reaction with CD_3OH support this bond-cleavage mechanism since CD_3^+ is the only product observed.

The results presented in Figure 1 can be explained in terms of proton transfer and two dissociative proton transfer channels involving H_2 and H_2O elimination form a $CH_3OH_2^+$ intermediate species. In addition, we conclude that the proton is initially transferred to the O atom and that H,D isotopic scrambling does not occur prior to elimination of H_2O by bond cleavage or vicinal elimination of hydrogen. These results also suggest that the activation energy required for H,D isotopic scrambling is equal to or greater than the barrier for vicinal H_2 elimination.

By considering information deduced from our earlier studies of proton transfer reactions,[5-10] one can qualitatively account for many aspects of the experimental data. Previous work[6] has shown that the initial proton transfer reaction

$$X_2H^+ + A \rightarrow AH^+ + X_2$$

for relaxed (ground state) reactant ions (X_2H^+) deposits a negligible amount of the heat of reaction in the diatomic neutral product, (X_2). Thus, we assume the full 62 kcal exothermicity of reaction 12 is usually deposited either as internal energy of the $CH_3OH_2^+$ product or as relative translational energy of the ion and neutral products. Previous work has also shown that, for a significant fraction of the products (10–50%), considerable translational energy (5–20 kcal/mol) may be deposited as relative translational energy of the products.[5,6,8] A polarization-

stripping model[30] was found to provide a reasonable rationalization of the results.[6] This model has one arbitrary parameter, the critical separation of the center of charge from the neutral (r) at the point of proton transfer. The value for this parameter (which has limited significance due to the simplicity of the model) found to give the best fit was r = 2.1–2.2 Å for ethylene[6] and r = 2.25 Å for ethane.[5] Assuming a value of r = 2.2 Å for the present reaction, this model predicts 9 kcal/mol will be deposited as relative translational energy of the products. The large permanent dipole moment of methanol (1.7×10^{18} esu) may be included in this model using an average dipole orientation derived from the ADO theory of Su and Bowers.[18] Consideration of this additional term suggests a total kinetic energy release of ca. 14 kcal/mol; accordingly we estimate that 9–14 kcal/mol is the average translational energy release in this reaction. This result is qualitatively useful, but is obviously incorrect in detail.

If the internal energy of the $CH_3OH_2^+$ product is well known (and if energy equilibration in the ground electronic state precedes decomposition), one can then apply a statistical theory (e.g., QET,[11] RRKM[12]) in an attempt to calculate the subsequent unimolecular reaction rates and branching ratios for comparison with experiment. Bowers, Chesnavich, and Huntress used the activation energy required for the vicinal H_2 elimination process as a variable parameter in their QET calculations.[16] The best fit to the experimental data required an activation energy of 25 kcal/mol for reaction 6.

Recently Huntress, Bowers, and Jennings have measured directly the kinetic energy release associated with the metastable unimolecular decompositions of $CH_3OH_2^+$ to form $CH_3^+ + H_2O$ and $CH_2OH^+ + H_2$.[31] They obtained 0.05 and 21 kcal/mol of kinetic energy release for the CH_3^+ and CH_2OH^+ products, respectively. This is the amount of internal energy of the $CH_3OH_2^+$ ion converted to relative translational energy of the products on decomposition. Additional knowledge of the internal energy of the products is required to determine the precise activation energy barrier; however, it is often assumed that the majority of the heat of reaction is partitioned as translational energy of the products.[32] Consequently these results support the earlier QET calculations of Bowers et al.[16]

Since the CH_2OH^- products will contain only a fraction of the available energy, it is not surprising that we fail to observe the subsequent H_2 elimination product, HCO^+. The kinetic energy release for reaction

$$CH_2OH^+ \rightarrow HCO^+ + H_2 \qquad (19)$$

was measured to be 32.2 kcal/mol,[33] implying a barrier of at least this size. This large barrier, plus the energy partitioning discussed above, explain our failure to observe CHO^+ for even the most excited N_2H^+ reactants.

Another problem which must be confronted in justifying the application of statistical theories is whether the assumed mechanism is correct. For the present problem of rationalizing the decomposition branching ratios of $CH_3OH_2^+$ to form CH_3^+ and CH_2OH^+, we must be concerned with the possibility of a competing direct mechanism for formation of CH_2OH^+ by hydride abstraction;[5] e.g.

$$N_2H^+ + CH_3OH \rightarrow CH_2OH^+ + N_2 + H_2 \qquad (14)$$
$$\Delta H = -31 \text{ kcal/mol}$$

Both the present and previous studies using isotopically labeled reactants show that hydride abstraction is not important for reaction of N_2H^+ or relaxed H_3^+ ions with CH_3OH.[13,14] This reaction channel closes at a higher energy than dissociative proton transfer. Since both these reactions have identical overall exothermicities (31 kcal/mol), the results suggest an even larger barrier (>50 kcal/mol) to H^- abstraction. Such a large barrier for a simple reaction of H^- abstraction would be quite difficult to rationalize.

An alternative explanation for this result is that H^- abstraction[5] is not the true reaction mechanism; rather the actual process is proton transfer followed by prompt H_2 elimination (always involving the transferred proton) before energy equilibration occurs. This model avoids invoking an additional mechanism having an unusually high activation energy.

Finally, the results in Figure 1 show that the abundance of both the CH_3^+ and CH_2OH^+ products drop significantly as N_2H^+ is collisionally relaxed. Since these products represent competing fragmentation pathways of the $CH_3OH_2^+$ ion, one can suggest that the thermodynamic constraints are quite similar.[32] This is also suggested by the work of Huntress et al.[31] where both processes were observed as "metastable transitions" (i.e., unimolecular reactions occurring on the microsecond time scale) of approximately equal intensity. Ions undergoing unimolecular reactions on the microsecond time scale are usually considered to contain a very small amount of internal energy (≤3 kcal/mol) in excess of the thermodynamic requirement of the lowest energy reaction. Accordingly, assuming a negligible barrier to reaction 7, we estimate an activation energy of ~33 kcal/mol for H_2 elimination from $CH_3OH_2^+$. This value is greater than the experimentally measured kinetic energy release of 21 kcal/mol and suggests that about two-thirds of the excess energy is partitioned as relative translational energy.

In summary, the present results are consistent with previous experimental results[13,14] and provide qualitative support for the detailed reaction mechanism discussed elsewhere.[16] However, these QET calculations should be modified to account for energy partitioning in the initial proton transfer step. It is also suggested (based on current thermodynamic information) that the activation energy of 25 kcal suggested for reaction 6 is too low and a value of ~33 kcal is more appropriate. Making this change would require adjustment of other parameters of the QET calculation to bring it into line with experiment.

Acknowledgment. The authors wish to acknowledge the support of the National Science Foundation through Grant No. GP 33870X.

References and Notes

(1) (a) D. K. Bohme in "Interactions between Ions and Molecules", P. Ausloos, Ed., Plenum Press, New York, N.Y., 1975, p 489; (b) D. K. Bohme, presented at the Twenty-Fourth Annual Conference on Mass Spectrometry and Allied Topics, San Diego, Calif., May 9–14, 1976.
(2) A. E. Roche, M. M. Sutton, D. K. Bohme, and H. I. Schiff, *J. Chem. Phys.*, **55**, 5480 (1971).
(3) D. K. Bohme, R. S. Hemsworth, R. W. Rundle, and H. I. Schiff, *J. Chem. Phys.*, **58**, 3504 (1973).
(4) F. H. Field in "Ion-Molecule Reactions", J. L. Franklin, Ed., Plenum Press, New York, N.Y., 1972, p 261.
(5) R. D. Smith and J. H. Futrell, *Int. J. Mass Spectrom. Ion Phys.*, **20**, 347 (1976).
(6) R. D. Smith and J. H. Futrell, *Int. J. Mass Spectrom. Ion. Phys.*, **19**, 201 (1976).
(7) R. D. Smith and J. H. Futrell, *Int. J. Mass Spectrom. Ion Phys.*, **20**, 33 (1976).
(8) R. D. Smith and J. H. Futrell, *Int. J. Mass Spectrom. Ion Phys.*, **20**, 43 (1976).
(9) R. D. Smith and J. H. Futrell, *Int. J. Mass Spectrom. Ion Phys.*, **20**, 59 (1976).
(10) R. D. Smith and J. H. Futrell, *Int. J. Mass Spectrom. Ion Phys.*, **20**, 71 (1976).
(11) M. L. Vestal in "Fundamental Processing in Radiation Chemistry", P. Ausloos, Ed., Interscience, New York, N.Y., 1968.

(12) (a) R. A. Marcus, *J. Chem. Phys.*, **20**, 359 (1952); (b) G. M. Wieder and R. A. Marcus, *ibid.*, **37**, 1835 (1962).
(13) W. T. Huntress, Jr., and M. T. Bowers, *Int. J. Mass Spectrom. Ion Phys.*, **12**, 1 (1973).
(14) A. S. Fiaux, D. L. Smith, and J. H. Futrell, *Int. J. Mass Spectrom. Ion Phys.*, **20**, 223 (1976).
(15) D. L. Smith and J. H. Futrell, *Int. J. Mass Spectrom. Ion Phys.*, **14**, 171 (1974).
(16) M. T. Bowers, W. J. Chesnavich, and W. T. Huntress, *Int. J. Mass Spectrom. Ion Phys.*, **12**, 357 (1973).
(17) G. Gioumousis and D. P. Stevenson, *J. Chem. Phys.*, **29**, 294 (1958).
(18) (a) T. Su and M. T. Bowers, *J. Chem. Phys.*, **52**, 3027 (1973); (b) *Int. J. Mass Spectrom. Ion Phys.*, **12**, 347 (1973).
(19) L. Bass, T. Su, W. J. Chesnavich, and M. T. Bowers, *Chem. Phys. Lett.*, **34**, 119 (1975).
(20) K. R. Ryan, *J. Chem. Phys.*, **61**, 1559 (1974).
(21) M. T. Bowers and D. Elleman, *J. Chem. Phys.*, **51**, 4606 (1969).
(22) J. A. Burt, J. L. Dunn, M. J. McEwan, M. M. Sutton, A. E. Roche, and H. I. Schiff, *J. Chem. Phys.*, **52**, 6062 (1970).
(23) V. Aquilanti, A. Galli, A. Giardini-Guidoni, and G. G. Volpi, *J. Chem. Phys.*, **43**, 1969 (1965).
(24) D. K. Bohme, R. S. Hemsworth, H. W. Rundle, and H. I. Schiff, *J. Chem. Phys.*, **58**, 3504 (1973).
(25) F. von Busch and G. H. Dunn, *Phys. Rev. A*, **5**, 1726 (1972).
(26) J. L. Franklin, J. G. Dillard, H. M. Rosenstock, J. T. Herron, K. Drazl, and F. H. Field, *Natl. Stand. Ref. Data Ser., Natl. Bur. Stand.*, **No. 26** (1969).
(27) P. M. Guyon, W. A. Chupka, and J. Berkowitz, *J. Chem. Phys.*, **64**, 1419 (1976).
(28) J. L. Beauchamp, Ph.D. Thesis, Harvard University, 1967.
(29) S. Chang and J. L. Franklin, *J. Am. Chem. Soc.*, **94**, 6347 (1972).
(30) P. M. Hierl, Z. Herman, and R. Wolfgang, *J. Chem. Phys.*, **53**, 660 (1970).
(31) (a) W. T. Huntress, M. T. Bowers, and K. R. Jennings, presented at the Twenty-Fourth Annual Conference on Mass Spectrometry and Allied Topics, San Diego, Calif., May 9–14, 1976. (b) W. T. Huntress, private communication.
(32) R. G. Cooks, J. H. Beynon, R. M. Capriali, and G. R. Lester, "Metastable Ions", Elsevier, New York, N.Y., 1973.
(33) J. H. Beynon, A. E. Fontaine, and G. R. Lester, *Int. J. Mass Spectrom. Ion Phys.*, **1**, 1 (1968).
(34) K. M. A. Refaey and W. A. Chupka, *J. Chem. Phys.*, **48**, 5205 (1968).

Chemical Effects of Low-Energy Electron Impact on Hydrocarbons in the Gas Phase. 2. Propene[1]

R. Derai* and J. Danon

Laboratoire de Physico-Chimie des Rayonnements (associé au CNRS), Université de Paris-Sud, Centre d'Orsay, 91405 Orsay, France
(Received March 8, 1976)

The chemical effects of low-energy (3.5–15.0 eV) electron impact on propene were investigated. The setup used for the irradiations has previously been described. Appearance curves for stable products were determined, from which correlations between products and precursors were deduced. In the excitation range, the main precursors are the triplet state at 4.4 eV and various singlet states around 7.0 and 9.0 eV. Above the ionization potential, contribution from superexcited molecules and ions was noted. Superexcited molecules are formed with a much higher cross section than excited molecules. A reaction scheme was proposed to account for the chemical effects associated with excited states and the yields of excited molecules in dissociating states were derived from experimental data. Results concerning the fragmentation of propene excited in singlet states conform to photolysis data. The following new results were obtained: (i) the decomposition of propene excited in the triplet state at 4.4 eV involves mainly C–C bond rupture; (ii) the decomposition processes of superexcited and excited molecules are similar. A higher degree of fragmentation is observed in the case of superexcited molecules.

Introduction

As shown in a previous paper,[2] low-energy electron impact experiments based on stable product determination (or "simulated radiolysis" studies) provide a useful tool for investigating the role played by low-energy secondary electrons in radiation chemistry. Such experiments are suitable for studying the chemical effects associated with excited and ionized states of molecules. This method is particularly appropriate for examination of the fragmentation processes resulting from triplet state excitation, since in electron impact experiments the interaction time between electron and molecule is long and optically forbidden transitions, such as singlet–triplet, may occur with a high probability.

The chemical effects induced by low-energy electron impact on propene in the gas phase are reported here. According to optical absorption studies,[3-5] several singlet excited states are involved: two valence states, S_2 and S_3, at 7.2 and 8.3 eV and four Rydberg states, S_1 and S_4 to S_6, at 6.7, 8.6, 8.9, and 9.4 eV. Comparison between optical absorption and electron impact excitation spectra[6,7] presented in Figure 1 provides evidence for the following optically forbidden transitions: a transient compound negative state at 2.2 eV and three triplet states, T_1 to T_3, located at 4.4, ~6.1, and 7.7 eV. The ionization potential of propene derived from mass spectrometry studies is 9.7 eV.[8] Fragment ions such as allyl, allene, vinyl, and allenyl ions appear at 11.9, 12.4, 13.8, and 14.1 eV, respectively.[8,9] Parent and fragment ions are known to react quickly with propene.[10-14] Literature on the photolysis[15-20] and radiolysis[21,22] of propene is also available.

Experimental Section

The apparatus and the experimental conditions have been described in detail previously.[2] They are briefly recalled here. We adopted a flow system in order to limit secondary effects on the products formed. This system involves three chambers, I, II, and III, separated by two holes of small conductance with a differential pumping between two of them, I and II. The electrons are produced by a tungsten filament located in source chamber I which is maintained at low pressure by high-speed pumping. The

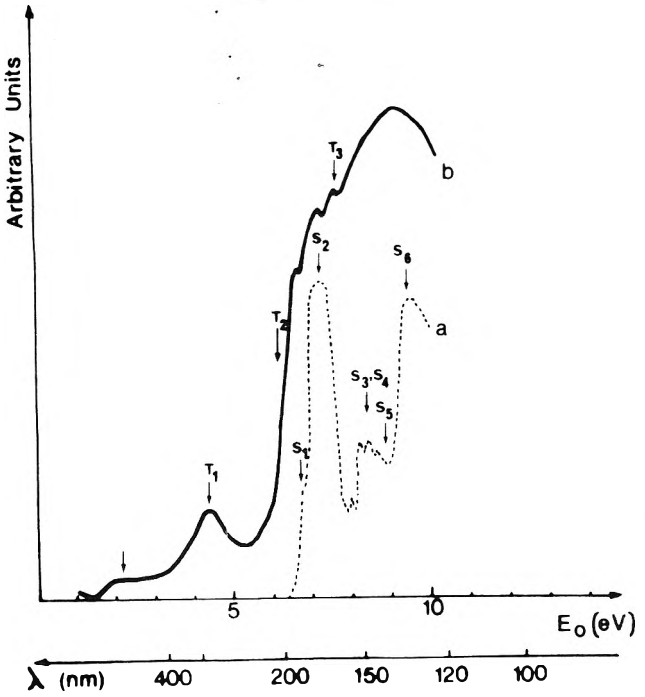

Figure 1. Comparison between excitation spectra of propene: (a) photon impact;[4] (b) electron impact.[7]

electron optics are such that the electrons are directed through the central compartment II, reach the desired energy at the entrance of reaction chamber III, and, in this last chamber, undergo collisions with the gas within a large equipotential volume (V = 5900 cm^3), at a constant pressure P_{III}. The gas sample is introduced at a constant flow rate in the reaction chamber and is removed through the central compartment by a second pump. This compartment allows one to obtain a high pressure gradient between the electron source and the reaction zone and permits a satisfactory electron flow. The electron beam is confined by a 300-G magnetic field. The design of the electron optics permits a determination to be made of the energy spread of the incident electron beam by the retarding potential method before each irradiation.

Irradiation of flowing propene (c = 35 cm^3 s^{-1}) was performed at 1×10^{-2} Torr with electrons having energies E_0 between 3.5 and 15.0 eV. The electron energy definition was ±0.6 eV. The average residence time in the reaction chamber, $t_R = V/c$ = 170 s, is long enough for the reactions of transient species (free radicals and ions) to be complete even at the low pressure used. Free radicals react not only in the gas phase but also on the walls since, in spite of the large dimensions of the reaction chamber, they diffuse rapidly to the walls. At 1×10^{-2} Torr, diffusion rate constants are $(k_D)_P = 57.5$ s^{-1} and $(k_D)_H = 1.7 \times 10^3$ s^{-1} for species having the size of parent molecules and hydrogen atoms, respectively. Owing to the use of the magnetic field and of equipotential conditions, ions react mainly in the gas phase within a volume between 10 and 60 cm^3 (see ref 2 for details).

Stable products up to C_5 were analyzed by gas chromatography. The detection limit was 10^{-4} molecules of product formed per incident electron. Product yields, which were corrected for blank run contributions, are expressed as the number of molecules of product formed per incident electron. The yield of a given product X is characterized by [X].

Commercial propene from Air Liquide was used without further purification. Main impurities were ethane (0.10%) and propane (0.14%).

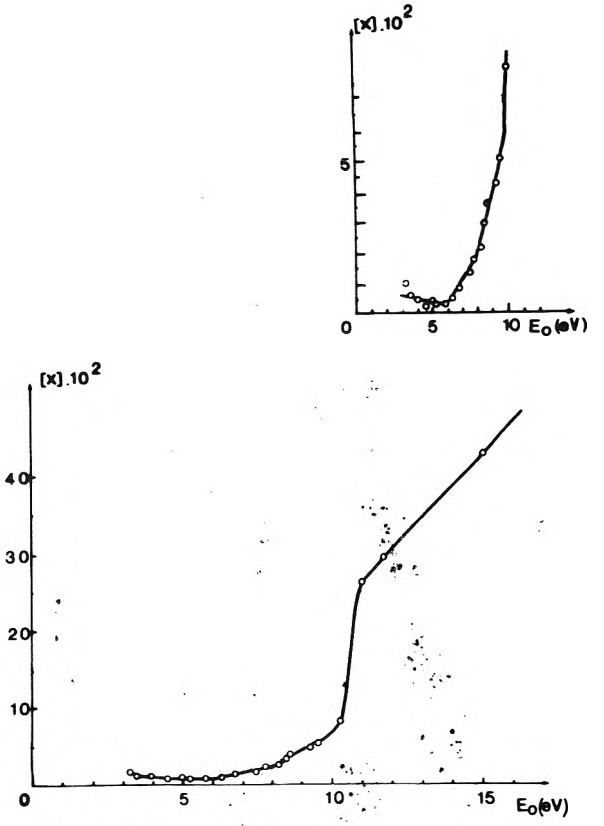

Figure 2. Appearance curve for ethylene.

Results

Nature of the Products. Products such as ethylene, acetylene, 1-butene, methane, hydrogen, isobutane, and allene are formed below and above the ionization potential of propene (IP = 9.7 eV). Propyne, ethane, and several C_4 and C_5 compounds[23] appear at 10.2 eV, i.e., at an energy which corresponds rather well to the ionization potential of propene. Among these last products, only C_4H_8 compounds (methylcyclopropane and *cis*- and *trans*-2-butenes) were systematically analyzed. The other products are always formed in very low yields, less than 10^{-3} molecules per incident electron.

A problem arose with the analysis of ethane and propane. The detection limit for these compounds, which were important impurities in the starting material propene, is high: 10^{-2} molecules per incident electron. Ethane was detected from 10.2 eV but, as will be seen in the Discussion, is likely to be formed in the whole excitation range in yields less than the detection limit. Propane, which was never detected, is formed in negligible quantities.

Carbon–Hydrogen Balance. The H/C ratio is always different from the expected value, 2. A hydrogen deficit is noted below 8.0 and above 10.2 eV. A hydrogen excess is found between 8.0 and 10.2 eV. The differences observed are always less than 10%.

Appearance Curve Characteristics. Product appearance curves, i.e., product yields as functions of incident electron energy, are presented in Figures 2–9. According to these curves, products are already formed at 3.5 eV, the lowest energy studied, and positive breaks are noted at 6.0, 8.0, and 10.2 eV. The break at 7.5 eV, which is observed only in isobutane and hydrogen appearance curves (Figure 6), cannot be distinguished from the break at 8.0 eV, which is observed for five products, ethylene, acetylene, 1-butene, methane, and allene (Figures 2–5 and 7), due to the fact that the energy difference between the two breaks is less than the electron energy definition. Four energy domains

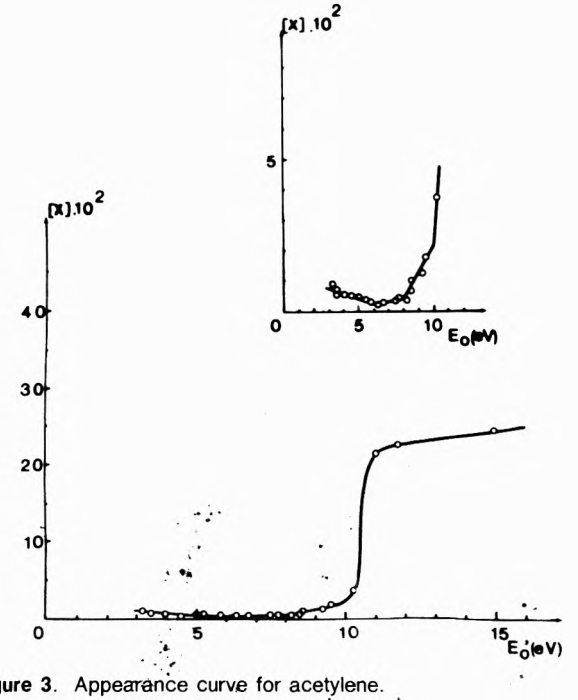

Figure 3. Appearance curve for acetylene.

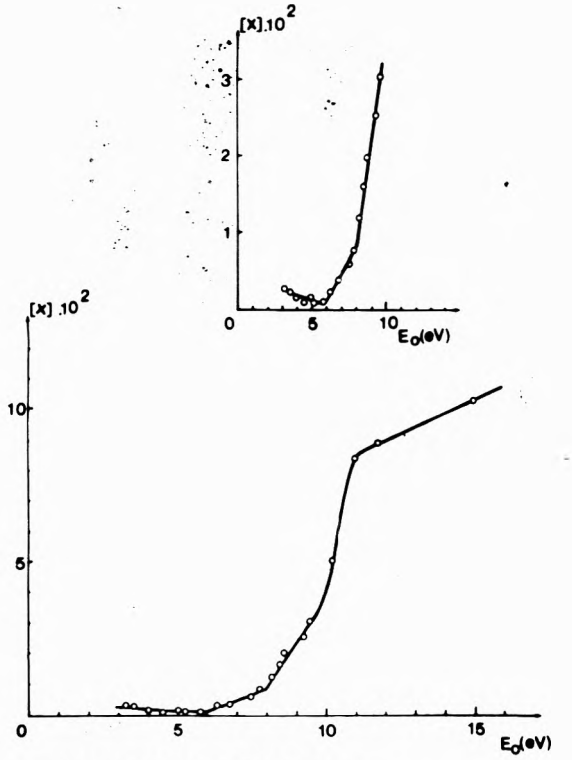

Figure 4. Appearance curve for 1-butene.

can consequently be considered:

D_1	$E_0 < 6.0$ eV
D_2	$6.0 < E_0 < 8.0$ eV
D_3	$8.0 < E_0 < 10.2$ eV
D_4	$E_0 > 10.2$ eV

The observations below 10.2 eV, i.e., in the excitation range, may be summarized as follows: the products formed in domain D_1 include ethylene, acetylene, 1-butene, and methane (Figures 2–5). These products are also characteristic of domains D_2 and D_3 since their appearance curves exhibit positive breaks at 6.0 and 8.0 eV. Isobutane, hydrogen, and allene (Figures 6 and 7) are characteristic

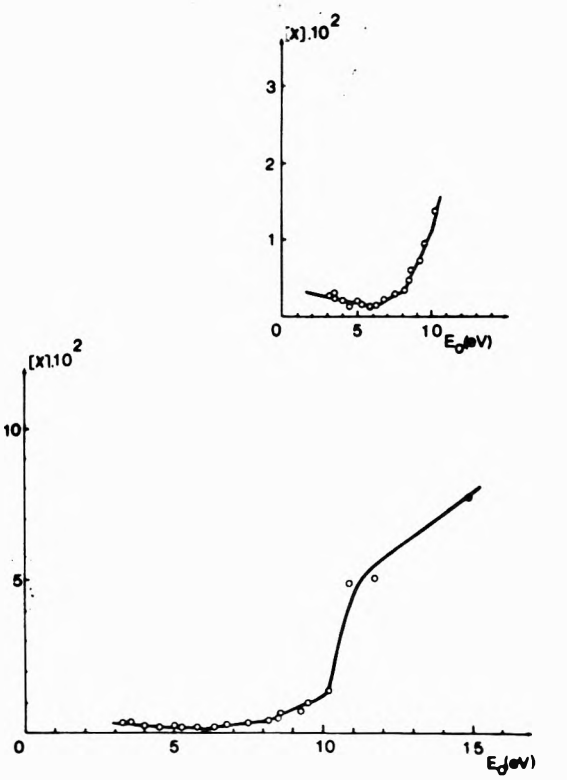

Figure 5. Appearance curve for methane.

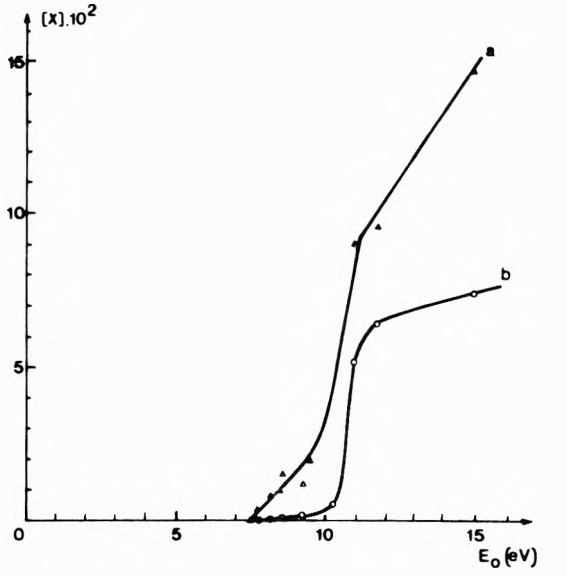

Figure 6. Appearance curve for (a) hydrogen and (b) isobutane.

of domain D_3 only. In domain D_1, the product yields decrease as electron energy increases and extrapolation at higher energies indicates that they become zero around 7.0 eV. In domains D_2 and D_3, the yields increase nearly linearly with electron energy.

Above 10.2 eV, i.e., in the ionization range, the observed products can be classified into three groups according to the shape of their appearance curves:

Group A allene (Figure 7)

Group B ethylene, acetylene, 1-butene, methane, hydrogen, isobutane, ethane, and propyne (Figures 2–8)

Group C methylcyclopropane, isobutene, and *trans*- and *cis*-2-butenes (Figure 9)

Products of groups A and B are those formed in the excitation range plus propyne. Their yields exhibit a steep increase by a factor of about 4 up to 11 eV, i.e., at the

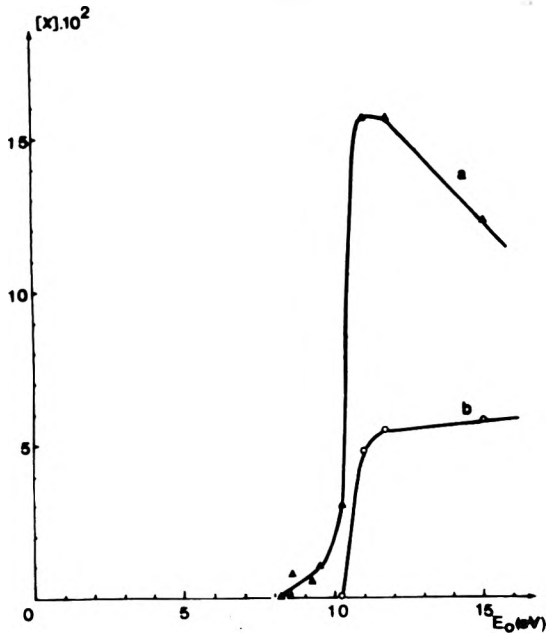

Figure 7. Appearance curve for (a) allene and (b) propyne.

TABLE I: Comparison between Product Appearance Potentials (AP) and Literature Data

Lit. data[d] Excited state[a] or ion	E, eV AP, eV	Present results: Characteristic products	Present results: Domain AP, eV
$C_3H_3^+$	14.1	C_4 and C_5	
$C_2H_3^+$	13.8	compounds	
$C_3H_4^+$	12.4	Ethylene,[c]	
$C_3H_5^+$	11.9	acetylene,[c] methane,[c] 1-butene,[c] propyne,[c] ethane,[c] hydrogen,[c] isobutane[c]	D_4
SE	?	Allene[c]	
			10.2
$C_3H_6^+$(IP)	9.7	Ethylene,	
S_6	9.4	acetylene,	
S_5	8.9	methane,	
S_4	8.6	1-butene,	D_3
S_3	8.3	allene, hydrogen, isobutane	
			8.0
T_3	7.7		
S_2	7.2	Ethylene,	
S_1	6.7	acetylene,	D_2
T_2	6.1	methane, 1-butene	
			6.0
T_1	4.4	Ethylene,[b] acetylene,[b] methane,[b] 1-butene[b]	D_1
			3.5

[a] S; singlet state; T, triplet state; SE, superexcited states. [b] Yield decreases as electron energy increases. [c] Yield increases steeply at the ionization threshold. [d] Spectroscopic[6,7] and mass spectrometric[8,9] data.

ionization threshold and then either decrease (group A) or slightly increase (group B). Products of group C all appear at the ionization potential. Their yields increase gradually with electron energy. The appearance curves

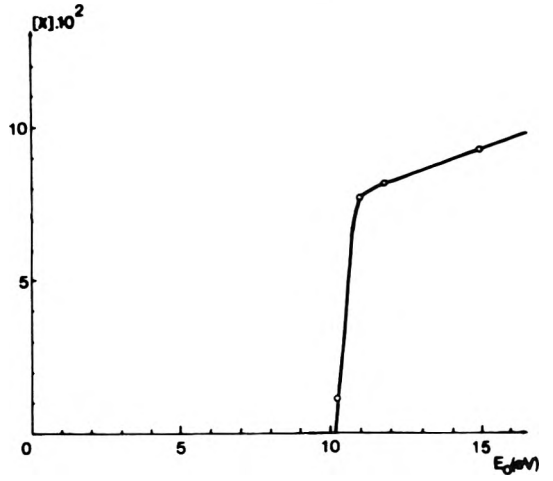

Figure 8. Appearance curve for ethane.

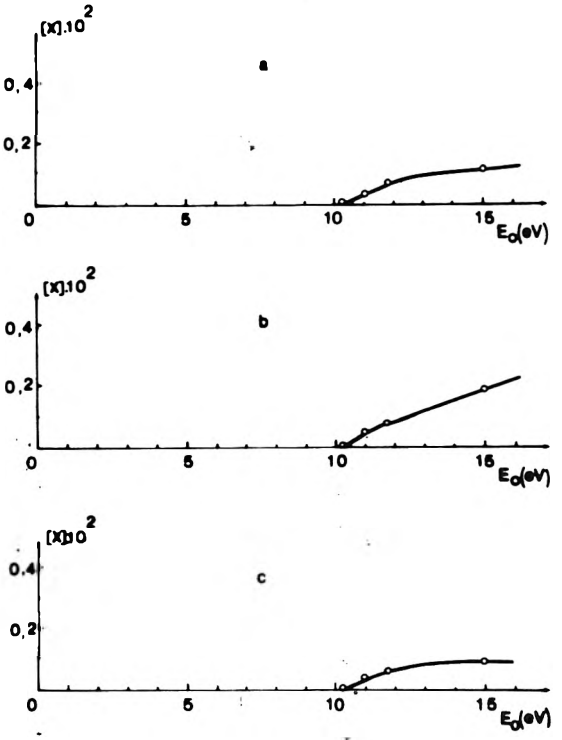

Figure 9. Appearance curve for (a) methylcyclopropane, (b) *trans*-2-butene, and (c) *cis*-2-butene.

relative to group B can be considered as superpositions of those characteristic of groups A and C. These features are similar to those reported in the simulated radiolysis of neopentane.[2]

Discussion

A. *Correlations between Products and Excited and Ionized States of Propene.* A comparison between the appearance potentials of the products and the energies of the excited and ionized states of propene is presented in Table I. Relationships of the products which characterize a given domain of energy to the possible precursor states were deduced from this comparison.

Excitation Range. The transient compound negative state observed at 2.2 eV cannot be involved in the product formation since its energy is less than the energy required for a C–C or a C–H bond rupture. The products formed in domain D_1 ($E_0 < 6.0$ eV), which is located at energies less than the optical absorption threshold, 6.4 eV, can be correlated with the first two triplet states of propene at

4.4 and ~6.1 eV. The appearance curves in this domain can be visualized as the envelope of two resonant functions ascribed to these two forbidden transitions with a preponderant contribution from the transition at 4.4 eV.

Product formation in domains D_2 ($6.0 < E_0 < 8.0$ eV) and D_3 ($8.0 < E_0 < 10.2$ eV) can be assigned to the singlet states reached by the optically allowed transitions at 6.7 and/or 7.2 eV and at 8.3 and/or 8.6, 8.9, 9.4 eV, respectively. This assignment is in good agreement with the linear shape of the appearance curves in the two domains. The triplet state, T_3, at 7.7 eV seems to have a negligible contribution.

Ionization Range. According to the detailed analysis presented in the paper on the simulated radiolysis of neopentane,[2] the steep increase in the yields of products in groups A and B (products observed in the excitation range plus propyne), which is noted at the ionization threshold where ionization is negligible, can be correlated with superexcitation. The conclusion, reached in the case of neopentane, that electron impact produces superexcited molecules with a much higher cross section than excited molecules, also applies to propene.

Above the ionization threshold, ionization and excitation both occur, and a complete knowledge of the reaction scheme is needed for establishing the detailed correlations between the products and the neutral and ionic precursors. This was impossible to achieve due to the complexity of the reaction scheme (mainly ionic reactions). Rough relationships can, however, be proposed by analogy with the analysis made in the simulated radiolysis of neopentane.[2]

(1) Products of group C whose yields, like electron impact ionization cross sections, increase gradually with electron energy can be ascribed to ionic precursors.

(2) Superexcited molecules are the main precursors of allene. This product has the same typical appearance curve as 2,2-dimethylbutane formed in the simulated radiolysis of neopentane which has been demonstrated to be representative of the production of such precursors (see ref 2).

(3) Products of group B are due both to ionic and neutral precursors as indicated by the shape of their appearance curves.

B. *Chemical Effects Associated with Excitation.* A reaction mechanism which explains the results obtained in the excitation range and at the ionization threshold is shown in Scheme I.

Primary Processes. Up to 8.0 eV, excited propene molecules ($C_3H_6^*$) dissociate according to processes I–III. This is in conformity with data from photolysis experiments using 6.7-eV photons[15-17] and accounts for the fact that the same products are observed in domains D_1 and D_2. Above 8.0 eV processes I–VI must be considered as proposed in photolysis experiments using 8.4-eV photons[18,19] and as shown by allene appearance at 8.0 eV. It must be noted that processes V and VI cannot be distinguished from processes I and II followed by fragmentation of allyl and vinyl radicals when these species have excess internal energy.

$$C_3H_5^* \rightarrow C_3H_4 + H$$

$$C_2H_3^* \rightarrow C_2H_2 + H$$

Superexcited molecules ($C_3H_6^{**}$) dissociate also according to processes I–VI; processes IV and V lead not only to allene but also to propyne. This conclusion is justified by the fact that the products observed at the ionization threshold include those noted in domain D_3 plus propyne.

Secondary Reactions. Reactions 1–4 describe the fate of hydrogen atoms formed in primary processes I, V, and VI. Hydrogen atoms are involved only in reactions with propene. These reactions, which occur either in the gas phase or on the walls, include addition to the double bond of propene as well as hydrogen atom abstraction. Addition of hydrogen atoms to propene in the gas phase (reaction 1) is likely to occur since it has a rate constant equal to 8×10^{-13} cm^3 molecule^{-1} s^{-1},[24,25] and is only a factor of 6 less rapid than the diffusion to the walls of hydrogen atoms under our conditions. It leads to excited isopropyl radicals which dissociate according to reaction 2.[26] Wall-catalyzed reactions 3 and 4 involving adsorbed hydrogen atoms and propene molecules are also important. Reaction 3 leads to stabilized isopropyl radicals. This reaction becomes noticeable above 7.5 eV since isobutane, which originates from isopropyl radicals (reaction 10), appears at this energy. Reaction 4 is suggested by the fact that in domain D_3 hydrogen is formed in yields higher than C_3H_4 compounds and cannot consequently be entirely attributed to process IV. The simultaneous appearance of hydrogen and isobutane at 7.5 eV indicates that, up to this energy, all hydrogen atoms are intercepted in the gas phase (reaction 1) and that, above this energy, the probability for these species to reach the walls and to react according to wall reactions 3 and 4 is no more negligible. The situation is less straightforward for the hydrogen atom abstraction reaction occurring in the gas phase. According to literature data,[27] this reaction competes with gas-phase addition reaction only when the reacting hydrogen atoms are hot. Present observations do not define whether the hydrogen atoms formed in primary processes are hot and then undergo hydrogen atom abstraction in the gas phase.

Concerning the methylene radicals resulting from process III the following comments are appropriate. Process III does not lead to singlet methylene radicals since products such as methylcyclopropane and 2-butenes, which would result from gas-phase reactions of these species with propene,[28] are not observed in the excitation range. Consequently, process III must lead to methylene radicals in the ground triplet state. Gas-phase reactions of these species with hydrocarbons are known to be slow.[29,30] On the other hand, according to observations made in the simulated radiolysis of cyclopropane,[31] gas-phase or wall reactions of these species with themselves and with methyl, vinyl, and allyl radicals are unimportant. Triplet methylene radicals are therefore assumed to react on the walls

Scheme I

Primary processes	ΔH°, eV	
$C_3H_6^*, C_3H_6^{**} \rightarrow C_3H_5 + H$	3.8	(I)
$\rightarrow C_2H_3 + CH_3$	4.2	(II)
$\rightarrow C_2H_4 + CH_2$	4.1	(III)
$\rightarrow C_3H_4 + H_2$	1.8[a]	(IV)
$\rightarrow C_3H_4 + 2H$	6.3[a]	(V)
$\rightarrow C_2H_2 + CH_3 + H$	5.9	(VI)
Secondary reactions		
$H + C_3H_6 \rightarrow C_3H_7^*$		(1)
$C_3H_7^* \rightarrow CH_3 + C_2H_4$		(2)
$H + C_3H_6 \xrightarrow{w} C_3H_7$		(3)
$H + C_3H_6 \xrightarrow{w} H_2 + C_3H_5$		(4)
$CH_3 + C_2H_3 \rightarrow CH_4 + C_2H_2$		(5)
$C_2H_3 + C_2H_3 \rightarrow C_2H_4 + C_2H_2$		(6)
$C_3H_5 + CH_3 \rightarrow C_4H_8$		(7)
$C_3H_5 + C_3H_5 \rightarrow C_6H_{10}$		(8)
$CH_3 + CH_3 \xrightarrow{w} C_2H_6$		(9)
$C_3H_7 + CH_3 \rightarrow C_4H_{10}$		(10)

[a] Values calculated for allene. Values relative to propyne are not very different since ΔH_f°(allene) and ΔH_f° (propyne) are very close, 1.99 and 1.92 eV, respectively.

TABLE II: Yields of Excited Molecules Decomposed at Different Electron Energies ($4.0 < E_0 < 11.0$ eV)[a]

Yield	D_1 4.0 eV	D_1 5.0 eV	D_1 6.0 eV	D_2 7.0 eV	D_2 8.0 eV[f]	D_3 9.0 eV	D_3 10.0 eV	D_3 11.0 eV
N_I[b]	0.16	0.10	0.08	<0.89	>1.14[d]	>1.78[d]	>1.59[d]	
N_I[c]	0.18	0.13	0.08	>0.46				>0[e]
N_{II}	0.98	0.64	0.28	0.46	0.62	>0.71 <1.89	>1.19 <3.17	>4.16 <27.8
N_{III}	0	0	0	<0.43	<1.06	<1.95	<2.53	13.5
N_{IV}						} 0.59	} 1.98	<8.41
N_V								>12.1 <20.5
N_{VI}						<0.59	<0.99	>5.48 <17.2
N_E	1.14	0.74	0.36	1.35	>2.82[d]	>6.80[d]	>11.2[d]	>55.4[e]

[a] Yields are expressed as 10^{-2} events per incident electron. Subscript refers to the decomposition process involved. [b] Determined from hydrogen atom yield. [c] Determined from primary allyl radical yield. [d] Underestimated by the yield of trapped secondary isopropyl radicals. [e] Underestimated by the yields of diallyl and of trapped secondary allyl radicals. [f] Results relative to this energy are not presented in domain D_2 since wall reactions of hydrogen atoms occur.

with propene and to lead to a nonanalyzed high molecular weight compound, $(CH_2)_n$.

As regards the other primary and secondary radicals, it must be noted that even in the most favorable case (methyl radicals), addition to the propene double bond is unimportant: (i) gas-phase addition has a very small rate constant;[32] (ii) wall addition would lead to butyl radicals which are not evidenced in the excitation range. Abstraction which is less rapid than addition[32] is a fortiori excluded. It follows that primary methyl, vinyl, and allyl as well as secondary methyl, isopropyl, and allyl radicals react mainly with each other. The free radicals formed in the gas phase under reactions 5–9. Although they lead to diallyl, which is not analyzed, and ethane, which is not detected below 10.2 eV, reactions 8 and 9 are probable. There is indeed no reason to exclude them. Among reactions 5–9, only reaction 9 involving two methyl radicals requires the walls for stabilization of the recombination product. Thus primary and secondary methyl radicals have a lower probability of reaction in the gas phase and consequently a higher probability for diffusion to the walls than primary vinyl and allyl radicals. Therefore, secondary allyl and isopropyl radicals resulting from wall reactions 4 and 3 react mainly with those methyl radicals which reach the walls (reactions 7 and 10). It must be noted, however, that all secondary allyl and isopropyl radicals do not react according to reactions 7 and 10. This is evidenced by the carbon–hydrogen balance above 10.2 eV which, in contrast to that below 10.2 eV, cannot be entirely explained by the lack of diallyl and ethane among the observed products. The hydrogen deficit noted above 10.2 eV, where the ethane yield is measured, suggests that saturated species other than ethane are not recovered. These species could be secondary isopropyl radicals which remain trapped in the adsorption sites where they are formed. A similar fate is likely for secondary allyl radicals, and such a situation must occur above 7.5 eV.

A last point in this discussion concerns the omitted reactions between radicals. Disproportionation reactions involving allyl radicals are neglected since combination is the most probable fate of such radicals.[33] On the other hand, allene, which would result from disproportionation of allyl radicals, is not observed in domains D_1 and D_2 where these radicals are present. Combination reactions involving vinyl radicals are also omitted. The expected products, butadienes and C_5 compounds, are not observed in agreement with the fact that disproportionation is preponderant when two vinyl radicals interact.[20,34] The disproportionation reaction between methyl and isopropyl radicals is also of negligible importance.[33] Interaction between vinyl and allyl radicals is also omitted since combination would lead to methylbutadienes and disproportionation to either ethylene plus allene (or propyne), or acetylene plus propene. Methylbutadienes and allene (or propyne) are not observed in domains D_1 and D_2. The latter possibility is also excluded by analogy with the results obtained in the simulated radiolysis of cyclopropane.[31]

C. *Yields of Excited Molecules Involved in Product Formation.* The total and individual yields of excited molecules which dissociate according to processes I–VI, N_E and N_I to N_{VI}, are calculated from product yields using the relations derived from Scheme I and presented in the Appendix. The results are summarized in Table II, and the following comments are appropriate.

Except for N_I in domain D_1 and N_{II} in domains D_1 and D_2, only broad limits are found for the yields of excited molecules. In domain D_1, the N_I values derived from the yields of hydrogen atoms and allyl radicals (see relations h and i in the Appendix) are in very good agreement. Uncertainties on N_{III} in domains D_2 and D_3 are related to the lack of information on ethane yields. Distinction between processes IV and V, which lead to the same products, is possible at the ionization threshold only. Distinction between processes II and VI, which also lead to the same products, is possible in domain D_3 as well as at the ionization threshold. The limits to N_{II} and N_{VI} are, however, quite ill-defined.

The results in domain D_1 clearly demonstrate that process III does not occur (see Appendix). It follows that propene excited in both triplet states at 4.4 and ~6.1 eV dissociates according to processes I and II as in the mercury ($^3P_1$) photosensitized decomposition of propene.[35-37] The relative importance of processes I and II is $N_I/N_{II} = 15/85$ at 4.0 eV and does not vary much above this energy, suggesting that propene excited in the triplet state at 4.4 eV, which is the prominent contributing species in the whole domain D_1 (see above), dissociates mainly according to process II (C–C bond rupture). This is consistent with the fact that this state is reached through a $\pi \rightarrow \pi^*$ transition which involves an electron of the double bond. This process is also known to be the main fragmentation mode of chemically excited propene.[38] It is therefore possible that the observed decomposition occurs via conversion of this triplet state into vibrationally excited levels of the ground state. Comparison between observations in this energy range and data from mercury ($^3P_1$) photosensitized experiments are presented else-

TABLE III: Yields of Excited Molecules Dissociating According to Process III[a]

Domain	D_1			D_2
Electron energy, eV	4.0	5.0	6.0	7.0
$[C_2H_4] + [CH_4] - [C_2H_2]$	0.16	0.10	0.08	0.89
$[C_4H_8]$	0.18	0.13	0.08	0.46
N_{III}	≃0	≃0	≃0	<0.43

[a] Yields are expressed as 10^{-2} events per incident electron.

where.[39]

The results at 7.0 eV correspond to the decomposition of propene in the singlet states at 6.7 and/or 7.2 eV since, as seen above, the contribution of the triplet states at 4.4 and ~6.1 eV is zero at this energy. These results, which are not conclusive about the occurrence of process III, indicate that processes I and II are characteristic of the singlet states mentioned above and that the N_I/N_{II} ratio is between 1 and 2. A slightly different observation is made in photolysis experiments using 6.7-eV photons,[17] where the N_I/N_{II} ratio is found to be approximately unity.

According to the results in domain D_3, processes IV and/or V and processes II and/or VI are among the decomposition modes of propene in the singlet states at 8.3 eV and/or 8.6, 8.9, and 9.4 eV. No definite conclusion can be reached concerning processes I and III. These results are too qualitative to be correlated with data from photolysis experiments using 8.4-eV photons.[18,19]

The results at the ionization threshold show that processes III, V, and VI are characteristic of the decomposition of superexcited molecules, but do not allow a decision as to whether superexcited molecules dissociate according to processes I, II, and IV. It is noteworthy that processes V and VI, which release three fragments, are important decomposition channels of superexcited molecules. The same conclusion has been obtained in the simulated radiolysis of cyclopropane.[31]

Comparison with Radiolysis. As already mentioned, ionic mechanisms in propene are complex due to the high reactivity of parent and fragment ions toward propene. It is consequently impossible to derive a reaction scheme for ionic species and to separate and estimate the relative contribution from excitation and ionization.

Conclusion

This work reports on the decomposition of propene induced by low-energy ($3.5 < E_0 < 15.0$ eV) electron impact. A great deal of information was obtained from the structures observed on the appearance curves of the products. It was possible to distinguish the main precursors: (i) excited molecules in the triplet state at 4.4 and in various singlet states around 7.0 and 9.0 eV; (ii) superexcited molecules; (iii) ions.

Other data were deduced from a detailed analysis of the chemical reactions of the species resulting from the decomposition of excited molecules. The observations relative to the singlet states conform to photolysis data. New results were obtained: (i) the main dissociation mode of propene excited in the triplet states at 4.4 eV is C–C bond rupture and it is possible that this fragmentation occurs via internal conversion into vibrationally excited levels of the ground state; (ii) superexcited molecules dissociate according to the same processes as excited molecules. However, the degree of fragmentation is higher in the first case.

Results concerning superexcited molecules confirm the observations made in the simulated radiolysis of neopentane.[2] These species are produced with a much higher cross section than excited molecules.

Appendix

Yields of Excited Molecules Involved in Product Formation. The yields, N, of excited molecules of propene which dissociate according to primary processes I–VI are given by the following general relations deduced from Scheme I:

$$N_I = [H]_I = [H] - 2[H]_V - [H]_{VI} \quad (a)$$

$$N_I = [C_3H_5]_I = [C_3H_5] - [C_3H_5]_4 \quad (b)$$

$$N_{II} = [C_2H_3] \quad (c)$$

$$N_{III} = [C_2H_4]_{III} = [C_2H_4] - ([C_2H_4]_2 + [C_2H_4]_6) \quad (d)$$

$$N_{IV} + N_V = [C_3H_4]_{IV} + [C_3H_4]_V = [C_3H_4] \quad (e)$$

$$N_{VI} = [C_2H_2]_{VI} = [C_2H_2] - ([C_2H_2]_5 + [C_2H_2]_6) \quad (f)$$

Subscripts refer to the reaction leading to the product considered.

The total yield of excited molecules in dissociating states, N_E, is then

$$N_E = N_{I \to VI} \quad (g)$$

Domains D_1 and D_2. Processes IV–VI and reactions 3, 4, and 10 do not occur. Relations a–d and g are then simplified. They can be expressed as functions of product yields and become

$$N_I = 2[CH_4] + [C_4H_8] + 2[C_2H_6] - 2[C_2H_2] \quad (h)$$

$$N_I = [C_4H_8] + 2[C_6H_{10}] \quad (i)$$

$$N_{II} = 2[C_2H_2] - [CH_4] \quad (j)$$

$$N_{III} = [C_2H_4] + [C_2H_2] - [CH_4] - [C_4H_8] - 2[C_2H_6] \quad (k)$$

$$N_E = [C_2H_2] + [C_2H_4] \quad (l)$$

with

$$N_I + N_{III} = [C_2H_4] + [CH_4] - [C_2H_2] \quad (m)$$

The two unknown terms, $[C_2H_6]$ and $[C_6H_{10}]$, involved in relations h, i, and k can be estimated as follows.

In domain D_1, product yields verify the following relation (see Table III)

$$[C_2H_4] + [CH_4] - [C_2H_2] = [C_4H_8] \quad (n)$$

which, compared to eq m and i, leads to

$$N_{III} + 2[C_6H_{10}] = 0 \quad (o)$$

This means that (i) diallyl is formed in negligible quantities in this energy range; (ii) excited molecules dissociate only according to processes I and II as in mercury photosensitized decomposition of propene.[35-37] The ethane yield can then be deduced from relation k

$$[C_2H_6] = {}^1/_2([C_2H_4] + [C_2H_2] - [CH_4] - [C_4H_8]) \quad (p_1)$$

The situation is different in domain D_2 where, according to Table III, relation n is not verified. Estimation of diallyl yield is then impossible. Limits to the ethane yield are obtained from relation k

$$0 < [C_2H_6] < {}^1/_2([C_2H_4] + [C_2H_2] - [CH_4] - [C_4H_8]) \quad (p_2)$$

which allows the individual yields N_I and N_{III} to be bracketed.

Domains D_3 and D_4 at the Ionization Threshold. The whole reaction scheme applies in these energy ranges. The yields of excited molecules are given by general relations a–g. Relations a–d and f can be explicited as follows:

$$N_I = [H]_I = [C_4H_8] + [H_2] + 2([CH_4] + [C_4H_{10}] + [C_2H_6] - [C_2H_2] - [C_3H_4]) + [C_3H_4]_{IV} + [C_3H_7]_T \quad (q)$$

$$N_I = [C_3H_5]_I = [C_4H_8] - [H_2] + 2[C_6H_{10}] + [C_3H_5]_T \quad (r)$$

$$N_{II} = 3[CH_4] + 2([C_4H_8] + [C_4H_{10}] + 2[C_2H_6] - [C_2H_2] - [C_2H_4]_2) \quad (s)$$

$$N_{III} = [C_2H_4] + [C_2H_2] - [CH_4] - [C_4H_8] - [C_4H_{10}] - 2[C_2H_6] \quad (t)$$

$$N_{VI} = 2([C_2H_2] - [CH_4] - [C_2H_6]) - [C_4H_8] - [C_4H_{10}] + [C_2H_4]_2 \quad (u)$$

$[C_3H_7]_T$ and $[C_3H_5]_T$ are the yields of secondary isopropyl and allyl radicals, which are formed by reactions 3 and 4 and remain trapped on the walls. These terms, as well as $[C_6H_{10}]$, are impossible to evaluate in contrast to the other unknown terms involved in these relations: $[C_2H_6]$ (in domain D_3 only), $[C_3H_4]_{IV}$, and $[C_2H_4]_2$. Limits to $[C_2H_6]$ are deduced from relation t:

$$0 < [C_2H_6] < {}^1/_2([C_2H_4] + [C_2H_2] - [CH_4] - [C_4H_8] - [C_4H_{10}]) \quad (v)$$

Limits to $[C_3H_4]_{IV}$ are derived from relation e. In domain D_3 where $[H_2] > [C_3H_4]$:

$$0 < [C_3H_4]_{IV} < [C_3H_4] \quad (w)$$

At the ionization threshold where $[H_2] < [C_3H_4]$:

$$0 < [C_3H_4]_{IV} < [H_2] \quad (x)$$

Limits to $[C_2H_4]_2$ take into account the fact that ethylene is formed by process III and reactions 2 and 6:

$$0 < [C_2H_4]_2 < [CH_4] + [C_4H_8] + [C_4H_{10}] + 2[C_2H_6] - [C_2H_2] \quad (y)$$

In domain D_3 where the ethane yield is given by relation v, this relation becomes:

$$0 < [C_2H_4]_2 < [C_2H_4] \quad (z)$$

The individual yields, N_{II} to N_{VI}, can consequently be bracketed. Only lower limits are obtained for N_I. The highest lower limit is deduced from relations q and r in domain D_3 and at the ionization threshold respectively. N_I is then underestimated by the yield of trapped secondary isopropyl radicals in domain D_3 and by the yields of diallyl and of trapped secondary allyl radicals at the ionization threshold. In such conditions the total yield of excited molecules, N_E, cannot be bracketed and only lower limits are found.

TABLE IV: Ethane Yields in the Excitation Range[a]

Electron energy, eV	4.0	5.0	6.0	7.0	8.0	9.0	10.0
$[C_2H_6]$	0.38	0.22	0.08	<0.34	<0.53	<1.00	<1.25

[a] Yields are expressed as 10^{-2} events per incident electron.

A last remark concerns the ethane yields given by relations p_1, p_2, and v. Table IV shows that as expected values always below or around the detection limit are observed.

References and Notes

(1) This work is a part of the These de Doctorat d'Etat of R. Derai.
(2) R. Derai, P. Nectoux, and J. Danon, *J. Phys. Chem.*, **80**, 1664 (1976).
(3) (a) W. C. Price and W. T. Tutte, *Proc. R., Soc. London, Ser. A*, **174**, 207 (1940); (b) J. A. R. Samson, F. F. Marmo, and K. Watanabe, *J. Chem. Phys.*, 36, 783 (1962).
(4) A. A. Iverson, B. R. Russel, and P. R. Jones, *Chem. Phys. Lett.*, **17**, 98 (1972).
(5) A. J. Merer and R. S. Mulliken, *Chem. Rev.*, **69**, 639 (1969).
(6) C. R. Bowman and W. D. Miller, *J. Chem. Phys.*, **42**, 681 (1965).
(7) D. F. Dance and I. C. Walker, *Proc. R. Soc. London, Ser. A*, **334**, 259 (1973).
(8) J. L. Franklin, J. G. Dillard, H. M. Rosenstock, J. T. Herron, K. Draxl, and F. H. Franklin, *Natl. Stand. Ref. Data Ser., Natl. Bur. Stand.*, **No. 26** (1969).
(9) F. H. Field and J. L. Franklin, "Electron Impact Phenomena," Academic Press, New York, N.Y., 1957.
(10) R. Gorden, Jr., R. Doepker, and P. Ausloos, *J. Chem. Phys.*, **44**, 3733 (1966).
(11) L. W. Sieck and J. H. Futrell, *J. Chem. Phys.*, **45**, 560 (1966).
(12) F. P. Abramson and J. H. Futrell, *J. Phys. Chem.*, **72**, 1994 (1968).
(13) A. A. Herod and A. G. Harrison, *J. Phys. Chem.*, **73**, 3189 (1969).
(14) L. W. Sieck and P. Ausloos, *J. Res. Natl. Bur. Stand, Sect. A*, **76**, 253 (1972).
(15) S. Arai, S. Shida, and T. Nishikawa, *Bull. Chem. Soc. Jpn.*, **39**, 2548 (1966).
(16) H. Okabe, H. D. Beckey, and W. Groth, *Z. Naturforsch. A*, **21**, 135 (1966).
(17) P. Borrell, A. Cervenka, and J. W. Turner, *J. Chem. Soc. B*, 2293 (1971).
(18) D. A. Becker, H. Okabe, and J. R. McNesby, *J. Phys. Chem.*, **69**, 538 (1965).
(19) E. Tschuikow-Roux, *J. Phys. Chem.*, **71**, 2355 (1967).
(20) D. R. A. Cuff, G. R. Johnston, and D. Price, *J. Photochem.*, 3, 107 (1974).
(21) K. Yang, *J. Phys. Chem.*, **65**, 42 (1961).
(22) M. Trachtman, *J. Phys. Chem.*, **70**, 3382 (1966).
(23) C_4 and C_5 compounds observed in the ionization range are: C_4H_6, 1,3- and 1,2-butadienes; C_4H_8, methylcyclopropane, *cis*- and *trans*-2-butenes; C_5H_8, isoprene and 1,4-pentadiene; C_5H_{10}, 3-methyl-1-butene, 2-methyl-1-butene, 2-methyl-2-butene, and 1-pentene; C_5H_{12}, isopentane.
(24) B. de B. Darwent and R. Roberts, *Discuss. Faraday Soc.*, **14**, 55 (1953).
(25) K. Yang, *J. Am. Chem. Soc.*, **84**, 719 (1962).
(26) W. E. Falconer, B. S. Rabinovitch, and R. J. Cvetanović, *J. Chem. Phys.*, **39**, 40 (1963).
(27) G. R. Woolley and R. J. Cvetanović, *J. Chem. Phys.*, **50**, 4697 (1969).
(28) M. G. Topor and R. W. Carr, Jr., *J. Chem. Phys.*, **58**, 757 (1973).
(29) W. Braun, A. M. Bass, and M. Pilling, *J. Chem. Phys.*, **52**, 5131 (1970).
(30) P. S. T. Lee, R. L. Russell, and F. S. Rowland, *Chem. Commun.*, 18 (1970).
(31) R. Derai and J. Danon, *Chem. Phys.*, **15**, 331 (1976).
(32) M. Miyoshi and R. K. Brinton, *J. Chem. Phys.*, **36**, 3019 (1962).
(33) M. J. Gibian and R. C. Corley, *Chem. Rev.* **73**, 441 (1973).
(34) K. O. McFadden and C. L. Currie, *J. Chem. Phys.*, **58**, 1213 (1973).
(35) M. Avrahami and P. Kebarle, *J. Phys. Chem.*, **67**, 354 (1963).
(36) C. A. Heller and A. S. Gordon, *J. Chem. Phys.*, **42**, 1262 (1965).
(37) J. W. Simons, B. S. Rabinovitch, and F. H. Dorer, *J. Phys. Chem.*, **70**, 1076 (1966).
(38) J. M. Figuera, E. Fernandez, and M. J. Avila, *J. Phys. Chem.*, **78**, 1348 (1974).
(39) R. Derai and J. Danon, *Chem. Phys. Lett.*, in press.

Temperature Dependence of Rate Constants and Branching Ratios for the Reaction of Oxygen Atoms with Carbon Disulfide

Ronald E. Graham and David Gutman*

Department of Chemistry, Illinois Institute of Technology, Chicago, Illinois 60616 *(Received August 4, 1976)*

Publication costs assisted by the National Science Foundation

The overall rate constant for the O + CS_2 reaction (k) and the branching ratio (k_2/k) for route 2 of this reaction, O + CS_2 → OCS + S, have been measured at seven temperatures between 249 and 500 K. The overall rate constant increases with temperature in a non-Arrhenius manner increasing from 2.9×10^{-12} cm^3 $molecule^{-1}$ s^{-1} at 249 K to 11.2×10^{-12} cm^3 $molecule^{-1}$ s^{-1} at 500 K. The fraction of the reaction proceeding by route 2 decreases slightly with increasing temperature from 0.098 (±0.004) to 0.081 (±0.007) over the same temperature range.

Introduction

The reaction between oxygen atoms and carbon disulfide has been shown to proceed by all three possible exothermic channels[1-4]

$$O + CS_2 \xrightarrow{k} \begin{cases} \xrightarrow{k_1} CS + SO + 31\ kcal & (1) \\ \xrightarrow{k_2} OCS + S + 55\ kcal & (2) \\ \xrightarrow{k_3} CO + S_2 + 83\ kcal & (3) \end{cases}$$

This reaction has received considerable attention in recent years because of its usefulness as a source of CS for producing chemical CO lasers through the important secondary reaction in these systems[5]

$$O + CS \rightarrow CO^{\ddagger} + S \qquad (4)$$

The chemical kinetics of $CS_2 + O_2(O)$ laser systems have been modeled to better understand the factors governing their performance.[7-9] It has been found that the products of routes 2 and 3 are also involved in determining laser performance. The OCS produced by route 2 selectively relaxes the lower excited vibrational states of $CO^{\ddagger}$,[9] and can enhance laser output from higher levels. Nielsen has modeled an electrically discharged CS_2–O_2 chemical laser, and has found that the OCS produced by route 2 is the dominant relaxer of CO[5] (CO in the fifth vibrational level) soon after the flash and continues to be one of the most important relaxers of CO near $v = 5$ at later times.[8] The importance of OCS in determining laser performance has also been observed experimentally. Using a continuous wave chemical laser produced by reactions 1 and 4, Suart, Arnold, and Kimbell found significant laser power enhancement (up to 500%) when small amounts of OCS were added to the system.[10]

Hudgens, Gleaves, and McDonald have found that the CO produced by route 3 is also vibrationally excited but has a markedly different vibrational population distribution than that of the CO produced in reaction 4, favoring the lower v levels instead of being peaked at $v = 9$.[4] There is some evidence that this additional source of vibrationally excited CO effects laser performance. In Nielsen's modeling study he did not include the production of excited CO from route 3, and he was unable to account for a "moderate rate of CO production in lower v levels".[8]

For a better understanding of the chemical factors which govern the performance of CO lasers driven by the O + CS_2 reaction, more quantitative information is needed on the importance of its various routes. Although there have been several determinations of the overall rate constant for the O + CS_2 reaction, very little is known about the rate constants into each reactive channel, k_1–k_3. Slagle, Gilbert, and Gutman have directly measured the branching ratio ($R_2 = k_2/k$) for route 2 at 302 K and find it is 0.093.[3] Earlier estimates of R_2, which vary from less than 0.015 to 0.22, were reviewed in their report of this study.[3] There have been no direct determinations of R_1 (k_1/k) or R_3 (k_3/k). Experimental evidence clearly suggests that route 1 is dominant ($R_1 \approx 0.8$),[1,3,4] and that route 3 may account for about 10% of the overall reaction at room temperature.[3,4]

We have now measured R_2 over an extended temperature range, 250–500 K, to learn whether the importance of route 2 changes with temperature. Estimates of k_2 over 1000 K suggest R_2 might be increasing with temperature.[11] Such a suggested increase has already been used to model $CS_2 + O_2$ combustion behind shock waves.[12] Calculation of "prior" branching ratios predict essentially no temperature dependence of R_2.[13] The temperature range covered overlaps that in which $CS_2 + O_2$ lasers operate, thus this study provides measured values of R_2 for modeling these systems. Values of k, the overall rate constant for the O + CS_2 reaction, were also measured in the same temperature range and are also reported here.

Experimental Section

Oxygen atoms (produced by the N + NO → N_2 + O) reaction and CS_2 were mixed in a 1.27 cm i.d. fast-flow reactor. The rate of CS_2 loss and OCS production were simultaneously monitored by mass spectrometric analyses of gas sampled through a 0.033-cm diameter hole in the end of the reactor. The temperature of the reactor was established by circulating a heating or cooling fluid (silicone oil or ethanol) from a thermostated bath through a concentric jacket surrounding the reactor. A chromel–alumel thermocouple inside the movable central inlet tube was used to determine the temperature inside the flow reactor. Temperature uniformity along the reactor was within 1 K as was the temperature stability during an experiment.

The experimental details and data analysis were the same as described before.[3] The branching ratio for route 2 was obtained from the relation

$$R_2 = k_2/k = \Delta[OCS]_t/\Delta[CS_2]_t \qquad (I)$$

where $\Delta[OCS]_t$ is the OCS concentration at time t, and $\Delta[CS_2]_t = [CS_2]_0 - [CS_2]_t$ is the decrease in $[CS_2]$ from its initial value.[3]

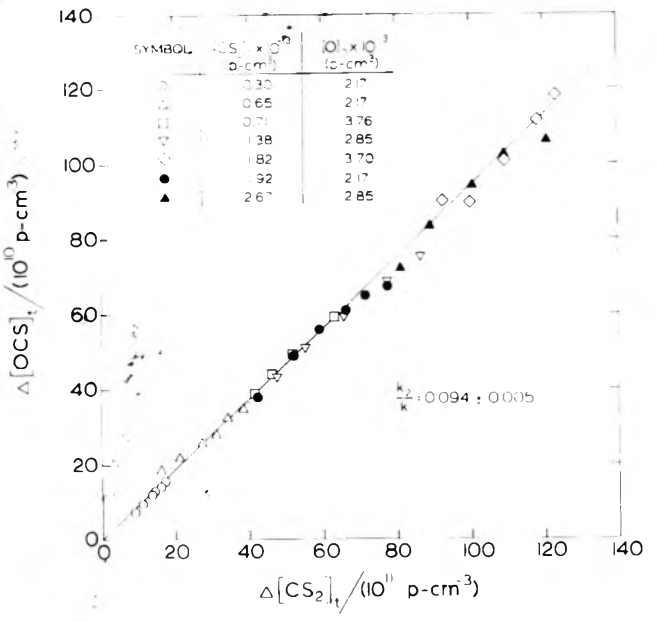

Figure 1. Plot of OCS production vs. CS_2 loss from seven experiments at 335 K. Initial CS_2 and O concentrations given in the figure. Slope of line through points yields R_2 (see text). Error limits on R_2 is the standard deviation of R_2 values calculated for each point from the average slope.

At each of seven temperatures between 249 and 500 K, R_2 was measured in six–nine experiments and found to be independent of $[O]_0$, $[CS_2]_0$, [M] flow velocity, and extent of reaction. Graphical evidence for this independence of R_2 on reaction variables can be seen in Figure 1, a plot of $\Delta[OCS]_t$ vs. $\Delta[CS_2]_t$ measurements obtained during the seven experiments at 355 K. Each point in Figure 1 yields a value of R_2, and, according to eq I, the totality of points from all experiments should lie along a straight line passing through the origin. Within the experimental scatter this is indeed the case. The value of R_2 selected at each temperature was the slope of the straight line fitted through all data points plotted as in Figure 1. The line was not constrained to pass through the origin, but always passed extremely close to it.

Implicit in the derivation of eq I is the assumption that the OCS produced by route 2 is not subsequently consumed by the O atoms in the system. Experiments were performed which verified the assumption. At each temperature OCS was mixed with the O atoms in the absence of CS_2. Under the experimental conditions used to determine R_2, there was no detectable OCS consumption (<3%) at all temperatures except the highest. At 500 K about 5% of the OCS was consumed by the O atoms. In order to negate the need for minor corrections for this effect, the experiments at 500 K were not done with large O atom excesses. This assured the absence of O atoms after CS_2 consumption was complete and the negligible loss of OCS by a secondary reaction.

The results of the experiments to determine R_2 at different temperatures are given in Table I. In experiments in which O was in great excess, $[CS_2]$ vs. t profiles were used to also obtain k, the overall rate constant for the O + CS_2 reaction. The results of these experiments are also given in Table I.

TABLE I: Results of Experiments to Measure O + CS_2 Rate Constants and Branching Ratios[a]

Temp, K	10^2R_2 (k_2/k)	$10^{12}k$,[d] cm^3 p^{-1} s^{-1}
249	9.8 (±0.4)[b]	2.9 (±0.2)[c]
273	9.8 (±0.5)	3.6 (±0.3)
295	9.6 (±0.6)	4.1 (±0.2)
335	9.4 (±0.5)	5.1 (±0.6)
376	8.7 (±0.5)	6.6 (±0.3)
431	8.2 (±0.1)	8.5 (±0.6)
500	8.1 (±0.7)	11.2 (±0.8)

[a] Details of all experiments performed to determine R_2 and k are available as microform material. [b] Average of at least six experiments with one standard deviation given in parentheses. Estimated accuracy ±15%. [c] Average of at least six experiments with one standard deviation given in parentheses. Estimated accuracy ±30%. [d] p = particle (atom or molecule).

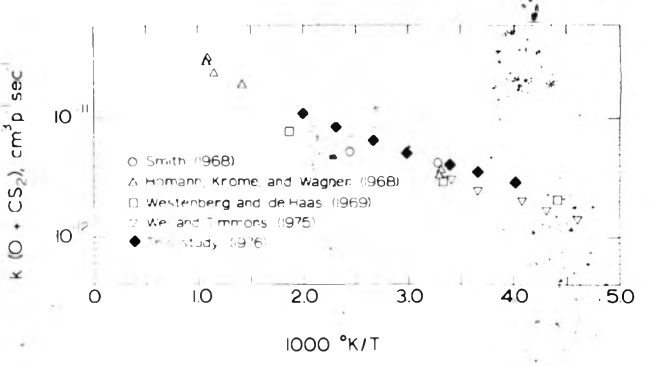

Figure 2. Arrhenius plot of O + CS_2 overall rate constants.

Discussion

Overall Rate Constant k. The overall rate constants for the O + CS_2 reaction obtained in this study and those obtained by others are shown together on an Arrhenius plot in Figure 2. Agreement with earlier studies is fairly good. The upward curvature of our k values at the higher temperatures in this figure, if continued, extrapolates to the values of k above 700 K obtained by Homan, Krome, and Wagner.[14] The results of two ESR flow reactor studies of the O + CS_2 reaction, by Westenberg and deHaas[16] and by Wei and Timmons,[17] yield values of k which are consistently slightly lower than comparable rate constants from our study. In both of these ESR studies a stoichiometric factor of 2 (determined by Westenberg and deHaas) was used to divide into experimental rate coefficients to obtain k. Very recently Bida, Breckenridge, and Kolln, using a computer simulation of the O + CS_2 reaction kinetics under the conditions of these ESR studies, found that the assumed stoichiometric factor of 2 is too high because the intermediate CS does not reach steady state during the observed reaction time.[18] They further determined that a stoichiometric factor in the range 1.2–1.5 would have been more appropriate in these studies (at room temperature). A stoichiometric factor below 2 would yield higher calculated values of k from the two ESR studies, and would yield better agreement with the values of k we report here.

We have not calculated an Arrhenius activation energy for k from our results because the individually determined values do not lie on a straight line in Figure 2. In Schofield's 1973 review of O + CS_2 rate constant studies, a recommended Arrhenius expression for k is offered which relies heavily on the Westenberg and deHaas study.[15] The high temperature results of Homan et al. are considered suspect and ignored probably because they lie a factor of 2 above the extrapolated Arrhenius expression which runs through the lower temperature rate constants. The upward curvature of our k values in Figure 2 indicates an Arrhenius expression is not well suited for fitting O + CS_2 rate constants over a significant temperature range. If the stoichiometric factor correction suggested by Bida et al. is applied to the data of the ESR studies, all rate constants in the five studies mentioned (ref 1, 14, 16, 17, 19, and this

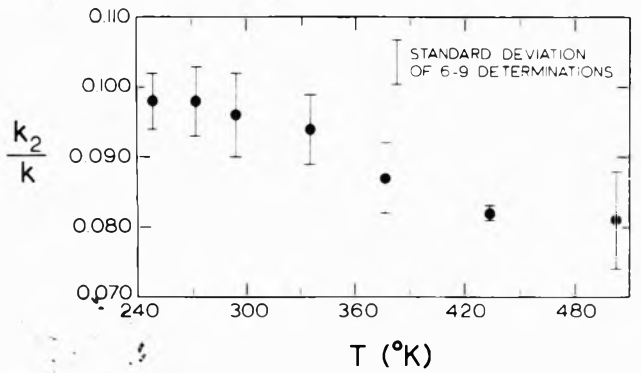

Figure 3. Plot of branching ratios for the O + CS_2 → OCS + S reaction vs. temperature.

study) lie reasonably close together on an Arrhenius plot, along a line curving smoothly upward at high temperatures.

Branching Ratio R_2. The branching ratios for route 2 are displayed in Figure 3 where they are plotted against temperature. The branching ratio decreases only slightly in importance between 249 and 500 K dropping from 0.098 ± 0.004 to 0.081 ± 0.007. The small monatomic decrease in R_2, although statistically evident, cannot be used for lenghty extrapolations to other temperatures due to the uncertainty of each determination, about ±15%. (The accuracy of R_2 is greater than that of k since it is derived from the ratio of similar measurements, a feature which reduces absolute error.) We would suggest a value of R_2 = 0.085 as probably being most appropriate in the 400–600 K range where CS_2 + O_2(O) lasers often operate.

Zetzsch has measured $k_2/(k_1 + k_2)$ at 1100 K and found it to be about 0.14.[11] Assuming $k_2 \approx k_3$ this would yield a value of R_2 of 0.11 at this temperature. The uncertainty reported for $k_2/(k_1 + k_2)$ is rather large. In addition this reported ratio is considered to be an upper limit.[19] This being the case, these results are in substantial agreement with those we report here.

We continue to have an interest in also directly determining the branching ratios for routes 1 and 3 of the O + CS_2 reaction. Unfortunately secondary reactions in this system make these determinations in a flow reactor extremely difficult, and we have not yet been successful in this pursuit.

Acknowledgment. The authors gratefully acknowledge the support for this work from the National Science Foundation.

Supplementary Material Available: Table IA contains the initial gas concentrations, flow velocity, and rate constants (k) for all experiments (a total of 46 experiments at 7 temperatures), and Table IB contains the initial gas concentrations, flow velocity, and branching ratios determined from all experiments (a total of 53 experiments at 7 temperatures) (4 pages). Ordering information is given on any current masthead page.

References and Notes

(1) I. W. M. Smith, *Trans. Faraday Soc.*, **64**, 378, 3183 (1968).
(2) P. L. Moore, P. N. Clough, and J. Geddes, *Chem. Phys. Lett.*, **17**, 608 (1972).
(3) I. R. Slagle, J. R. Gilbert, and D. Gutman, *J. Chem. Phys.*, **61**, 704 (1974).
(4) J. W. Hudgens, J. T. Gleaves, and J. D. McDonald, *J. Chem. Phys.*, **64**, 2529 (1976).
(5) G. Hancock and I. W. M. Smith, *Trans. Faraday Soc.*, **67**, 2586 (1976).
(6) R. D. Suart, P. H. Dawson, and G. H. Kimbell, *J. Appl. Phys.*, **43**, 1022 (1972).
(7) D. W. Howgate and T. A. Barr, Jr., *J. Chem. Phys.*, **59**, 2815 (1973).
(8) N. A. Nielsen, Jr., Ph.D. Thesis, Department of Chemistry, Cornell University, 1975.
(9) G. Hancock and I. W. M. Smith, *Appl. Opt.*, **10**, 1827 (1971).
(10) R. D. Suart, S. J. Arnold, and G. H. Kimbell, *Chem. Phys. Lett.*, **7**, 337 (1970).
(11) C. Zetzsch, Diplomarbeit, Universitat Gottingen, 1969. Results obtained for $k_2/(k_1 + k_2)$ presented by K. H. Homann, G. Krome, and H. Gg. Wagner, *Ber. Bunsenges. Phys. Chem.*, **74**, 654 (1970).
(12) J. Hardy and W. G. Gardiner, Paper presented at 16th Symposium (International) on Combustion, August 1976, Cambridge, "Shock Tube Study of Carbon Disulfide Oxidation".
(13) R. E. Graham, Department of Chemistry, unpublished results.
(14) K. H. Homann, G. Krome, and H. Gg. Wagner, *Ber. Bunsenges. Phys. Chem.*, **72**, 998 (1968). The actual measured rate constants can be found in ref 15.
(15) K. Schofield, *J. Phys. Chem. Ref. Data*, **2**, 25 (1973).
(16) A. A. Westenberg and N. deHaas, *J. Chem. Phys.*, **50**, 707 (1969).
(17) C. N. Wei and R. B. Timmons, *J. Chem. Phys.*, **62**, 3240 (1975).
(18) G. T. Bida, W. H. Breckenridge, and W. S. Kolln, *J. Chem. Phys.*, **64**, 3296 (1976).
(19) C. Zetzsch, private communication.

Pressure and Temperature Dependence of NH_2 Recombination Rate Constant

Pham Van Khe, J. C. Soulignac, and R. Lesclaux*

Laboratoire de Chimie Physique A,† Université de Bordeaux I, 33405 Talence, France *(Received April 22, 1976; Revised Manuscript Received November 2, 1976)*

Publication costs assisted by Laboratoire de Chimie Physique, Université de Bordeaux I

The recombination rate constant of the NH_2 radical is measured by flash photolysis of ammonia as a function of total pressure from 0.3 to 1000 Torr of nitrogen. The recombination kinetics is third order between 0 and 20 Torr and the relative third body efficiencies of ammonia, nitrogen, and argon, determined in this pressure range, are 4.0, 1.0, and 0.4, respectively. The termolecular rate constant is, in the case of nitrogen, $k_{1a,N_2} = 2.5(\pm 50\%) \times 10^{12}$ M^{-2} s^{-1}. The high pressure limiting value of $k_{1a}(\infty) = 1.5(\pm 50\%) \times 10^{10}$ M^{-1} s^{-1} is reached at about 1000 Torr of nitrogen. A low pressure limit $k_1(0) = 8.5(\pm 50\%) \times 10^8$ M^{-1} s^{-1} is found when the pressure tends to zero. The disproportionation reaction of amino radicals seems to be the principal reaction at pressures lower than 1 Torr. No significant temperature effect is found either near the high pressure limit or at the low pressure limit. A small negative temperature coefficient ($-1 < E < -0.5$ kcal/mol) is observed at 20 Torr of nitrogen, when the reaction is essentially termolecular. These results are discussed in connection with previous data concerning this reaction.

Introduction

Data concerning the rate constant of NH_2 radical reactions are relatively scarce to date. The radical is known to be weakly reactive[1-3] and among the NH_2 reactions, the recombination process

$$NH_2 + NH_2 \rightarrow \text{products} \qquad (1)$$

appears to be one of the fastest. As a result it often competes with other NH_2 reactions and it follows that reaction mechanisms involving the NH_2 radical cannot be completely elucidated unless the recombination kinetics is well known over a wide range of conditions. This is particularly true for the pressure dependence of the process

$$NH_2 + NH_2 + M \rightarrow N_2H_4 + M \qquad (1a)$$

The first evaluation of the recombination rate constant was made by Hanes and Bair[4] using a pulsed radio frequency discharge in ammonia and simultaneously monitoring NH_2 concentrations by visible absorption spectroscopy. They measured a value of 2.3×10^9 M^{-1} s^{-1} at room temperature under pressures of 0.4–0.8 Torr. Later, Diesen[5] found that around 10 Torr the recombination rate was pressure dependent and suggested that the rate constant measured by Hanes and Bair corresponded in fact to the following disproportionation process rather than to the combination reaction 1a:

$$NH_2 + NH_2 \rightarrow NH + NH_3 \qquad (1b)$$

In a new investigation, Salzmann and Bair[6] again found a pressure dependence of the NH_2 disappearance rate between 0 and 10 Torr and determined a low pressure limiting rate of 0.46×10^9 M^{-1} s^{-1} that they attributed to process 1b. The occurrence of this reaction at low pressure was shown by Mantei and Bair in a flash photolysis study of ammonia[7] while Gehring et al.[8,9] measured $k_{1a}/k_{1b} = 4.7 \times 10^3$ M^{-1} (M = Ar) using a fast flow reactor coupled to an ESR spectrometer and a mass spectrometer.

The first high pressure determination of the rate constant k_1 was performed by Gordon et al.[10] by pulse radiolysis of ammonia. They found that k_1 reached the high pressure limiting value of 6.2×10^{10} M^{-1} s^{-1} for 250 Torr of ammonia. Back and Yokota[11] obtained about the same value (4.7×10^{10} M^{-1} s^{-1}) in the same range of pressure.

† Equipe de Recherche Associée au CNRS No. 167.

Despite these attempts, not enough attention has been paid to NH_2 recombination reactions in order to be able to relate all the available data obtained at different pressure. It thus appeared to us necessary to have a complete determination of the kinetics of reaction 1 in a range of pressure continuously covering the falloff region. This is important not only to obtain precise data needed for a complete understanding of reaction mechanisms involving NH_2 but also for a better theoretical approach to the forward and reverse processes.

This paper reports measurements of the rate constant of reaction 1 by flash photolysis of ammonia in the pressure range 0.3–1000 Torr, using NH_3, N_2, and Ar as third bodies, and the temperature dependence between 300 and 500 K. One of the features of this study is that all the measurements are made using a single technique under all conditions.

Experimental Section

Materials and Apparatus. Ammonia (99.96%) was dried over sodium and distilled at low temperature. Nitrogen (99.99%) and argon (99.99%) were used without further purification. SF_6 (99.5%) was distilled at low temperature.

The flash photolysis apparatus and the method for transient absorption measurements were described in detail in a preceding paper.[12] The apparatus was essentially composed of the following: a pulsed 150-W xenon arc as the analyzing light source; two flashlamps of 400 J emitting pulses of light with a duration of about 20 μs; a multipath cell set for path lengths from 3 to 15 m; a monochromator selecting the strong NH_2 absorption lines around 5977 Å; a differential absorption measurement system allowing determination of light absorptions smaller than 5%. For such low absorptions and except for the lowest pressures, the measured optical densities are a linear function of NH_2 concentration in spite of the fact that the monochromator band width is broader than the absorption line.[12] Therefore no correction were necessary for pressures higher than 20 Torr to take into account deviations from the Beer–Lambert law. Figure 1 shows typical plots of the measured absorbance vs. the number of passes in the cell. At low pressure, the correction was applied directly from these calibration curves. Kinetic measurements were made with absorbances smaller than 0.05.

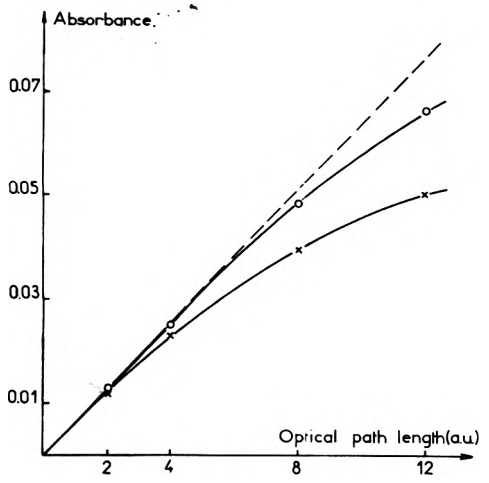

Figure 1. Measured NH_2 absorbance as a function of the optical path length: (O) total pressure = 20 Torr; (×) total pressure lower than 5 Torr.

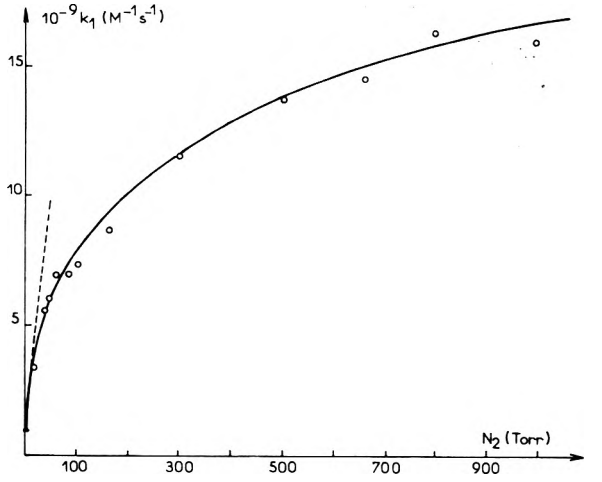

Figure 2. Recombination rate constant k_1 of NH_2 radicals as a function of nitrogen pressure.

Second-Orders Kinetics Measurements. In all measurements performed, the NH_2 disappearance kinetics is essentially second order. It was thus necessary to determine the absolute radical concentration or the apparent extinction coefficient of the absorption line. Two methods were used for this determination.

First, the transient absorption of NH_2 was measured by flash photolysis of 5 Torr of NH_3 in the presence of 600 Torr of isobutane. Ammonia is dissociated according to

$$NH_3 \xrightarrow{h\nu} NH_2 + H \quad (2)$$

while hydrogen atoms react very fast (during the flash duration) and quantitatively with the isobutane in excess

$$H + iC_4H_{10} \rightarrow H_2 + C_4H_9 \quad (3)$$

The amount of molecular hydrogen produced by 100 flashes was measured by mass spectrometry and was related to the NH_2 initial concentration. The amino radicals disappeared by various radical recombination reactions with a half-life of about 150 μs. No change in the NH_2 absorption was found from the first to the last flash and H atoms could not react with the products of the reaction, given the large excess of isobutane.

In the second method 5 Torr of ammonia was flashed in the presence of 0.04 Torr of NO and 700 Torr of nitrogen. The reaction of NH_2 + NO being very fast, the following reactions were assumed to take place[12]

$$NH_2 + NO \rightarrow N_2 + H_2O \quad (4)$$

$$H + NO + M \rightarrow HNO + M \quad (5)$$

$$2HNO \rightarrow N_2O + H_2O \quad (6)$$

Two NO molecules were thus consumed for one NH_2 radical produced. By measuring the increase of the NH_2 lifetime (about 5%) as NO is consumed from one flash to the other it was possible to relate the initial NH_2 concentration to the initial NH_2 absorption. Both methods gave similar values, resulting in an apparent extinction coefficient ϵ of 330 ± 50 M^{-1} cm^{-1} for our particular experimental conditions.

The question arises here as to the extinction coefficient variation with pressure due to the pressure broadening of NH_2 absorption lines. In fact, the apparent extinction coefficient was found constant over the range 0.3–1000 Torr because the spectral width of the analyzing light (1.2 Å) is much broader than the NH_2 absorption lines (the NH_2 absorption was actually due to a group of three rotational lines around 5977 Å[13]). Thus the absorption measured was not really proportional to the extinction coefficient value at a particular wavelength, but rather to the oscillator strength of the lines which is constant with pressure. It should be noted that the measured apparent extinction coefficient is independent of line broadening only for low absorption (i.e., <10%).

Second-order kinetics measurements necessitate a uniform irradiation of ammonia in the cell. This was achieved by a symmetrical excitation of the cell and by always flashing at the lowest possible ammonia pressure (0.3 Torr) so that only a small fraction of the excitation light was absorbed (an indication on the amount of light absorbed is given by the fact that the maximum yield of NH_2 radicals was obtained for 10 Torr of ammonia). From the geometrical characteristics of the optical arrangement it could be determined that the variation of the excitation intensity was about 10% in the analyzing zone, for the lowest ammonia pressures.

Results

It cannot be asserted that NH_2 disappearance kinetics were strictly second order in all cases since it was not possible to follow these kinetics over two half-lifes. This was mainly due to the weak absorption necessary for accurate measurements and also, to some extend, to the fact that in some experiments the decay curve did not come back exactly to zero absorption, especially for pressure lower than 100 Torr. Though this fact was not fully understood it was tentatively attributed either to some electronic artifact or to secondary reactions of hydrogen atoms with hydrazine yielding NH_2 radicals,[19] such as

$$H + N_2H_4 \rightarrow N_2H_3 + H_2 \quad (7a)$$

$$H + N_2H_4 \rightarrow NH_3 + NH_2 \quad (7b)$$

$$H + N_2H_3 \rightarrow 2NH_2 \quad (8)$$

Hydrazine came either from preceding flashes necessary to set the best measurement conditions or from the hydrazine adsorbed on the cell walls. However, this small residual absorption which never exceded 1% did not significantly affect the rate constant determination especially at high pressure, but did not allow an accurate analysis of the decay curve in order to evaluate small deviations from second-order kinetics.

Results obtained by photolyzing 0.3 Torr of ammonia and by using nitrogen as the third body are shown in Figure 2. Large variations of the NH_2 second-order disappearance rate are observed when the nitrogen

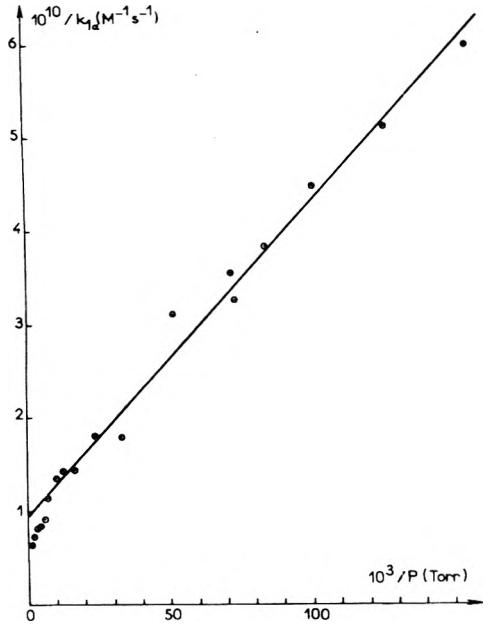

Figure 3. Plot of $1/k_{1a}$ against $1/P$. P is the total pressure (nitrogen + 0.3 Torr of ammonia); $k_{1a} = k_1 - k_1(0)$ (see text).

pressure is varied from 0 to 1000 Torr. The rate constant seems to be close to the high pressure limiting value around 1000 Torr of N_2.

In order to obtain a better value of the high pressure limit for the rate constant k_{1a}, $1/k_{1a}$ was plotted against $1/P$ (P is the total pressure). According to the simple mechanism

$$NH_2 + NH_2 \underset{k_{-1}'}{\overset{2k_1'}{\rightleftharpoons}} N_2H_4^* \qquad (1')$$

$$N_2H_4^* + M \xrightarrow{k_1''} N_2H_4 + M \qquad (1'')$$

$1/k_a$ is given by the following expression

$$\frac{1}{k_{1a}} = \frac{k_{-1}'}{k_1'k_1''[M]} + \frac{1}{k_1'} \qquad (I)$$

k_1' being the high pressure limiting value, here after called $k_{1a}(\infty)$.

The results are shown in Figure 3 and will be discussed later. It was assumed that $k_{1a} = k_1 - k_1(0)$; k_1 is the measured rate constant of the NH_2 disappearance at a given pressure; $k_1(0)$ is the low pressure limiting k_1 value (see Discussion).

The low pressure range (0–20 Torr) was examined in more detail by using NH_3, N_2, and Ar as third bodies (Figure 4). In the case of ammonia, the total pressure could not exceed 10 Torr in order to keep an homogeneous excitation which was fairly well verified according to the good linear plot obtained. The observed linear dependence between k_1 and the pressure indicates clearly that the recombination reaction kinetics is third order in this pressure range. A curvature is only observed over 30–50 Torr of N_2. From Figure 4 the following termolecular rate constants are deduced: $k_{1a,NH_2} = 10.2 \times 10^{12}\ M^{-2}\ s^{-1}$; $k_{1a,N_2} = 2.55 \times 10^{12}\ M^{-2}\ s^{-1}$; $k_{1a,Ar} = 1.00 \times 10^{12}\ M^{-2}\ s^{-1}$.

Relative third body efficiencies of 4.0, 1.0, and 0.4 for NH_3, N_2, and Ar, respectively, can be calculated. The relative error between these values does not certainly exceed 10%, however, the error on the absolute value of the rate constant is larger since it depends on the excitation coefficient uncertainty, as will be discussed later.

The plots in Figure 4 do not intercept the ordinate axis at the origin. A low pressure limit is thus observed for the

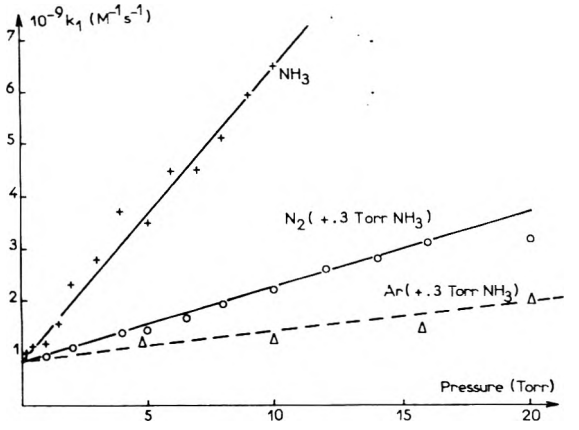

Figure 4. Recombination rate constant k_1 as a function of NH_3 (+), N_2 (O), and Ar (Δ) pressure.

NH_2 disappearance rate constant as already reported by Salzman and Bair.[6] The low pressure limiting value $k_1(0)$ is found to be $k_1(0) = 8.5 \times 10^8\ M^{-1}\ s^{-1}$.

Temperature Effect. The temperature effect on the rate of disappearance of NH_2 was measured between 300 and 500 K under the following conditions: (i) close to the high pressure limit in order to measure any activation energy of NH_2 combination reaction; (ii) at a pressure of 20 Torr of nitrogen, for which the termolecular process is the most efficient one; (iii) at the lowest possible pressure (0.3 Torr of ammonia) which correspond within experimental errors to the low pressure limiting value of the rate constant k_1.

Under high pressure, NH_3 was photolyzed in the presence of 350 Torr of SF_6. For this gas, having an intermediate third body efficiency between that of ammonia and of nitrogen, the measured k_1 value is close to the high pressure limit within experimental errors. This allowed us to eliminate the high nitrogen pressure (~2 atm) which would have developed in the cell upon heating.

No temperature effect greater than experimental errors could be detected either close the high pressure limit or at the low pressure limit. This would correspond to activation energies lower than ±0.5 kcal/mol.

The results obtained in the presence of 20 Torr of nitrogen indicate however a significant negative temperature coefficient in spite of the poor accuracy of measurements at high temperatures. This temperature effect corresponds to a negative activation energy $-1.0 < E < -0.5$ kcal/mol which is a usual value for termolecular reactions of this type.

Discussion

The disappearance of NH_2 following flash photolysis of ammonia is accounted for by the reactions

$$NH_2 + NH_2 \rightarrow \text{products} \qquad (1)$$

$$NH_2 + H + M \rightarrow \text{products} \qquad (9)$$

The rate of disappearance being at a given pressure:

$$-d[NH_2]/dt = 2k_1[NH_2]^2 + k_9[NH_2][H] \qquad (II)$$

It is generally admitted that at low pressure reaction 1 is much faster than reaction 9 and thus it can be considered as the only pathway for the observed NH_2 disappearance. The situation should be somewhat different at the highest pressure used in this study, as shown by Gordon et al.[10] who determined the relative rates of reactions 1 and 9 in the high pressure region, using NH_3 as a third body. According to the results shown in Figure 3, NH_3 is more efficient than N_2 as third body by a factor of 4. This means that the relative rates of reactions 1 and 9 should be about the same at 1000 Torr of N_2 and at about

250 Torr of NH_3, assuming that the relative efficiency of third bodies are similar for both reactions. At 250 Torr of NH_3, Gordon et al. found for k_9 a value of about $0.5k_1$. The kinetic analysis of NH_2 decays reported in our work are not accurate enough to reach a similar conclusion. However, an indication of the participation of reaction 9 in the NH_2 disappearance at high pressure may be obtained from Figure 3. According to eq I the plot should be a straight line and this is roughly the case for pressures lower than 300 Torr. At higher pressures, the values of the experimental rate constants are too high compared to those extrapolated by the straight line from low pressures. This does not appear clearly in Figure 3 due to the experimental errors. However, taking into account the fact that measurements are more accurate at high pressure than at low pressure, because of absorption line broadening, the difference observed is indeed significant. This deviation in the high pressure range might be interpreted by the occurrence of reaction 9, but eq I results from a simplified mechanism and it is known that more elaborate theories concerning termolecular recombination reaction predict a curvature of the plot $1/k_1$ against $1/P$ for the highest pressures, similar to the curvature obtained in Figure 3. RRKM calculations carried out by Tsang[15] concerning reaction 1a are consistent with such a curvature.

In order to take into account the occurrence of reaction 9 at high pressure it can be assumed that the measured rate constant is approximately $k_{1a} + k_9$ since the initial concentrations of NH_2 and H are the same. At 1000 Torr of nitrogen (or 250 Torr of NH_3) the measured value is 1.7×10^{10} M^{-1} s^{-1}. According to Gordon et al., $k_{1a} \simeq 2k_9$ at this pressure which would give $k_{1a} = 1.1 \times 10^{10}$ M^{-1} s^{-1} and $k_9 = 0.6 \times 10^{10}$ M^{-1} s^{-1}. It is seen that this calculated value of k_{1a} falls exactly on the extrapolated straight line in Figure 3, thus in agreement with eq I. It is therefore not obvious how the extrapolated high pressure value of $k_{1a}(\infty)$ should be obtained.

The extrapolation of the straight line and of the experimental points to infinite pressure gives respectively 1.15×10^{10} and 1.8×10^{10} M^{-1} s^{-1} for $k_{1a}(\infty)$. Taking into account that at high pressure a curved plot (Figure 3) is expected and that reaction 9 indeed occurs, $k_{1a}(\infty)$, consistent with our results, is intermediate between these last two values. Considering that they ary not very different, a value of $k_{1a}(\infty) = 1.5 \times 10^{10}$ M^{-1} s^{-1} is certainly within the experimental error from the true high pressure limit. Considering also the uncertainty in the extinction coefficient, an error of 50% can be estimated for this value.

The high pressure limit is reached at about 1000 Torr of N_2 and this is in agreement with Gordon et al. who found a constant value for k_{1a} over 250 Torr of NH_3.[10] However, an important discrepancy is observed between our absolute high pressure limiting value and that of Gordon et al. who found $k_{1a}(\infty) = 6.2 \times 10^{10}$ M^{-1} s^{-1}. Back and Yokota studying the photolysis of formamide vapor by the method of the rotating sector, found $k_{1a}(\infty) = 4.7(\pm 2) \times 10^{10}$ M^{-1} s^{-1} and taking into account new $G(NH_2)$ determinations in ammonia radiolysis,[11] they estimated that Gordon's value should be 5×10^{10} M^{-1} s^{-1}. There is still a ratio larger than 3 between the latter value and ours.

The difference cannot be totally explained by a discrepancy in the extinction coefficient determinations. Gordon et al.[10] found an ϵ of 775 M^{-1} cm^{-1} which gives 620 M^{-1} cm^{-1} after correcting the $G(NH_2)$ value, compared to an ϵ of 330 M^{-1} cm^{-1} determined from the present experiments. However, our value is expected to be lower than that of ref 10 since the spectral widths of the analyzing light were respectively 0.12 nm in our experiments and 0.08 nm in ref 10. Thus, the disagreement between the two values should not exceed a factor of 1.5 which can be accounted for considering that uncertainties in the extinction coefficient determinations are generally fairly large.

It is then difficult to explain the difference observed between the $k_{1a}(\infty)$ value we determined and that of Gordon et al.[10] (which is supposed to be more accurate than that of Back and Yokota[11]). It cannot be due to the Beer–Lambert relation used in ref 10 in which the absorbance was expressed as $(\epsilon cl)^n$ ($n = 0.77$), whereas no correction was applied in this work since very low absorptions were measured. Indeed an identical rate constant was found for the reaction $NH_2 + NO$ by Gordon et al.[10] and ourselves using the same experimental techniques.[12]

It is also interesting to compare the k_1 value in the low pressure region to those obtained by Bair and co-worker under similar conditions. In their first determination[4] they found a value of $2.3(\pm 0.2) \times 10^9$ M^{-1} s^{-1} at pressures lower than 1 Torr, which is about twice our value (Figure 4), and in their second investigations they determined a low pressure limiting value of 0.46×10^9 M^{-1} s^{-1} (almost half our value) and a rate constant $k_1 = 2.5 \times 10^9$ M^{-1} s^{-1} at a few Torr of NH_3, the exact pressure not being clearly stated. The latter results would then be in a better agreement with ours at low pressure than those of ref 10 at high pressure despite the poorly defined pressure conditions in ref 6. This shows again that the discrepancy with ref 10 is not only due to a discrepancy in the extinction coefficient determination.

Finally the absolute k_{1a} high pressure limiting value obtained from Figure 3 is at least a factor of 3 lower than that of Gordon et al.[10] and in the low pressure range (Figure 4), the results are in acceptable agreement with the average of Bair's results. No explanation can be found concerning the remaining discrepancy in the high pressure region.

The extrapolation to zero pressure of the straight lines in Figure 4 gives a k_1 low pressure limiting value of 8.5×10^8 M^{-1} s^{-1}. Salzman and Bair[6] who also found such a low pressure limiting rate constant, but their value is half ours, attributed this remaining reaction to the NH_2 disproportionation (reaction 1b) in agreement with Diezen.[5] As already mentioned the occurrence of reaction 1b was confirmed by Mantei and Bair.[7] The result obtained by Ghering et al.,[8] who measured the combination over disproportionation ratio in a flow tube in the presence of argon ($k_{1a}/k_{1b} = 4.4 \times 10^3$ M^{-1}), can be combined with the termolecular rate constant deduced from Figure 4 in the case of argon and one can determine $k_{1b} = 2.0 \times 10^8$ M^{-1} s^{-1}. Considering the quite different technique used by Gehring et al.[8] it can be considered that this last value is on the order of magnitude of the observed low pressure limiting value of k_1. It is then likely that the main reaction, at pressures lower than 1 Torr, is the disproportionation reaction 1b. However, no proof has yet been given for eliminating the possibility of occurrence of the following reaction at low pressure:

$$NH_2 + NH_2 \rightarrow N_2 + 2H_2 \quad (1c)$$

$$NH_2 + NH_2 \rightarrow N_2H_2 + H_2 \quad (1d)$$

It is therefore difficult to obtain precise information on the disproportionation–combination ratio of NH_2 radicals since the rate constants of reactions 1b, 1c, and 1d are not known accurately. It can only be said that at high pressure the ratio is smaller than $k_1(0)/k_{1a}(\infty) = 0.057$. More investigations on NH_2 recombination reaction at low pressure are necessary in order to determine the relative rates of

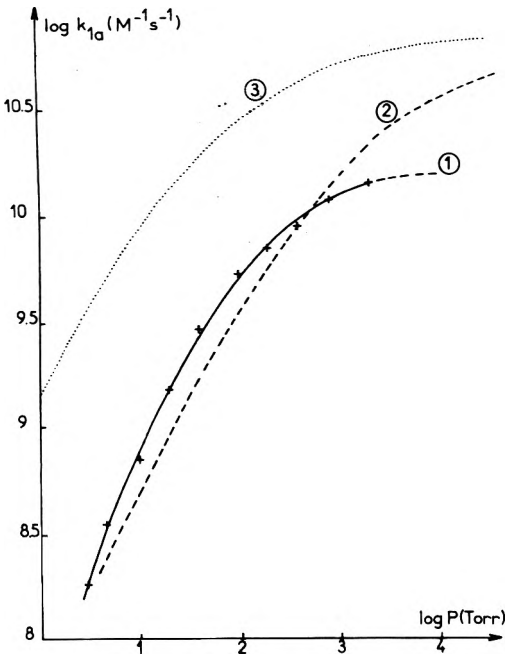

Figure 5. Dependence of k_{1a} on the total pressure of argon. Comparison of experimental results obtained in this work (1) with calculated values in ref 15 (2) and ref 18 (3).

reactions 1b, 1c, and 1d.

In a study of hydrazine thermal decomposition using a shock tube coupled with a mass spectrometer, Diesen[5] determined a value $k_{1b} = 2.5 \times 10^{10}$ M^{-1} s^{-1} at 2000 K. This value is one order of magnitude higher than those determined at room temperature (see above). It would correspond to a mean activation energy of 1.0 kcal mol^{-1}. This is in contradiction with the absence of variations of k_1 with temperature near the low pressure limit reported in this paper. Such an activation energy should correspond to k_1 variations larger than a factor of 2 in the range 300–500 K, which is much larger than experimental deviations. Diesen's value is then either too high or does not correspond to disproportionation reaction 1b only.

It is of interest to relate a radical combination reaction to the reverse dissociation reaction. Tsang[15] examined this question critically and tried, by using RRKM calculations, to develop a model in agreement with experimental results on both dissociation and combination reactions. The main result of the calculation, based on a "loose" transition state, was to show that both dissociation and combination reactions were pressure dependent in agreement with preceding predictions[16] and the present results. The thermochemical parameters employed were adjusted so that the calculated rate constants fitted the experimental results, especially the pulse radiolysis combination rate constant determination.[10] However, by using a different model, which gives a combination rate lower by a factor of 8, the best N–N bond energy of hydrazine was slightly closer than that expected[17] and the fit with experimental dissociation rate parameters was still obtained. The calculated temperature effects are in fairly good agreement with those reported in this study. However, the calculated dependence on third body effects of the recombination reaction is higher than that deduced from experimental data. This is shown in Figure 5 where our experimental results are compared to those of Tsang's calculations[15] in the case of argon used as a third body. Despite the fairly good agreement in the low pressure region, an important deviation appears at high pressure as expected from the higher value of $k_{1a}(\infty)$ in ref 10 as compared to ours.

Recently, Tsang[18] carried out new RRKM calculations which better reproduced the hydrazine decomposition rates at high temperature but postulated a negative threshold energy for the combination process. This results in a temperature dependence for the combination rate constant corresponding to fairly high negative temperature coefficients in disagreement with the small temperature effect found in the present experiments. It is interesting to note that Tsang[18] stated that the requirement for a zero threshold energy for the combination reaction would be a rate constant value one order of magnitude lower than that found in ref 10. This would certainly be in better agreement with our results. These new calculated data[18] for room temperature conditions are shown in Figure 5. In spite of the differences observed on the absolute values of k_{1a} due again to the discrepancy at the high pressure limit, the general variation of k_{1a} in the falloff region is in better agreement with our experimental results than those deduce from the preceding calculations.[15]

For a better comparison, RRKM calculations should be carried out again, taking into account our present data. However further investigations are necessary in order to clear the remaining discrepancy at high pressure and to determine the k_{1a} temperature dependence over a wider range of temperature. This latter point would allow a better correlation between the NH_2 recombination rate and hydrazine decomposition at high temperature than can be done with the present data.

Acknowledgment. The authors wish to thank Professor J. Joussot-Dubien for his encouraging interest in this work and valuable discussions.

References and Notes

(1) R. Lesclaux and P. V. Khe, *J. Chim. Phys.*, **70**, 119 (1973).
(2) Y. Ogata, Y. Izawa, and H. Tomioka, *Tetrahedron*, **23**, 1509 (1967).
(3) S. Shih, R. J. Buenker, S. D. Peyerimhoff, and C. J. Michejda, *J. Am. Chem. Soc.*, **94**, 7620 (1972).
(4) M. H. Hanes and E. J. Bair, *J. Chem. Phys.*, **38**, 672 (1963).
(5) R. W. Diesen, *J. Chem. Phys.*, **39**, 2121 (1963).
(6) J. D. Salzman and E. J. Bair, *J. Chem. Phys.*, **41**, 3654 (1964).
(7) K. A. Mantel and E. J. Bair, *J. Chem. Phys.*, **49**, 3248 (1968).
(8) M. Gehring, K. Hoyermann, H. Gg. Wagner, and J. Wolfrum, *Ber. Bunsenges. Phys. Chem.*, **75**, 1287 (1971).
(9) M. Gehring, K. Hoyermann, H. Schacke, and J. Wolfrum, *Symp. (Int.) Combust., [Proc.], 14th*, 99 (1973).
(10) S. Gordon, W. Mulac, and P. Nangia, *J. Phys. Chem.*, **75**, 2087 (1971); **79**, 3080 (1975).
(11) R. A. Back and T. Yokota, *Int. J. Chem. Kinet.*, **5**, 1039 (1973).
(12) R. Lesclaux, P. V. Khe, P. Dezauzier, and J. C. Soulignac, *Chem. Phys. Lett.*, **35**, 493 (1975).
(13) K. Dressler and D. A. Ramsay, *Philos. Trans. R. Soc. London, Ser. A*, **251**, 553 (1959).
(14) G. Hancock, W. Lange, M. Lenzi, and K. H. Welge, *Chem. Phys. Lett.*, **33**, 168 (1975).
(15) W. Tsang, National Bureau of Standards Report 10904, 171 (1972).
(16) D. W. Setser and W. C. Richardson, *Can. J. Chem.*, **47**, 2593 (1969).
(17) D. R. Stull and H. Prophet, *Natl. Stand. Ref. Data Ser., Natl. Bur. Stand.*, **No. 37**.
(18) W. Tsang, to be submitted for publication.
(19) M. Arvis, C. Devilliers, M. Gillois, and M. Curtat, *J. Phys. Chem.*, **78**, 1356 (1974).

Photoisomerization of Stilbene Following Direct Optical Excitation into the Triplet Manifold†

R. Benson‡ and D. F. Williams*

National Research Council of Canada, Division of Chemistry, Ottawa, Ontario K1A 0R6, Canada (Received August 9, 1976)

Publication costs assisted by the National Research Council of Canada

The initial rates of isomerization of stilbene following direct optical excitation into the triplet manifold are measured from 200 to 300 K. A temperature dependence of isomerization is found for both cis → trans and trans → cis processes. These results are discussed in terms of a curve avoidance at the 90° twisted configuration. Experiments at room temperature also show azulene quenches trans → cis stilbene isomerization more efficiently than anthracene.

I. Introduction

Isomerization is one of the simpler photochemical processes which one can study. In particular stilbene has been the subject of many investigations whose object has been to probe the mechanisms involved in this conversion process. Experimentally, it is relatively simple to populate and hence study singlet excited states of stilbene by direct optical absorption processes, for such optical transitions are highly allowed. For triplet states, however, the relevant absorption coefficient is very small, since this is a spin forbidden process. Triplet sensitizers have been used to obtain sufficient stilbene triplet populations to study the isomerization. It is necessary however that some triplet experiments be carried out in pure systems, to show if the assumptions used in sensitized experiments are valid, as well as to extend the knowledge of the role of triplets in the isomerization process. For these reasons we have studied the rate of isomerization of stilbene following excitation directly into the triplet state by an argon laser.

To understand more fully the process of cis–trans isomerization of stilbene in its triplet state one needs to know the shape of the potential energy profile for rotation about the central carbon double bond, and the rates of decay from this triplet state profile to the ground state profile. From thermochemical studies the shape of the ground state profile is known. The cis ground state (^{0}c) is 2.3 kcal/mol above the trans ground state (^{0}t).[1] The energy at 90° rotation (^{0}p state) is 46–50 kcal/mol above the ^{0}t state.[2,3] Absorption studies with high-pressure oxygen[4] or heavy atom perturbation[5] to increase the absorption probability place the ^{3}t (trans triplet) at 49 kcal/mol and the ^{3}c (cis triplet) at 57 kcal/mol above the ^{0}c state. No phosphorescence has ever been detected from either isomer. To obtain information about the shape of the triplet state profile away from the planar configurations one must turn to the results of photochemical studies.

Hammond et al.[6] found that *trans*-stilbene acted as a classical triplet energy acceptor, in that sensitizers with a triplet energy below the ^{3}t energy level transferred energy according to the Boltzmann law of energy distribution (efficiency of transfer $\propto \exp[(E_{triplet} + E_{thermal})/RT]$. From this result he concluded that ^{3}t was a minimum in the stilbene triplet energy profile. *cis*-Stilbene was found not to be a classical triplet energy acceptor, in that sensitizers with triplet energy below the ^{3}c energy level transferred energy with a greater efficiency than predicted by the Boltzmann law. It was concluded that ^{3}c is probably a maximum on the triplet energy profile.

Both Hammond et al.[6] and Saltiel[7] have discovered that triplet energy quenchers have the effect, on both photostationary states and initial ratios of isomerization, of increasing the decay rate to the trans ground state no matter which isomer is the starting material. From these results, since quenching is a vertical process, one can conclude that ^{3}c can rotate to ^{3}t.

Saltiel[7] has studied the effects of deuteration on the photostationary cis/trans ratios and found no effect of deuteration and only a small effect on the triplet lifetime, τ, ($\tau_d/\tau_h = 1.3$). Schulte-Frohlinde et al.[8] studied the effect of deuteration on the triplet lifetime of *trans*-stilbene in EPA at 77 K and found an increase in τ upon deuteration by a factor of about 4.1. Their measured lifetime of nondeuterated *trans*-stilbene was 2.2×10^{-2} s. Dainton et al.,[9] using pulse radiolysis techniques, measured a triplet lifetime of *trans*-stilbene at room temperature of 1.10×10^{-7} s. Thus at ~300 K, the triplet lifetime is five orders of magnitude smaller than at 77 K, and deuteration only slightly changes the room temperature triplet lifetime and has no influence on isomerization. It is the room temperature results which are anomalous. At 77 K the stilbene triplet lifetime and its change with deuteration are similar to those of other aromatics (i.e., pyrene with a triplet energy of approximately 48 kcal/mol has a lifetime of 0.05 s and $\tau_d/\tau_h = 6.4$).

One explanation for the behavior of stilbene at room temperature is that the ^{3}c and ^{3}t configurations rotate toward the twisted configuration (^{3}p) and then decay to the ground state. In the ^{3}p configuration the energy difference between the ground state and the triplet state is very small. With a small energy gap the lifetime will be much shorter and the deuterium effect will be nil. This analysis also offers a mechanism for the isomerization, namely, rotation on the triplet energy profile followed by decay to the ground state with partition to the cis and trans ground state. In short hand form the mechanism can be written as follows:

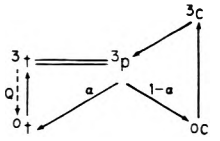

The next step in the elucidation of the isomerization mechanism is to measure the temperature dependence of

† Issued as NRCC No. 15735.

‡ Present Address: Chemistry Department, Kansas State University, Manhattan, Kansas.

isomerization. Both Hammond[6] and Saltiel et al.[10] have measured the temperature dependence on photostationary cis/trans ratios. They concluded that the energy of the ^{3}p state was higher than the ^{3}t state. Saltiel found that the enthalpy content of the ^{3}t state was 800 cal less than the ^{3}p state, but that the free energy content of the ^{3}p state was less than the ^{3}t state in the temperature range he used. Thus at equilibrium most molecules were in the ^{3}p state. Because he studied only the photostationary state, his results only give information on energy differences between states and not on activation energies, even if any are present. It should be mentioned that Saltiel studied the temperature dependence of sensitized isomerization with a quencher present. Thus in his experiments there are potentially three temperature-dependent processes, sensitization, (I), quenching (II), and any temperature-dependent process intrinsic to isomerization (III).

To obtain further information on the shape of the triplet state profile we have performed temperature-dependent studies on the initial rates of isomerization on solutions of the pure stilbenes (up to 5% conversion). We have used the 4880 Å (and 5145 Å) lines from a powerful argon laser to optically excite the stilbene triplet directly, without the use of heavy atoms or oxygen. No quenchers were used in the temperature-dependent studies. These experiments are relatively simple to interpret, and allow the temperature dependence of single rate constants to be obtained, giving information concerning any energy barriers which are present in the path of isomerization.

We have also studied at room temperature the effects of azulene and anthracene quenching of stilbene isomerization via its triplet state, both to compare results with previous work and to measure the effect of the different triplet energy levels of quenchers on their efficiency of quenching.

II. Experimental Section

trans-Stilbene (Matheson Coleman and Bell) was purified by three vacuum sublimations. A vapor phase chromatographic analysis indicated that about 1% cis isomer was present in the final product. *cis*-Stilbene (Aldrich) was purified by alumina chromatography using hexane as the eluent. A vapor phase analysis indicated that about 0.1% trans isomer was present in the final product. 2-Methylpentane and 2,3-dimethylbutane, the solvents, were Philips research grade and were used without further purification. The solutions of these stilbenes were produced following vacuum line techniques, in sealed glass tubes. The tubes were mounted inside a glass dewar, through which cold nitrogen gas could be passed. Sample temperature and temperature control were measured from thermocouples. The temperature could be controlled to ±2 K.

An argon laser, 10 W Spectraphysics, was used as the excitation source, normally tuned to the 4880-Å line, though several check experiments with the 5145-Å laser line were run. The tuned laser line was freed of possible background UV light, and fixed into a defined geometrical position with respect to the sample by passing the beam in turn through a prism, pin hole, and a solution of sodium nitrite in water (1% V/W). The laser was always used in a light modulated control mode, which kept the intensity of the excitation light stable to better than one part in 200. A photodiode was used to monitor the laser intensity throughout the experiment, and to normalize the laser intensity for each separate experiment.

The relative amounts of *cis*- and *trans*-stilbene present in the samples at the termination of the experiment were determined by gas chromatography and integrating the separate peaks by weight. A control sample, treated in the same way other than having no optical excitation, was run in each case.

The samples were exposed to the laser for either 4 h (trans starting material) or 16 h (cis starting material). This exposure gave 1–3% conversion, sufficiently small that any back reaction could be discounted. Decreasing the time and increasing the laser power gave the same results, and the above times were chosen simply for convenience.

TABLE I: Trans Starting Material

Temp, K	$10^5 R_c$,[a] M/M	ϕ_c[b]
296	5.07(4.60 → 5.43)[c]	0.42(0.38 → 0.45)[c]
282	4.23(4.08 → 4.38)	0.35(0.34 → 0.36)
268	3.62(3.33 → 3.90)	0.30(0.28 → 0.32)
238	2.53(2.28 → 2.65)	0.21(0.19 → 0.22)
	$10^5 R_t$[a]	ϕ_t
296	3.37(3.10 → 3.63)	0.22(0.20 → 0.24)
249	2.16(1.91 → 2.40)	0.14(0.12 → 0.16)
220	1.70(1.68 → 1.71)	0.111(0.110 → 0.112)
	$10^5 R_c$[d]	ϕ_c
296	5.1	0.42
235	2.0	0.16

[a] Solvent, 2-methylpentane. [b] Predicted quantum yields. [c] Average value and range. [d] Solvent, 2,3-dimethylpentane. Initial stilbene isomerization rate constants for trans → cis, R_c, and cis → trans, R_t, stilbene isomerization in 2-methylpentane. For comparison initial rate constants measured for t → c stilbene isomerization in a different solvent, data for 2,3-dimethylpentane are included.

III. Results and Discussion

(i) *Temperature Studies.* In Table I are shown the results of temperature dependence studies on initial rates of isomerization. R_c (R_t) is the rate of formation of *cis*-stilbene (*trans*-stilbene) from trans (cis) starting material and is simply the concentration of *cis*- (*trans*-) stilbene divided by the time, in hours, of exposure to 2 W of the 4880-Å argon laser line.

Before we can discuss these temperature results in terms of the energetics of isomerization we should examine possible other causes for the change. There are two other possibly temperature-dependent processes in these experiments: (1) the absorption of light and (2) the viscosity of the solvent.

First, we are exciting solutions, the solute will have broad absorption bands which are relatively temperature insensitive, and second, the excitation energy falls well within the triplet manifolds (4880 Å is equivalent to 58.4 kcal/mol) of both cis and trans isomers; hence, there should be no temperature dependence on absorption. The contraction of the solvent as the temperature decreases should increase the absorption, not decrease it as required to explain the experimental results. The second possible cause of temperature results is a solvent viscosity change. Saltiel[11] and Fischer[12,13] have studied the effect of viscosity on the isomerization and have found that it is indeed affected, but only at high viscosities. Fischer[14] has measured the viscosity of various organic solvents at low temperatures. He has shown that 2-methylpentane remains fluid to lower temperatures than used in our studies, so viscosity changes within our temperature range seem to be unimportant. Nevertheless, to further check the effect of viscosity on our results we repeated some of the experiments, with a second solvent 2,3-dimethylbutane (at 25 °C $\eta_{2,3DMB}/\eta_{2MP} = 1.35$, at −40 °C $\eta_{2,3DMB}/\eta_{2MP} = 1.5$).

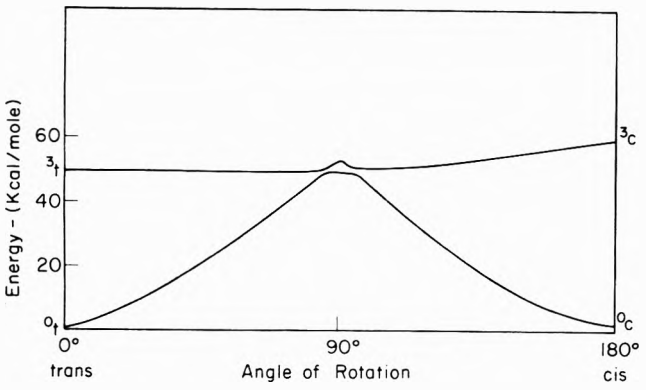

Figure 1. Energy of the first triplet state and ground state of stilbene as a function of the angle of rotation about the central carbon double bond.

These results are also listed in Table I and they fall within the experimental error of the 2-methylpentane solution results, showing viscosity cannot account for the measured changes in isomerization rate with temperature.

Thus the temperature results relate directly to effects in the stilbene isomerization processes. First it is seen that both the c → t and t → c initial rates decrease with decreasing temperature. This shows there is no temperature dependence on the intersystem crossing from the ^{3}p state, because in this case if the initial c → t rate decreased, then the t → c initial rate should increase.

A barrier between the ^{3}t and ^{3}p configuration hypothesized by Hammond et al.[6] also cannot explain our data because of two reasons: (1) lowering the temperature would then have increased the c → t initial rate and (2) such a barrier implies a transition from ^{3}t → ^{0}t which is competitive with movement over the barrier from ^{3}t to ^{3}p. Saltiel's deuteration experiment showed that the main decay route was from ^{3}p or near ^{3}p and not ^{3}t. The measured triplet lifetime at room temperature is 110 ns[9] compared to a ^{3}t lifetime[8] of 22×10^6 ns at 77 K. It is hard to rationalize this change of five orders of magnitude in the ^{3}t lifetime from 77 to 293 K, without postulating that these lifetimes are for different configurations of the molecule.

An energy barrier between ^{3}c and ^{3}p could explain the temperature results on c → t rates but cannot explain why quenchers have no effect on this rate. Again, a barrier between ^{3}c and ^{3}p implies a competition between the transition ^{3}c → ^{3}p and ^{3}c → ^{0}c. This implication also means that quenchers should quench ^{3}c to ^{0}c, and this is not observed experimentally.

The only position where this energy barrier could exist is at the 90° configuration, namely, the ^{3}p configuration, and ^{3}p as defined would no longer exist. The cause for the barrier could be a curve crossing or avoidance between the ground state and triplet state energy curves. Thermochemical studies have shown that the height of the ground state barrier for isomerization can be as high as 50 kcal/mol which would mean it is energetically higher than ^{3}t. Figure 1 shows such a curve avoidance scheme for stilbene. Energy profiles which exhibit curve avoidance can be used to explain the experimental results to date reported for stilbene isomerization via the triplet state. In the extreme case such curves can be described in terms of adiabatic or diabatic expressions, that is, perturbation via kinetic energy terms or spin–orbit coupling terms in the molecular Hamiltonian. Since we are discussing a molecular motion in a solution, which involves a rotation about the central stilbene C=C bond, the adiabatic approximation is probably appropriate, i.e., the nuclear motion is slow. The size of the splitting of the two curves is however a function of the magnitude of the spin–orbit coupling. Thus in this case where we have a soft potential, and spin–orbit coupling of 1–2 cm^{-1}, it is not simple to distinguish which theoretical approximation (diabatic or adiabatic) most closely resembles the true physical picture.

In Figure 1, an energy profile scheme for stilbene including curve avoidance, it is seen that instead of a common ^{3}p configuration, we now have a ^3p_c configuration which is definitely a minimum, together with a ^3p_t configuration which may or may not be a minimum. Such a profile does not contradict Saltiel's deuteration experiments nor the results of quenching experiments. Isomerization still occurs by rotation from ^{3}c and ^{3}p to the ^3p_i configuration from where decay would lead to the ground state. The temperature dependence is explained because isomerization only takes place by crossing over the barrier. Using this model for the isomerization the reaction rates can be written in terms of the following kinetic scheme:

$$^0t \xrightarrow{k_1} {}^3t$$

$$^3t \xrightarrow{k_2} {}^3p_t$$

$$^3p_t \xrightarrow{k_3} {}^0t$$

$$^3t + Q \xrightarrow{k_4} {}^0t + {}^3Q \qquad Q \text{ is a quencher}$$

$$^3p_t \xrightarrow{k_5} {}^3p_c$$

$$^3p_c \xrightarrow{k_6} {}^0c$$

$$^3p_c \xrightarrow{k_7} {}^3p_t$$

$$^0c \xrightarrow{k_8} {}^3c$$

$$^3c \xrightarrow{k_9} {}^3p_c$$

The fourth reaction, quenching, does not have to take place exactly at the transoid configuration, but can take place anywhere along the ^{3}t to ^3p_t profile where the energy gap is sufficiently large that energy transfer to the quencher can take place efficiently. Likewise the third reaction, decay from ^{3}p, can also take place along the profile anywhere from ^3p_t to ^{3}t, but the rate increases greatly as the energy gap decreases. To simplify this kinetic scheme we replace ^3p_t and ^3p_c with ^{3}t and ^{3}c eliminating steps 2 and 9, leaving:

$$^0t \xrightarrow{k_1} {}^3t$$

$$^3t \xrightarrow{k_2} {}^0t$$

$$^3t + Q \xrightarrow{k_3} {}^0t + {}^3Q$$

$$^3t \xrightarrow{k_4} {}^3c$$

$$^3c \xrightarrow{k_5} {}^3t$$

$$^3c \xrightarrow{k_6} {}^0c$$

$$^0c \xrightarrow{k_7} {}^3c$$

The expressions for the initial rates are now given by

$$R_c = \frac{d(c)}{dt} = \frac{k_6 k_4 k_1 (^0t)}{(k_2 + k_3(Q))(k_5 + k_6) + k_4 k_6} \qquad (1)$$

$$^0c(0) = 0$$

$$R_t = \frac{(k_2 + k_3(Q))k_5 k_7 (^0c)}{(k_2 + k_3(Q))(k_6 + k_5) + k_4 k_6} \qquad (2)$$

$$^0t(0) = 0$$

Since there is no quencher in the temperature dependent experiments, eq 1 and 2 reduce to

$$R_c = \frac{k_6 k_4 k_1(^0t)}{k_2k_5 + k_2k_6 + k_4k_6} \quad (3)$$

$$R_t = \frac{k_2 k_5 k_7(^0c)}{k_2k_5 + k_2k_6 + k_4k_6} \quad (4)$$

The rates of isomerization can be written as $R = K\phi$ where K is the rate of excitation and is independent of temperature, and ϕ is the quantum yield. From the measured initial rates, the temperature dependence of the quantum yields can thus be calculated, and the absolute values of ϕ obtained by normalization with reported values of ϕ at room temperature. The quantum yields of isomerization have been measured at room temperature using two techniques: (1) sensitization $\phi(c \rightarrow t) = 0.4$, $\phi(t \rightarrow c) = 0.6$ and (2) direct excitation using a high pressure of oxygen, $\phi(c \rightarrow t) = 0.22$, $\phi(t \rightarrow c) = 0.42$.[16] The latter measurements resemble most closely the experimental methods used in our experiments, and these values were used in our calculations.

From the kinetic scheme given earlier, we see

$$\phi_c = \frac{k_6k_4}{k_2k_5 + k_2k_6 + k_4k_6}$$

$$\phi_t = \frac{k_6k_4}{k_2k_5 + k_2k_6 + k_4k_6}$$

Hence

$$\left[\left(\frac{1}{\phi_c}\right) - 1\right] = \frac{k_2}{k_4}\left(\frac{k_5}{k_6} + 1\right)$$

$$\left[\left(\frac{1}{\phi_t}\right) - 1\right] = \frac{k_6}{k_5}\left(\frac{k_4}{k_2} + 1\right)$$

Only k_4 and k_5 are temperature dependent in these expressions and at low temperature, assuming $k_5/k_6 \ll 1$ and $k_4/k_2 \ll 1$, we can write

$$\left[\left(\frac{1}{\phi_c}\right) - 1\right] = \frac{k_2}{k_4} = \frac{k_2}{A_c}\exp\left(\frac{E_a^c}{RT}\right)$$

$$\left[\left(\frac{1}{\phi_t}\right) - 1\right] = \frac{k_6}{k_5} = \frac{k_6}{A_t}\exp\left(\frac{E_a^t}{RT}\right)$$

where E_a^c and A_c, and E_a^t and A_t are activation energy and preexponential factors for the trans → cis and cis → trans isomerization, respectively. Thus a plot of ln $[(1/\phi_{c,t}) - 1]$ vs. $1/T$ will have a slope equal to $E_{c,t}/R$ if the temperature assumption is true. In Figure 2 our results are shown in this form. Using only the two lowest temperature points we find $E_a^c = 2040$ cal/mol and $E_a^t = 1310$ cal/mol. From this $E(^3p_c) - E(^3p_t) = 730$ cal/mol, Figure 1, which compares favorably to the value for $E(^3p)$; 800 cal/mol, measured by Saltiel. The value of the intercepts in Figure 2 are equal to k_2/A_c and k_6/A_t, respectively. If we assume that A is the same for both k_4 and k_5, then from the intercept magnitudes we find k_2 and k_6 have a ratio of 7.9. With the measured triplet lifetime of 110 ns at room temperature, values of k_2 and k_6 are then given by

$$\frac{k_6}{k_2} \simeq 8, \text{ and } 1.1 \times 10^{-7}\ \text{s} = 1/k_2$$

and therefore $k_2 = 10^7\ \text{s}^{-1}$ and $k_6 = 8 \times 10^7\ \text{s}^{-1}$. From this

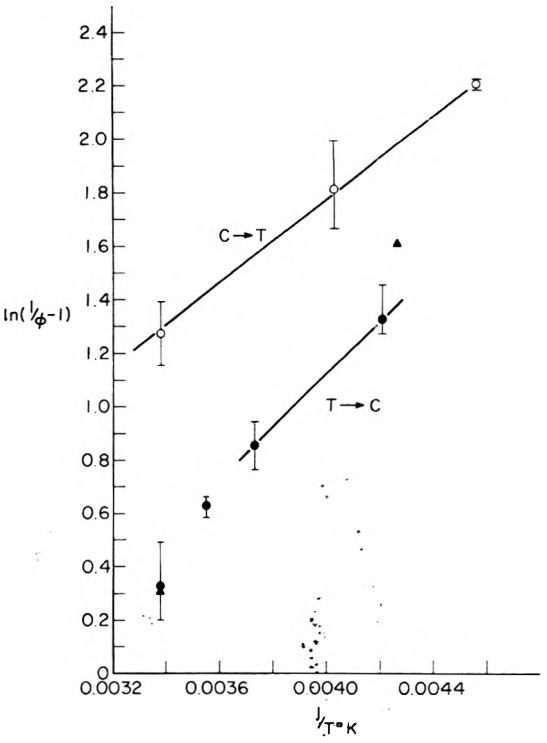

Figure 2. Plot of ln $[(1/\phi) - 1]$ against T^{-1} (K) for cis → trans and trans → cis stilbene isomerization: (O) c → t, (●) t → c in 2MP; (▲) t → c in 2,3DMB.

value of k_2, $A \simeq 2 \times 10^7\ \text{s}^{-1}$. These rate constants are subject to at least a 50% error even if the assumption made above is valid.

The assumption $k_5/k_6 \ll 1$ is really not a good approximation (at 235 K $k_5/k_6 = 0.15$ and at 270 K $k_5/k_6 = 0.21$) and thus extended lower temperature measurements, particularly to lower temperatures, are needed to obtain more accurate activation energies and rate constants, not forgetting that, at lower temperatures, viscosity may become a complicating factor.

(ii) *Isomerization Quenching Results.* In addition to temperature studies on the pure stilbene isomerization, similar experiments were carried out in the presence of triplet quenchers. These latter experiments were all performed at room temperature. Anthracene and azulene were chosen as quenchers, azulene due to its use in earlier studies and anthracene since it is a well-understood molecule with energy bands which are well separated from those of stilbene.

In Table II are shown the effects of the quencher on the trans → cis isomerization initial rates. In these experiments, an unknown but constant amount of xenon was present, hence the larger R_c compared to Table I.

According to our kinetic scheme

$$\left[\left(\frac{1}{\phi_c}\right) - 1\right]_{\text{quenchers}} = \left[\left(\frac{1}{\phi_c}\right) - 1\right]_0 + \frac{(k_5 + k_6)k_3(Q)}{k_6k_4}$$

where

$$\left[\left(\frac{1}{\phi_c}\right) - 1\right]_0 = \frac{k_2}{k_4}\left[\frac{k_5}{k_6} + 1\right]$$

In Figure 3 is plotted $[(1/\phi_c) - 1]_Q$ against quencher concentration of both azulene and anthracene. From the

TABLE II: Initial Stilbene Isomerization Rate Constants for Trans → Cis Isomerization R_c in 2-Methylpentane in the Presence of Triplet Quenchers Anthracene or Azulene[a]

Quencher	Quencher concn, M	$10^5 R_c$,[b] M/M	ϕ_c[b,c]	$(1/\phi_c - 1)$
None		9.73(9.47-10.2)	0.42(0.41-0.44)	1.38(1.44-1.27)
Anthracene	0.005	6.78(6.60-6.97)	0.29(0.285-0.30)	2.45(2.51-2.33)
Anthracene	0.01	5.00(4.80-5.20)	0.216(0.207-0.225)	3.63(3.83-3.44)
Azulene	0.005	1.67(1.60-1.81)[d]	0.072(0.069-0.078)	12.88(13.49-11.82)
Azulene	0.01	1.09(0.90-1.24)[d]	0.047(0.039-0.054)	20.28(24.64-17.52)

[a] A small constant concentration of xenon is present in these samples, hence the slight change in R_c compared to Table I for the neat *trans*-stilbene solution. [b] Mean value and range. [c] Predicted quantum yield. [d] Corrected for azulene absorption.

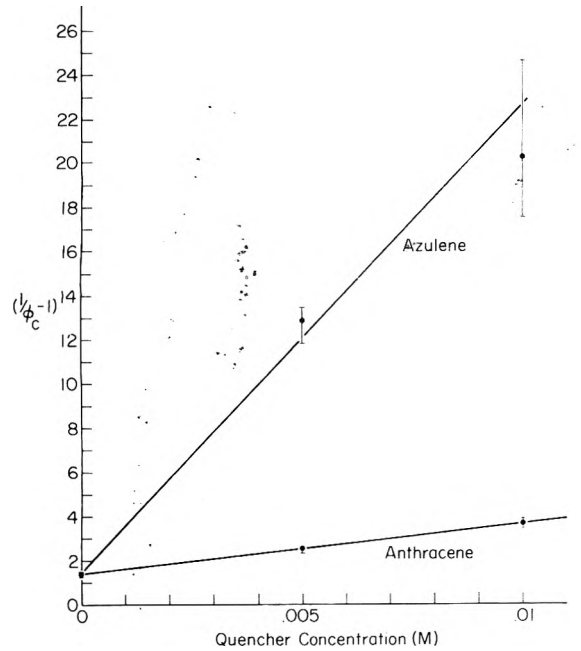

Figure 3. Plot of $[(1/\phi) - 1]$ found for different concentrations of the triplet quenchers anthracene and azulene.

ratio of the slopes of these two lines one obtains k_3(azul)/k_3(anth) = 9.8, in other words, azulene quenches the t → c isomerization with an efficiency 9.8 times greater than anthracene. This is an interesting and confusing result. Before we discuss this result we will derive values of k_3 using our previous values for k_2, k_4, k_5, and k_6. We assume that k_2 and k_6 are not affected by the presence of xenon which is probably a good assumption for the measured R_c value only increased by 1.92 times in the presence of xenon. We then see that

$$k_3(\text{azul}) = 9.4 \times 10^8 (M_Q)^{-1}$$
$$k_3(\text{anth}) = 9.5 \times 10^7 (M_Q)^{-1}$$

Saltiel, using Dainton's measurement of the triplet lifetime of 110 ns,[10] calculated k_3(azul) = $4 \times 10^8 (M_Q)^{-1}$,[10] i.e., the same as our own value within experimental error. Unfortunately Dainton's[10] measured value for k_3(anth) was $2.6 \times 10^9 (M_Q)^{-1}$, much larger than our value for anthracene or azulene, which also of course means that the use of the triplet lifetime of 110 ns is in question. Accepting both of these pulse radiolysis rate constants would mean that measured quantum yields of isomerization are approximately an order of magnitude too large, which seems unlikely in view of the close agreement for ϕ by many workers. More probable is the possibility of photochemical interference in the pulse radiolysis studies. However, we feel that the ratio of k_3(azul):k_3(anth) of ~10:1 is real. One can speculate that this result reflects the different times the stilbene molecule spends in a configuration where the energy gap between its triplet and singlet energy profiles is sufficient to transfer energy to anthracene or azulene. With a soft potential well between the 90° twisted configuration and ^{3}t, the influence of high vibrational quantum numbers is to shift the average position of the stilbene triplet molecule closer to the turning points, and hence quenchers with lower triplet energies would be more efficient.

IV. Summary

Measurements of the initial rate of isomerization for stilbene following direct optical excitation into the stilbene triplet level have been made. It is found that the initial rates of both cis → trans and trans → cis isomerization decrease as temperature decreases, effects which can be interpreted in terms of potential energy curve avoidance at the 90° twisted configuration. Results obtained from triplet sensitization experiments also can be interpreted in terms of this same physical picture. This agreement between results from direct and sensitized experiments shows the validity of the assumptions made in analyzing the latter experimental results.

The presence of an energy barrier for isomerization in both directions means that quantum yields for isomerization via the triplet state are temperature dependent. A simple kinetic analysis based on this model and including the experimental results shows that the overall *trans*-stilbene triplet rate of decay to the trans triplet ground state is about 10 times slower than found for the same cis transition. The preexponential factor for passing over the potential energy barrier is $\sim 10^7$ s^{-1}.

Quenching experiments, with azulene or anthracene as triplet quenchers, have shown azulene to be about 10 times as efficient as a triplet quencher.

Acknowledgment. We wish to thank Dr. W. Siebrand for his interest and participation in discussions concerning this work, and Mr. C. Halpin for valuable technical assistance.

References and Notes

(1) G. Fischer, K. A. Muszkat, and E. Fischer, *J. Chem. Soc. B*, 156 (1968).
(2) G. B. Kistiakowsky and W. R. Smith, *J. Am. Chem. Soc.*, **56**, 638 (1934).
(3) A. V. Santoro, E. J. Barrett, and H. H. Hoyer, *J. Am. Chem. Soc.*, **89**, 4545 (1967).
(4) A. Bylima and Z. R. Garbowski, *Trans. Faraday Soc.*, **65**, 458 (1969).
(5) R. H. Dyck and D. S. McCure, *J. Chem. Phys.*, **36**, 2326 (1962).
(6) G. S. Hammond, J. Saltiel, A. A. Lamola, N. J. Turro, J. S. Bradshaw, D. O. Cowan, R. C. Counsell, V. Vogt, and C. Dalton, *J. Am. Chem. Soc.*, **86**, 3197 (1964).
(7) J. Saltiel, *J. Am. Chem. Soc.*, **90**, 6394 (1968).
(8) G. Heinrich, H. Gusten, F. Mark, G. Olbrich, and D. Schulte-Frohlinde, *Ber. Bunsenges. Phys. Chem.*, **77**, 103 (1973).
(9) F. Dainton, E. A. Robinson, and G. A. Salmon, *J. Phys. Chem.*, **76**, 3897 (1972).
(10) J. Saltiel, D. N. L. Chang, E. D. Megarity, A. D. Rousseau, P. T. Shannon, B. Thomas, and A. K. Uriarte, *Pure Appl. Chem.*, **41**, 559 (1975).
(11) J. Saltiel, O. C. Zafiriou, E. D. Megarity, and A. A. Lamola, *J. Am. Chem. Soc.*, **90**, 4759 (1968).

(12) O. Gegiou, K. A. Muszkat, and E. Fischer, *J. Am. Chem. Soc.*, **90**, 12 (1968).
(13) K. A. Muszkat, D. Gegiou, and E. Fischer, *J. Am. Chem. Soc.*, **89**, 4814 (1967).
(14) H. Greenspan and E. Fischer, *J. Phys. Chem.*, **69**, 2446 (1965).
(15) H. A. Kierstead and J. Turkevich, *J. Chem. Phys.*, **12**, 24 (1944).
(16) J. Saltiel, J. T. D'Agostino, E. D. Megarity, L. Metts, K. R. Neuberger, M. Wrighton, and O. C. Zafiriou, *Org. Photochem.*, **3**, 1 (1971).

γ-Irradiated Hydrocarbon Crystals. Yields, Decay, and Photoreactions of Radicals: Carbanion Formation[1]

D. D. Wilkey, H. W. Fenrick, and J. E. Willard*

Department of Chemistry, University of Wisconsin, Madison, Wisconsin 53706 *(Received August 4, 1976)*

Publication costs assisted by the U.S. Energy Research and Development Administration

The G values of trapped radicals produced by the γ irradiation of polycrystalline n-alkanes at 77 K are independent of carbon number from C_6 to C_{10}, are ~70% higher than in the glassy branched alkanes, and are ~40% higher for the protiated forms than for perdeuterated. In an uncracked single crystal of n-C_6H_{14}, the $G(R\cdot)$ and decay kinetics are consistent with a rapid intraspur decay followed by second-order reaction of randomly distributed radicals, as observed in glasses, in contrast to the "stepwise" decays observed in polycrystalline samples. 30–35% of the radicals produced by γ irradiation of protiated n-alkanes are removable by exposure to 254-nm light, compared to 18% or less in deuterated n-alkanes. Thermally reversible photoisomerization of the remaining radicals occurs. Both the photoinduced removal of radicals and the photoisomerization occur at 4 K as well as at 77 K. Ultraviolet absorption by carbanions formed by the capture of electrons by radicals in γ-irradiated n-C_6H_{14} has been observed, and an upper limit of 0.25 has been set on $G(R:^-)_{initial}$. The carbanion concentration reaches a steady state after a dose of $\sim 2 \times 10^{20}$ eV g^{-1}. Phase effects on $G(R\cdot)$ in polycrystalline cyclohexane have been examined.

Introduction

We report here experiments designed to answer questions about the properties of radicals and the fate of charge carriers in γ-irradiated crystalline and polycrystalline alkanes. These questions, which are important to improved understanding of the radiation chemistry and solid state chemistry of these systems, include the following: (1) Is there a correlation between alkane chain length and radical yield? (2) What are the effects of phase on yield? When a compound can be obtained as either a glass or crystal at the same temperature, are the yields the same? (3) Why are the decay kinetics of radicals in polycrystalline hydrocarbons different (i.e., stepwise with temperature) than in glassy hydrocarbons? (4) Does the photoinduced removal of a limited fraction of trapped radicals, which has been observed in some alkane glasses, also occur in polycrystalline alkanes? (5) Does photoisomerization of radicals and thermal reversal of the process without loss of radical concentration occur in crystalline hydrocarbons as it does in glasses? (6) Do radical populations which differ in their photoresponse differ in ESR saturation characteristics? (7) Does charge stabilization by carbanion formation occur in γ-irradiated crystalline hydrocarbons?

These data have been sought against the background of earlier work on solid hydrocarbons which includes: (1) Evidence that the G values (radicals produced per 100 eV absorbed) of trapped radicals produced from aromatic compounds are more than tenfold lower than for radicals produced from alkanes or alkenes.[2] This has been interpreted[2] as indicating that the probability of bond rupture is related to the energy of the lowest electronic excited state relative to the bond strength. (2) Evidence for intramolecular energy transfer from alkane side chains to aromatic groups,[3] for intermolecular energy transfer to solutes with resultant selective bond rupture in the solute molecules,[4] and for transfer to toluene solute with subsequent luminescence from the toluene.[5] (3) $G(R\cdot)$ in glassy branched chain alkanes is uniformly lower (~3.0) than in polycrystalline n-alkanes (~5.0).[6a,b] (4) $G(R\cdot)$ in deuterated glassy and polycrystalline hydrocarbons in uniformly 30% or more lower than in protiated hydrocarbons,[6a,b] and the localization of bond rupture is different in n-$C_{10}H_{22}$ than n-$C_{10}D_{22}$.[7] (5) Different radicals are formed by γ irradiation of different solid state phases of some compounds.[4c] (6) Trapped hydrogen atoms are not formed by the γ irradiation of hydrocarbon crystals and glasses,[6c] other than CH_4. (7) Optical absorption in the 300–400-nm range,[8a,b] photostimulated luminescence,[8c,d] and photostimulated conductivity[8e,f] indicate carbanion formation and photoionization in hydrocarbon glasses

$$R\cdot + e_t^- \underset{h\nu}{\overset{h\nu(IR)}{\rightleftharpoons}} R:^-$$

(8) Radicals produced by γ radiolysis of hydrocarbon glasses show a relatively rapid time-dependent first-order decay (~50%) resulting from intraspur radical–radical reaction and a slower second-order decay resulting from random encounters.[9] (9) Radicals produced by γ irradiation of polycrystalline hydrocarbons undergo stepwise decay as the temperature is raised to successively higher temperatures, indicating selective softening of crystallites of different sizes, or radical trapping sites of different energies.[10] (10) Different species of radicals in the same polycrystalline pure hydrocarbon matrix show different ESR relaxation times.[11] (11) Paired radicals, as well as more widely separated radicals are formed in both polycrystalline[7,11] and glassy hydrocarbons,[12] the yields of pairs being higher at 4 K than at 77 K.[11c,d] (12) Illumination of trapped radicals in hydrocarbon glasses with 254-nm light accelerates intraspur decay[12b] and causes a reversible change in the ESR spectrum attributable to isomerization[12b] or, alternatively,[13] to C–C bond rupture.

TABLE I: Yields of Trapped Radicals in γ-Irradiated Hydrocarbons at 77 K

Compound	State	G(radicals)[a] Perprotiated	G(radicals)[a] Perdeuterated	$G(R\cdot)_H/G(R\cdot)_D$[b]
n-Hexane	Polycrystal	5.3 ± 0.4 (12)	3.9 ± 0.1 (5)	1.4
n-Hexane	Cracked single crystal	5.2 ± 0.3 (3)		
n-Heptane	Polycrystal	5.6 ± 0.2 (3)	3.6 ± 0.2 (2)	1.6
n-Octane	Polycrystal	5.7 ± 0.3 (3)	4.5 ± 0.4 (2)	1.3
n-Nonane	Polycrystal	5.9 ± 0.1 (2)		
n-Decane	Polycrystal	6.0 ± 1.0 (3)		
Neopentane	Polycrystal	2.5 ± 0.3 (2)		
Cyclohexane	Polycrystal	3.8 ± 0.3 (7)	3.0 ± 0.2 (2)	1.3
Methylcyclohexane	Polycrystal	4.3 ± 0.3 (3)	3.0 (1)	1.4
Benzene	Polycrystal	0.15 ± 0.02 (4)	0.065 ± 0.007 (3)	2.3
3-Methylpentane	Glass	3.0[c]	2.0[c]	1.5
Methylcyclohexane	Glass	3.4 ± 0.4 (6)[d]	2.6 ± 0.2 (4)	1.3
3-Methylheptane	Glass	3.5 ± 0.1 (6)	2.7 ± 0.3 (4)	1.3
3-Ethylpentane	Glass	3.2 ± 0.4 (4)		
3-Methylhexane	Glass	3.0 ± 0.2 (4)		
2-Methylhexane	Glass	3.3 ± 0.2 (4)		
2,4-Dimethylpentane	Glass	3.2 ± 0.3 (4)		
2,4-Dimethylhexane	Glass	3.2 ± 0.3 (4)		
2,5-Dimethylhexane	Glass	3.6 ± 0.3 (4)		
Ethylcyclohexane	Glass	3.7 ± 0.3 (4)		
Isopropylcyclohexane	Glass	3.6 ± 0.1 (3)		

[a] The number of determinations made on each compound is shown in the parentheses. The error limits given are the average deviation from the average. [b] Ratio of the G(radicals) for the protiated form to that for the deuterated form. [c] Values from ref 9, to which determinations in the present work have been normalized.[6a] [d] Two of the data points used in arriving at the G values for each of the last ten compounds in the table are from the work of N. Bremer, M.S. Thesis, University of Wisconsin-Madison, 1975.

(13) Many investigations of radicals in polymers.[14]

Experimental Section

The methods used for sample preparation, γ irradiations, and ESR measurements have been described.[6a]

For photolysis of trapped radicals at 254 nm, γ-irradiated ESR samples under liquid nitrogen were placed in the center of a Vycor spiral low-pressure mercury discharge lamp giving an intensity of ~35 mW cm^{-2} on the sample. For photolysis at 185 nm the lamp was a Suprasil spiral and the finger of the Suprasil sample dewar was enclosed in a box made of interference filters to cut out the 254-nm radiation. Photobleaching of carbanions was accomplished by focusing the light from a General Electric AH-4 lamp, filtered to limit the output to ≥350 nm, on samples in either Suprasil ESR tubes or Suprasil optical cells with 0.25-cm optical path. Optical spectra of semiopaque polycrystalline samples were measured with a Cary-14 recording spectrophotometer equipped with a Sylvania DXN high-intensity lamp.

ESR measurements at temperatures >77 K were made with the sample in the dewar sleeve of a Varian variable temperature (VT) device which passed through the microwave cavity. Temperature measurements were made using a Fluke 2100A digital thermometer with a thermocouple positioned in the VT dewar at the center of the cavity. The control of temperature by cold nitrogen gas flowing through the VT dewar resulted in a vertical temperature gradient of about 0.5° over the 1-cm length of the sample in the sensitive region of the cavity. For any vertical position, and for all temperatures used, the sample temperature was maintained at a constant value within ±0.2°. Two light exposures at 4 K were made with the sample in an Air Products Heli-Tran LTD-3110 unit.

With the exception of methylcyclohexane (MCHx) and cyclohexane (CHx), all glassy and polycrystalline samples were prepared by quench freezing the room temperature liquid to 77 K in liquid nitrogen. MCHx glasses were prepared by quench freezing, while the polycrystalline state was obtained by either slowly cooling from the bottom of the sample, or by warming above the glass–crystal transition point after quench cooling to the glassy state at 77 K. Cyclohexane was prepared in different crystalline phases as described in the literature[15] and noted in the Results section. Each of these phases was investigated in this work. We have grown single crystals of *n*-hexane by placing the sample in the VT dewar at a temperature slightly above the freezing point (178 K) and decreasing the temperature to 173 K over a period of 2–3 h. Further cooling of these crystals at the same rate invariably resulted in their cracking at ~171 K. In two experiments designed to study radical decay in uncracked hexane single crystals, the sample was slowly frozen to a single crystal in a butyraldehyde slush bath at 173 K, irradiated at 173 K in the bath, and transferred to the VT dewar which was set at the desired decay temperature (≥173 K).

Results

Radical Yields. The G values from the present work and earlier work[6] for radical production at 77 K by γ irradiation of five normal alkanes, of eight branched chain alkanes, and of neopentane, cyclohexane, three substituted cyclohexanes, and benzene, including the perdeuterated forms of eight of the compounds, are given in Table I. (Hereafter perdeuterated and perprotiated hydrocarbons will be referred to as "deuterated" and "protiated".) The normal alkanes, cyclohexane, and benzene all crystallize at 77 K, whereas the branched chain alkanes and substituted cyclohexanes form glasses. Methylcyclohexane can be obtained at 77 K in either form.

The average radical yields from the *n*-alkanes (including carbon numbers C_6, C_7, C_8, C_9, C_{10}) are equivalent, i.e., G = 5–6, within the experimental uncertainty. In *n*-hexane, the one case where tests were made on cracked single crystals (obtained by slow freezing to a single crystal near the melting point followed by immersion in liquid nitrogen), as well as on polycrystalline samples (obtained by quenching the liquid at 77 K), the G values were the same in the two types of matrix. The polycrystalline compounds of different structure than the *n*-alkanes give different yields, G = 3.8 for cyclohexane, 4.3 for methylcyclohexane, and 0.15 for benzene. The eleven glasses, including a

variety of branched alkanes and three substituted cyclohexanes, all give yields within the range of 3.0–3.7, which are ~0.7 of the values for the normal alkanes. In every case the radical yield in the protiated form of a compound is greater than in the deuterated form by 40 ± 15%, except for benzene where the yield in the protiated form is higher by a factor of ~2.3.

Cyclohexane forms three distinct crystalline phases:[15] a high temperature face-centered cubic plastic crystal phase (I) stable from the freezing point (279 K) to 186 K, a monoclinic crystal phase stable at temperatures below 186 K (II), and a metastable phase (III) which cannot be maintained above 120 K and may be phase I frozen in by fast quenching. In an endeavor to resolve discrepancies in the literature, we have determined $G(R\cdot)$ for CHx crystals prepared in the following ways: (1) quenched to 77 K, held 2 h at 163 K; (2) frozen at 233 K, cooled in 10° intervals to 183 K, held at 183 K until transition to the low temperature phase was complete, cooled in 5° intervals to 83 K; (3) quenched to 77 K, annealed 41 h at 198 K; (4) quenched to 77 K. ESR measurements were made at 77 K following γ irradiation at 77 K to a dose of 5×10^{19} eV g^{-1}. Sample preparation methods 1–3 are reported to yield the stable phase II, while method 4 produces the metastable crystal phase III. The G values obtained were 4.4, 4.2, 3.8, and 3.8, respectively. Previous determinations gave $G(R\cdot) = 1.2$–1.4 for methods 3[16] and 4[16] and 1.6 for a sample irradiated at 153 K.[3] However, in better agreement with our results, Charlesby et al.[17] report $G(R)$ of 3.1 ± 1.2, independent of the method used to freeze the sample, and Voevodskii et al.[2b] have found 3.8 for samples prepared by method 4. A sample which we have frozen to the stable plastic crystal phase at 196 K, annealed for 47 h at 196 K, and γ irradiated to a dose of 7.5×10^{19} eV g^{-1} at 196 K gave no ESR signal at 196 K 7.5 min after the end of the irradiation, even though 196 K is only 0.7 of the melting point. A signal equivalent to $G(R\cdot) = 0.01$ would have been detected.

Photoeffects on Trapped Radicals in Protiated Matrices. When the protiated forms of *n*-hexane, *n*-heptane, *n*-octane, *n*-decane, or cyclohexane, which have been γ irradiated at 77 K, are exposed at 77 K to a 254-nm intensity of 35 mW cm^{-2} for 30 min or more, the radical concentration decreases by 30–35%, after which it remains constant with continued illumination. A similar decrease (limiting value 23%) has been found for a *n*-hexane sample held at 4 K during the 254-nm exposure, with the γ irradiation and ESR measurements being made at 77 K. Photolysis of *n*-hexane at 77 K with ~7 mW cm^{-2} of 185-nm light for 120 min removed 34% of the radicals, and an additional 120-min exposure caused no further decrease. Qualitatively similar photoinduced decreases in radical concentration, in γ-irradiated 3-methylpentane (3MP), 3-ethylpentane (3EP), and 3-methylheptane (3MHp) glasses and polycrystalline *n*-hexane have been found using a medium-pressure mercury arc with lower 254-nm intensity.[12b]

Concurrent with the loss in radical concentration resulting from exposure of the γ-irradiated protiated normal alkanes and cyclohexane to 254-nm light, there is a dramatic change in the ESR spectra. This is illustrated for *n*-hexane by the contrast between the spectrum of an unphotolyzed sample (Figure 1A) and a sample which has been exposed for 30 min to a 254-nm intensity of 35 mW cm^{-2} (Figure 1C). There is an improvement in resolution, several lines disappear, and the overall width of the spectrum decreases from ~170 to ~120 G. The spectrum showed no further change during a subsequent 15-min

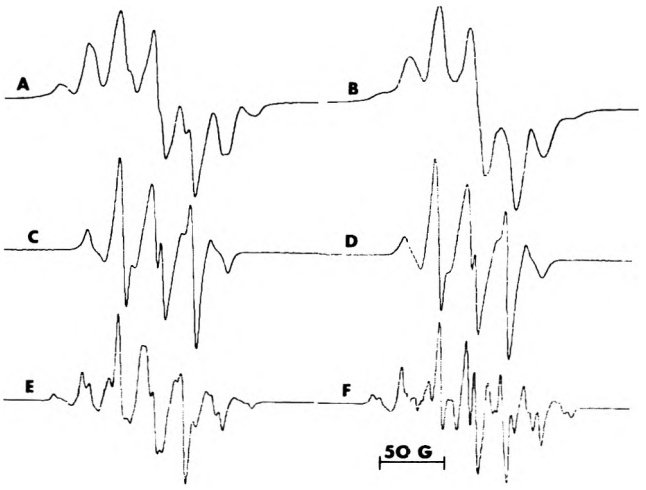

Figure 1. ESR spectra of polycrystalline *n*-hexane γ irradiated at 77 K to a dose of 5×10^{19} eV g^{-1}. A and B are the 77 K spectra at microwave powers of 0.1 and 20 mW, respectively. C and D are 77 K spectra at 0.1 and 20 mW, respectively, after 30-min photolysis with 254-nm light. E and F are the 173-K spectra observed following 120-min thermal decay at 173 K of a photobleached sample and a sample which had not been photobleached, respectively (power = 0.1 mW). In each case the modulation amplitude was 3.2 G.

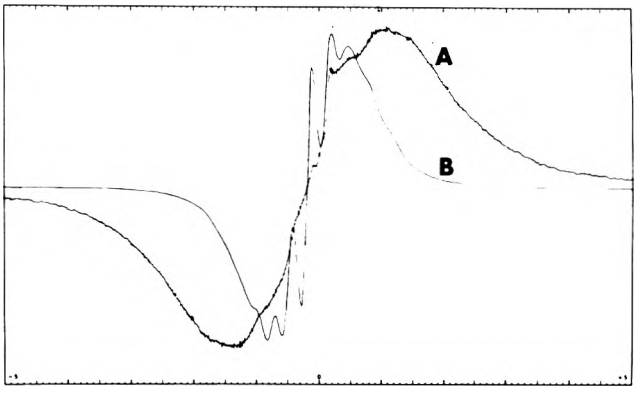

Figure 2. ESR spectra of polycrystalline cyclohexane-d_{12}: (A) after γ irradiation at 77 K to a dose of 5×10^{19} eV g^{-1}; (B) after subsequent 30-min photolysis with 254-nm light. Microwave power, 0.1 mW; modulation amplitude, 3.2 G. Spectrum A was recorded at a fivefold higher gain setting than spectrum B. The spin concentrations determined by double integration are equal.

254-nm exposure, or during storage for 46 h at 77 K, but, as described in a later section, changed to Figure 1E on standing at 173 K. A test with *n*-hexane has shown that the change occurs for 254-nm exposure at 4 K as well as at 77 K, the γ irradiation and measurement being at 77 K.

Photoeffects on Trapped Radicals in Deuterated Matrices. By contrast with the 30–35% reduction in radical concentration caused by exposure of protiated *n*-alkanes to 254-nm light following γ irradiation, the maximum reduction produced in *n*-C_6D_{14}, *n*-C_7D_{16}, *n*-C_8D_{18}, and c-C_6D_{12} were 13, 14, 18, and 0%, respectively.

The ESR spectrum of deuterated polycrystalline cyclohexane following γ irradiation at 77 K is a broad unresolved singlet (Figure 2A) which develops superimposed line structure when exposed to 254-nm radiation (Figure 2B), with no change in spin concentration. Since no chemical isomerization is possible with the symmetrical c-C_6D_{12} molecule the change in spectrum must result from a change in interaction of the unpaired electron with the hydrogen atoms of the radical as a result of change from one rotamer configuration of the ring to another under the influence of the energy of the photon absorbed by the

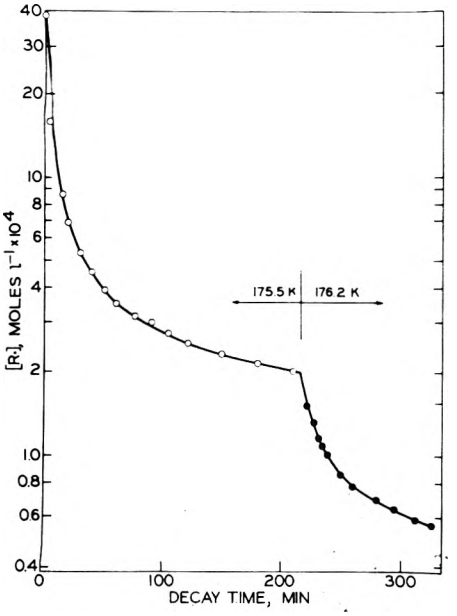

Figure 3. Decay of radicals in severely cracked crystals of *n*-hexane following γ irradiation at 77 K: (O) decay at 175.5 K; (●) decay at 176.2 K. The concentration at zero time was determined at 77 K. All other concentrations were determined at the temperature of decay. The dose was 5 × 10^{19} eV g^{-1}.

TABLE II: Extent of Stepwise Decay of Radicals as a Function of Temperature

Sample	Crystal type	*T*, K	Time, min	Fraction remaining[b]
n-C_6H_{14}	Poly	135	⩽120[a]	0.89
		157	⩽70[a]	0.77
		166	⩽140[a]	0.48
		169.8	60[b]	0.57
		172.6	30[b]	0.50
		173.0	60[b]	0.24
	Cracked single	175.5	110[b]	0.16
		175.5	110[b]	0.10
n-C_6D_{14}	Poly	158	30[a]	0.77
		173	60[a]	0.33
		158.0	20[b]	0.80
		168.0	10[b]	0.65
c-C_6H_{12}	Poly	*c*	30[a]	0.75
		c	60[a]	0.58
		c	120[a]	0.20

[a] Minutes required to reach point where <5% decay occurs in 60 min. [b] Minutes required to reach the "linear" portion of plots such as those of Figures 4 and 5. [c] Three successively higher temperatures in the range about 15 K below the transition temperature of 186 K.

radical. The initial spectrum from c-C_6D_{12} is in contrast to the well-developed structure found immediately after γ irradiation of both deuterated and protiated *n*-alkanes (all polycrystalline), and of protiated branched alkanes (all glasses). However, glassy 3MHp-d_{18}, like the c-C_6D_{12}, gives a broad singlet after γ irradiation and develops resolved structure on 254-nm exposure. Spectra from γ-irradiated MCHx-d_{14} show similar though less dramatic changes.

Thermal Decay of Radicals. No measurable decay of the radicals produced by γ irradiation of the *n*-alkanes studied takes place in 1 week at 77 K. As the temperature is raised, observable decay begins at about 0.8 of the melting point. As previously observed for radicals in γ-irradiated polycrystalline organic compounds[10] and for the metastable products produced by recoil atoms from nuclear processes in organic[18] and inorganic crystals,[19] there is initial rapid decay at each new temperature followed by a decrease in rate to a very low value (i.e., the decay is "stepwise"). This is illustrated for severely cracked crystals

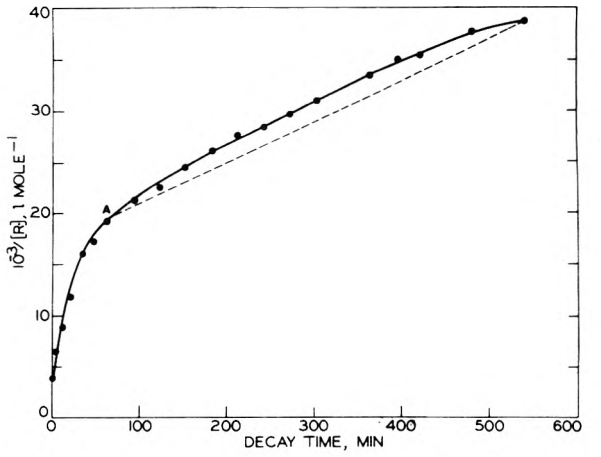

Figure 4. 1/[R·] vs. *t* plot of decay of radicals in polycrystalline *n*-hexane at 173 K following γ irradiation at 77 K. The dose was 5 × 10^{19} eV g^{-1}. Dashed line added to allow easier visualization of changing slope of second-order plot.

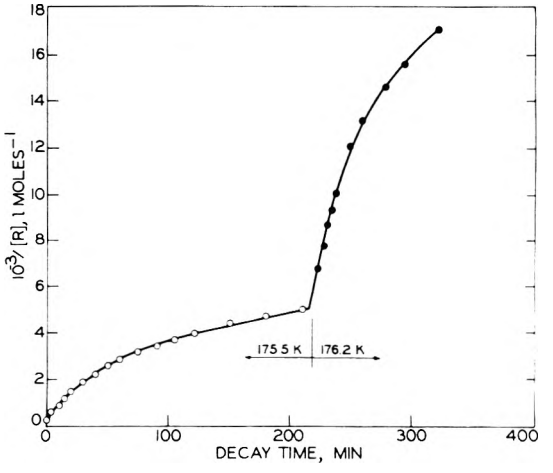

Figure 5. 1/[R·] vs. *t* plot of the data of Figure 3: (O) 175.5 K; (●) 176.2 K.

of *n*-hexane in Figure 3 and we have obtained similar stepwise curves for polycrystalline *n*-hexane-d_{14} and cyclohexane. Table II indicates the fraction of the initial radicals in γ-irradiated *n*-hexane which decayed rapidly at successively higher temperatures. Two methods of defining the "rapid decay" were used. Some samples were held at each temperature until no observable decay (<5%) occurred over a period of 60–120 min. For others, the time indicated in the table is that at which the changing initial slope of a plot of 1/[R·] appears to enter a relatively straight line region (e.g., point A of Figure 4). Neither during the rapid decay nor the slow decay does the decay follow a linear second-order plot (Figure 4). Some decay is observable in *n*-hexane at 135 K which is 0.76 of the melting point of 178 K. 50% rapid decay requires ~166 K or 0.93 of the melting point. A change from 175.5 K (0.98 of the melting point) to 176.2 K after the "linear" decay has been established at 175.5 K changes the differential half-life from ~500 to ~20 min (Figures 3 and 5).

To test the hypothesis[10c] that the stepwise decay is the result of varied softening points of crystallites and surface irregularities of different size and/or strain in the polycrystalline and cracked single crystal samples, we have measured the radical decay in single crystals of γ-irradiated *n*-hexane, starting at the lowest temperature (~173 K) at which they could be prepared without cracking (Figure 6). In contrast to polycrystalline and cracked single crystal

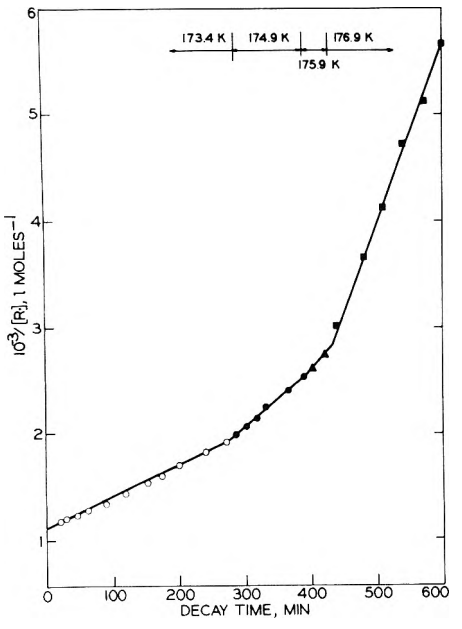

Figure 6. $1/[R\cdot]$ vs. t plot of radical decay in *n*-hexane uncracked single crystal. Decay was followed sequentially at 173.4 K (○), 174.9 K (●), 175.9 K (▲), and 176.9 K (■). The dose was 5×10^{19} eV g^{-1}.

samples (Figures 4 and 5), the uncracked single crystals show no evidence of stepwise decay. The plots of $1/[R\cdot]$ vs. t are linear for all temperatures tested. Since a time-dependent first-order mechanism may give a linear plot of $1/[R]$ vs. t in radiolyzed samples, the linear $1/[R\cdot]$ plots do not unequivocally establish a second-order mechanism. Decay data at the same temperatures for samples which had received different γ doses and hence had different initial concentrations would be required to do so. Such comparisons have not been possible because of the difficulty in obtaining the same temperature for different samples in the range above 173 K where the decay rate is highly sensitive to temperature. However, the $G(R\cdot)$ value in the single crystals at 173 K is only 1.5 ± 0.3 (i.e., ~0.28 of the value at 77 K), suggesting that high localized intraspur concentrations of radicals such as are expected to yield composite first-order decay are not present at the end of irradiation, in which case the straight lines of Figure 6 correctly imply a second-order mechanism.

When a γ-irradiated sample of either cracked single crystals or polycrystalline *n*-hexane-h_{14} is exposed to 254-nm light at 77 K until the radical concentration has reached the minimum value which can be achieved by bleaching (~67% of the initial value) and is then warmed to 172–175 K, the residual radical concentration after completion of the fast thermal decay is about the same as in samples which received no 254-nm exposure. This indicates that the photobleaching at 77 K removes radicals which are part of the same population removed by rapid thermal decay at elevated temperatures.

When a sample that had been photobleached at 77 K was allowed to decay at 172.7 K for 120 min, the ESR signal gradually changed from that of Figure 1C to that of Figure 1E, with an accompanying decrease of 69% in the radical concentration. The radical species which is represented by the two lines which are outermost in the spectra of Figures 1A and 1E but absent in 1C is removed by 254-nm exposure and grows back on standing at 172.7 K. Examination of the wings of the spectrum of Figure 1C at a sensitivity 160 times higher than used for the spectrum in Figure 1A showed that 254-nm photolysis reduced the intensity of the two outermost lines of the unbleached sample by at least 93%, confirming that these lines increase in intensity relative to the inner lines during subsequent thermal decay to the spectrum shown in Figure 1E.

The ESR spectrum for a sample which decayed for 122 min at 172.3 K without prior illumination is shown in Figure 1F. Cooling of the samples of Figures 1E and 1F to 77 K caused no change in the spectra. Subsequent exposure of the samples to 254 nm caused both spectra to revert to that of 1C. This change occurred with no loss in radical concentration, in contrast to the 30% loss which occurred when a γ-irradiated sample was photolyzed prior to decay.

Power Saturation Measurements. The radicals present in polycrystalline *n*-hexane immediately after γ irradiation at 77 K show the onset of ESR power saturation at ~300 μW, while the radicals which remain after 254-nm illumination do not show saturation below 1.2 mW.

At relatively high powers (20 mW) the two outer lines of the unbleached sample are significantly decreased relative to the five major inner lines (Figure 1B as compared to 1A), suggesting that the radical species which is preferentially bleached by 254-nm light, with resultant loss of the outer lines, is also the species which is most easily saturated in the unbleached mixture. The shape of the ESR spectrum of the bleached sample is essentially identical at powers of 0.1 and 20 mW (Figure 1C and 1D), consistent with the conclusion that only one paramagnetic species is present unless there are two or more with the same power saturation characteristics.

Orientation Effects on Radical Spectra. In contrast to the ESR spectra of radicals in organic glasses, where the radicals are produced with random orientation, all of the spectra observed in the crystalline samples of the present work showed differences in total breadth and ESR line structure dependent on the angle of rotation of the sample around its vertical axis in the ESR cavity. These differences were greater for samples frozen in the ESR tube to a single crystal near the melting point and then cooled to 77 K (with accompanying cracking) than for polycrystalline samples prepared by immersing the sample tube from room temperature directly into liquid nitrogen. Typically the cracked single crystals of *n*-hexane showed some 22 detectable lines, similar to earlier results,[20] and gave a change in width of ~40 G between maximum and minimum orientation while the relatively poorly resolved polycrystalline samples showed some 11 distinguishable lines and width change of ~12 G. The anisotropic effects shown by the polycrystalline samples indicate that the crystallites are not produced with completely random orientation. G value determinations were unaffected by orientation or whether the samples were polycrystalline or cracked single crystals.

Carbanion Formation in γ-Irradiated Polycrystalline n-Hexane. γ-Irradiated polycrystalline *n*-hexane shows optical spectra which rise continuously from their high wavelength onset to the limit of the measurements at 300 nm[21] (spectra A and B of Figure 7). Exposure of the samples to the light of an AH4 medium-pressure Hg lamp through a filter which removes wavelengths <340 nm removed most of the radiation-induced absorption (curve C of Figure 7). These results are similar to those attributed to carbanions in 3MHx glass (Figure 7D)[22a] and 3MP glass.[22b] The residual absorption at 300 nm following bleaching may be presumed to be the tail of the spectrum of trapped free radicals which for hydrocarbons typically has a maximum at ~240 nm.[23]

The optical densities at 350 nm for the two experiments of Figure 7 indicate that the carbanion concentration

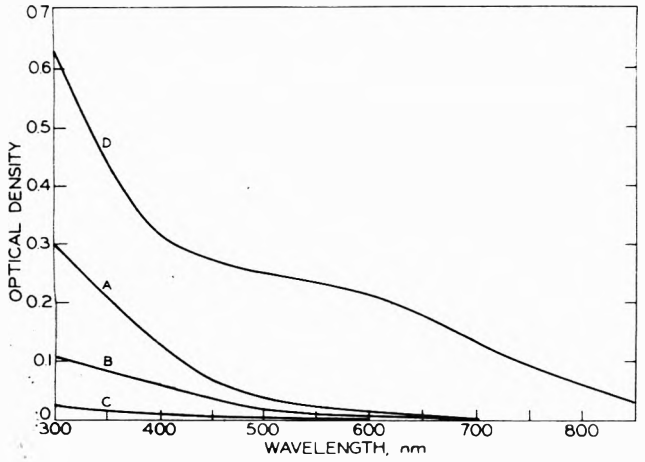

Figure 7. Absorption spectra of γ-irradiated polycrystalline *n*-hexane: (A) following a dose of 1.4×10^{20} eV g^{-1}; (B) following a dose of 7×10^{19} eV g^{-1}; (C) spectrum of sample A after a 15-min exposure to the light of an AH4 lamp filtered to cut out wavelengths <350 nm; (D) spectrum attributed to carbanions in γ-irradiated 3-methylhexane glass.[22a]

increases linearly with dose up to 1.4×10^{20} eV g^{-1}. Another experiment in which a single sample was irradiated to 1.6×10^{20}, 2.4×10^{20}, and 3.2×10^{20} eV g^{-1} without melting showed no change in $R:^-$ concentration over this range, within experimental error, indicating that a plateau or maximum had been reached.

An attempt has been made to determine the concentration of carbanions responsible for the absorption of Figure 7 from the change in radical concentration during bleaching as determined by ESR. Samples of *n*-hexane, *n*-hexane-d_{14}, and cyclohexane-d_{12} which had received doses of 4.7×10^{19} eV g^{-1} were each exhaustively bleached in the ESR cavity with light from the AH4 lamp equivalent to that which removed the carbanion optical spectrum of Figure 7. An additional experiment was done in which an irradiated *n*-hexane sample was exposed outside the ESR cavity to the focused light of the AH4 lamp filtered to remove all light of <350 nm. No change in the doubly integrated first derivative signal (<5%) was observed in any case. This result sets an upper limit on the concentration of the carbanions of <5% that of the radicals, and a limit on their G value of <0.25.

We have examined samples of γ-irradiated polycrystalline hydrocarbons by ESR at powers down to 1 μW for evidence of the singlet signal characteristic of trapped electrons. Consistent with a recent report,[24a] our evidence indicates that electrons are not trapped in these matrices.

Discussion

Radical Yields. The data of Table I allow the following generalizations about radical yields in γ-irradiated polycrystalline and glassy hydrocarbons: (1) for the polycrystalline *n*-alkanes from C_6 through C_{10}, $G(R\cdot)$ values are independent of carbon number, within the experimental uncertainty; (2) $G(R\cdot)$ values are also independent of carbon number for the glassy branched chain alkanes (including methyl and ethyl branching, single branching, and double branching and differences in branching position), but are only ~60% of the values in the polycrystalline *n*-alkanes; (3) the values for polycrystalline cyclohexane, methylcyclohexane, and neopentane are lower than for the polycrystalline *n*-alkanes, and that for benzene is still much lower; (4) complete deuteration lowers the yield by about 40 ± 15% from that of the protiated analogue, essentially independent of structure and glassy vs. crystalline states except for benzene where the effect is much greater; (5) the yield from *n*-hexane is the same in cracked single crystals as in a polycrystalline matrix.

It is also of interest that the $G(R\cdot)$ values for irradiation of 3MP, MCHx, 3MHp, and 3EP glasses[24d] and crystalline $C_{10}H_{22}$[11d] irradiated at 4 K and measured at higher temperatures are not significantly different from those for irradiations at 77 K, but that the yields determined at 4 K following irradiation at 4 K may be higher[11d] than when the determination is made at 77 K.

There is a contrast between our value of 6.0 ± 1 for $G(R\cdot)$ in *n*-$C_{10}H_{22}$ at 77 K and a recent report[11d] of 3.1 ± 0.5 for both *n*-$C_{10}H_{22}$ and *n*-$C_{10}D_{22}$. We have not measured the latter but the data for other compounds in Table I would predict a higher yield for the protiated species. (*Note Added in Proof*: Dr. Iwasaki has just informed us that, due to a numerical error, the 3.1 value should be revised upward and also that it is the average of values for deuterated and protiated samples which were consistently higher for the latter.)

The difference between the yields for the polycrystalline *n*-alkanes and the glassy branched alkanes indicates that either branching, or the amorphous state, or both, favors lower yields. The lower yield for MCHx glass than polycrystalline MCHx demonstrates that, for this compound, the glassy state favors the lower yield. Thus, the nature of the phase (glassy as compared to crystalline), isotopic substitution (i.e., perdeuteration), and possibly chain branching as compared to nonbranching seem to be much more significant in influencing the yield than the carbon number or the specific type of branching.

It has been suggested[6a] that the effect of deuteration on $G(R\cdot)$ in hydrocarbon matrices is due to the change in vibrational energy level spacings with deuteration, which results in less favorable Franck–Condon factors for intersystem crossing, thus decreasing[25] the probability of radiationless loss of excitation relative to radiative loss from excited molecules formed as a result of the ionizing radiation. This shift might be expected to be accompanied by a decrease in bond rupture, although little is known about what factors determine the ratio between bond rupture and loss of energy to the vibrational modes of the matrix for the radiationless deexcitation.

Data on fluorescence yields (θ_f) of photoexcited glassy and crystalline alkanes would be useful in evaluating the hypothesis that competition between radiative and radiationless excitation transfer determines relative G values. In the liquid phase, for which data are available[26] on the effects of branching, deuteration and temperature on θ_f, these yields are all less than 1%, which is inconsequential relative to the changes in G value in the solid state caused by deuteration and by the change from glassy to polycrystalline matrices. However, the θ_f values of the *n*-alkanes increase by more than an order of magnitude (from 6×10^{-4} to 8×10^{-3} for *n*-C_6H_{14}) when the temperature is lowered from 25 to −78 °C,[26] and may be very much higher in the matrices at 77 K. A test of the effect of isotopic substitution on θ_f in the liquid state has given yields of 1×10^{-2} for *n*-C_8D_{18} and 2.5×10^{-3} for C_8H_{18}.[26] This difference is in a direction consistent with the lower $G(R)$ observed for deuterated compounds at 77 K. However, θ_f values for branched alkanes are higher than for *n*-alkanes at 25 °C, whereas $G(R\cdot)$ values at 77 K fall in the opposite order.

It has been suggested[4c] that the data on fluorescence yields in liquid hydrocarbons can be helpful in reasoning as to mechanisms of energy transfer and selectivity in radical formation in hydrocarbon crystals at 77 K. For the reasons noted above, and also because bond rupture se-

lectivity seems to be different in the glassy phase than in the liquid and gas phases of the same compound,[27] such application seems to be precluded.

An early summary[2] of $G(R\cdot)$ for 16 aromatic compounds and 19 other compounds including compounds with nonconjugated double bonds, alcohols, bicyclic and monocyclic alkanes, and branched and linear hydrocarbons shows values of ≤ 0.3 for all of the aromatics and ≥ 3 for nearly all of the others. For cyclohexane, the only compound which was reported in both the present and earlier investigations, agreement is good. The authors suggest that $G(R\cdot)$ is related to the energy of the lowest excited state of the molecule in excess of the C–H bond energy in the compound, consistent with the observation that the estimated first excited state energies are higher than C–H energies in the nonaromatic compounds but about the same or lower than the bond energies in the aromatics. This hypothesis cannot explain the differences between crystalline and glassy and between deuterated and protiated hydrocarbons shown in Table I.

The near equality of $G(R\cdot)$ values of the crystalline *n*-alkanes of Table I with each other and with several bicyclic saturated hydrocarbons of the earlier work, and the independence of $G(R\cdot)$ for the glasses of Table I on the type of chain branching are remarkable, and particularly so when contrasted with the significant effects caused by deuteration and by the glass–crystal phase change. If proton transfer is insensitive to molecular structure changes of the type involved here, but not to deuteration and phase, it could explain the differences. It has been noted[6a] that $G(\text{ion pairs})_{\text{initial}}$ is high enough so that the total radical yields may possibly result from the sequence $RH^+ + RH \rightarrow RH_2^+ + R\cdot$; $RH_2^+ + e^- \rightarrow R\cdot + H_2$.

There is evidence[28] that the radicals formed in the crystalline protiated *n*-alkanes are a mixture of secondary radicals in which those with the radical center at the 2 position predominate for short chains, with other secondary positions becoming more important with increasing chain length. In the perdeuterated *n*-alkanes only the latter are found. In the branched alkanes, all of which are glasses at 77 K, the radical center is predominately on the secondary position of the CH_3CH_2 group of the longest branch.[27] When branching is in the 3 or 4 position, no tertiary radicals are detected but some are found when branching is in the 2 position. This rather high selectivity indicates considerable intramolecular or intermolecular energy migration before bond rupture, as do other lines of evidence.[3-5] It is surprising that this should be accompanied by the uniformities of G value which are observed.

Whereas the $G(R\cdot)$ values for the glassy branched alkanes are the same within experimental error, the G values of electron trapping in the glasses at 77 K[29] vary from 0.02 to 1.1. No correlation would be expected between the yields of C–H rupture and the ability of the matrices to trap electrons, but it is notable that the variations in amorphous structure implied by the variation in $G(e_t^-)$ have no appreciable influence on $G(R\cdot)$.

Thermal Decay of Radicals. The decay of radicals in polycrystalline and cracked single crystal alkanes does not follow second-order kinetics over at least the first 95% of radical removal (e.g., Figures 3–5), although the mechanism may be assumed to be bimolecular combination and disproportionation of radicals. This is in contrast to the decay of radicals in 3-methylpentane glass where 57% disappear by intraspur radical–radical reaction, giving time-dependent first-order kinetics, and the remainder give good second-order plots, indicating removal by random encounters.[9] The ~1.7-fold higher $G(R\cdot)$ values in the crystals suggest that more radicals are formed per spur than in glasses, so that the fraction which decays by intraspur reaction would be larger. This cannot, however, be predicted with certainty since the distance between radical production sites may be altered by differences in the energy transfer, hole migration, or electron migration properties of the two types of phase. Such differences alone would only alter the proportion of second-order decay to time-dependent first-order decay relative to that in glasses.

The data of Figure 6 for decay in uncracked single crystals, which show second-order kinetics with an increased rate constant at each successively higher temperature, but no stepwise effect, support the suggestion[10c] that the shapes of the decay curves for radicals in polycrystalline and cracked single crystal samples are determined by a range of "softening" temperatures which is determined by crystallite sizes and strains.

Photoinduced Removal of Radicals. There are two conceivable mechanisms by which absorption of 254-nm light by radicals in γ-irradiated alkanes at 77 K may promote radical–radical encounters, and hence radical removal by combination or disproportionation. One is by warming the immediate environment of the radicals which absorb photons to a temperature at which they can diffuse and encounter other radicals, and the other is to excite radicals in such a way as to produce migration of the vacant bond by intermolecular or intramolecular hydrogen hopping. Whichever mechanism is responsible, it can only affect radicals within a limited distance of each other. About one third of the radicals in the protiated C_6 to C_{10} normal alkanes and cyclohexane must be within this limiting distance, as indicated by the fraction removed by exhaustive 254-nm illumination. These must be the radicals in closest proximity in the spurs. Consistent with this conclusion, removal of radicals by 254-nm light at 77 K reduces the fraction which decay thermally when the sample is heated to temperatures below the melting point but above the onset of thermal decay.

Assuming an average heat capacity of 0.24 cal g^{-1} °C^{-1} [30] over the temperature range of interest for the crystalline alkanes, it may be estimated that the energy of a 254-nm photon evenly distributed in a sphere of 15-Å radius around a radical would raise the temperature by ~65°. For a sphere of 12-Å radius the increase would be ~125°. In *n*-C_6H_{14} the lowest temperature at which the onset of thermal decay of radicals has been observed is 135 K which is 58 K above the 77 K temperature of illumination. In *n*-decane the onset of decay occurs at ~174 K, 117 K above 77 K. There is some evidence from ESR relaxation time experiments that the radical–radical distances in the spurs in γ-irradiated 3MP glass are <15 Å. From these considerations the photoinitiated thermal diffusion mechanism seems possible. However, this model leads to the prediction of: (1) higher fractional radical removal for matrices with lower softening temperatures, because larger volumes would be heated to the temperature necessary for rapid diffusion to occur; (2) higher fractional radical removal with 185-nm light than 254-nm light, because the energy per photon is 40% higher and so would heat a larger volume; (3) lower fractional radical removal for 254-nm illumination at 4 K than at 77 K. The experimental observations of the present work are contrary to all of these predictions, thus seeming to eliminate the thermal diffusion hypothesis which was proposed earlier.[12b]

The hydrogen hopping hypothesis is attractive as an alternative to the thermal diffusion hypothesis to account

for the photoinduced removal of radicals because it seems more probable that such a process would be independent of the melting point. There is no firm evidence of which we know for the hopping process, but it has been postulated as a mechanism for migration of radical centers in polymers,[14c] and in n-$C_{12}D_{22}$ samples when warmed to 35 and 200 K after γ irradiation at 4 K.[11d]

It is plausible that the smaller fraction of radicals removable by 254-nm radiation in the perdeuterated than in the protiated n-alkanes (13–18% as compared to 30–35%) reflects the presence of fewer radicals per spur, consistent with the lower G values in the deuterated matrices. Cyclohexane for which 30% of the R· are bleachable in the protiated matrix and 0% in the deuterated, and benzene where only 16% are bleachable in the protiated, but 29% in the deuterated must then be cases where the molecular or crystal structures result in unique spatial distributions of the radicals as they are produced.

Photoinduced Changes in ESR Spectra. The changes in the spectrum of γ-irradiated polycrystalline n-C_6H_{14} on increasing the power (Figure 1B compared to 1A) and on exposure to 254-nm light (Figure 1C compared to 1A) indicate that more than one radical is present and that the radicals which saturate more easily are removed by the light. There is evidence[28] that the radicals which saturate more easily are $-CH_2\dot{C}HCH_2-$ type radicals (II) and those which saturate less easily are $CH_3\dot{C}HCH_2-$ type (I). It appears that 254-nm light causes photoisomerization of type II radicals to type I at 77 K while the system relaxes to an equilibrium mixture of I and II at 173 K.[31] Both an intramolecular isomerization and abstraction from an adjacent molecule with reversal by tunneling must be considered as possible mechanisms. Similar effects have been observed in glassy hydrocarbon matrices in our laboratory[12b] and by others.[32] The present work has shown that the photoisomerization process in n-hexane occurs at 4 K as well as 77 K.

Although the 30–35% loss in radical concentration produced by 254-nm exposure is accompanied by the Figure 1A to 1C spectral change, the radical loss and the spectral change are independent processes. This is evident from the effect of 254-nm light in converting the radical population represented by E and F of Figure 1 to that of C without loss in radical concentration. It is further evident that the photoactivated combination of radicals which reduces the initial spin concentration is not limited to radicals of only type I or only type II since the maximum decrease in radical concentration caused by the light is independent of the length of the carbon chain, whereas the fraction of the radicals which are type II increases with increasing chain length from 34% in n-C_6H_{14} to 57% in n-$C_{19}H_{22}$.[28]

Carbanion Formation. The data of Figure 7 and the related observations reported in the Results section indicate that carbanions are formed during the γ irradiation of n-hexane crystals at 77 K, but with a low G value. The low G value indicates that the absence of physically trapped electrons in γ-irradiated polycrystalline hydrocarbons[24a] is not due to their capture by free radicals but rather to a higher probability than in glassy matrices of their encountering and being neutralized by cations. The steady state reached by the carbanion concentration as the dose is increased in the range of 1.4×10^{20} to 2.4×10^{20} eV g^{-1} is similar to the leveling off of the concentration of trapped electrons in hydrocarbon glasses,[33] but occurs at a somewhat higher dose. Unlike the e_t^- concentration in glasses, the R:$^-$ does not pass through a maximum and then decrease, at least up to 3.2×10^{20} eV g^{-1}. Assuming G(R:$^-$) = <0.25 for the carbanion production, it may be estimated that the steady state concentration is $<10^{-2}$ mol %. Among the mechanisms which may account for the removal are the encounter of freshly formed migrating positive charge with carbanions before the positive charge is trapped, and tunneling of electrons from carbanions to cations as their average proximity increases with increasing concentration.

References and Notes

(1) This work has been supported in part by the U.S. Energy Research and Development Administration under Contract No. AT(11-1)-1715 and by the W. F. Vilas Trust of the University of Wisconsin.
(2) (a) Y. N. Molin, I. I. Chkheidze, N. Y. Buben, and V. V. Voevodskii, *Kinet. Katal.*, **2**, 192 (1961); (b) V. V. Voevodskii and Y. N. Molin, *Radiat. Res.*, **17**, 366 (1962).
(3) Y. N. Molin, I. I. Chkheidze, A. A. Petrov, N. Y. Buben, and V. V. Voevodskii, *Dokl. Akad. Nauk*, **131**, 125 (1960).
(4) (a) T. Miyazaki, T. Wakayama, M. Fukaya, Y. Saitake, and Z. Kuri, *Bull. Chem. Soc. Jpn.*, **46**, 1030 (1973); (b) M. Fukaya, T. Wakayama, T. Miyazaki, Y. Saitake, and Z. Kuri, *ibid.*, **46**, 1036 (1973); (c) M. Kato, Y. Saitake, T. Miyazaki, and Z. Kuri, *ibid.*, **46**, 2004 (1973); (d) T. Gillbro and A. Lund, *Chem. Phys. Lett.*, **27**, 300 (1974).
(5) T. Miyazaki, Y. Saitake, Z. Kuri, and S. Sakai, *Bull. Chem. Soc. Jpn.*, **46**, 70 (1973).
(6) (a) D. D. Wilkey, H. W. Fenrick, S. L. Hager, N. Bremer, and J. E. Willard, *J. Chem. Phys.*, in press; (b) N. Bremer, M.S. Thesis, University of Wisconsin–Madison, 1975; (c) D. Timm and J. E. Willard, *J. Phys. Chem.*, **73**, 2403 (1969).
(7) T. Gillbro and A. Lund, *J. Chem. Phys.*, **61**, 1469 (1974).
(8) (a) A. Ekstrom, R. Suenram, and J. E. Willard, *J. Phys. Chem.*, **74**, 1888 (1970); (b) D. P. Lin and J. E. Willard, *ibid.*, **78**, 1135 (1974); (c) V. J. Nikol'skii, V. A. Tochin, and N. Ya. Buben, *Fiz. Tverd. Tela*, **5**(8), 2248 (1963); (d) T. B. Truong, A. Bernas, and J. Roncin, *J. Phys. Chem.*, **78**, 867 (1974); (e) B. S. Yakovlav and E. L. Frankevich, *Isv. Akad. Nauk. SSSR, Ser. Khim.*, **3**, 402 (1966); (f) J. E. Willard, *Int. J. Radiat. Phys. Chem.*, **4**, 405 (1972).
(9) M. A. Neiss and J. E. Willard, *J. Phys. Chem.*, **79**, 1469 (1974).
(10) For examples and references see: (a) D. K. Ermolaev, Yu. N. Molin, and N. Ya. Buben, *Kinet. Katal.*, **3**, 58 (1962); (b) D. K. Ermolaev, Yu. N. Molin, and N. Ya. Buben, *ibid.*, **3**, 314 (1962); (c) A. I. Mikhailov, Ya. S. Lebedev, and N. Ya. Buben, *ibid.*, **6**, 48 (1965); (d) R. Bensasson, M. Durup, A. Dworkin, M. Magat, R. Marx, and H. Swarc, *Discuss. Faraday Soc.*, **36**, 177 (1963).
(11) (a) M. Iwasaki, T. Ichikawa, and T. Ohmori, *J. Chem. Phys.*, **50**, 1991 (1969); (b) T. Gillbro, P. O. Kinnell, and A. Lund, *J. Phys. Chem.*, **73**, 4167 (1969); (c) T. Gillbro and A. Lund, *Chem. Phys. Lett.*, **34**, 375 (1975); (d) M. Iwasaki, K. Toriyama, H. Muto, and K. Nunome, *J. Chem. Phys.*, **65**, 596 (1976).
(12) (a) D. P. Lin and J. E. Willard, *J. Phys. Chem.*, **78**, 2233 (1974); (b) E. D. Sprague and J. E. Willard, *J. Chem. Phys.*, **63**, 2603 (1975).
(13) (a) M. Ya Mel'inkov, V. I. Sklyarenko, and N. V. Fok, *Dokl. Akad. Nauk SSSR*, **218**, 875 (1974)[*Dokl. Phys. Chem.*, **218**, 939 (1975)]; (b) V. I. Sklyarenko, M. Ya Mel'inkov, and N. V. Fok, *J. Chem. Soc., Chem. Commun.*, 167 (1975).
(14) See for example: (a) S. Nara, S. Shimada, H. Kashiwabara, and J. Sohma, *J. Polym. Sci.*, **6**, 1435 (1968); (b) M. Iwasaki, T. Ichikawa, and T. Ohmori, *J. Chem. Phys.*, **50**, 1984 (1969); (c) M. Dole in "The Radiation Chemistry of Macromolecules", Vol. I, M. Dole, Ed, Academic Press, New York, N.Y., 1972, p 335.
(15) (a) M. Renaud and R. Fourme, *J. Chim. Phys.*, **63**, 27 (1966); (b) R. Kahn, R. Fourme, D. Andre, and M. Renaud, *Acta Crystallogr., Sect. B*, **29**, 131 (1973).
(16) (a) H. Swarc and R. Marx, *J. Chim. Phys.*, **57**, 680 (1960).
(17) A. Kabi, A. D. Lenherr, M. G. Ormerod, and A. Charlesby, *Int. J. Radiat. Phys. Chem.*, **1**, 45 (1969).
(18) K. E. Collins and J. E. Willard, *J. Chem. Phys.*, **37**, 1908 (1962).
(19) For examples and references see: G. Harbottle and N. Sutin, *Adv. Inorg. Chem.*, **1**, 268 (1959); G. Harbottle, *Ann. Rev. Nucl. Sci.*, **15**, 89 (1965).
(20) T. Gillbro, P. Kinell, and A. Lund, *J. Phys. Chem.*, **73**, 4167 (1969).
(21) (a) Each of these samples had been exposed to $1–2 \times 10^{20}$ eV g^{-1} in previous experiments before melting and refreezing for this experiment. (b) The 300-nm limit was determined by the increasingly intense light scattering by the polycrystalline matrix at lower wavelengths.
(22) (a) G. C. Dismukes, Ph.D. Thesis, University of Wisconsin–Madison, 1975; (b) D. P. Lin and J. E. Willard, *J. Phys. Chem.*, **78**, 2233 (1974).
(23) For example and references see: N. Bremer, B. J. Brown, G. H. Morine, and J. E. Willard, *J. Phys. Chem.*, **79**, 2187 (1975).
(24) (a) T. Ichikawa and H. Yoshida, *Int. J. Radiat. Phys. Chem.*, **8** 391 (1976), (b) Determined by Dr. Toyoaki Kimura in our laboratory.
(25) For examples and references see: (a) B. T. Henry and W. Siebrand in "Organic Molecular Photophysics", Vol. I, J. B. Birks, Ed., Wiley, New York, N.Y., 1973; (b) B. Brocklehurst, *Radiat. Res. Rev.*, **2**, 149 (1970); (c) A. H. Kalantar, *Chem. Phys.*, **1**, 207 (1973); (d) T. E. Martin and A. H. Kalantar, *J. Chem. Phys.*, **48**, 4996 (1968).

(26) (a) W. Rothman, F. Hirayama, and S. Lipsky, *J. Chem. Phys.*, **58**, 1300 (1973); (b) S. Lipsky in "Chemical Spectroscopy and Photochemistry in the Vacuum Ultraviolet", C. Sandorfy, P. J Ausloos, and M. B. Robin, Ed., D. Reidel Publishing Co., Boston, Mass., 1974, pp 495–512.
(27) D. J. Henderson and J. E. Willard, *J. Phys. Chem.*, **91**, 3014 (1969).
(28) T. Gillbro and A. Lund, *Chem. Phys.*, **5**, 283 (1974).
(29) T. Kimura, N. Bremer, and J. E. Willard, *J. Chem. Phys.*, in press.
(30) D. R. Douslin and H. M. Huffman, *J. Am. Chem. Soc.*, **68**, 1704 (1946).
(31) The differences in the spectra of Figure 1F and 1E are probably due to differences in orientation. It is of interest that 1F is essentially identical with the spectrum reported for a cracked single crystal of n-C_6H_{14} at 77 K immediately after irradiation.[20]
(32) See references given in ref 12b.
(33) The properties of trapped electrons in organic glasses are reviewed and references given in J. E. Willard, *J. Phys. Chem.*, **79**, 2966 (1975).

Reactions of Radiation-Induced Free Radicals in Solid Halodeoxyuridines. Single Crystals of 5-Chloro- and 5-Bromodeoxyuridine

J. Hüttermann,* W. A. Bernhard,[2] E. Haindl, and G. Schmidt

Institut für Biophysik und Physikalische Biochemie, Universität Regensburg, D-8400 Regensburg, West Germany

(Received August 17, 1976)

Publication costs assisted by Universität Regensburg

The kinetics of the decay and the formation of three different radicals formed by X irradiation of both 5-chloro- (ClUdR) and 5-bromodeoxyuridine (BUdR) has been measured by ESR spectroscopy of single crystals between about 90 K and room temperature. Two of the radicals reside on the ribose moiety, the third is located at the pyrimidine base. The reaction sequence is found to start from a radical which results from hydrogen abstraction of the $O_{5'}$ position in the sugar. This alkoxyl radical decays between about 90 and 120 K under concurrent formation of another ribose-located radical at position $C_{5'}$. The apparent activation energy for this process is 5 ± 1 kcal/mol (ClUdR) and 7 ± 1 kcal/mol (BUdR). Between about 200 and 240 K, the $C_{5'}$-centered radical converts into a pyrimidine base radical which is formed by hydrogen addition to carbon C_6 of the 5,6 double bond. An activation energy for the latter reaction cannot be given because of kinetic irregularities brought about by crystal phase transitions in both ClUdR and BUdR in this temperature region. The possible mechanisms for the two conversion reactions and their relation to radiation-damage pathways in nucleic acid constituents are discussed.

Introduction

The radiation chemistry of the nucleic acid constituent analogues deriving from 5-halogen-substituted uracil has attracted considerable interest owing to their radio-sensitizing properties when incorporated into nucleic acids.[3] Electron spin resonance (ESR) studies in dilute aqueous solutions[4] or glasses[5,6] in accord with other radiation-chemical findings[7] have brought about the view that halogen elimination from the base upon dissociative electron attachment or OH· radical attack is a major reaction pathway for all halogen substituents except fluorine and, to a lesser extent, chlorine. As a consequence, the σ type uracilyl radical resulting from dehalogenation has been inferred to mediate the sensitizing reactions of the halo uracils in nucleic acids.[8,9]

These findings contrast with ESR studies at room temperature on single crystals of the deoxyribosides 5-chloro- (ClUdR), 5-bromo- (BUdR), and 5-iododeoxyuridine (IUdR) in which α halogen radicals RCH_2–$\dot{C}$–hal–R′ formed effectively by hydrogen addition to the 5,6 double bond of the pyrimidine base have been observed as dominant species.[10-12] In view of this apparent discrepancy we have sought to gain more information about the radiation-induced free-radical reactions in solid halo deoxyuridines. We have examined single crystals of ClUdR and BUdR between 4.2 K and room temperature. Among others, major concentrations of two radicals in the sugar moiety were detected between about 30 and 240 K in both crystal systems. One of these is formed by hydrogen abstraction from the $O_{5'}$ position (I). Similar alkoxyl type

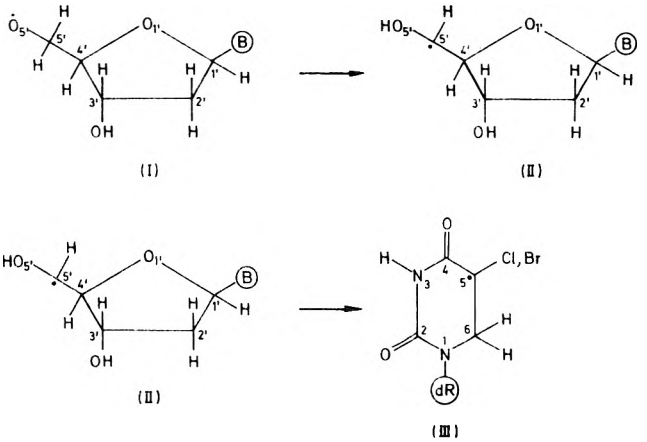

radicals have been observed in serine,[13] thymidine,[14] and in an arabinoside derivative of uracil.[15] The second deoxyribose-located radical (II) is centered at the $C_{5'}$ position. Its spectral parameters are analogous to those of related radicals observed in deoxyadenosine[16] and 3′-cytidylic acid.[17]

The two sugar radicals were found to be linked in a decay-formation type reaction from radical I to radical II. In a further process, the decay of the latter radical was found to be connected to the formation of the α-halogen radicals (III) which are stable at room temperature. The present report deals with the kinetic measurements of the two reactions in both ClUdR and BUdR single crystals. A detailed description of the spectral parameters of

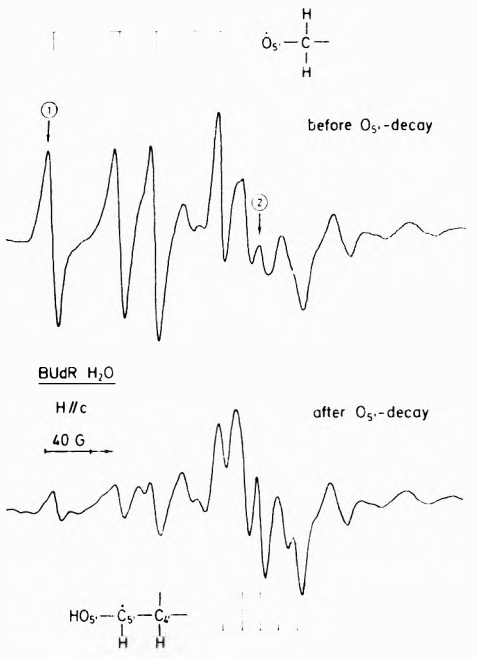

Figure 1. ESR spectra of BUdR single crystals in the orientation $H \| c$ before (top) and after (bottom) decay of $C_{5'}$ radicals showing conversion to the C_5 species. Stick diagrams refer to line positions of both radicals. Lines 1 and 2 are used in the kinetic evaluation.

radicals I and II will be given elsewhere.

Experimental Section

The experimental procedures for crystal growing, X irradiation, and ESR measurements have been described previously.[18] ClUdR and BUdR grow as isomorphous monoclinic crystals of space group $P2_1$ with two molecules in the unit cell.[19,20] For ESR measurements an orthogonal axis set a^*bc was chosen containing the crystallographic b and c axes. Radical decay and formation was measured at X-band frequencies with crystals irradiated at 77 K to about 10 Mrads and placed in a conventional variable temperature insert (Varian E-257). The sample temperature was monitored continuously with a chromel–alumel thermocouple mounted about 2 cm away from the crystals in thermal contact with the stainless-steel crystal holders.

Results

1. $\dot{O}_{5'} \rightarrow \dot{C}_{5'}$ *Conversion.* Radical I, abbreviated $\dot{O}_{5'}$ to indicate the site of its main unpaired spin-density concentration, is characterized by a quartet pattern of nearly isotropic component spacings of about 55 and 85 G due to interaction with the two β protons at carbon $C_{5'}$. Its g factor is highly anisotropic ranging from about 2.09 to 1.99. This latter feature provides for crystal orientations in which overlap with lines of other radicals centered around the free-spin g factor is minimal. One such orientation is $H \| c$ for which the spectrum is shown in Figure 1, using BUdR as the sample compound. ClUdR shows nearly identical features. The four-line stick spectrum of $\dot{O}_{5'}$ is indicated above the spectrum. The group of five lines of intensities 1:2:2:2:1 centered near the free-spin g factor in Figure 1 arises from radical II, abbreviated $\dot{C}_{5'}$, which shows hyperfine interaction to an α proton, the β proton at $C_{4'}$, and the $OH_{5'}$ proton. Its center lines are free from overlap with lines from $\dot{O}_{5'}$ in this specific orientation.

The $\dot{O}_{5'}$ radical is formed upon irradiation below 77 K and is unstable at 77 K but reasonable decay times cannot be measured below about 90 K. Figure 2 shows a typical plot of the peak-to-peak intensity of the first quartet line

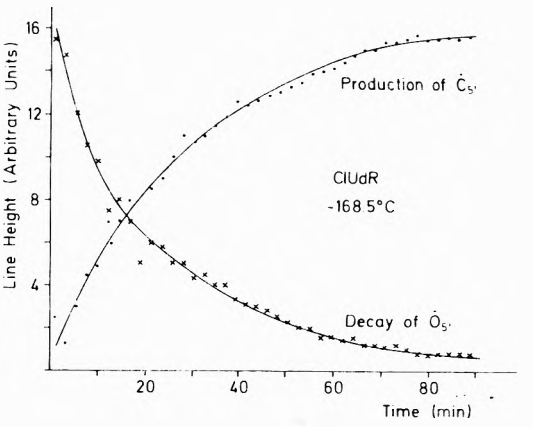

Figure 2. Linear plot of the decay of $\dot{O}_{5'}$ and the formation of $\dot{C}_{5'}$ in ClUdR at −168.5 °C.

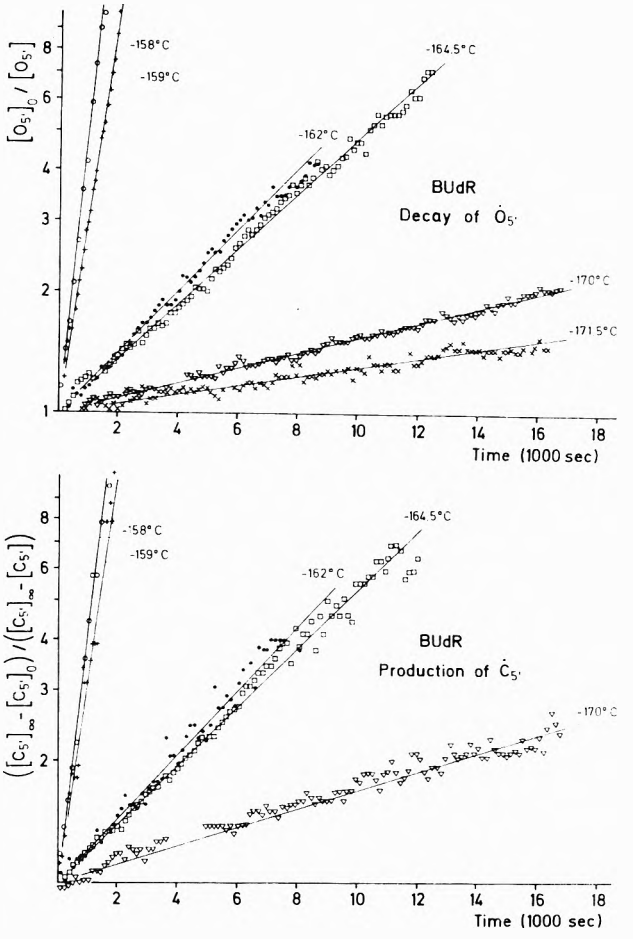

Figure 3. Normalized semilog plot of the decay of $\dot{O}_5$ (left) and the production of $\dot{C}_{5'}$ (right) in BUdR at various temperatures of measurement.

in Figure 1 (encircled 1) vs. the time which is obtained in the temperature range between 90 and 120 K. Concurrent with the decay of the $\dot{O}_{5'}$ radical indicated by the line-intensity decrease is the formation of $\dot{C}_{5'}$ judged from the increase of the peak-to-peak intensity of one of the center lines in Figure 1 (encircled 2) at the same temperature which is also plotted in Figure 2.

Similar decay–formation curves were measured for a variety of temperatures in both ClUdR and BUdR using freshly irradiated crystals for each temperature. Differences in the irradiation dose resulted in varying relative concentrations of $\dot{O}_{5'}$ vs. $\dot{C}_{5'}$. In order to assess the kinetic behavior of the conversion, the linear curves were normalized and plotted on a semilogarithmic scale. The results are given in Figure 3 for BUdR as an example.

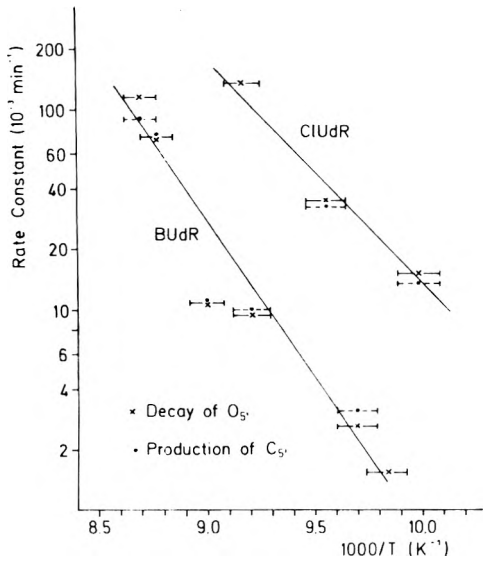

Figure 4. Arrhenius graph of the rate constants for the conversion $O_{5'} \rightarrow C_{5'}$ in BUdR and ClUdR vs. temperature.

Similar findings were obtained in ClUdR except that the reactions were shifted to lower mean temperatures by about 7 °C as judged from the values of the reaction constants. At each temperature in Figure 3, the $O_{5'}$ decay and the $C_{5'}$ production curves are approximately linear and have a nearly identical slope. This result suggests that the reaction should be of first order and that the conversion is nearly 1:1. Under these assumptions, the first-order rate constants k can be evaluated from the equations

$$\ln ([d_0]/[d]) = k_d t \quad (1)$$

$$\ln \{([p_\infty] - [p_J])/([p_\infty] - [p])\} = k_p t \quad (2)$$

where the letters d and p refer to decay and production, respectively. In these equations, $[d_0]$ and $[p_0]$ are the initial concentrations and $[p_\infty]$ is the asymptotic value of the linear production curve. The determination of this latter value is, besides the uncertainty in the temperature which was estimated to be correct within 1 °C, the main source of error in the kinetic analysis of the production process both for slow and fast experimental runs. For the former, nitrogen consumption is the limiting factor preventing measurements above about 6 h. In fast runs, especially when the initial concentration of the product was substantial, asymptotic values for the production were often not obtainable owing to too much scatter of the experimental points. The best set of reaction constants obtained plotted as a function of the temperature for both the decay of the $O_{5'}$ radical and the production of the $C_{5'}$ radical in ClUdR and BUdR is presented in Figure 4. Using the Arrhenius equation

$$k_{d,p} = f_{d,p} \exp(-\Delta E_{d,p}/kT) \quad (3)$$

activation energies $\Delta E_{d,p}$ of 5 ± 1 kcal/mol (ClUdR) and 7 ± 1 kcal/mol (BUdR) are obtained for the conversion. Insertion of these values in eq 3 yields preexponential or "frequency" factors $f_{d,p}$ of about 1×10^9 and 2×10^{12} min^{-1}, respectively. The larger activation energy and the higher preexponential factor for BUdR reflect the finding that the mean temperature of conversion is slightly higher in this crystal system as compared to ClUdR.

2. $C_{5'} \rightarrow$ *5-yl Conversion.* Warming of single crystals of ClUdR and BUdR to higher temperatures results in the decay of the $C_{5'}$ radical and concurrent formation of the α-halogen radical (III), abbreviated 5-yl according to its

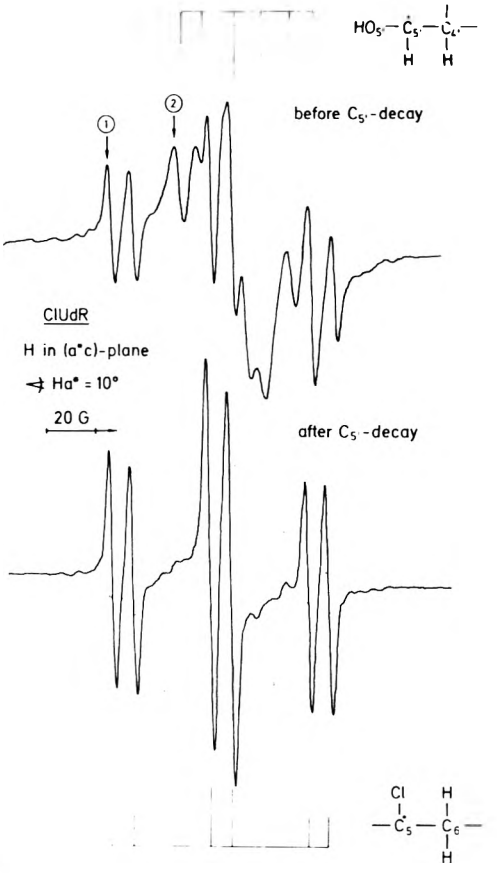

Figure 5. ESR spectra of ClUdR single crystals with the magnetic field in the a^*c plane before (top) and after (bottom) decay of the $C_{5'}$ radical showing conversion to the 5-yl α-chloro radical. Stick diagrams indicate line positions of both radicals. Marks 1 and 2 refer to lines used in kinetic measurements.

main site of spin-density localization on the pyrimidine ring. Again, varying concentrations of the 5-yl radical are present already before the conversion takes place. This may be visualized from the lower spectrum in Figure 1 in which all lines not marked by the $C_{5'}$ stick diagram are associated with the α-bromo radical in BUdR.[10] The kinetic data were taken at crystal orientations where overlap from lines of the two radicals is minimal. In ClUdR, one such orientation, where the magnetic field in the a^*c plane is about 10° off the a axis, is shown in Figure 5. The α-chloro radical (III) exhibits a gross triplet pattern resulting from the two β protons at C_6 together with a chlorine "doublet" subsplitting[12] as is indicated by the stick diagram beneath the bottom half spectrum.

A normalized semilog plot of the increase of line 1 indicating the production of the 5-yl radical and of the decrease of line 2 as a measure for the decay of the $C_{5'}$ species vs. time is shown in Figure 6 for a variety of temperatures. Apparently, there are kinetic irregularities since the steepness of the slope of the curves does not increase steadily with the temperature. However, the curves are linear indicating a first-order process and, in addition, at each temperature, the slope for the decay curve is identical with that of the production curve. This documents the connection between $C_{5'}$ decay and the 5-yl formation.

The irregular kinetic behavior which prevents the evaluation of an activation energy for the $C_{5'}$ conversion is probably due to higher-order phase transitions which have been observed in both BUdR and ClUdR in the temperature range from −10 to −60 °C.[21] They may cause a dependence of the rate constants on the "history" of the crystals used in the actual experiments, i.e., on the velocity

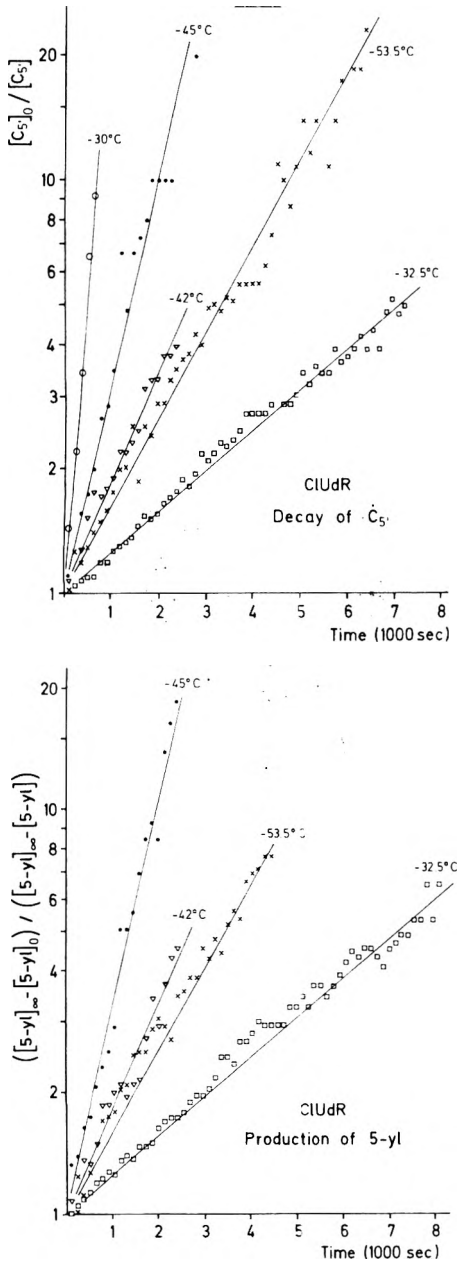

Figure 6. Normalized semilog plot of the decay of $\dot{C}_{5'}$ (left) and the production of 5-yl radicals (right) in ClUdR at various temperatures of measurement.

of the warming of the crystal from the irradiation temperature 77 K to the temperature of measurement. Other factors, such as the geometrical arrangement of the molecules, may also influence the rate constants. In view of this we restricted the measurements of the $\dot{C}_{5'}$ decay and 5-yl formation in BUdR to one temperature. These results, given in Figure 7, demonstrate again the first-order behavior of the conversion.

Discussion

The kinetic measurements have shown the occurrence of a two-step reaction pathway in ClUdR and BUdR involving deoxyribose radicals as primary and secondary species and the α-halogen base radical as tertiary product. The first radical in this sequence, the alkoxyl-type $\dot{O}_{5'}$ species, has been considered the result of a pristine event of radiation, the oxidation of the molecule.[13,14]

Its conversion to the $\dot{C}_{5'}$ radical most probably involves hydrogen abstraction which is known to be the common mode of reactions of alkoxy radicals.[22] The process could

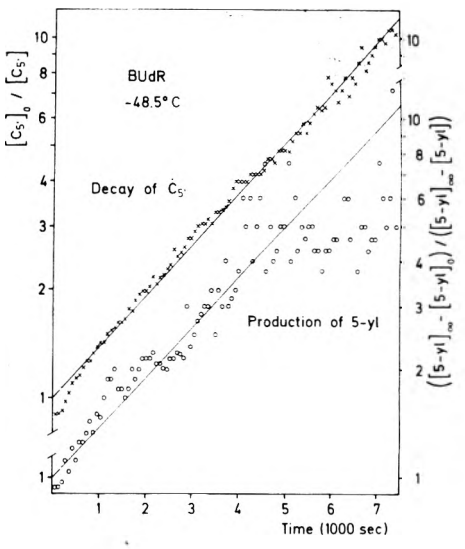

Figure 7. Normalized semilog plot of $\dot{C}_{5'} \rightarrow$ 5-yl conversion in BUdR at −48.5 °C.

be intramolecular from the adjacent $C_{5'}$ position or intermolecular. In the former case, the hyperfine interaction to the OH proton in the $\dot{C}_{5'}$ radical should involve a nonexchangeable hydrogen. Experiments with ClUdR and BUdR crystals grown from D_2O show unequivocally that the OH proton is exchanged. Therefore, the alkoxy radical should convert to $\dot{C}_{5'}$ via an intermolecular process. We propose that it abstracts a hydrogen from the $C_{5'}$ position of a neighboring molecule forming the $\dot{C}_{5'}$ radical there. According to the crystallographic data, the hydrogen atom in question is about 2.7 Å away from the $\dot{O}_{5'}$ locus making its abstraction quite feasible.

The conversion of the $\dot{C}_{5'}$ radical to the α-halogen species is probably more complex in nature. Again, experiments with deuterated crystals shed some light on the reaction. Thus, both at 77 K and room temperature the spectra exhibit a mixture of α-halogen radicals resulting from H and D addition to carbon C_6 of the base. However, when crystals, irradiated at 77 K are warmed slowly to room temperature, only the concentration of the H-adduct radicals increases. Therefore, the decay of the $\dot{C}_{5'}$ radical involves the liberation of a nonexchangeable hydrogen atom which adds to the base. A detailed scheme for this reaction is, however, not proposed since the radiation chemistry of the sugar moiety in the solid nucleosides is not yet sufficiently understood.

It would be of interest to compare the reaction sequence in ClUdR and BUdR with those in other nucleosides and nucleotides. However, there are only a few kinetic measurements on nucleic acid constituent radicals available in the literature. One report involving the conversion of a ribose-located radical is for 3′-cytidylic acid.[23] In that case, a $\dot{C}_{5'}$ centered radical decays into still another radical on the sugar moiety without affecting the cytosine base.

It remains to relate the observed reaction pathway to radiation-chemical findings in nucleic acid constituents and, specifically, in halouracils. Most of the radiation-damage mechanisms postulated on the basis of ESR investigations in the solid state have emphasized the mode of formation hydrogen-adduct radicals on pyrimidine and purine bases,[24] which are the main stable species observed at room temperature. It has been proposed that they should be formed either by attack of hydrogen atoms, probably released from the sugar, to the unsaturated bonds or by protonation of base anions. Evidence for the latter reaction has derived mainly from studies in frozen solu-

tions or glasses[25,26] whereas indirect arguments, for example, measurements of radical yields[27] have been advanced in support of the hydrogen atom attack mechanism. Our results in ClUdR and BUdR present the first direct demonstration of the hydrogen atom addition reaction with the hydrogen liberated as a consequence of deoxyribose damage. On the other hand, the experiments with deuterated crystals indicate that the reductive protonation (deuteration) pathway should also be operative in the production of hydrogen-adduct radicals observed in the two systems. This reaction requires an anion as a precursor which we have not observed so far. It is reasonable to assume that protonation occurs at very low temperatures in the halouracils. This argument would explain the observation that a fraction of hydrogen-adduct radicals is invariably observed prior to the decay of the $\dot{C}_5$ radical in both ClUdR and BUdR.

It is interesting to note that major concentrations of radical species resulting from halogen elimination have not been observed in the temperature range from about 30 K to room temperature. For ClUdR, the observed reaction sequence $\dot{O}_5 \rightarrow \dot{C}_5 \rightarrow$ 5-yl includes the main fraction of all radicals observed. The pathway does, however, not account for the total radical balance in BUdR. There is a small fraction of Br_2^- centers observed at 77 K and below. At room temperature, one or more radicals besides the hydrogen-adduct radical contribute to the spectra.[10] Another indication that the reaction sequence should be more complex in this crystal is the observation that the $\dot{O}_5$ radical converts into $\dot{C}_5$ only upon slow warming whereas another radical, not yet identified, is formed otherwise. In ClUdR, no such restriction was detected. Further measurements are necessary to unravel a more detailed radical-reaction scheme for BUdR. The results are sufficient, however, to suggest that both ClUdR and BUdR in the solid phase are rather resistant to halogen elimination on both attack of electrons and hydrogen atoms. Comparing these findings with the radiation-chemical evidence derived from aqueous solution or glasses, it becomes apparent that radiation-induced dehalogenation of halouracils should depend strongly on the microscopic environment of the base. This view should be taken into consideration when predictions about the radiation effects of halouracil-substituted DNA in vivo are made on the basis of model compound studies.

References and Notes

(1) To whom correspondence and reprint requests should be addressed.
(2) On leave from the University of Rochester, supported by NIH Career Development Award No. 5K04 GM-70337, NIH Research Grant No. 1 R01 GM 20688-01, and University of Rochester Biomedical and Environmental Research Project Report No. UR-3490-900.
(3) For a recent review see W. Szybalski, *Cancer Chemother. Rep., Part 1*, **58**, 539 (1974).
(4) P. Neta, *J. Phys. Chem.*, **76**, 2399 (1972).
(5) M. D. Sevilla, R. Failor, and G. Zorman, *J. Phys. Chem.*, **78**, 696 (1974).
(6) L. D. Simpson and J. D. Zimbrick, *Int. J. Radiat. Biol.*, **28**, 461 (1975).
(7) K. M. Bansal, L. K. Patterson, and R. H. Schuler, *J. Phys. Chem.*, **76**, 2386 (1972).
(8) J. D. Zimbrick, J. F. Ward, and L. S. Myers, Jr., *Int. J. Radiat. Biol.*, **16**, 505 (1969).
(9) J. D. Zimbrick, J. F. Ward, and L. S. Myers, Jr., *Int. J. Radiat. Biol.*, **16**, 525 (1969).
(10) J. Huttermann and A. Muller, *Int. J. Radiat. Biol.*, **15**, 297 (1969).
(11) J. Huttermann, G. W. Neilson, and M. C. R. Symons, *Mol. Phys.*, **32**, 269 (1976).
(12) J. Huttermann, W. A. Bernhard, E. Haindl, and G. Schmidt, *Mol. Phys.*, **32**, 1111 (1976).
(13) J. Y. Lee and H. C. Box, *J. Chem. Phys.*, **59**, 2509 (1973).
(14) H. C. Box and E. E. Budzinski, *J. Chem. Phys.*, **62**, 197 (1975).
(15) R. Bergene and R. A. Vaughan, *Int. J. Radiat. Biol.*, **29**, 145 (1976).
(16) C. Alexander, Jr., and C. E. Franklin, *J. Chem. Phys.*, **54**, 1909 (1971).
(17) W. A. Bernhard, D. M. Close, K. R. Mercer, and J. C. Corelli, *Radiat. Res.*, **66**, 19 (1976).
(18) J. Huttermann, G. Schmidt, and D. Weymann, *J. Magn. Reson.*, **21**, 221 (1976).
(19) D. W. Young and E. M. Morris, *Acta Crystallogr., Sect. B*, **29**, 1259 (1973).
(20) J. Iball, C. H. Morgan, and H. R. Wilson, *Proc. R. Soc. London., Ser. A*, **295**, 320 (1966).
(21) K. Rossler, personal communication.
(22) J. A. Howard, *Adv. Free Radical Chem.*, **4**, 49 (1972).
(23) W. A. Bernhard, J. Huttermann, A. Muller, D. M. Close, and G. W. Fouse, *Radiat. Res.*, in press.
(24) A. Muller and J. Huttermann, *Ann. N.Y. Acad. Sci.*, **222**, 411 (1973).
(25) M. D. Sevilla, *J. Phys. Chem.*, **75**, 626 (1971).
(26) A. D. Lenherr and M. G. Ormerod, *Nature (London)*, **225**, 546 (1970).
(27) A. Muller, *Prog. Biophys. Mol. Biol.*, **17**, 99 (1967).

Pressure Dependence of the Glass Transition Temperature in Ionic Liquids and Solutions. Evidence Against Free Volume Theories

E. Williams* and C. A. Angell

Department of Chemistry, Purdue University, West Lafayette, Indiana 47907

(Received April 12, 1976)

Publication costs assisted by the National Science Foundation and the Office of Water Resources Research

A simple DTA method of determining the glass transition temperature, T_g, of a supercooled liquid using small samples under high pressure has been developed and applied to the study of several anhydrous ionic liquid binary systems, and salt + water systems. Values of the pressure dependence of T_g have been compared with those predicted (a) from the pressure dependence of electrical conductance and (b) from the changes of heat capacity and expansion coefficient observed at T_g by use of the quasi-thermodynamic relation $dT_g/dP = T_g V_g \Delta\alpha/\Delta C_p$. In the case of alkali acetate + water systems, T_g is almost independent of pressure, and, in the case of the composition $LiOAc \cdot 10\ H_2O$, dT_g/dP is actually negative. This result, which implies a decrease in expansion coefficient on increase of temperature through the glass transition, is conceptually incompatible with a free volume interpretation of liquid relaxational properties.

The glass transition as a phenomenon has frequently been studied in relation to composition changes in multicomponent systems, but the effect of the other common thermodynamic variable, the external pressure, has been given much less attention. Data are available for only a few polymeric and molecular liquids,[1-3] while the only data on inorganic systems are from Tammann's brief study of B_2O_3, a lead silicate glass, and a phosphoric acid solution.[4] Information derived from pressure dependence studies should be useful both for the purpose of clarifying the

thermodynamic factors which help determine the occurrence of the glass transition phenomenon[5] and for interpreting the effect of pressure on liquid transport properties at temperatures well above that of the glass transition temperature, T_g. The present study was conducted with both of the above interests in mind. In particular, predictions of values of dT_g/dP have been available for some time from the analysis of the effect of pressure on electrical conductances in molten calcium nitrate + potassium nitrate mixtures,[6] and an experimental test of the predictions has been needed to assess the validity of the data analysis and the principles underlying it.

For the same ionic liquids, sufficient data are now available to test the applicability of the quasi-thermodynamic relation

$$\frac{dT_g}{dP} = T_g V_g \frac{\Delta\alpha}{\Delta C_p} \tag{1}$$

where V_g is the molar volume at T_g, and $\Delta\alpha$ and ΔC_p are the changes in volume expansion coefficient and constant pressure heat capacity which occur at T_g. Equation 1 is of the form originally derived by Ehrenfest[7] for the relation between thermodynamic quantities at a second-order thermodynamic transition, by using the fact that $\Delta S = \Delta(dG/dT) = 0$ at such a transition.

Although the glass transition is not an equilibrium phenomenon, it has been proposed[5,8] that eq 1 should apply at the glass transition (a) if the temperature of the transition is determined by a condition of constant excess entropy or (b) if the thermodynamic state of the liquid can be specified at any T and P by a single ordering parameter (e.g., the number of holes per mole).[9] In the latter case a second equation[5,8]

$$dT_g/dP = \Delta\kappa/\Delta\alpha \tag{2}$$

which is analogous to an equation derived by Ehrenfest[7] from the other condition obtaining at a second-order transition, $\Delta V = \Delta(dG/dP)_T = 0$, should also be valid. In eq 2 $\Delta\kappa$ is the change in isothermal compressibility at T_g. A constant excess entropy condition will coincide with a constant excess volume condition only where a single ordering parameter is adequate for a thermodynamic description of the liquid state. In view of the molecular complexity of the liquid state it is therefore not expected that condition b will be fulfilled nor, therefore, that both eq 1 and 2 will be valid. In fact, the finding that, experimentally, one of them, eq 1, is valid in all the cases tested to date is of considerable interest.

Although few data are available to test eq 2, it appears that dT_g/dP is only about $0.5\Delta\kappa/\Delta\alpha$. However there is some suggestion from the values of $\Delta\kappa$ determined on different time scales by ultrasonic methods[10] that eq 2 may become more accurate as the time scale on which the transition is observed tends to infinity (i.e., as $T_g \rightarrow T_g$-(ideal)).

It will be seen that our results on simple ionic glasses not only affirm the common validity of eq 1, and hence of the excess entropy criterion for the glass transition in such materials, but also provide positive evidence against the physical reasonableness of a free volume criterion for glass formation in certain cases.

Experimental Section

Materials. Compositions in the system $Ca(NO_3)_2$ + KNO_3 were prepared by weighing of reagent grade KNO_3 and $Ca(NO_3)_2{\cdot}4H_2O$, fusing, and removing the water by purging the liquid with dry N_2. The organic chloride solutions were prepared from components which had been carefully dried by sublimation procedures. The other systems studied were all reagent grade materials and were used without further purification, or after the appropriate additions of distilled water.

Apparatus. Glass transition temperatures were determined using a simple differential thermal analysis technique in which the thermocouples were arranged collinearly in order that both the sample and reference materials could be contained within the same 4 cm long × 2 mm i.d. Pyrex glass tube. The position of the tube with respect to the thermocouples was fixed by the use of epoxy resin at the tube mouth. The thermocouples, which were of 1 mm Thermocoax, were brazed into a standard Aminco pressure plug and this assembly was screwed into a 4-mm i.d. steel pressure tube (Figure 1). Temperature uniformity over the sample area during heating runs was ensured by means of a 1-in. thick aluminum sleeve around the pressure tube. Heat was supplied to the system by a heating tape wrapped around the aluminum sleeve.

Pressure was applied to the system by means of an oil pressure pump generating a maximum pressure of 40 000 psi. The arrangements of the valves, gauges, etc. is depicted schematically in Figure 1. The accuracy of the pressure gauge (American Instrument Co. No. 47-18340) is not stated but the gauge was easily readable to ±100 psi in the range between 15 and 30 000 psi (1–2000 bars). The differential EMF and the sample temperature were recorded on a Honeywell Electronik 194 two-pen recorder, using full scale settings which permitted the sample temperature to be determined with an accuracy ±0.1 °C, and allowed differential EMF's of 5 to 100 μV to be recorded. T_g was determined as shown in the inset to Figure 1, with an accuracy considered to be ±1.0 °C, the uncertainty arising mainly from the subjective treatment of the differential EMF traces. Reproducibility was generally good except for the case of $Mg(C_2H_3O_2)_2{\cdot}4H_2O$, for which the glass transition region is very extended and generally abnormal.[11]

Procedure. The sample tube was half filled with the material of interest in liquid form, and the remaining (reference) section was filled with the pump pressure-transmitting oil, for samples with $T_g > 0$ °C, or with a low-melting easily supercooled fluid, e.g., methylcyclohexane, for samples with lower T_g values, since the pump oil froze at ~−50 °C. The sample and thermocouple assembly were then mounted in the pressure tube which itself was prefilled with either oil or methylcyclohexane (down to valve A, Figure 1) depending on the sample T_g value. The sample was then cooled to a temperature 10–20 °C below T_g, by pouring a steady stream of liquid nitrogen onto the exterior of the pressure cell. The differential EMF was then recorded during heating at a constant dT/dt, usually 12 °C min^{-1}, to establish the 1 atm pressure value of T_g. Since data on T_g at 1 atm pressure have been reported previously for all the solutions studied,[11] it was possible to check, by this initial measurement, whether or not (a) any sample crystallization had occurred during the (rather slow) cool-down of the metal apparatus and (b) the sample–reference configuration had remained undisturbed.

The pressure was then increased while the sample was above T_g after which the temperature was decreased in order to form the glass. T_g, which was now that pertaining to the glass formed under the high pressure condition, was then determined as before during reheating at a rate of 12 °C min^{-1}. Since the pressure changed continuously during this heating process, it was necessary to monitor

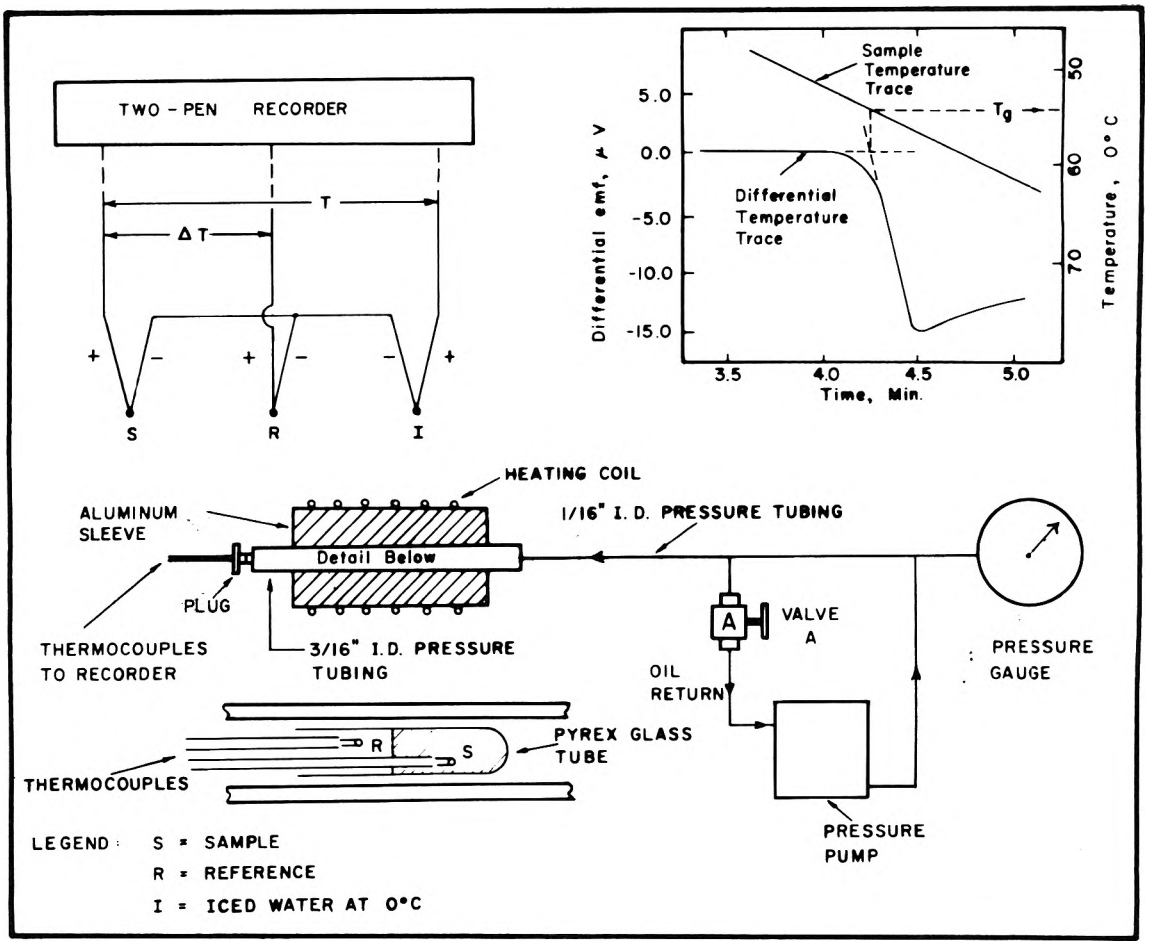

Figure 1. Schematic diagram of the high pressure cell and associated equipment used to determine the glass transition temperature, T_g, as a function of pressure. The inset shows how T_g was determined from a typical DTA trace.

it, and to determine later the value obtaining at T_g.

This process was repeated at increasing pressures up to the maximum value (~2 kbars), after which the pressure was released and the value of T_g at 1 atm pressure redetermined. Any discrepancy would indicate the occurrence of some crystallization or degradation during the series. This rarely was found, due to the precautionary avoidance of temperatures more than 10–20 °C above T_g at any pressure. This was the normal procedure and it is shown schematically as procedure 1 in Figure 1 of the following paper.

In some cases T_g was also determined at various pressures which progressively decreased from the maximum value. The pressure changes were made as before, i.e., while the sample was in the liquid state, but the results differed neither systematically nor significantly from the data obtained in the increasing pressure series.

In principle, the value of T_g at a given pressure should depend on whether the sample is pressurized while in the glassy state (fixed configuration) or liquid state (structure can respond to pressure increase). In polymeric materials, in which T_g is commonly very responsive to pressure changes, this distinction is of great importance. Quach and Simha,[12] for instance, found that for polystyrene, dT_g/dP = 74.2 °C kbar^{-1} when pressure is applied to the glass formed at 1 atm pressure, and 31.6 °C kbar^{-1} when it is pressurized in the liquid state. For poly(o-methylstyrene) the respective values of dT_g/dP were 73.0 and 34.2 °C kbar^{-1}. Still different behavior was obtained if the glass was vitrified isothermally by sufficient pressure increase. The sensitivity of the present ionic systems to any such differences in pressure–temperature cycles was only studied systematically for the case of $ZnCl_2$ (see following paper), for which case no dependences of T_g on pressure–temperature history could be observed so long as the rate of temperature change during the T_g determination itself was kept constant.

Isolated determinations of T_g for the $Ca(NO_3)_2$–KNO_3 glasses using procedure 2 of the following paper (pressure imposed below T_g) also failed to show any discordance with the generally adopted procedure 1 results (pressure imposed while $T > T_g$). Therefore, while the dT_g/dP values reported in this study are based primarily on results from procedure 1 type experiments, we feel they can probably be taken as procedure-independent values. It seems that in these simply structured, molecularly isotropic, ionic systems, for which dT_g/dP is not large, the path by which the glassy state is reached is not of the same order of importance as the pressure imposing on the sample while T_g is measured.

Results

Data are presented in Figures 2–6 and in Table I for various anhydrous ionic liquids with both inorganic and organic ions, for molten hydrates, and for concentrated aqueous solutions. All measurements refer to heating rates of 12 °C min^{-1}. A representative DTA trace in the glass transition region is shown as an inset in Figure 1. The data on anhydrous $ZnCl_2$, which proves unusual, will be presented in the following paper,[13] together with heat capacity measurements for this substance.

Discussion

First we compare our results for the mixed nitrate glasses with the predictions[6] based on the analysis of mass transport behavior at temperatures well above T_g.

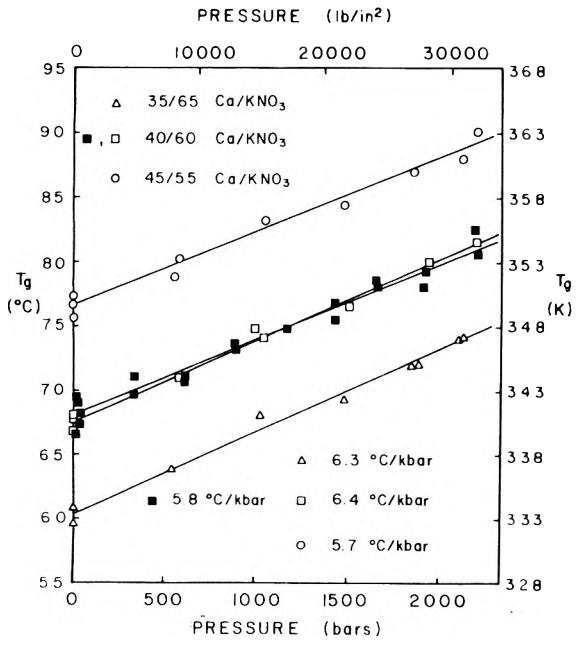

Figure 2. Pressure dependence of T_g for three anhydrous $Ca(NO_3)_2$ + KNO_3 mixtures.

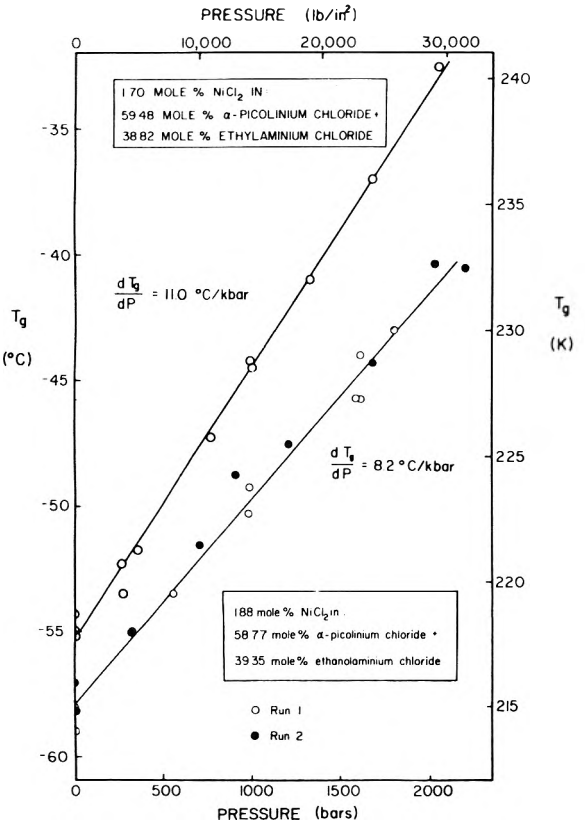

Figure 3. Pressure dependence of T_g for two anhydrous organic salt mixtures. Results for two independent series of determinations are distinguished.

In an investigation of the pressure dependence of the electrical conductance of molten $Ca(NO_3)_2$–KNO_3 solutions, Angell et al.[6] found that, within their experimental uncertainty, data covering four orders of magnitude change in conductance, obtained in the temperature range 120–200 °C and the pressure range 1–2000 bars, could be fitted to a Vogel–Tammann–Fulcher (VTF) type equation:

$$\kappa(T,P) = AT^{-1/2} \exp\left[\frac{-B_\kappa}{T - T_0(P)}\right] \qquad (3)$$

TABLE I

System	T_g, °C	dT_g/dP, deg kbar^{-1}
35/65 Ca/KNO_3	60.3 ± 0.3	6.3 ± 0.2
40/60 Ca/KNO_3, run 1	68.1 ± 0.2	5.8 ± 0.2
40/60 Ca/KNO_3, run 2	67.6 ± 0.3	6.4 ± 0.3
45/55 Ca/KNO_3	76.6 ± 0.3	5.7 ± 0.3
Ethylaminium + α-picolinium chlorides	−55.4 ± 0.3	11.0 ± 0.3
Ethanolaminium + α-picolinium chlorides	−57.8 ± 0.3	8.2 ± 0.3
$Ca(NO_3)_2 \cdot 4H_2O$	−57.3 ± 0.4	4.3 ± 0.4
$Ca(NO_3)_2 \cdot 8H_2O$	−91.9 ± 0.2	3.6 ± 0.2
$Mg(OAc)_2 \cdot 4H_2O$	−14.2 ± 0.4	4.4 ± 0.4
$Li(OAc) \cdot 6H_2O$	−95.1 ± 0.2	0.83 ± 0.15
$Li(OAc) \cdot 10H_2O$	−107.5 ± 0.3	−0.60 ± 0.24
$Na(OAc) \cdot 10H_2O$	−99.0 ± 0.2	0.48 ± 0.15

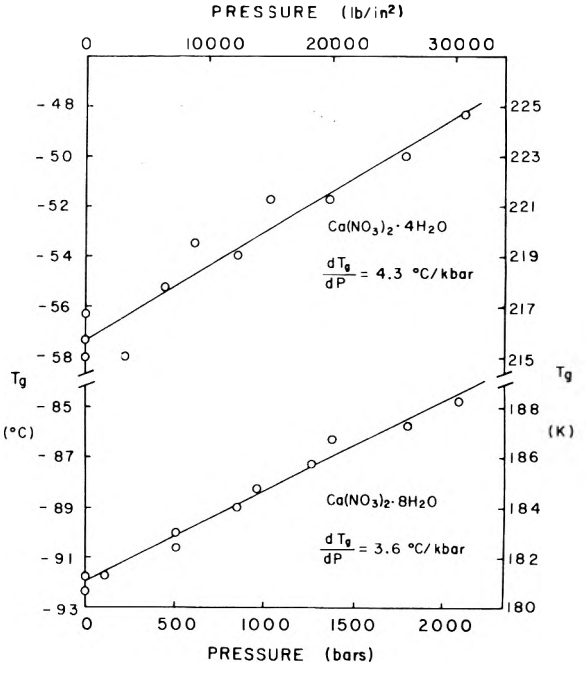

Figure 4. Pressure dependence of T_g for $Ca(NO_3)_2 \cdot 4H_2O$ and $Ca(NO_3)_2 \cdot 8H_2O$.

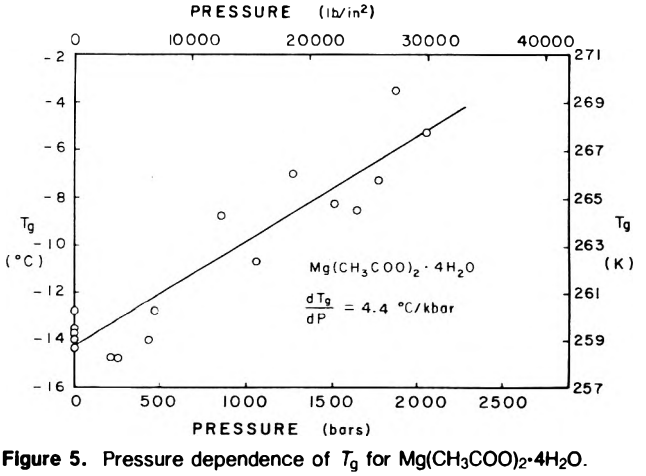

Figure 5. Pressure dependence of T_g for $Mg(CH_3COO)_2 \cdot 4H_2O$.

in which only the constant $T_0(P)$ varied with pressure. $T_0(P)$, as obtained from an eq 3 type analysis of data in the conductance studies by Angell et al., generally falls a little below T_g. When P = 1 bar, it agrees well with the value of T_0 obtained from a similar analysis of viscosity data taken in the same temperature region.[14] Since

TABLE II

Composition, mole % $Ca(NO_3)_2$	T_g, °C	T_g, K	V_g, cm^3 $equiv^{-1}$	$\Delta\alpha$, deg^{-1} $\times 10^{-4}$	ΔC_p, cal deg^{-1} $equiv^{-1}$	dT_g/dP, °C $kbar^{-1}$ Calcd	Expt
35	60.3	333.5	41.93	2.540	11.4	7.5	6.3 ± 0.2
40	68.1	341.3	41.40	2.316	12.8	6.1	5.8 ± 0.2
40	67.6	340.8	41.40	2.316	12.8	6.1	6.4 ± 0.2
45	76.6	349.8	40.65	2.091	13.8	5.2	5.7 ± 0.3

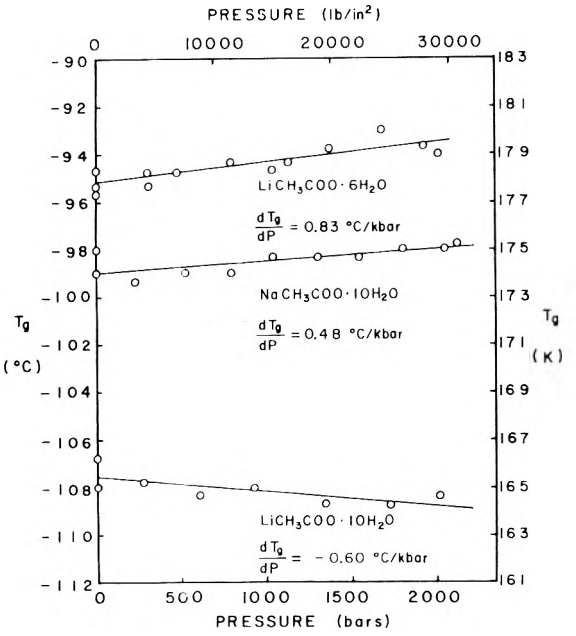

Figure 6. Pressure dependence of T_g for $NaCH_3COO \cdot 10H_2O$, $LiCH_3COO \cdot 6H_2O$, and $LiCH_3COO \cdot 10H_2O$. Note that dT_g/dP is negative for the latter.

theories for eq 3,[15] although inadequate,[16] relate T_0 and T_g intimately, it is of interest to know whether or not the value of dT_0/dP as obtained from the conductance study is confirmed by the direct determination of dT_g/dP. Angell et al. quoted dT_0/dP (1–2000 bars) as = 8 ± 2 °C $kbar^{-1}$ [6] for the 38% $Ca(NO_3)_2$ + 62% KNO_3 solution, which was reduced to 7 ± 2 °C in Pollard's final computer-assisted data analysis.[6b] This value compares rather well with the present result of 5.8 ± 0.2 °C $kbar^{-1}$ for our 40/60 mixture. Since the latter quantity has a smaller uncertainty than the former, the small difference between them suggests that the parameter B_K in eq 3 is in fact not constant but increases slightly with increasing pressure, a conclusion which is of marginal interest.

Of more significance is the test of eq 1 which our data permit for the above system. Rao, Helphrey, and Angell[17] have recently determined: (i) the changes of heat capacity which occur at T_g for a series of compositions in the Ca/KNO_3 system, using differential scanning calorimetry, and (ii) the changes of volume expansion coefficient at T_g using data from the temperature dependence of the refractive index. We take, as an example, the composition 40 mol % $Ca(NO_3)$ + 60 mol % KNO_3, for which the most extensive and reliable data are available. Using their values of T_g = 341 K, V_g = 41.4 cm^3 $equiv^{-1}$, $\Delta\alpha = 2.32 \times 10^{-4}$ deg^{-1}, and ΔC_p = 12.8 cal deg^{-1} $equiv^{-1}$, eq 1 leads to the prediction that $dT_g/dP = 6.1 \pm 0.4$ °C $kbar^{-1}$ which is in good accord with the present experimental value found from the more accurate data (denoted by solid squares) in Figure 2. For the other compositions studied, we obtain the results listed in Table II.

The only other case for which a value of $\Delta\alpha$ is available is that of $LiOAc \cdot 10H_2O$.[18] This datum was acquired, using a simple dilatometric technique, in order to test the implication of the data on $LiOAc \cdot 10H_2O$, which is shown in Figure 6, that $\Delta\alpha$ should have a small *negative* value. The value of $\Delta\alpha$ calculated using eq 1, in which an unpublished value[11] for ΔC_p of 65 cal mol^{-1} deg^{-1} is used, is $-0.4 \pm 0.2 \times 10^{-4}$ deg^{-1} which is on the threshold of measurability by common techniques. Our measured value, reported elsewhere,[18] was found to be $-0.4 \pm 0.4 \times 10^{-4}$ deg^{-1}. This is good agreement in terms of absolute magnitudes ($\Delta\alpha$ values of 5 to 20 $\times 10^{-4}$ deg^{-1} being common) but the relative uncertainties are so large that such agreement as exists obviously cannot be used to test the validity of eq 1.

While these calculated and measured $\Delta\alpha$ values are almost indistinguishable from zero within measurement accuracy, they are nevertheless of great significance to theoretical interpretations of glass transition phenomenology, since negative or even zero values of $\Delta\alpha$ are simply untenable in terms of free volume theories of glass formation. The latter require that additional or "free" volume, V_f, become available above T_g, in an amount given by

$$V_f = V_{f(T_g)} + V_g \Delta\alpha (T - T_g) \qquad (4)$$

before molecular motion can be free enough for structural equilibrium to be established on a time scale less than the relaxation time characteristic of the glass transition temperature (order of seconds). Free volume would have to be defined in a very special way, which would permit negative values to be physically meaningful, before such theories could explain the production of relatively mobile liquids during a negative configurational expansion ($\Delta\alpha$) regime.

It seems preferable, therefore, to seek as a basis for a general treatment of relaxational phenomena in viscous liquids, a configurational property which *always* increases with increasing temperature. Such properties are the entropy,[15c] which would be consistent with the common validity of eq 1, or the enthalpy,[15a] or some enthalpy-related excitation parameter, e.g., a "broken-bond fraction".[19] Free volume theories might however be expected to have a limited validity for molecularly simple substances, in which volume and enthalpy are simply and consistently correlated.

The explanation for the behavior of the $LiOAc-H_2O$ solutions is no doubt to be found in the low energy associated with linear hydrogen bonds, and the open structure this tends to promote when the steric conditions for three-dimensional H-bonded structures are fulfilled. In this connection the presence of the strongly proton-attracting acetate ion and a large fraction of water molecules (which in the supercooled pure liquid state exhibit a pronounced anomalous negative total thermal expansion regime) is no doubt of significance.

The presence of a hydrogen-bond-promoted open structure at low temperatures that tends to collapse as increasing temperature ruptures the bonds may also be responsible for the rather small values of dT_g/dP for the other hydrated glasses studied. Consistent with this idea are the small values of $\Delta\alpha$ which we calculate using eq 1

for those cases for which ΔC_p values are available.[11] For $Ca(NO_3)_2 \cdot 4H_2O$, $Ca(NO_3)_2 \cdot 8H_2O$, and $Mg(CH_3CO-O)_2 \cdot 4H_2O$, these values are 3.7, 3.4, and 2.6×10^{-4} deg^{-1}, respectively, values which are much smaller than the $\sim 20 \times 10^{-4}$ deg^{-1} values characteristic of molecular and polymeric liquids.[1]

By contrast, the values of dT_g/dP for the mixed ionic chloride glasses are closer to those of the molecular liquids referred to previously.[1-3] The values of dT_g/dP for these two binary mixtures, which differ only by the presence of an –OH group at the neutral end of one organic cation, are in the same order as the total liquid state expansion coefficients, and the molar volumes.[20] This is consistent with the general rule that –OH groups promote cohesion, and decrease both compressibility and expansivity, etc.[21] Interestingly enough, the dT_g/dP values stand in essentially the same ratio, 1.37, as the expansion coefficients, 1.30, as would be predicted by simple two-state models for the configurational thermodynamic properties.[19] These substances were included in the present study primarily because data were needed in connection with their use as solvents in a separate high pressure spectral investigation,[22] and they will not be discussed further here. We note, however, that the spectroscopic observation of a glass transition whose pressure dependence is known was found to be a successful way of determining pressure under conditions where direct measurements were not possible.[22]

Finally we should point out that the failure of free volume concepts to embrace glasses with behavior such as that exhibited by $LiOAc \cdot 10H_2O$ by no means implies that eq 2 must fail to apply to such glasses, since there is nothing in the derivation of eq 2 which prevents $\Delta\alpha$ from taking negative values. A desirable extension of this work therefore would be the study of isothermal compressibility changes occurring at T_g so the question of whether or not eq 2 fails for ionic glasses as clearly as it does for the (few) molecular liquids so far studied could be answered directly. Some evidence is already at hand. In the case of the nitrate glass $40Ca/60KNO_3$, the Prigogine-Defay ratio $(T_g V_g[(\Delta\alpha)^2/\Delta C_p \Delta\kappa])$ has been shown recently[25] to have a value of approximately 4 rather than of unity as would be the case for a single ordering parameter description of the viscous liquid. Thus, since eq 1 was found above to be valid for this composition, it seems that eq 2 must fail by a factor of approximately 4 also. There is also direct spectroscopic evidence, for the organic salts of this study, that the structural states frozen in at T_g depend on the pressure at which the transition occurs,[22] i.e., that a single ordering parameter is insufficient to describe the glass state, and hence that at least one of eq 1 and 2, presumably the latter, should fail. Combining these observations with the acetate glass findings, the general conclusion may be drawn that volume is not a useful variable on which to focus attention in attempts to understand the thermodynamic aspects of the glass transition.

Acknowledgment. The authors gratefully acknowledge support of different aspects of this work by the National Science Foundation under Grant G.P. 30722 and by the Office of Water Resources Research under Water Resources Research Act 1964, Project No. B-051-IND (Agreement No. 14-31-0001-3883).

References and Notes

(1) J. M. O'Reilly, *J. Polym. Sci.*, **57**, 429 (1962).
(2) A. Gilchrist, J. E. Early, and R. H. Cole, *J. Chem. Phys.*, **26**, 196 (1957).
(3) J. E. McKinney, H. V. Belcher, and R. S. Marvin, *Trans. Soc. Rheol.*, **4**, 374 (1960).
(4) G. Tammann and G. Bandel, *Z. Anorg. Alleg. Chem.*, **129**, 192 (1930).
(5) M. Goldstein, *J. Chem. Phys.*, **39**, 3369 (1963); *J. Phys. Chem.*, **77**, 667 (1973).
(6) (a) C. A. Angell, L. J. Pollard, and W. Strauss, *J. Chem. Phys.*, **50**, 2694 (1969); (b) L. J. Pollard, Ph.D. Thesis, Melbourne University, 1969.
(7) P. Ehrenfest, *Commun. Kamerlingh Onnes Lab. Univ. Leiden*, **756**, (1933); H. B. Callen, "Thermodynamics", Wiley, New York, N.Y., 1960.
(8) R. O. Davies and G. O. Jones, *Adv. Phys.*, **2**, 370 (1953); *Proc. R. Soc. London, Ser. A*, **217**, 26 (1953).
(9) N. Hirai and H. Eyring, *J. Appl. Phys.*, **29**, 810 (1958); *J. Polym. Sci.*, **37**, 51 (1959).
(10) T. A. Litovitz and T. Lyon, *J. Accoust. Soc. Am.*, **30**, 856 (1958).
(11) J. C. Tucker, private communication; E. J. Sare, Ph.D. Thesis, Purdue University, 1970.
(12) A. Quach and R. Simha, *J. Phys. Chem.*, **76**, 416 (1972).
(13) C. A. Angell, E. Williams, K. J. Rao, and J. C. Tucker, *J. Phys. Chem.*, following paper in this issue.
(14) S. Blaser, P. B. Macedo, and R. Weiler, *J. Phys. Chem.*, **73**, 4147 (1969).
(15) (a) F. Bueche, *J. Chem. Phys.*, **30**, 748 (1959); (b) M. H. Cohen and D. Turnbull, *ibid.*, **31**, 1163 (1959); (c) G. Adam and J. H. Gibbs, *ibid.*, **43**, 139 (1965).
(16) H. Tweer, J. H. Simmons, and P. B. Macedo, *J. Chem. Phys.*, **54**, 1952 (1971).
(17) K. J. Rao, D. B. Helphrey, and C. A. Angell, *Phys. Chem. Glasses*, **14**, 26 (1973).
(18) E. Williams and C. A. Angell, *J. Polym. Sci., Polym. Lett. Edit.*, **11**, 383 (1973).
(19) C. A. Angell and K. J. Rao, *J. Chem. Phys.*, **57**, 470 (1972).
(20) M. L. Abkemeier, Ph.D. Thesis, Purdue University, 1972.
(21) P. W. Bridgman, *Proc. Am. Acad. Art Sci.*, **67**, 1 (1932).
(22) C. A. Angell and M. L. Abkemeier, *Inorg. Chem.*, **12**, 1462 (1973).
(23) (a) N. Hirai and H. Eyring, *J. Appl. Phys.*, **29**, 810 (1958); *J. Polym. Sci.*, **73**, 51 (1959); (b) T. Nose, *Polym. J.*, **2**, 437 (1971).
(24) P. B. Macedo, W. Capps, and T. A. Litovitz, *J. Chem. Phys.*, **44**, 3357 (1966).
(25) P. K. Gupta and C. T. Moynihan, to be submitted for publication.

Heat Capacity and Glass Transition Thermodynamics for Zinc Chloride. A Failure of the First Davies–Jones Relation for dT_g/dP

C. A. Angell,* E. Williams, K. J. Rao, and J. C. Tucker

Department of Chemistry, Purdue University, West Lafayette, Indiana 47907 *(Received April 16, 1976)*

Publication costs assisted by the National Science Foundation

Measurement of the heat capacities of the liquid, glass, and crystal (α-polymorph) forms of $ZnCl_2$, and of the pressure dependence of the glass transition temperature, are reported. The excess heat capacity, and the temperature dependence of the viscosity as well, may be described using two-parameter equations from the bond–lattice model. The glass transition temperature at a given pressure is independent, within experimental error, of the pressure–temperature history of the sample. The observed pressure dependence, however, is only half the value predicted from the changes in heat capacity and expansion coefficient at T_g by the Davies–Jones equation. This uncommon failure of the equation is attributed to a small ΔC_p associated with the network structure of zinc chloride.

Among pure liquid inorganic halides, $ZnCl_2$ and BeF_2 are unusual for their high viscosities at their respective freezing points, and for their consequent abilities to supercool and vitrify in macroscopic quantities. Although much work has been done on the structure[1-8] and nonequilibrium properties (viscosity,[9-11] diffusivity,[12,13] and electrical conductivity[14-17]) of these liquids and the glasses they form, little is known of their thermodynamic properties. This is particularly true for the temperature range about their glass transition temperatures, T_g, of 375[12,18] and 592 K,[11] respectively.

Among glass-forming liquids the mass transport properties of $ZnCl_2$ and BeF_2 are unusual for their small departures from Arrhenius behavior. As there is some evidence that mass transport behavior and changes in thermodynamic derivative properties at T_g are closely related[19,20] the paucity of thermodynamic data for these liquid halides is unfortunate. In the present paper we go some way toward improving this position by presenting measurements of the heat capacity of the supercooled liquid and glassy states of $ZnCl_2$, and of the pressure dependence of the temperature T_g at which the change in heat capacity is manifested at fixed heating rate. According to observations on a considerable number of glass-forming liquids the latter pressure dependence, dT_g/dP, should be quantitatively related to the changes in heat capacity ΔC_p and expansion coefficient $\Delta\alpha$ by the expression first suggested by Davies and Jones.[21] It will be seen that for the case of $ZnCl_2$ this relation

$$dT_g/dP = T_g V_g \Delta\alpha/\Delta C_p \quad (1)$$

does not hold.

Experimental Section

1. *Materials.* Liquid $ZnCl_2$ was prepared in the anhydrous condition by fusion of "anhydrous" reagent-grade salt (Mallinkrodt) in a stream of pure dry HCl gas, followed by a dry nitrogen flush. The product was converted to glass beads by pouring dropwise into dry liquid nitrogen, and was stored under molecular sieve.

2. *Heat Capacity Measurements.* Heat capacity measurements were made using both Perkin-Elmer Model 1B and Model 2 differential scanning calorimeters. Samples for study were prepared by adding one of the glass beads to a weighed gold sample pan, remelting it to obtain good pan contact, allowing it to solidify, and then hermetically sealing the sample pan. Finally, a vitreous sample was obtained by remelting the bead and dropping the pan and its contents into dry liquid nitrogen. All these operations were carried out in a low dew point drybox.

In standard DSC practice, calibration runs covering each temperature interval are carried out using the same pans as will later contain the sample. In the present work, because of the difficult nature of the sample, calibration runs were made using a separate pan of mass identical with that of the sample pan. Heat capacities of the vitreous, liquid, and crystalline states were obtained by the following sequence of measurements, using up-scans in all cases: (a) vitreous state, from −100 °C to T_g in 30 °C intervals; (b) supercooled liquid state, from T_g to 140 °C (when crystallization to the α-polymorph always took place) in a single interval; (c) crystalline state, from −100 to 300 °C (when fusion of the α-polymorph occurred) in 30 °C intervals; (d) liquid state, from 300 to 360 °C in 30 °C intervals. This sequence was repeated four times using the DSC-1B instrument to improve data reliability. On a later occasion the measurements in the vicinity of the glass transition temperature were repeated using the improved DSC-2 instrument.

3. *Melting and Heat of Fusion of α-$ZnCl_2$.* Although $ZnCl_2$ can exist in three polymorphic forms,[24] only the α and β forms are produced from the anhydrous liquid. The β polymorph, which is the most stable, forms during very slow cooling, when crystallization occurs not too far below the stable freezing point. The α form is produced, unreliably, on very fast cooling and, invariably, on reheating a sample which has been first quenched into the vitreous state. In this study the initial crystallization was thus always to the α form, and it was this form whose solid state heat capacity was determined in the experiments described above. The α form, although metastable, persists to high temperatures as shown by the absence of solid state transitions in the present study, and by the persistence of spectral characteristics of the α form up to at least 274 °C in the far IR study of Angell et al.[5b] The fusion studied in this work was therefore that of the α form. Fusion was observed to occur over a relatively narrow temperature range (297–302 °C) considering instrument lag and the inevitability of some residual contamination by water. The fusion enthalpy was obtained by comparison of the area under the fusion peak for a sample of known mass with the corresponding area for fusion of a known mass of

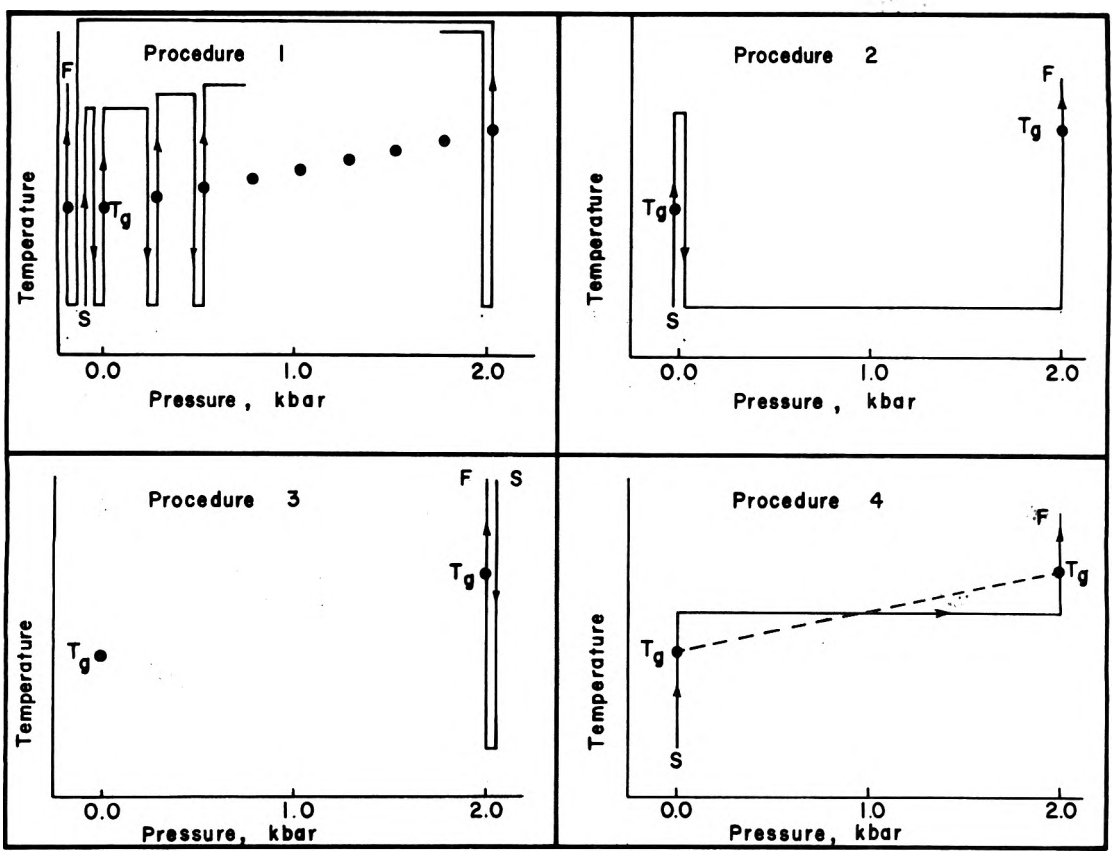

Figure 1. Schematic representations of the various procedures used to determine T_g. Procedure 1 was the normally adopted procedure. Closely spaced vertical lines are essentially coincident, but have been separated for clarity: ● P, T_g data points, (S) start, (F) finish.

indium metal, or, secondary standard, analytical grade KNO_3. Fusion of the β polymorph, which occurs at 318 °C in the absence of water contamination, was not studied in this work.

4. *Determination of* dT_g/dP. The pressure dependence of the glass transition temperature was measured using the collinear sample–reference differential thermal analysis technique described in the preceding paper.[22] Because the value of dT_g/dP for $ZnCl_2$ proves to be unexpectedly low, the measurements were performed using several different pressurization–measurement sequences in order to determine whether or not pressure–temperature histories were systematically influencing the T_g values being recorded. As noted in the preceding paper, for some polymers with large dT_g/dP values, the values of T_g and its apparent pressure dependence are strongly affected by whether the pressure is applied to the sample when it is in the liquid state when configurational changes can occur or in the solid state when they can not. Samples of $ZnCl_2$ were studied according to the following procedures, schematically shown in Figure 1, with the results noted.

Procedure 1. The glass transition temperature was measured during heating at 1 atm pressure. While the temperature was maintained *above* T_g, the pressure was increased to some chosen value, and the sample was then quenched to the glass, so that the structure characteristic of the compressed liquid was frozen in. Maintaining the same pressure, T_g was then determined during heating at the same rate dT/dt as in the previous run. Once the supercooled liquid state was reached the pressure was again increased incrementally and the procedure repeated. After a sequence of several such runs the pressure imposing on the system reached the apparatus maximum. The pressure was then released, again above T_g, and the value of T_g at 1 atm pressure was redetermined. In some cases the pressure was only partially released. The T_g values obtained in such a decreasing pressure sequence were consistent with those obtained with increasing pressures.

Procedure 2. The sample temperature was raised 10–20 °C above T_g at 1 atm, the sample was quenched to the glassy state, after which a pressure of ~2 kbars (close to the apparatus limit) was imposed, and T_g was determined during heating. The value agreed with that of procedure 1.

Procedure 3. The pressure obtaining at T_g during procedure 2 was maintained on the sample while it was cooled from above T_g at the end of the procedure 2 run. Maintaining this pressure on the now-glassy sample, T_g was determined during heating. The value of T_g was indistinguishable from that obtained in procedure 2 even though any possible differences would have been maximized by the use of the maximum pressure.

Procedure 4. Commencing at a pressure of 1 atm, with the temperature constant at a value 10 °C above the 1 atm T_g value, the pressure was increased continuously to the apparatus maximum. During pressurization the sample vitrified since, as will be seen later, T_g (2 kbars) > [T_g (1 bar) + 10 °C]. The value of T_g of the now-vitreous sample was determined again during heating under the 2-kbar maximum pressure. Again the value was unchanged within our normal reproducibility limits.

Results

Heat capacities for $ZnCl_2$ in the vitreous, liquid, and crystalline states as obtained in this work, are shown in Figure 2. The scatter for data obtained with the DSC-1B is greater than with the improved DSC-2. Despite the multiple determinations, data for the crystalline state between 160 and 290 K were considered unacceptable and are not reported. For the remainder, the average of the four separate runs is plotted and the standard deviation for the set of values at each temperature is indicated by

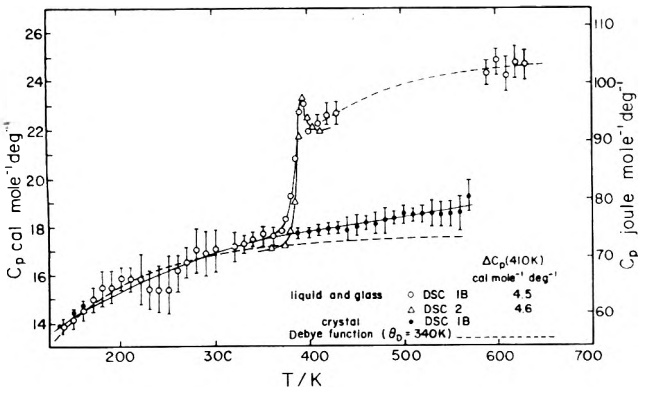

Figure 2. Heat capacities of liquid, glassy, and crystalline states of $ZnCl_2$. The dashed curve is a plot of the Debye heat capacity function for a value of θ_D = 340 K.

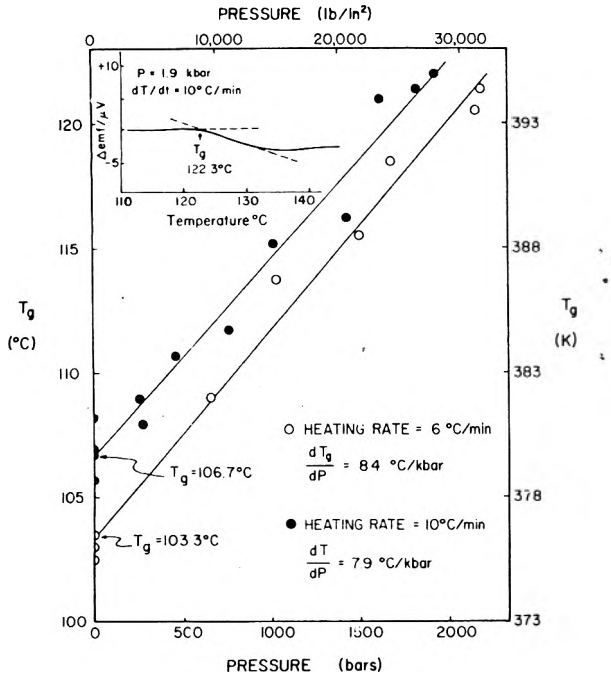

Figure 3. Pressure dependence of T_g for $ZnCl_2$: (○) at a heating rate of 6 °C/min; (●) at a heating rate of 10 °C/min.

the error bars. The value of the quantity of major interest to this paper, the change of heat capacity at T_g, ΔC_p, is the same within experimental uncertainty for both DSC-1B and DSC-2 determinations. The value obtained is 4.5 ± 0.3 cal mol^{-1} deg^{-1} which is considerably less than the value expected from the drop calorimetry data on liquid and crystalline states of $ZnCl_2$ reported by Cubiciotti and Eding[23] and utilized in an earlier discussion of the glass transition thermodynamics of $ZnCl_2$.[5a]

The heat of fusion was found to be 2.33 kcal/mol, yielding an entropy of fusion for the observed melting range of 3.97 eu. This is 4% smaller than the earlier drop calorimetry value of 4.13 eu obtained by Cubiciotti and Eding,[23] which is probably more appropriate to a mixed α- and β-polymorphic product. A small entropy difference between α and β polymorphs would be consistent with the observability of independent polymorph fusions, a parallel case being that of the SiO_2 polymorphs.

The values of T_g obtained at two different heating rates are shown as a function of imposed pressure in Figure 3. The glass transition is quite well defined (see inset) despite the rather small value of ΔC_p. As the least-squares best fit lines in Figure 3 show, both scan rates yield the same value of dT_g/dP, 8.2 °C kbar^{-1}, within the standard error of 0.4 °C kbar^{-1}.

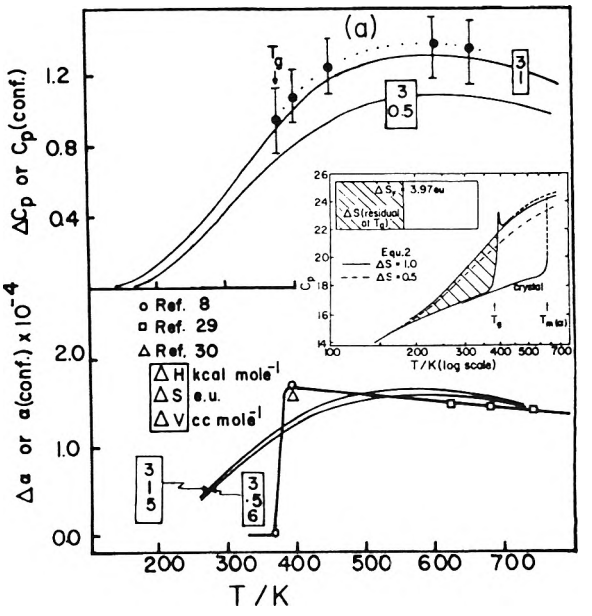

Figure 4. Comparison of excess heat capacity of liquid $ZnCl_2$ per mole of Zn–Cl bonds with configurational heat capacity of the bond–lattice model for bond excitation parameters ΔH = 3 kcal mol^{-1} and ΔS = 1.0 or 0.5 eu. The inset shows the experimental and theoretical C_p vs. T relations for $ZnCl_2$ using a log scale for T so that area is proportional to entropy. Areas corresponding to the measured fusion entropy and residual entropy at T_g are shown. The residual entropy predicted by the bond–lattice model for parameters ΔH = 3.0 kcal mol^{-1} and ΔS = 1.0 eu is shown as a cross hatched area between experimental crystal and calculated supercooled liquid curves.

Discussion

1. *Heat Capacity of Vitreous and Crystalline $ZnCl_2$.* Figure 2 shows that the heat capacities of $ZnCl_2$ glass and crystal have almost the same values. This is expected if only vibrational modes contribute in each case since the densities of the crystal (α polymorph) and glass differ by only ~10%.[24] The observed decreases of solid state heat capacity with decreasing temperature can be accounted for by a Debye model with characteristic temperature 340 K. As frequently observed,[25] the Debye temperature and glass transition temperature are not very different (cases with T_g as high as $1.4\theta_D$, however, have been observed[26]).

2. *Excess Heat Capacity and Other Properties of Liquid $ZnCl_2$.* Using the heat capacity of the crystal as a guide to the heat capacity of the amorphous solid at "short" response times, the excess heat capacity ΔC_p of the liquid state over that of the nonrelaxing solid has been assessed and is plotted in Figure 4. Since the instantaneous structure of the amorphous phase at $T > T_g$ is somewhat "looser", hence more anharmonic, than at $T \leq T_g$, the actual "short time" or "glassy" heat capacity will presumably increase with temperature a little more rapidly than does that of the crystal due to increasing anharmonicity contributions. Thus the above construction will tend to exaggerate the magnitude of ΔC_p at $T >> T_g$. Both the expansion coefficient and the heat capacity for liquid $ZnCl_2$, however, are unusually small for an ionic liquid and, since this implies slowly varying short-range order, the above source of error in ΔC_p is expected to be small.

ΔC_p for $ZnCl_2$, which is associated with the excitation of configurational degrees of freedom, is unusual by comparison with most other liquids (molecular, ionic, or covalent) in that it appears to be decreasing as T_g is approached and possibly to have a maximum value at $T_g < T_{max} < T_m$. Heat capacities of this form can be accounted for by the Schottky-type heat capacity associated with "n-state" models, and it is significant in this con-

nection that some spectroscopic evidence for well-defined "on" and "off" bonding states in $ZnCl_2$ has been reported.[5a] Since these observation led originally to the development of the "bond-lattice" model for network glasses,[27] we show, in Figure 4a, how well the experimental ΔC_p plot can be reproduced by the two-parameter bond-lattice model equations

$$\Delta C_p = \frac{\Delta H}{RT^2} \frac{\exp\left(\frac{\Delta H - T\Delta S}{RT}\right)}{\left[1 + \exp\left(\frac{\Delta H - T\Delta S}{RT}\right)\right]^2} \quad (2)$$

$$= \frac{\Delta H}{RT^2} (N_x(1 - N_x)) \quad (3)$$

Here ΔC_p is the heat capacity increment per mole of bonds and is to be compared with one-fourth the molar heat capacity change of $ZnCl_2$ since there are four Zn–Cl bonds per mole of $ZnCl_2$. ΔH is the energy per mole required to break the Zn–Cl bonds, and ΔS is the entropy change per mole associated with the consequent changes in structural and vibrational degeneracy. In the simplified form eq 3, N_x is simply the fraction of bonds in the lattice which are broken at temperature T, and is given[27] by

$$N_x = (1 + \exp(\Delta H - T\Delta S)/RT)^{-1} \quad (4)$$

In the case of parameters ΔH = 3 kcal/mol and ΔS = 0.5 or 1 eu, the equilibrium heat capacity form is also capable of accounting approximately for that fraction of the entropy of fusion ($\sim 0.4\Delta S_F$) which is retained in the glassy state when internal equilibrium is lost at T_g. This is shown by the semilog plot (Kauzmann plot) inset in Figure 4a. Although two-state models are generally discredited by such findings as those given in the preceding paper, we believe it worthwhile to note (see Figure 4b) that with the addition of a single parameter (the excitation volume), the excess expansivity of the liquid over that of the glass at normal pressure can also be adequately described. Leidecker et al.[28] have shown that an adequate description of pressure effects also may be obtained, at least for the case of B_2O_3, if the two-state model is modified by inclusion in the analysis of a second excited state which is degenerate in energy with the first but lower in volume.

As a final illustration of the use which can be made of the heat capacity data through the simple two-state model, we show that the temperature dependence of the mass transport properties of $ZnCl_2$ can be accounted for very well using the exponential relationship between the probability of a mass transporting particle rearrangement, $p(r)$, and the state of configurational excitation, N_x, suggested by Angell and Rao,[27] and recently derived by Van Damme and Fripiat.[41]

The proposed relationship, given by

$$p(r) = p_0 \exp(\zeta/N_x) \quad (5)$$

where viscosity, $\eta = \eta_0 \exp(\zeta_\eta/N_x)$, etc. ($p_0$, η_0, and ζ are constants), accounts well for the mass transport properties of liquid $ZnCl_2$ as shown below. Because of the nearly linear dependence of N_x on temperature such that $N_x = C(T - T_0)$ in the relevant temperature range 400–700 K, this expression has the virtue of accounting for the success of the Vogel–Tammann–Fulcher (VTF) transport equation

$$\eta = \eta_0 \exp\left[\frac{B}{(T - T_0)}\right] \quad (6)$$

(where η_0, B, and T_0 are constants) without actually requiring the existence of a unique transition at T_0.

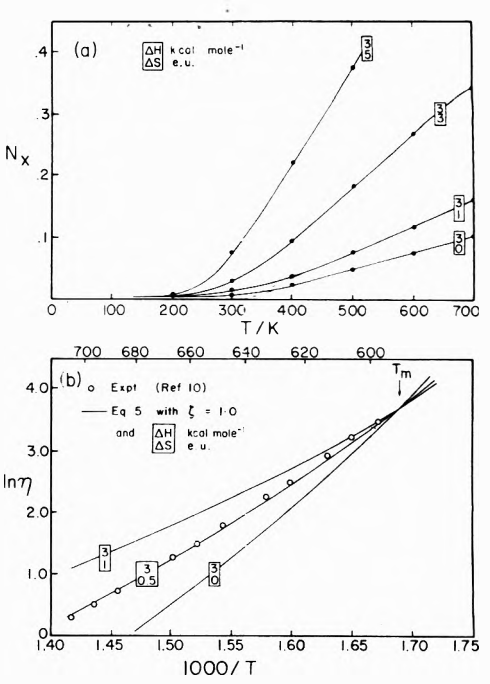

Figure 5. (a) Excited bond fraction vs. temperature for different excitation entropy parameters and ΔH = 3 kcal mol^{-1} showing linear temperature dependence, $N_x = C(T - T_0)$, in the region N_x = 0.1 to 0.4. (b) Comparison of experimental viscosity temperature dependence with values calculated from eq 5 (—) normalized to the experimental value at the melting point.

The linearity of the N_x vs. T relation for several choices of excitation parameters is shown in Figure 5a, and the good fit of the non-Arrhenius viscosity–temperature relation predicted by eq 5 using only the parameters ΔH = 3.0 kcal/mol and ΔS = 0.5 U (i.e., with ζ = 1.0) is shown in Figure 5b. If ζ is treated as a free parameter then an equally good fit to the viscosity data can be obtained with other ΔS parameters. For instance, with ΔS = 1.0, the ΔS value which best describes the excess heat capacity in Figure 4a, a value of ζ = 1.35 must be used. To permit comparisons with experiment, in Figure 5b, the calculated η–T functions were scaled to the experimental curve by making the experimental and calculated curves coincident at the normal melting point 591 K (318 °C). This amounts to assigning to the preexponential parameter η_0 an appropriate value for each set of ΔH, ΔS, and ζ parameters.

The viscosity and other transport properties of $ZnCl_2$ are equally well fitted by the VTF equation yielding, in different studies, T_0 = 250 ± 30 K[10] from viscosity data, and 340 ± 20,[14] 320 ± 10,[15] and 280 ± 10 K[16] from electrical conductance data. Values of T_0 in the range 320–350 K are suggested by the extrapolated N_x–T relations (Figure 5a) which account for the excess heat capacity of this substance. Extrapolation of the heat capacity, assuming a linear rather than curvilinear decrease with decreasing temperature, indicates a vanishing of the excess entropy (S(liquid) – S(crystal)) at about 250 K.[27]

$ZnCl_2$ is unusual among viscous molten salts for the large (average) Arrhenius coefficient and the relatively small departures from Arrhenius behavior which it shows.[9-16] According to eq 5 this is to be related to the comparatively sluggish rate of increase in broken bond fraction with increasing temperature, see Figure 5a, which also causes the value of ΔC_p to be smaller than usual. The rate of increase of N_x with T is itself determined by the magnitude of ΔS, a small value of which implies that not much increase in local system probability (configurational or vibrational degeneracies, $\Delta S = R \ln \Delta W$ or $R \ln \nu_2/\nu_1$) ac-

companies bond rupture. An extreme case of such behavior is provided by the other glass-forming halide, BeF_2, and also by the oxide glass-formers GeO_2 and SiO_2. In these network liquids, which are even more highly structured than $ZnCl_2$, the heat capacity barely changes at T_g and the viscosity temperature dependence is strictly Arrhenius.[11,19]

We conclude that, although this simple one-order parameter model may be inadequate to describe both temperature and pressure effects, it is useful and economic, in terms of adjustable parameters, in the description and interpretation of constant pressure behavior.

Pressure Dependence of T_g, and an Exception to the First Davies–Jones Equation. Compared with the nitrate glasses of the previous paper, $ZnCl_2$ has a rather large pressure dependence of T_g. It is not as large, however, as one would anticipate from the observed values of $\Delta\alpha$ and ΔC_p, assuming that eq 1 is valid. Taking values from the data shown in Figures 4b and 2 ($\Delta\alpha = 1.74 \times 10^{-4}$ deg^{-1},[18] $\Delta C_p = 4.5$ cal/mol^{-1} deg^{-1} at 375 K) and using $V_g = 50.61$ cm^3 mol^{-1} [29] one obtains from eq 1 $dT_g/dP = 17.5$ deg kbar^{-1}. Restating this result, we see that the experimental $\Delta\alpha$ is larger, relative to the observed ΔC_p, than eq 1 would suggest from the observed dT_g/dP. An earlier value of $\Delta\alpha$, obtained by Eisenberg and Hileman,[30] is somewhat smaller (viz. 1.56×10^{-4} deg^{-1}) than the datum of Goldstein and Nakonecznyi[18] used above, but still leads to a predicted dT_g/dP which is far too large, 15.8 deg kbar^{-1}.

This is only the second clear-cut failure of eq 1 reported and it is therefore desirable that the accuracy of the data involved be confirmed. We have noted in this laboratory that small amounts of second components cause rather rapid increases in the value of C_p(liquid)/C_p(glass) for $ZnCl_2$, and similar changes would presumably also be found for $\Delta\alpha$. It is possible therefore that contamination by water (which is notoriously difficult to remove from $ZnCl_2$) may have affected the two $\Delta\alpha$ results quoted above. Both laboratories, however, appear to have taken appropriate measures to remove water and we do not expect that further measurements will change the qualitative conclusion that eq 1 fails for $ZnCl_2$ (and will therefore have to be abandoned as a general law of glass transition thermodynamics). We expect it will also fail for GeO_2,[19] SiO_2, and BeF_2 (if the glass transition thermodynamic manifestation can in fact be detected for the latter two substances). The implications of the observed eq 1 breakdown must therefore be examined.

For a true (equilibrium) second-order transition, eq 1 with dT_g/dP replaced by dT_2/dP can be deduced from the recognition that $\Delta S = 0$ at such a transition.[31] Goldstein[32] has shown that eq 1 may be expected to hold for a kinetically determined transition, if the transition at constant cooling rate occurs at a constant value of the excess entropy. Only in such a case can glass formed at one pressure pass through the glass transition at another pressure and still satisfy the condition $\Delta S = 0$ from which eq 1 is derived.[32c] This situation is depicted in Figure 6 which shows a liquid entropy surface undergoing a discontinuous change of slope along a P–T line which falls a constant entropy increment (S_{ex}) above the P–T line at which an equilibrium transition to an "ideal" glass state would occur for hypothetical infinite-time-scale experiments. The projection of this line in the P–T plane (see Figure 6) gives a slope dT_g/dP which would conform to eq 1. In view of the validity of eq 1 for so many vitreous systems investigated previously, the glass surface commencing along this P–T–S line is designated "normal glass". Since the experimental dT_g/dP for $ZnCl_2$ is smaller

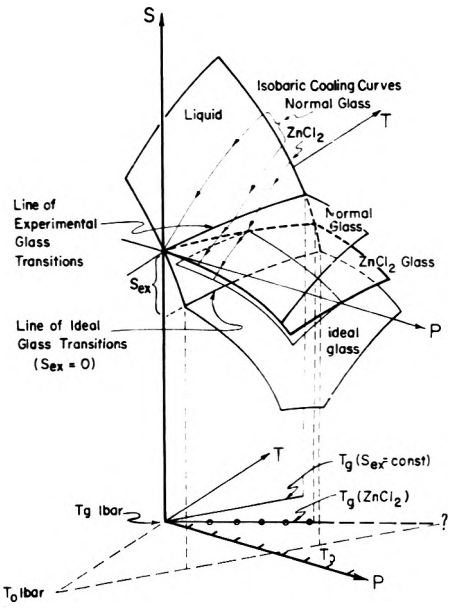

Figure 6. Entropy surfaces for liquid, ideal glass, and a "normal" glass (i.e., glass obeying eq 1). A pseudo-surface for $ZnCl_2$, the intersection of which with the liquid surface qualitatively describes the experimental dT_g/dP behavior, is also shown. This surface actually must be a composite of isobaric "strips" of different glass surfaces each of which is characterized by a constant excess entropy, and each of which can only be accessed from the liquid surface at a single T, P point of entrance. A portion of one such surface is shown. The diagram also poses the question of whether an ideal glass ($S_{ex}(T_g) = 0$, or $T_g = T_0$) could be produced under sufficiently high pressure.

than predicted, the geometrical requirements of Figure 6 show that for $ZnCl_2$ the value of the excess entropy must decrease with increasing pressure, i.e., $ZnCl_2$ glass becomes more nearly ideal (S_{ex} decreases) as the pressure at which the glass is formed increases.[33]

This may be more easily seen from the following thermodynamic relations and the recognition that the glass transition at constant cooling rate occurs when the average structural relaxation time τ_{av} reaches a fixed value. We write

$$dS_{ex} = \frac{\Delta C_p}{T} dT - V\Delta\alpha\, dP \neq 0 \tag{7}$$

whence

$$\left(\frac{\partial S_{ex}}{\partial P}\right)_\tau = \frac{\Delta C_p}{T_g}\left(\frac{\partial T_g}{\partial P}\right)_\tau - V_g\Delta\alpha \tag{8}$$

so that

$$\left(\frac{\partial T_g}{\partial P}\right)_\tau = T_g V_g \frac{\Delta\alpha}{\Delta C_p} + \frac{T}{\Delta C_p}\left(\frac{\partial S_{ex}}{\partial P}\right)_\tau \tag{9}$$

Since dT_g/dP proves to be less than $T_g V_g \Delta\alpha/\Delta C_p$ it is clear from eq 9 that $(\partial S_{ex}/\partial P)_\tau$ must be negative.

The failure of eq 1 for $ZnCl_2$ is in many ways less surprising than its success for the general case. The validity of eq 1 for the general case would seem to require that average relaxation times for liquids near T_g are determined by the excess entropy content alone

$$\tau = f(S_{ex}) \tag{10}$$

implying a very simple connection between thermodynamic and relaxational properties.

Failure of such a simple connection would be expected to show up most prominently in a system in which S_{ex} varies relatively slowly with temperature, as in the case of zinc chloride. Even in the relaxation theory of Adam

and Gibbs,[20] in which the excess (or configurational) entropy of the supercooled liquid plays a central role, τ is not a function of S_{ex} alone. Rather, according to Adam and Gibbs

$$\tau = f(TS_{ex}) \quad (11a)$$

$$= \tau_0 \exp(-C/TS_{ex}) \quad (11b)$$

The Adam and Gibbs function, although failing near T_g for many glasses,[25,34] is actually of the right form to rationalize the present data since at higher T_g (generated by increased pressure) a smaller S_{ex} is needed to yield the same τ (the constancy of which determines T_g). Goldstein[36] has shown that if constancy of TS_{ex} rather than of S_{ex} determines T_g then eq 1 should be replaced by

$$\frac{dT_g}{dP} = \frac{T_g V_g \Delta\alpha}{S_{ex} + \Delta C_p} \quad (12)$$

According to observations on molecular and polymeric liquids by Wunderlich[37] and by Bestul and Chang[38] ΔC_p and S_{ex} have "universal" values of ~2.7 cal deg^{-1} per "bead" and ~0.7 eu per "bead". Thus eq 12 suggests that ~25% discrepancies with eq 1 should be the general rule. Such deviations are generally indistinguishable against the accumulated experimental uncertainties of the quantities in eq 1, although a trend to deviations in the expected direction has been noted elsewhere.[39] On the other hand, for inorganic network liquids which exhibit small values of ΔC_p (1.5 cal deg^{-1} per bead in the present case, assuming each atom in the $ZnCl_2$ molar unit satisfies Wunderlich's "bead" criterion), eq 12 predicts more pronounced failures of eq 1, such as we have observed. Using the entropy residual at T_g according to Figure 4a (1.79 eu mol^{-1}) in eq 12 we calculate a considerably reduced value of dT_g/dP, 12.5 deg kbar^{-1} which, however, still exceeds the experimental value. It is possible that the strong network glasses, e.g., GeO_2 for which $\Delta\alpha$ and ΔC_p values are available,[39] may exhibit even more pronounced departures from eq 1. Certainly it is reasonable to expect further failures of eq 1 and experiments to determine the range of its validity are desirable.

Finally some comment should be made on the apparent independence of T_g for $ZnCl_2$ on the sample pressure–temperature history. As noted earlier, for the typical polymer glass the glass temperature of a sample under a given uniform pressure depends strongly on whether the pressure was applied initially while the sample was in the liquid or in the glassy state. This is due to the very strong dependence of the relaxation time of a polymer on its configuration. Because moderate pressure applied below T_g produces only elastic compression, the configuration is fixed primarily by the temperature and pressure prevailing when complete internal equilibrium was initially lost, i.e., by the so-called fictive temperature and pressure. In $ZnCl_2$, because of the small ΔC_p, the relaxation time is proportionately more dependent on the external variables, pressure and temperature. The greater dependence of τ_{av} for $ZnCl_2$ on pure temperature has been previously remarked on by Goldstein.[18,40] Presumably a high precision search would reveal some systematic pressure–temperature history dependence for T_g for $ZnCl_2$ also but the present work establishes that it must be a minor effect. The relatively large dependence of τ_{av} on pure temperature is seen also in the shift of T_g by 3 °C for a change in dT/dt of only 4°C/min (Figure 3).

Acknowledgment. The authors are indebted to the National Science Foundation for support of this work under Grant No. GP 30722, and to Professor M. Goldstein for some very helpful discussion of the pressure dependence anomaly.

References and Notes

(1) W. Bues, *Z. Anorg. Allg. Chem.*, **279**, 104 (1955).
(2) J. K. Wilmshurst, *J. Chem. Phys.*, **39**, 1779 (1963).
(3) D. E. Irish and T. F. Young, *J. Chem. Phys.*, **43**, 1765 (1965).
(4) J. R. Moyer, J. C. Evans, and G. Y.-S. Lo, *J. Electrochem. Soc.*, **113**, 158 (1966).
(5) (a) C. A. Angell and J. Wong, *J. Chem. Phys.*, **53**, 2053 (1970); (b) C. A. Angell, G. Wegdam, and J. van der Elsken, *Spectrochim. Acta, Part A*, **30**, 665 (1974).
(6) A. H. Narten, *J. Chem. Phys*, **56**, 1905 (1972).
(7) A. S. Quist, J. B. Bates, and G. E. Boyd, *Spectrochim. Acta*, in press.
(8) A. Rahman, R. H. Fowler, and A. H. Narten, *J. Chem. Phys.*, **57**, 3010 (1972).
(9) G. J. Gruber and T. A. Litovitz, *J. Chem. Phys.*, **40**, 13 (1964).
(10) A. J. Easteal and C. A. Angell, *J. Chem. Phys.*, **56**, 4231 (1972).
(11) C. T. Moynihan and S. Cantor, *J. Chem. Phys.*, **48**, 115 (1968).
(12) C.-A. Sjoblom and A. Behn, *Z. Naturforsch. A*, **23**, 495 (1968).
(13) J. O'M. Bockris, S. R. Richards, and I. Nanis, *J. Phys. Chem.*, **69**, 1627 (1965).
(14) J. O'M. Bockris, E. H. Crook, H. Bloom, and N. E. Richards, *Proc. R. Soc. London, Ser. A*, **255**, 558 (1960).
(15) H. Bloom and I. A. Weeks, *J. Chem. Soc. A*, 2028 (1969).
(16) A. J. Easteal and C. A. Angell, *J. Phys. Chem.*, **74**, 3987 (1970).
(17) G. D. Robbins and J. Braunstein in "Molten Salts: Characterization and Analysis", G. Mamantov, Ed., Marcel Dekker, New York, N.Y., 1969, p 44; and private communication.
(18) M. Goldstein and M. Nakoneczryi, *Phys. Chem. Glasses*, **6**, 126 (1965).
(19) C. A. Angell and J. C. Tucker in "Chemistry of Process Metallurgy", J. H. E. Jeffes and R. J. Tait, Ed., Institute of Mining and Metallurgy, 1974, p 207.
(20) G. Adam and J. H. Gibbs, *J. Chem. Phys.*, **43**, 139 (1965).
(21) R. O. Davies and G. O. Jones, *Adv. Phys.*, **2**, 370 (1953); *Proc. R. Soc. London, Ser. A*, **217**, 26 (1953).
(22) E. Williams and C. A. Angell, *J. Phys. Chem.*, preceding paper in this issue.
(23) D. Cubiciotti and H. Eding, *J. Chem. Phys.*, **40**, 978 (1964).
(24) B. Brehler, *Naturwissenschaften*, **46**, 554 (1959); *Fortschr. Mineral.*, **38**, 187 (1960); *Z. Kristallogr.*, **115**, 373 (1961).
(25) (a) C. A. Angell, *J. Am. Ceram. Soc.*, **51**, 117 (1968); (b) N. Smirl and J. P. Devlin, *J. Phys. Chem.*, **76**, 3093 (1972).
(26) V. E. Schnaus, C. T. Moynihan, R. W. Gammon, and P. B. Macedo, *Phys. Chem. Glasses*, **11**, 213 (1970).
(27) C. A. Angell and K. J. Rao, *J. Chem. Phys.*, **57**, 470 (1972).
(28) H. W. Leidecker, J. H. Simmons, T. A. Litovitz, and P. B. Macedo, *J. Chem. Phys.*, **55**, 2028 (1971).
(29) This value of V_g is assessed from the liquid density data of W. Klemm (*Z. Anorg. Chem.*, **152**, 235 ('926)) which was confirmed by Angell and Wong (ref 5), in combination with the expansivity data of Goldstein and Nakonecznyi (ref 13) and is believed accurate to ±0.2%.
(30) A. Eisenberg and B. J. Hileman, Technical Report No. 3, Contract No. 233 (87), Chemistry Branch, Office of Naval Research.
(31) L. D. Landau and I. M. Lifschitz, "Statistical Physics", R. F. Pierls, Ed., Addison-Wesley, Reading, Mass., 1958, p 437.
(32) (a) M. Goldstein, *J. Chem. Phys.*, **39**, 3369 (1963); (b) *J. Phys. Chem.*, **77**, 667 (1973); (c) *J. Appl. Phys.*, in press.
(33) Thus the surface in Figure 6 designated "$ZnCl_2$ glass" should be regarded as a composite of infinitesimal slices of different glass surfaces. Each surface element has in common the same relaxation time along the *T–P* line connecting it to the equilibrium liquid surface.
(34) B. Bose, R. Weiler, and P. B. Macedo, *Phys. Chem. Glasses*, **11**, 117 (1970).
(35) W. T. Laughlin and D. R. Uhlmann, *J. Phys. Chem.*, **76**, 2317 (1972).
(36) M. Goldstein, private communication.
(37) B. Wunderlich, *J. Phys. Chem.*, **64**, 1052 (1960).
(38) A. B. Bestul and S. S. Chang, *J. Chem. Phys.*, **42**, 3731 (1964).
(39) C. A. Angell and W. Sichina, *Trans. N.Y. Acad. Sci.*, in press. (Proceedings of the Workshop on the Glass Transition and Nature of the Glassy State, Dec, 1975.)
(40) M. Goldstein, *J. Chem. Phys.*, **44**, 1852 (1965).
(41) H. Van Damme and J. J. Fripiat, *J. Chem. Phys.*, **62**, 3365 (1976).

Electrosorption of 2-Butanol at the Mercury–Solution Interface 2. Theory of Noncongruent Electrosorption

David M. Mohilner,*[1] Hisamitsu Nakadomari,[2] and Patricia R. Mohilner

Departments of Chemistry and Computer Science, Colorado State University, Fort Collins, Colorado 80523 *(Received July 23, 1976)*

Publication costs assisted by the Air Force Office of Scientific Research

A theory is proposed to explain noncongruent electrosorption of organic compounds at the metal–solution interface in the absence of specific ionic adsorption. Under this theory the inner (compact) part of the electrical double layer is treated as a two-component nonelectrolyte solution called the surface solution. By means of this theory it is possible to calculate the excess Gibbs free energy of mixing of the surface solution as well as the activities and activity coefficients of the adsorbed organic compound and of the adsorbed water in the inner layer. It is shown that in a certain range of excess charge densities on the metal the dilute surface solutions exhibit positive deviations from Raoult's law, and it is proposed that, like bulk aqueous solutions of aliphatic alcohols, the properties of the surface solution are under entropy control. For this reason, it is concluded that the so-called Flory–Huggins electrosorption isotherm is probably incorrect because the statistical mechanical theory on which that isotherm is based predicts that the excess electrochemical entropy of mixing of the surface solution will be positive. It is shown that in one extreme limiting case this theory leads to the Frumkin isotherm, but the interpretation of the parameter appearing in the exponential term of that isotherm would be quite different under this theory than under the theory of Frumkin.

I. Introduction

In part 1[3] the experimental measurements of the electrosorption of 2-butanol on mercury from aqueous sodium sulfate solutions and the thermodynamic analysis of the data were described. It was shown that the electrosorption is congruent neither with respect to the electrode potential nor with respect to the excess charge density on the metal surface. In the present paper we develop a general theory of the adsorbed layer in the absence of specific ionic adsorption in terms of a model, the *surface solution*, in which the inner (compact) part of the electrical double layer is treated as a two-component nonelectrolyte solution. We then apply this theory to our data for 2-butanol in the horizontal orientation and calculate the electrochemical excess free energy of mixing of the surface solution and the activity and activity coefficients of the 2-butanol and water in the inner layer as functions of the surface mole fraction and the electrical state of the system. It will be shown that at constant composition in the surface solution the magnitude of the deviations from ideality (Raoult's law) depends on the electrode potential or excess charge density. The noncongruence of the electrosorption isotherm is a direct consequence of this dependence of the nonideality on the electrical state.

II. Theory

A. *The Model.* We consider the electrosorption of a neutral organic compound on a metal electrode from an aqueous electrolyte solution in the absence of specific ionic adsorption. Therefore, the inner part of the electrical double layer is populated only by organic molecules and water molecules. We shall treat this inner layer as a two-component nonelectrolyte solution, the *surface solution*. It is assumed that the organic molecules adsorb in a given orientation to form only a monolayer or fraction of a monolayer. The thickness of the surface solution is given by the distance from the metal surface to a hypothetical mathematical surface placed just on the solution side of the adsorbed organic molecules. This mathematical surface will serve as the *dividing surface* for the purpose of calculating the derelativized (Gibbsian) surface excesses[4,5] of the organic compound, Γ_A, and of the water, Γ_W. The region between the metal surface and the dividing surface thus contains only one layer of organic molecules but a *multilayer* of water molecules due to the relatively smaller size of the water molecules. Thus our model of the inner layer is *not* a monolayer model for water.

The surface excesses, Γ_A and Γ_W, reckoned at this dividing surface will be identical with the absolute surface concentrations (in mol cm^{-2}) of the organic compound and of the water in the inner layer. In order to apply the theory developed here to experimental electrosorption data which yield only the relative surface excess, Γ_{AW}, of the organic compound, it will be necessary to derelativize the relative surface excess on the basis of molecular models. The method of derelativization was described in part 1.[3] In order to develop the theory of the inner layer in as parallel a fashion as possible to ordinary bulk nonelectrolyte solution theory,[6,7] the concentration units we shall employ will be the mole fractions, x_A^{ads} and x_W^{ads}, of the adsorbed organic compound and water, respectively, in the inner layer. These surface mole fractions are given by

$$x_A^{ads} = \Gamma_A/(\Gamma_A + \Gamma_W) \quad (1)$$

and

$$x_W^{ads} = \Gamma_W/(\Gamma_A + \Gamma_W) \quad (2)$$

The surface solution model of the inner layer adopted here is quite different from the two-dimensional gas model employed by Parsons[4,8] in which the presence of the adsorbed solvent molecules is not explicitly considered, so that the intermolecular interactions in the inner layer are formally attributed to organic–organic intermolecular forces. In Parson's model the goal was to develop a two-dimensional "equation of state" for the adsorbed organic molecules analogous to the three-dimensional equations of state for real gases, and the measured surface pressure was equated with the pressure of the two-dimensional gas. In contrast, the goal of the present theory will be to develop equations for the excess electrochemical free energy of mixing of the surface solution and for the activity coefficients of the adsorbed organic compound and of the adsorbed water in the inner layer as functions of

x_A^{ads} and the electrical state of the system. The theory developed here has some similarities to, but also significant differences from, the theory of Frumkin[9,10] in which an analogy was drawn between the measured surface pressure and the osmotic pressure of a two-dimensional solution. It will be shown in section III.E that the Frumkin isotherm does indeed result from the present theory in one particular limiting case.

B. *Standard States for the Adsorbed Species.* In the treatment of two-component bulk nonelectrolyte solutions it is common[6,7] to choose as the standard state for each component the pure substance at the temperature of interest, i.e., to choose the fugacity, f°, of each component in its standard state to be equal to the value, $f^\bullet$, which is the fugacity of the pure component at the specified temperature. This choice of standard states is often described as the *symmetrical choice*. Another choice, which is sometimes convenient to make, is the *unsymmetrical choice* of standard states.[11] With this choice, the standard state of component 1, which is called the *solvent*, is taken as the pure component at the temperature of interest, so that $f_1^\circ = f_1^\bullet$. However, for component 2, which is called the *solute*, the standard state fugacity is taken as the extrapolation of the fugacity of component 2 along the Henry's law line to unit mole fraction, i.e., $f_2^\circ = f_2^\bullet = k_{2H}$ where k_{2H} is the slope of the Henry's law line for component 2. (We shall hereafter use the Plimsoll mark, $\ominus$, as the superscript to denote this hypothetical, Henry's law standard state.) The activity coefficient for component 2 under this unsymmetrical choice of standard states is called the *rational* activity coefficient.[11]

In our treatment of the inner layer as a two-component nonelectrolyte solution, we shall use at different times both of these choices of standard states. In the beginning, for the direct use of the experimental electrosorption data, it will be convenient to use the unsymmetrical choice of standard states, i.e., to consider the adsorbed water as the solvent and the adsorbed organic compound as the solute in the surface solution. This will enable us to calculate from the experimental data the ratio of the rational activity coefficient, γ_{Ar}^{ads}, of the adsorbed organic compound to the nth power of the activity coefficient of the adsorbed water, $(\gamma_W^{ads})^n$. Here n is the number of water molecules in the inner layer replaced by one adsorbing organic molecule. We shall then fit this ratio, $[\gamma_{Ar}^{ads}/(\gamma_W^{ads})^n]$, to a theoretical equation (eq 22) and calculate the individual activity coefficients, γ_A^{ads} and γ_W^{ads}, of the adsorbed organic compound and water on the basis of the symmetrical choice of standard states.

The fugacity of the adsorbed species in the standard state will depend not only on the temperature, but also on the electrical state of the system. The electrical state of the system can be specified either by fixing the potential of the electrode, $E^\pm$, with respect to an indicator electrode[4] or by fixing the value of the excess surface charge density, σ^M. The standard state fugacities of the adsorbed molecules depend on the electrical state of the system because the adsorbed molecules interact with the electric field in the inner layer. To emphasize their dependence on the electrical state, we shall call these standard fugacities the *standard electrochemical fugacities.*

For any fixed electrical state of the system the two kinds of activity coefficients for the adsorbed organic compound are given by equations of the usual form[11]

$$\gamma_{Ar}^{ads} = f_A^{ads}/x_A^{ads} f_A^{\ominus} \tag{3}$$

and

$$\gamma_A^{ads} = f_A^{ads}/x_A^{ads} f_A^{\bullet} \tag{4}$$

In eq 3 and 4 f_A^{ads} is the electrochemical fugacity of the adsorbed organic compound at the specified temperature, electrical state, and surface mole fraction. $f_A^\ominus$ is the standard electrochemical fugacity of the adsorbed organic compound at the specified temperature and electrical state in the hypothetical, Henry's law standard state. $f_A^\bullet$ is the electrochemical fugacity of the adsorbed organic compound at the specified temperature and electrical state when the actual mole fraction of the organic compound in the inner layer is unity, i.e., when the electrode surface is fully covered with the organic compound. It follows from eq 3 and 4 that

$$\gamma_{Ar}^{ads} = \gamma_A^{ads}(f_A^\bullet/f_A^\ominus) \tag{5}$$

C. *Method of Determination of the Standard Electrochemical Free Energy of Adsorption, $\Delta\bar{G}_{ads}^\ominus$, and of the Activity Coefficient Ratio, $[\gamma_{Ar}^{ads}/(\gamma_W^{ads})^n]$, from Experimental Data.* The adsorption equilibrium is described by the following chemical equation:

$$A(b) + nH_2O(ads) \rightleftarrows A(ads) + nH_2O(b) \tag{6}$$

where (b) denotes the species in the bulk solution and (ads) denotes the species adsorbed in the inner layer. By equating the electrochemical potentials of the species on both sides of eq 6 we can derive the electrosorption isotherm in terms of the bulk activities, the surface mole fractions, and the surface activity coefficients.

$$\{\exp[-\Delta\bar{G}_{ads}^\ominus/RT]\}[a_A/(a_W)^n] = [x_A^{ads}/(x_W^{ads})^n][\gamma_{Ar}^{ads}/(\gamma_W^{ads})^n] \tag{7}$$

In eq 7 a_A and a_W denote the activities of the organic compound and of water, respectively, in the bulk electrolyte solution on the basis of the symmetrical choice of bulk standard states (cf. part I[3]). γ_{Ar}^{ads} and γ_W^{ads} are the activity coefficients of the adsorbed species based on the unsymmetrical choice of standard states, and $\Delta\bar{G}_{ads}^\ominus$, the standard electrochemical free energy of adsorption, is given by

$$\Delta\bar{G}_{ads}^\ominus = \bar{\mu}_A^\ominus - \mu_A^\bullet - n\bar{\mu}_W^\bullet + n\mu_W^\bullet \tag{8}$$

In eq 8 $\bar{\mu}_A^\ominus$ is the standard electrochemical potential of the adsorbed organic compound based on the hypothetical, Henry's law standard state at the specified temperature and electrical state. $\mu_A^\bullet$ is the chemical potential of pure bulk organic compound at the specified temperature. $\bar{\mu}_W^\bullet$ is the standard electrochemical potential of the adsorbed water based on the standard state of the surface fully covered with adsorbed water at the specified temperature and electrical state, and $\mu_W^\bullet$ is the chemical potential of pure bulk water at the specified temperature. x_A^{ads} and x_W^{ads} are given by eq 1 and 2. In the region of very low Γ_A, the rational activity coefficient of the adsorbed organic compound, γ_{Ar}^{ads}, will equal unity (Henry's law), and the activity coefficient of the adsorbed water, γ_W^{ads}, will also equal unity, since according to the Gibbs–Duhem equation whenever the solute obeys Henry's law the solvent must obey Raoult's law.[11]

The procedure adopted for determination of $\Delta\bar{G}_{ads}^\ominus$ was the following. First a least-squares fit of the relative surface excess, Γ_{AW}, to the bulk activity, a_A, was constrained to pass through the origin because when $a_A = 0$ it is required that $\Gamma_{AW} = 0$ also. In the very low concentration region the fitted values of Γ_{AW} were derelativized and the corresponding values of x_A^{ads} and x_W^{ads} were calculated. Then at each electrical state determined by the value of E^+ or σ^M in the very low concentration region $\ln [a_A/(a_W)^n]$ was plotted against $\ln [x_A^{ads}/(x_W^{ads})^n]$, and in each case the plot was found to be a straight line with

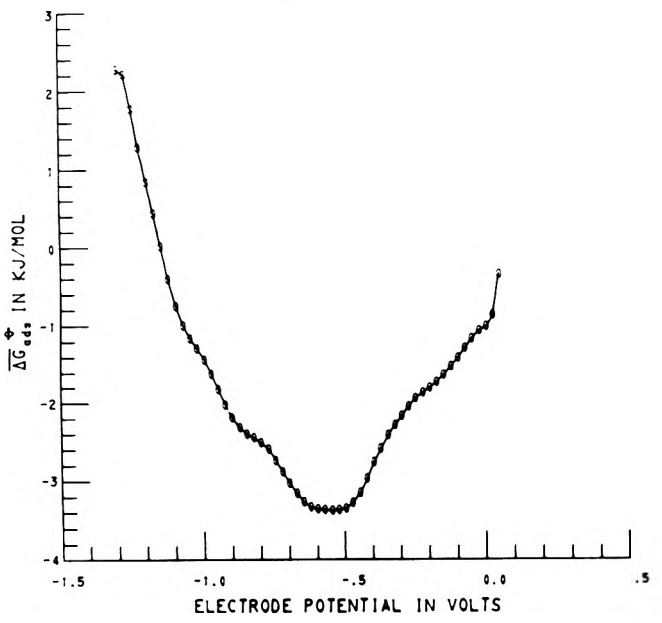

Figure 1. Standard electrochemical free energy of adsorption of 2-butanol on mercury from aqueous sodium sulfate solutions as a function of the electrode potential.

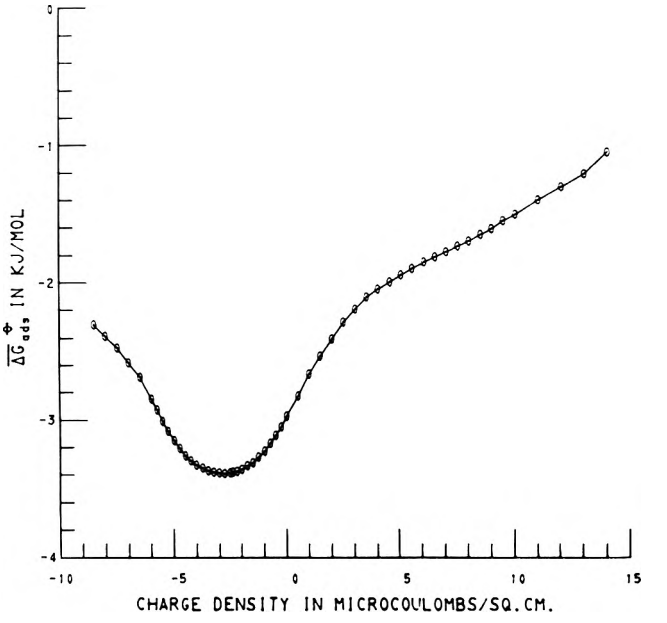

Figure 2. Standard electrochemical free energy of adsorption of 2-butanol on mercury from aqueous sodium sulfate solutions as a function of the excess charge density on the metal.

unit slope. According to eq 7 such a plot should have unit slope in the Henry's law region because in that region ln $[\gamma_{Ar}^{ads}/(\gamma_W^{ads})^n] = 0$. The intercept of this plot at each value of the electrode potential or excess charge density yields the corresponding value of the standard electrochemical free energy of adsorption, $\Delta\bar{G}_{ads}^{\bullet}$. Figure 1 is a plot of $\Delta\bar{G}_{ads}^{\bullet}$ vs. electrode potential for the electrosorption of 2-butanol in the horizontal orientation. Figure 2 is the corresponding plot of $\Delta\bar{G}_{ads}^{\bullet}$ vs. the excess charge density, σ^M. It will be noted that in each of these figures $\Delta\bar{G}_{ads}^{\bullet}$ passes through a minimum at the electrode potential or excess charge density of maximum adsorption for the horizontal orientation (cf. part 1[3]), and the value of $\Delta\bar{G}_{ads}^{\bullet}$ at each of these minima is the same, −3.40 kJ mol^{-1}, as it should be since the σ^M–E^+ curves for the 15 lowest bulk concentrations of 2-butanol crossed at a single point.

The value of $\Delta\bar{G}_{ads}^{\bullet}$ can then be used to calculate the ratio $[\gamma_{Ar}^{ads}/(\gamma_W^{ads})^n]$ for all higher concentrations from the experimental ratios of the bulk activities $[a_A/(a_w)^n]$ and of the surface mole fractions, $[x_A^{ads}/(x_W^{ads})^n]$ by substituting into eq 7. Thus from the experimental electrosorption data it is possible to calculate the ratio of the activity coefficients of the adsorbed species on the basis of the unsymmetrical choice of standard states.

D. *The Excess Electrochemical Gibbs Free Energy of Mixing of the Surface Solution and the Activity Coefficients of the Adsorbed Species on the Basis of the Symmetrical Choice of Standard States.* At fixed electrical state we shall denote the excess electrochemical Gibbs free energy of mixing by the symbol, $\Delta\bar{G}^E$. We define $\Delta\bar{G}^E$ in a manner exactly analogous to the definition of the excess Gibbs free energy of mixing of ordinary bulk solutions, ΔG^E, which was introduced in 1938 by Scatchard and Raymond,[12] namely: ΔG^E is the difference between the Gibbs free energy of mixing of the real solution[11] and the Gibbs free energy of mixing of the same solution if it behaved ideally.[11] The only reservation we must make in order to apply these classical solution concepts to the surface solution is to specify that the mixing process consists of mixing x_A^{ads} moles of the organic compound in its *electrochemical standard state* with x_W^{ads} moles of water in its *electrochemical standard state* to form the surface solution in which the activity of the organic compound is $a_A^{ads} = x_A^{ads}\gamma_A^{ads}$ and the activity of the water is $a_W^{ads} = x_W^{ads}\gamma_W^{ads}$. We specify further that we are using the symmetrical choice of standard states for the adsorbed species. If the surface solution behaved ideally we would have $\gamma_A^{ads} = 1$ and $\gamma_W^{ads} = 1$ over the entire composition range, $0 \le x_A^{ads} \le 1$. The electrochemical Gibbs free energy of mixing of the real surface solution is

$$\Delta\bar{G}_m = [x_A^{ads}(\bar{\mu}_A^{\bullet} + RT \ln a_A^{ads}) + x_W^{ads}(\bar{\mu}_W^{\bullet} + RT \ln a_W^{ads})] - x_A^{ads}\bar{\mu}_A^{\bullet} - x_W^{ads}\bar{\mu}_W^{\bullet}$$

or

$$\Delta\bar{G}_m = RT(x_A^{ads} \ln a_A^{ads} + x_W^{ads} \ln a_W^{ads}) \quad (9)$$

Similarly, the electrochemical Gibbs free energy of mixing of the surface solution if it behaved ideally would be

$$\Delta\bar{G}_m^I = RT(x_A^{ads} \ln x_A^{ads} + x_W^{ads} \ln x_W^{ads}) \quad (10)$$

The excess electrochemical free energy of mixing of the surface solution at the specified temperature, electrical state, and composition is therefore given by

$$\Delta\bar{G}^E = \Delta\bar{G}_m - \Delta\bar{G}_m^I \quad (11)$$

or

$$\Delta\bar{G}^E = RT(x_A^{ads} \ln \gamma_A^{ads} + x_W^{ads} \ln \gamma_W^{ads}) \quad (12)$$

It follows from eq 12 and the Duhem–Margules relation that[13] the activity coefficients, γ_A^{ads} and γ_W^{ads}, may be calculated from $\Delta\bar{G}^E$ and its rate of variation with x_A^{ads} by the means of the following equations

$$RT \ln \gamma_A^{ads} = \Delta\bar{G}^E + (1 - x_A^{ads})(\partial\Delta\bar{G}^E/\partial x_A^{ads}) \quad (13)$$

and

$$RT \ln \gamma_W^{ads} = \Delta\bar{G}^E - x_A^{ads}(\partial\bar{G}^E/\partial x_A^{ads}) \quad (14)$$

where R is the gas constant and T is the absolute temperature.

Rather than assuming that the surface solution behaves according to any particular nonideal nonelectrolyte solution model such as the regular solution model of Hil-

debrand,[6] we shall simply express $\Delta\bar{G}^E$ as a polynomial in x_A^{ads}. Thus

$$\Delta\bar{G}^E = RT \sum_{j=1}^{k} \alpha_j (x_A^{ads})^j \quad (15)$$

This polynomial of degree k is subject to two constraints[13] which follow from the properties of the excess free energy of mixing; namely, $\Delta\bar{G}^E$ must equal zero when $x_A^{ads} = 0$ and also when $x_A^{ads} = 1$. The first of these constraints is satisfied by having no term for $j = 0$ in eq 15. The second constraint is satisfied by specifying that

$$\sum_{j=1}^{k} \alpha_j = 0 \quad (16)$$

The coefficients, α_j, in eq 15 are functions of the temperature and of the electrical state of the system. Substitution of eq 15 into eq 13 yields the following equation for the activity coefficient, γ_A^{ads}, of the adsorbed organic compound

$$\ln \gamma_A^{ads} = \sum_{j=2}^{k} (1-j)\alpha_j (x_A^{ads})^j + \sum_{j=1}^{k} j\alpha_j (x_A^{ads})^{j-1} \quad (17)$$

Substitution of eq 15 into eq 14 yields the following equation for the activity coefficient, γ_W^{ads}, of the adsorbed water

$$\ln \gamma_W^{ads} = \sum_{j=2}^{k} (1-j)\alpha_j (x_A^{ads})^j \quad (18)$$

E. *Method of Determination of the Set of Coefficients* $\{\alpha_j\}$ *in the Equations for* $\Delta\bar{G}^E$, $\ln \gamma_A^{ads}$, *and* $\ln \gamma_W^{ads}$. The equation for the ratio of the activity coefficients of the adsorbed species on the basis of the unsymmetrical choice of standard states, $[\gamma_{Ar}^{ads}/(\gamma_W^{ads})^n]$, which can be determined from the experimental electrosorption data (cf. section II.C), is obtained in the following manner. First it follows from eq 5 that

$$\ln [\gamma_{Ar}^{ads}/(\gamma_W^{ads})^n] = \ln [\gamma_A^{ads}/(\gamma_W^{ads})^n] + \ln (f_A^{\bullet}/f_A^{\ominus}) \quad (19)$$

Then in the limit of infinite dilution in the surface solution, i.e., as $x_A^{ads} \to 0$, Henry's law will be obeyed by the organic compound, and Raoult's law will be obeyed by the adsorbed water. Thus

$$\lim_{x_A^{ads} \to 0} \{\ln [\gamma_{Ar}^{ads}/(\gamma_W^{ads})^n]\} = 0$$

$$= \lim_{x_A^{ads} \to 0} \{\ln [\gamma_A^{ads}/(\gamma_W^{ads})^n]\} + \ln (f_A^{\bullet}/f_A^{\ominus}) \quad (20)$$

Therefore, the required ratio of the standard electrochemical fugacities of the adsorbed organic compound, $(f_A^{\bullet}/f_A^{\bullet})$, in eq 19 is obtained by combination of eq 17, 18, and 20.

$$\ln (f_A^{\bullet}/f_A^{\ominus}) = -\lim_{x_A^{ads} \to 0} \{\ln [\gamma_A^{ads}/(\gamma_W^{ads})^n]\} = -\alpha_1 \quad (21)$$

Substitution of eq 17, 18, and 21 into eq 19 then yields

$$\ln [\gamma_{Ar}^{ads}/(\gamma_W^{ads})^n] = -\alpha_1 + (n-1)\sum_{j=2}^{k} (j-1)\alpha_j (x_A^{ads})^j + \sum_{j=1}^{k} j\alpha_j (x_A^{ads})^{j-1} \quad (22)$$

The procedure for evaluating the set of coefficients $\{\alpha_j\}$ is to fit the experimentally determined $\ln [\gamma_{Ar}^{ads}/(\gamma_W^{ads})^n]$ to the polynomial in x_A^{ads} given in eq 22 by the method of least squares, subject to the constraint given in eq 16. A discussion of the computer procedure used for this least-squares fitting is given in Appendix A available as supplementary material.

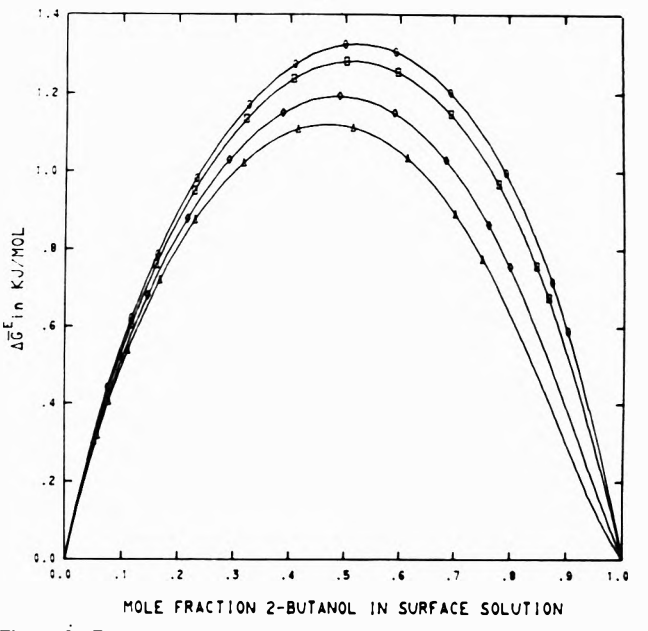

Figure 3. Excess electrochemical free energy of mixing of the surface solution at various electrode potentials. E^+ values in volts: ⊙, −0.450; ⊡, −0.625; ◇, −0.750; △, −0.800.

III. Results and Discussion

A. *The Excess Electrochemical Free Energy of Mixing of the Surface Solution,* $\Delta\bar{G}^E$, *and the Noncongruence of the Electrosorption Isotherm.* At each constant value of the electrode potential, E^+, or of the excess surface charge density, σ^M (cf. part 1[3]), the value of $\ln [\gamma_{Ar}^{ads}/(\gamma_W^{ads})^n]$ was calculated at each experimental value of x_A^{ads}. Then at each fixed electrical state, $\ln [\gamma_{Ar}^{ads}/(\gamma_W^{ads})^n]$ was fitted by the method of least squares (cf. Appendix A) to the polynomial of degree k given in eq 22 subject to the constraint given by eq 16, and the values of the coefficients, α_j, were determined. Least-squares fits were made for all values of k from 2 to 9, and at each point the difference between the fitted value and the experimental value of $\ln [\gamma_{Ar}^{ads}/(\gamma_W^{ads})^n]$ was calculated. In all cases the fits for $k = 2$ and $k = 3$ were so poor that these values of k could be rejected immediately. With increasing k the closeness of the least-squares fit to the experimentally determined $\ln [\gamma_{Ar}^{ads}/(\gamma_W^{ads})^n]$ improved, but to a decreasing extent as the value of k increased. At the same time, of course, as the degree, k, of the polynomial was increased, the number of degrees of freedom of the least-squares fit, and thus the amount of smoothing, decreased. On the basis of careful examination of the results of the least-squares fitting, it was decided that the degree $k = 7$ was optimum. Therefore all of the discussion which follows is based on the fitting of $\ln [\gamma_{Ar}^{ads}/(\gamma_W^{ads})^n]$ to the seventh degree polynomial in x_A^{ads}. At each value of E^+ or σ^M the coefficients, α_j, were substituted into eq 15 to calculate the excess electrochemical free energy of mixing, $\Delta\bar{G}^E$, of the surface solution as a function of x_A^{ads}. Figure 3 illustrates the behavior of $\Delta\bar{G}^E$ at selected constant electrode potentials.

Just as is true of the excess free energy of mixing, ΔG^E, of ordinary bulk solutions, the excess electrochemical free energy of mixing of the surface solution must be zero throughout the entire concentration range, $0 \leq x_A^{ads} \leq 1$, for an ideal solution; it will be positive for a surface solution which exhibits positive deviations from Raoult's law; it will be negative for a surface solution which exhibits negative deviations from Raoult's law. The magnitude of $\Delta\bar{G}^E$ is a direct measure of the extent of nonideality of the surface solution. It is clear from Figure 3 that the extent of

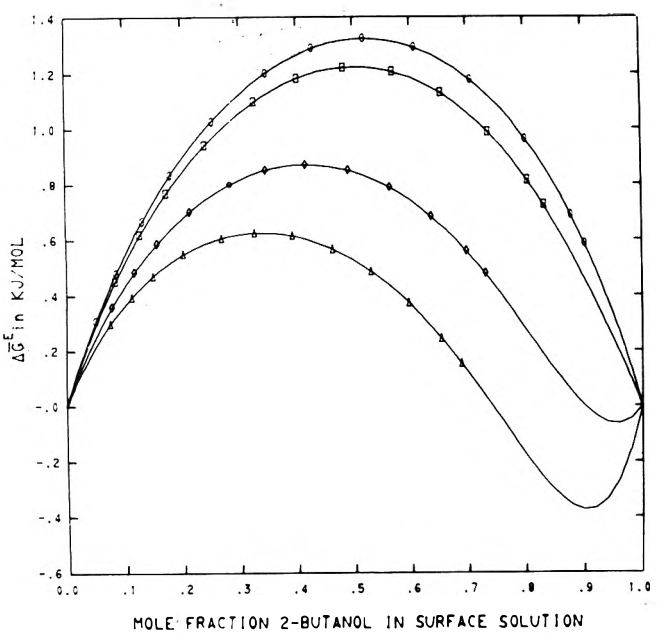

Figure 4. Excess electrochemical free energy of mixing of the surface solution at various values of the excess charge density. σ^M values in μC cm^{-2}: ⊙, −2.20; ⊡, −3.25; ◊, −4.00; △, −4.25.

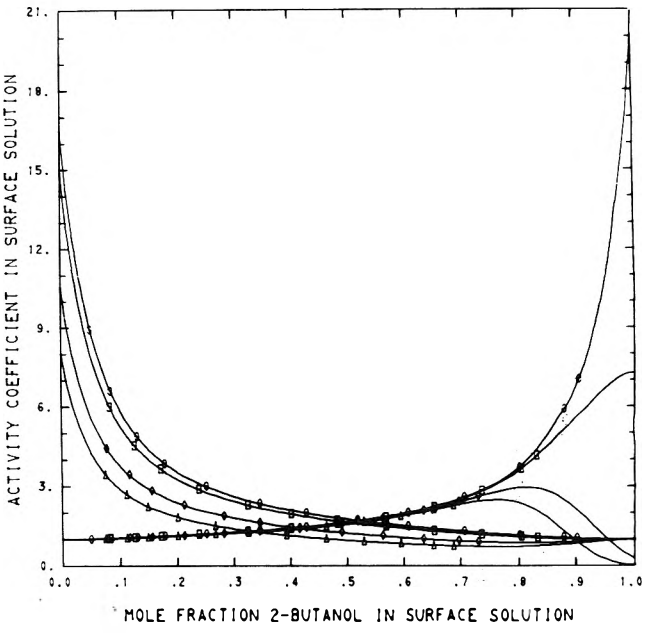

Figure 5. Activity coefficients of adsorbed 2-butanol (curves running down from left to right) and of adsorbed water (curves running up from left to right) on the basis of the symmetrical choice of standard states at various values of the excess charge density. σ^M values are same for corresponding symbols as in Figure 4.

nonideality of the inner layer (surface solution) in the case of the electrosorption of 2-butanol from aqueous sodium sulfate solutions is dependent on the value of the electrode potential. At fixed mole fraction of the 2-butanol in the inner layer, the excess electrochemical free energy of mixing and also its rate of variation with x_A^{ads}, i.e., $(\partial\Delta\bar{G}^E/\partial x_A^{ads})$, changes with electrode potential. It follows, therefore, from eq 12, 13, and 14 that the activity coefficients of the adsorbed 2-butanol and of the adsorbed water also vary with electrode potential at constant composition in the inner layer.

At constant temperature, the only way the electrosorption isotherm could be congruent with respect to electrode potential would be for the activity coefficients, γ_A^{ads} and γ_W^{ads}, to be independent of electrode potential and to be functions only of the surface mole fraction, x_A^{ads}. Only in this way would it be possible to express the right-hand side of the electrosorption isotherm, eq 7, as a function only of the relative surface excess, $F(\Gamma_{AW})$, which is the basic requirement for congruence (cf. part 1[3]). In terms of the surface solution model of the inner layer, the noncongruence of the electrosorption with respect to electrode potential arises because the extent of nonideality of the surface solution is a function not only of the composition, but, also, of the electrode potential. In part 1[3] it was shown that the electrosorption of 2-butanol on mercury from aqueous sodium sulfate solution is not congruent with respect to electrode potential.

Figure 4 illustrates the behavior of $\Delta\bar{G}^E$ at various constant values of the excess charge density, σ^M. It can be seen from these figures that at constant x_A^{ads} both $\Delta\bar{G}^E$ and $(\partial\Delta\bar{G}^E/\partial x_A^{ads})$ change as σ^M is changed, and therefore the electrosorption of 2-butanol should not be congruent with respect to excess charge density. Such noncongruence with respect to σ^M was shown in part 1.[3]

The noncongruence illustrated by the behavior of $\Delta\bar{G}^E$ is, we believe, due to a change in the structure of the surface solution and, hence, a change of the intermolecular forces within the surface solution with changing electric field in the inner layer. Although the noncongruence with respect to both E^- and σ^M means, fundamentally, that neither of these electrical variables has any more special significance than the other, we think that there may be some advantage in concentrating our attention on the constant excess charge density behavior of the surface solution because σ^M is equal to the magnitude of the component of the electric displacement vector, **D**, perpendicular to the electrode surface inside the inner layer.[4] A calculation of the electric field, **E**, in the inner layer from first principles, taking account of the molecular polarizability and permanent dipole orientation, would seem to be more direct from **D**, through the fundamental relation, $\mathbf{D} = \epsilon_0\mathbf{E} + \mathbf{P}$, where ϵ_0 is the permittivity of free space and **P** is the polarization vector, than a calculation from the electrode potential. Therefore, in the remainder of this article we shall restrict our detailed discussion of the properties of the surface solution to the condition of constant excess charge density.

B. *The Activity Coefficients, γ_A^{ads} and γ_W^{ads}, and the Activities, a_A^{ads} and a_W^{ads}, of the Adsorbed 2-Butanol and of the Adsorbed Water in the Inner Layer on the Basis of the Symmetrical Choice of Standard States, and Their Dependence on the Excess Surface Charge Density, σ^M.* The activity coefficients, γ_A^{ads}, of the adsorbed 2-butanol and, γ_W^{ads}, of the adsorbed water on the basis of the symmetrical choice of standard states were calculated from the set of coefficients, $\{\alpha_j\}$, and the surface mole fraction of the adsorbed 2-butanol, x_A^{ads}, by means of eq 17 and 18, respectively. The results of these calculations are illustrated in Figure 5. The values of σ^M chosen for the activity coefficient curves displayed in Figure 5 are the same as those chosen for the excess electrochemical free energy of mixing curves, $\Delta\bar{G}^E$, shown in Figure 4. The plots of the activity coefficients vs. x_A^{ads} for a series of σ^M values more positive than $\sigma^M = -2.2$ μC cm^{-2} have a similar appearance to those shown in Figure 5, i.e., at any fixed x_A^{ads}, γ_A^{ads} $(\sigma^M) < \gamma_A^{ads}$ $(\sigma^M = -2.2)$. From the activity coefficients the corresponding activities of the adsorbed species were then calculated from the following equations:

$$a_A^{ads} = x_A^{ads}\gamma_A^{ads} \quad (23)$$

$$a_W^{ads} = (1 - x_A^{ads})\gamma_W^{ads} \quad (24)$$

Figure 6 shows the activities of the adsorbed 2-butanol and

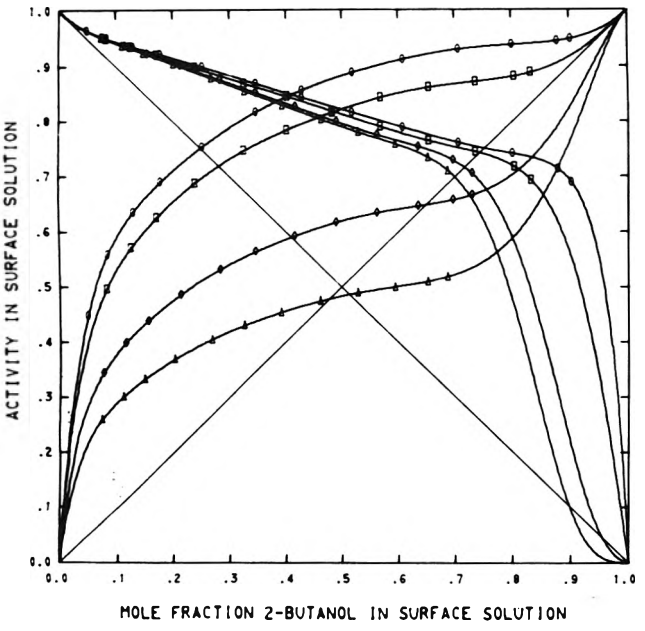

Figure 6. Activity of adsorbed 2-butanol (curves running up from left to right) and adsorbed water (curves running down from left to right) on basis of symmetrical choice of standard states. σ^M values are same for corresponding symbols as in Figure 4.

of the adsorbed water at the same σ^M values as in Figure 4. The activity curves for $\sigma^M > -2.2$ μC cm^{-2} have a similar appearance, i.e., at any fixed x_A^{ads}, a_A^{ads} $(\sigma^M) < a_A^{ads}$ $(\sigma^M = -2.2)$. In all three of these figures (Figures 4–6) the smooth curves were calculated from the set of coefficients, $\{\alpha_j\}$, and the surface mole fraction, x_A^{ads}, in the range $0 \leq x_A^{ads} \leq 1$ at intervals of 0.01 in x_A^{ads}. The points on the curves in these figures indicate the experimental values of x_A^{ads} which were actually used at the specified value of σ^M to determine the set of coefficients, $\{\alpha_j\}$. One value of σ^M is common to all three of these figures. This particular value, $\sigma^M = -2.2$ μC cm^{-2}, gave the largest positive deviations from Raoult's law, i.e., at any fixed value of the surface mole fraction, x_A^{ads}, the value of ΔG^E, γ_A^{ads}, and a_A^{ads} is greater than for any other value of σ^M.

Focusing our attention first on the activity curve (Figure 6) for $\sigma^M = -2.2$ μC cm^{-2}, we note the following salient features. First, a_A^{ads} shows positive deviations from Raoult's law throughout the entire composition range, $0 \leq x_A^{ads} \leq 1$. Second, in the limit as $x_A^{ads} \to 1$, the activity of the adsorbed 2-butanol asymptotically approaches the Raoult's law line. Third, in the range of very low x_A^{ads} the activity, a_A^{ads}, of the adsorbed 2-butanol approaches the origin linearly with a finite positive slope (Henry's law), and simultaneously the activity of the adsorbed water, a_W^{ads}, asymptotically approaches the Raoult's law line for water. Fourth, the water activity also exhibits positive deviations from Raoult's law over the entire composition range.

These four features of the activity curves for the adsorbed species in the inner part of the electrical double layer at $\sigma^M = -2.2$ μC cm^{-2} are identical with those of many two-component bulk solutions of organic compounds which are miscible with water in all proportions such as 1-propanol in water.[14] We interpret this behavior of the surface solution as indicating that the structure and intermolecular interactions in the inner layer at this value of σ^M must have considerable similarity to the structure and intermolecular interactions of two-component bulk solutions of an organic compound in water. However, the magnitudes of the positive deviations from Raoult's law in the surface solution of 2-butanol in water at this value of σ^M, although large, are nevertheless smaller than those of the corresponding bulk solutions[15] (cf. Figure 6, ref 15). In the case of the bulk solutions of 2-butanol in water, the positive deviations from Raoult's law are so great that at a mole fraction, x_A, of 2-butanol of 0.05 the solution breaks into two phases, a water rich phase with $x_A = 0.05$ and an alcohol rich phase with $x_A = 0.35$, and no solutions with mole fractions in the range $0.05 < x_A < 0.35$ (the miscibility gap) are capable of existence. The surface solutions of 2-butanol in water exhibit no miscibility gap, i.e., in the surface solution, unlike the bulk solution, 2-butanol and water are miscible in all proportions. The surface solution of 2-butanol in water is thus more like the bulk solution of 1-propanol in water.

As the excess surface charge density, σ^M, is caused to deviate either negatively (Figure 6) or positively away from the value, -2.2 μC cm^{-2}, the activity, a_A^{ads}, of the adsorbed 2-butanol at any fixed value of the surface mole fraction, x_A^{ads}, diminishes. This fact means that a shift of σ^M away from the value -2.2 μC cm^{-2} decreases the magnitude of the positive deviations from Raoult's law, and eventually negative deviations from Raoult's law begin to appear. (At more extreme values of σ^M than those shown in the figures, the negative deviations from Raoult's law begin to appear at lower and lower values of x_A^{ads}.) The behavior of the activity coefficients (Figure 5) and of the excess electrochemical free energy of mixing (Figure 4) is consistent with the behavior of the activities of the adsorbed species (Figure 6).

C. *The Standard Electrochemical Fugacity Ratio, $f_A^{\ominus}/f_A^{\bullet}$, and Its Implications About the Dependence of the Water Structure in the Inner Layer on the Excess Charge Density, σ^M.* The ratio of the electrochemical fugacity of the adsorbed organic compound in each of its two alternative standard states (cf. section II.B) is obtained directly from the least-squares fits of the activity coefficient ratio, $[\gamma_{Ar}^{ads}/(\gamma_W^{ads})^n]$, to the surface mole fraction, x_A^{ads}. Thus it follows from eq 21 that

$$(f_A^{\ominus}/f_A^{\bullet}) = \exp(\alpha_1) \tag{25}$$

This ratio of standard state electrochemical fugacities is equal to the limiting value at infinite dilution in the surface solution of the activity coefficient, γ_A^{ads}, on the basis of the symmetrical choice of standard states,[11] i.e.

$$(f_A^{\ominus}/f_A^{\bullet}) = \lim_{x_A^{ads} \to 0} (\gamma_A^{ads}) \tag{26}$$

Thus the standard electrochemical fugacity ratio is equal to the slope of the activity plots for the adsorbed 2-butanol in Figure 6 in the Henry's law region. Whenever $(f_A^{\ominus}/f_A^{\bullet}) > 1$, the surface solution will exhibit positive deviations from Raoult's law, at least in the dilute solution region. If $(f_A^{\ominus}/f_A^{\bullet}) < 1$, the surface solution will exhibit negative deviations from Raoult's law.

From eq 26, $(f_A^{\ominus}/f_A^{\bullet})$ is a direct measure of the intermolecular interactions in the surface solution between the adsorbed organic compound and the adsorbed water under conditions such that there are no complications from any organic–organic intermolecular interactions. Therefore, the determination of $(f_A^{\ominus}/f_A^{\bullet})$ as a function of σ^M provides an indication of how the water structure in the inner layer changes with σ^M. Figure 7 shows how $(f_A^{\ominus}/f_A^{\bullet})$ varies with σ^M in the case of the electrosorption of 2-butanol in the horizontal orientation on mercury in the absence of specific ionic adsorption. This ratio passes through a maximum at $\sigma^M = -2.2$ μC cm^{-2} which was the value of the excess charge density at which the surface solution exhibited the maximum positive deviations from Raoult's law (cf. Figures 4–6).

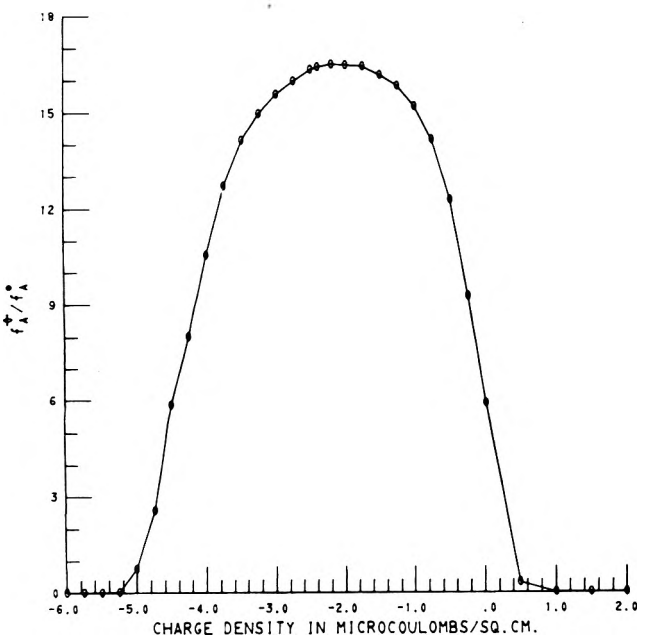

Figure 7. Standard electrochemical fugacity ratio for adsorbed 2-butanol as function of excess charge density.

We believe that at $\sigma^M = -2.2\ \mu C\ cm^{-2}$ the water in the inner layer is more bulklike than at any other value of σ^M, i.e., at this value of σ^M the water molecules in the inner layer have the most opportunity to form intermolecular hydrogen bonds with each other, which is the chief structural feature of bulk liquid water. Even at this value of σ^M the surface water must not be as highly structured as bulk water because the positive deviations from Raoult's law exhibited by the aqueous surface solutions of 2-butanol, although large, were not large enough to produce the miscibility gap which is the chief characteristic of the bulk aqueous solutions of this compound.

It might be asked why the surface water would be more bulklike in structure at this negative value of σ^M than at the point of zero charge. Our answer is that evidently there is a tendency for water molecules to form some sort of quasi-chemical bond to the uncharged mercury with the oxygen atoms attached to the metal surface. One strong piece of evidence in favor of such a preferential orientation of the water dipoles on the uncharged metal is the shift of the potential of zero charge in the positive direction with increasing adsorption of the organic compound (cf. Figure 5, part 1[3]). At the point of zero charge the water molecules in the first layer are evidently strongly oriented with their oxygen atoms toward the metal, so the water molecules in this layer have little opportunity to participate in intermolecular hydrogen bonding with each other or with the next layer of water molecules. When $\sigma^M = 0$ the value of $f_A^\circ/f_A^\bullet$ is only 5.9, whereas at $\sigma^M = -2.2\ \mu C\ cm^{-2}$ the value of $f_A^\circ/f_A^\bullet$ is 16.5. In the bulk solutions the limiting value of the activity coefficient of 2-butanol at infinite dilution was 23.8 (cf. Table I, part 1[3]). In order to overcome this preferential orientation of the water molecules with their oxygen atoms toward the metal, it is necessary to apply a negative electric field which will interact with the permanent dipoles and tend to reorient the water molecules. Apparently, when $\sigma^M = -2.2\ \mu C\ cm^{-2}$ the negative electric field has just overcome the natural tendency of the first layer of water molecules to bond their oxygen atoms to the mercury. At this value of σ^M we can say that the surface water has its most random orientation, meaning that the orientation of the water molecules *toward the metal* is most random, but simultaneously the water molecules' orientation *to each other* is most organized through intermolecular hydrogen bonding, i.e., the structure of the surface water is most bulklike. When we make σ^M even more negative the water dipoles will tend to become oriented with their hydrogen atoms toward the metal, and this electrostatic effect will tend to break up the intermolecular hydrogen bonding and make the surface solutions less bulklike.

Our basic contention about the structure of the water in the inner layer is therefore that, depending on the value of σ^M, the surface water retains a remnant of bulk water structure. The natural inclination of the water molecules to orient themselves with their oxygen atoms toward the mercury, on the one hand, and the interaction of the permanent molecular dipoles with the electric field, on the other, tend to break up this bulklike structure. Therefore, it is only in the vicinity of the maximum in the plot of $f_A^\circ/f_A^\bullet$ vs. σ^M that the surface solution exhibits very close resemblance to bulk aqueous solutions of the organic compound as indicated by strong positive deviations from Raoult's law. The standard electrochemical fugacity ratio, $f_A^\circ/f_A^\bullet$, thus serves as an indicator of the water structure in the surface solution at infinite dilution. Consequently, it is possible to use the electrosorption of an organic compound as a probe into the nature of the water structure in the inner layer.

D. *Implications of the Positive Deviations from Raoult's Law in the Dilute Surface Solutions for the Excess Electrochemical Entropy of Mixing, $\Delta\bar{S}^E$, and the Relevance of the Regular Solution Model of the Inner Layer and of the Flory–Huggins Electrosorption Isotherm.* It can be seen from Figure 7 that for all values of the excess charge density in the range $-4.9 < \sigma^M < +0.5\ \mu C\ cm^{-2}$ the standard electrochemical fugacity ratio, $(f_A^\circ/f_A^\bullet) > 1$, and therefore throughout this range of σ^M the dilute surface solutions will exhibit positive deviations from Raoult's law. Consequently, in this range of σ^M at low values of x_A^{ads} one has $\gamma_A^{ads} > 1$ and $\Delta\bar{G}^E > 0$ (cf. Figures 4–5). The excess electrochemical free energy of mixing is related to the excess electrochemical enthalpy of mixing,[16] $\Delta\bar{H}^E$, and the excess electrochemical entropy of mixing, $\Delta\bar{S}^E$, by

$$\Delta\bar{G}^E = \Delta\bar{H}^E - T\Delta\bar{S}^E \tag{27}$$

The universal behavior[17] for dilute aqueous bulk solutions of aliphatic alcohols is that the mixing process is exothermic, i.e., that $\Delta H^E < 0$. Such solutions always exhibit positive deviations from Raoult's law because $\Delta S^E < 0$ and

$$T|\Delta S^E| > |\Delta H^E| \tag{28}$$

In other words, as Franks and Reid[17] have said, "the solution properties are under entropy control". The origin of the large negative entropy of mixing is believed to be a solute-induced shifting of the water-structure equilibrium in the direction of greater structuredness,[18] i.e., as Frank and Evans[19] stated in their classic 1945 paper, when the organic molecule dissolves in water at room temperature it modifies the water structure in the direction of greater "crystallinity"—"the water so to speak, builds a microscopic iceberg around it".

It seems unreasonable to believe that the mixing process in the case of dilute surface solutions would be so unlike the bulk mixing process that it has changed from exothermic in the bulk to endothermic in the surface solution. Therefore, we believe that the iceberg effect must also play a role in the surface solution, i.e., that the surface mixing process is also under entropy control. Thus we think that it is likely that $\Delta\bar{S}^E < 0$, and $\Delta\bar{G}^E > 0$ although $\Delta\bar{H}^E < 0$ because

$$T|\Delta\bar{S}^E| > |\Delta\bar{H}^E| \quad (29)$$

If inequality 29 is true, we can immediately eliminate from further consideration two statistical mechanical models which have been proposed to account for organic electrosorption; namely, the regular solution model which was indicated by Frumkin[10] to be consistent with his electrosorption isotherm[20] which was first proposed in 1925, and the so-called Flory–Huggins isotherm which was introduced by Parsons[21] in 1964 and was later strongly supported in slightly modified form by Conway et al.[22] None of these workers considered the entropic implications of their proposed models. If the surface solution were a regular solution[6] it would be required that $\Delta\bar{S}^E = 0$. Thus, the regular solution model must be eliminated. On the other hand, if the surface solution obeyed lattice statistics with Flory's approximation,[7] the excess entropy of mixing would be given by

$$\Delta\bar{S}^E = -R\{x_W^{ads} \ln [1/(x_W^{ads} + nx_A^{ads})] + x_A^{ads} \ln [n/(x_W^{ads} + nx_A^{ads})]\} \quad (30)$$

According to eq 30, whenever $0 < x_A^{ads} < 1$, $\Delta\bar{S}^E > 0$, and so this approximate statistical mechanical model which leads directly to the so-called Flory–Huggins isotherm[21,22] must also be eliminated from consideration.

In the future it should be possible to actually measure $\Delta\bar{S}^E$ and to determine $\Delta\bar{H}^E = \Delta\bar{G}^E + T\Delta\bar{S}^E$. To determine $\Delta\bar{S}^E$ it will be required to measure the electrosorption of the organic compound at a series of different temperatures, calculate ΔG^E at each temperature as indicated in this paper, and then obtain $\Delta\bar{S}^E$ by means of the relation

$$\Delta\bar{S}^E = -(\partial\Delta\bar{G}^E/\partial T)_{\sigma^M, x_A^{ads}} \quad (31)$$

Such experiments would require that the emf measurements to determine the recipe for preparation of the series of solutions at constant electrolyte activity be done at each temperature. The gas chromatographic measurements of the bulk activity of the organic compound would also have to be done at each temperature (cf. part 1[3]). Fortunately, however, it would not be necessary to carry out measurements at each of the different temperatures at *constant chemical potential* of the electrolyte and of the organic compound as would be required for a determination of the relative surface excess of entropy.[4,23,24] A major practical advantage in working with the excess electrochemical mixing functions is that they do not contain any standard state quantities. In future work, we plan to carry out such studies at different temperatures to test whether inequality 29 is actually true.

E. *The Electrosorption Isotherm in Terms of the Fractional Surface Coverage, θ.* In the past,[21,22,25] a great amount of attention has been given to the mathematical form of the equation of the electrosorption isotherm in terms of the fraction, θ, of the surface actually covered by the adsorbed organic compound, and a major criterion which was generally used for accepting or rejecting a particular theory was how well the experimental data fitted the theoretical isotherm. In light of the present theory we think that the excess electrochemical free energy of mixing, $\Delta\bar{G}^E$, the activity coefficients, γ_A^{ads} and γ_W^{ads}, and the activities, a_A^{ads} and a_W^{ads}, are much more important than the isotherm in terms of θ. Nevertheless, in view of the emphasis which has been placed on this subject in the past, we conclude this article with a brief discussion of the isotherm in terms of θ which is consistent with our theory. In order to do this it is only necessary to express the surface mole fractions of the adsorbed organic compound and of the adsorbed water in terms of θ and then to substitute into the electrosorption isotherm, eq 7.

It follows directly from eq 16 and 17 in part 1[3] that

$$10^{-16}LS_A\Gamma_A = \theta \quad (32)$$

and

$$10^{-16}L(S_A/n)\Gamma_W = 1 - \theta \quad (33)$$

Therefore, substituting for Γ_A and Γ_W in eq 1 and 2 by means of eq 32 and 33 we obtain

$$x_A^{ads} = \{\theta/[1 + n(1 - \theta)]\} \quad (34)$$

and

$$x_W^{ads} = \{n(1 - \theta)/[1 + n(1 - \theta)]\} \quad (35)$$

Therefore the ratio, $[x_A^{ads}/(x_W^{ads})^n]$, which appears in the electrosorption isotherm, eq 7, is given by[26]

$$[x_A^{ads}/(x_W^{ads})^n] = \theta[\theta + n(1 - \theta)]^{n-1}/n^n(1 - \theta)^n = Z(\theta) \quad (36)$$

Thus the electrosorption isotherm takes the form

$$\{\exp[-\Delta\bar{G}_{ads}^{\ominus}/RT]\}[a_A/a_W^n] = Z(\theta)[\gamma_{Ar}^{ads}/(\gamma_W^{ads})^n] \quad (37)$$

or

$$\{\exp[-\Delta\bar{G}_{ads}^{\bullet}/RT]\}[a_A/a_W^n] = Z(\theta)[\gamma_A^{ads}/(\gamma_W^{ads})^n] \quad (38)$$

depending on whether one wishes to use the unsymmetrical (eq 37) or the symmetrical (eq 38) choice of standard states for the adsorbed species. The standard electrochemical free energy of adsorption, $\Delta\bar{G}_{ads}^{\bullet}$, for the symmetrical choice of standard states is related to the standard electrochemical free energy, $\Delta\bar{G}_{ads}^{\ominus}$, for the unsymmetrical choice of standard states by the following equation

$$\Delta\bar{G}_{ads}^{\bullet} = \Delta\bar{G}_{ads}^{\ominus} + RT \ln (f_A^{\bullet}/f_A^{\ominus}) \quad (39)$$

(For a derivation of eq 39 see Appendix B available as supplementary material.)

The ratio of activity coefficients for the adsorbed species on the basis of the unsymmetrical choice of standard states, $[\gamma_{Ar}^{ads}/(\gamma_W^{ads})^n]$, which appears in eq 37 can be expressed in terms of θ by substituting eq 34 into eq 22. The corresponding ratio of activity coefficients of the adsorbed species on the basis of the symmetrical choice of standard states, $[\gamma_A^{ads}/(\gamma_W^{ads})^n]$, which appears in eq 38 can be obtained in terms of θ by substituting eq 34 into eq 17 and 18. It is clear that the mathematical form of the electrosorption isotherm in terms of θ yielded by this theory is rather complicated whenever $n > 1$ and $k > 2$. Figure 8 shows the electrosorption isotherms for the adsorption of 2-butanol in the horizontal position for several different values of the excess charge density, σ^M. The smooth curves in this figure are calculated from the least-squares fits of $[\gamma_{Ar}^{ads}/(\gamma_W^{ads})^n]$ to x_A^{ads} with $n = 5$ and $k = 7$ used to determine the set of coefficients $\{\alpha_j\}$ at each value of σ^M. The points are the experimental values of θ.

In the limiting case when $n = 1$ and $k = 2$, the electrosorption isotherm, eq 37, for the unsymmetrical choice of standard states of the adsorbed species reduces to

$$\{\exp[-\Delta\bar{G}_{ads}^{\ominus}/RT]\}[a_A/a_W^n] = [\theta/(1 - \theta)][\exp(-2\alpha_1\theta)] \quad (40)$$

This equation is identical in form with the Frumkin isotherm;[28] however, the interpretation in terms of the

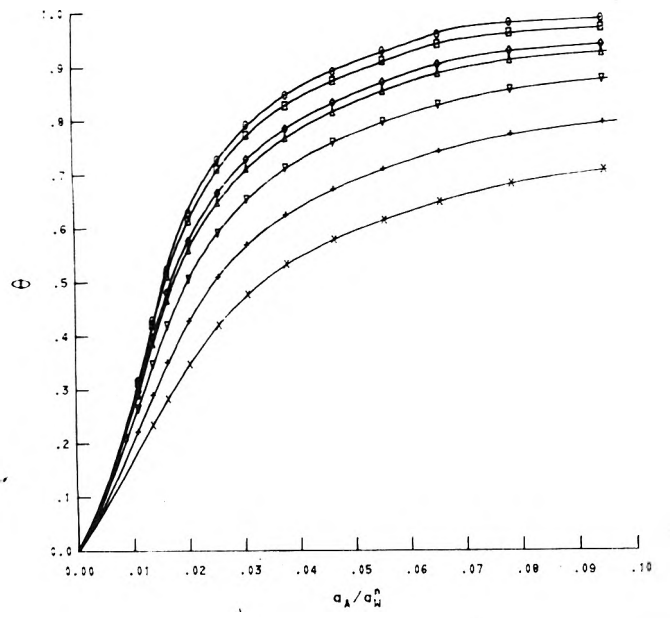

Figure 8. Electrosorption isotherms for 2-butanol in terms of the fractional surface coverage at various values of the excess charge density as function of the bulk activity ratio, (a_A/a_W^0). σ^M values in $\mu C\ cm^{-2}$: ⊙, -2.20; ⊡, -3.25; ◇, -4.00; △, -4.25; ▽, -5.00; +, -6.00; ×, -7.00.

present theory would be quite different from that of Frumkin. Frumkin's interpretation of the parameter, α_1, in eq 40 was that it was a van der Waals interaction constant indicating the extent of organic–organic intermolecular interaction. If $\alpha_1 > 0$, Frumkin concluded that there was organic–organic attraction. In terms of the present theory, $\alpha_1 = \ln (f_A^\circ/f_A^\bullet)$. Thus, in terms of our theory, $\alpha_1 > 0$ implies that the surface solution will exhibit positive deviations from Raoult's law not only in dilute surface solutions but throughout the entire concentration range, $0 < x_A^{ads} < 1$, because when $k = 2$, $\Delta\bar{G}^E$ is a parabola with an extremum at $x_A^{ads} = 0.5$. The fact that the Frumkin isotherm (eq 40) can be consistent with two quite different theories of the inner layer indicates that it cannot be used as a basis for acceptance or rejection of either theory. In the case of this study, the fit of the experimental data to the Frumkin isotherm was very poor because n is certainly not unity and the fits at $k = 2$ were very poor.

IV. Conclusions

A theory has been proposed to explain noncongruent electrosorption of organic compounds at the metal solution interface in the absence of specific ionic adsorption. Under this theory the inner (compact) part of the electrical double layer is treated as a two-component nonelectrolyte solution called the surface solution. By means of this theory it is possible to calculate the excess electrochemical free energy of mixing of the surface solution and the activities and activity coefficients of the adsorbed organic compound and of the adsorbed water in the inner layer. It is shown that in a certain range of excess charge density the dilute surface solutions exhibit positive deviations from Raoult's law. It is proposed that the properties of these dilute surface solutions are under entropy control as is true for dilute bulk aqueous solutions of aliphatic alcohols. It is shown that in an extreme limiting case this theory predicts that the Frumkin isotherm will be obeyed, but the interpretation of the parameter appearing in the exponential term of that isotherm will be quite different under this theory than under the theory of Frumkin. It is concluded that the so-called Flory–Huggins isotherm is probably incorrect because the statistical mechanical theory on which that isotherm is based predicts that the excess electrochemical entropy of mixing of the surface solution is positive.

Acknowledgment. This research was supported by the United States Air Force Office of Scientific Research under Grant No. AF-AFOSR-70-1887. We thank Professor Gary W. Schnuelle, Department of Chemistry, Colorado State University, for helpful discussions.

Supplementary Material Available: Appendix A, which is a detailed discussion of the digital computer method used for determination of the set of coefficients, $\{\alpha_j\}$, and Appendix B, which is a derivation of eq 39 (3 pages). Ordering information is available on any current masthead page.

References and Notes

(1) To whom correspondence and requests for reprints should be addressed at the Department of Chemistry.
(2) Present address: Department of Applied Science, Brookhaven National Laboratory, Upton, N.Y. 11973.
(3) H. Nakadomari, D. M. Mohilner, and P. R. Mohilner, *J. Phys. Chem.*, **80**, 1761 (1976).
(4) D. M. Mohilner in "Electroanalytical Chemistry", Vol. 1, A. J. Bard, Ed., Marcel Dekker, New York, N.Y., 1966, pp 241–409.
(5) This choice of the location of the dividing surface ensures that Γ_A is equal to the actual surface concentration of adsorbed organic molecules (cf. part 1,[3] note 44).
(6) J. H. Hildebrand and R. L. Scott, "The Solubility of Nonelectrolytes", 3d ed, Dover Publications, New York, N.Y., 1964.
(7) E. A. Guggenheim, "Mixtures", Clarendon Press, Oxford, England, 1952.
(8) R. Parsons, *Trans. Faraday. Soc.*, **51**, 1518 (1955); "Soviet Electrochemistry", Proceedings of the 4th Conference on Electrochemistry, 1956, USSR, Vol. 1, Consultants Bureau, New York, N.Y., 1961, p 18.
(9) A. N. Frumkin, *Z. Phys. Chem.*, **116**, 466 (1926).
(10) A. N. Frumkin, *J. Electroanal. Chem.*, **7**, 152 (1964).
(11) I. M. Klotz, "Chemical Thermodynamics", Revised Edition, W. A. Benjamin, New York, N.Y., 1964.
(12) G. Scatchard and C. L. Raymond, *J. Am. Chem. Soc.*, **60**, 1278 (1938).
(13) E. A. Guggenheim, "Thermodynamics", 3d ed, North-Holland Publishing Co., Amsterdam, The Netherlands, 1957.
(14) J. A. V. Butler, D. W. Thomson, and W. H. Maclennan, *J. Chem. Soc.*, 674 (1933).
(15) D. M. Mohilner, L. M. Bowman, S. J. Freeland, and H. Nakadomari, *J. Electrochem. Soc.*, **120**, 1658 (1973).
(16) The excess electrochemical enthalpy of mixing, $\Delta\bar{H}^E$, is equal to the electrochemical enthalpy of mixing, ΔH_m, of the nonideal surface solution since the electrochemical enthalpy of mixing for an ideal surface solution, ΔH_m^I, will be zero, just as is true for an ideal bulk solution.[11]
(17) F. Franks and D. S. Reid, *Water, Compr. Treat.*, **2**, Chapter 5 (1973).
(18) H. S. Frank and F. Franks, *J. Chem. Phys.*, **48**, 4746 (1968).
(19) H. S. Frank and M. W. Evans, *J. Chem. Phys.*, **13**, 507 (1945).
(20) A. N. Frumkin, *Z. Phys. Chem.*, **116**, 466 (1925).
(21) R. Parsons, *J. Electroanal. Chem.*, **8**, 93 (1964).
(22) H. P. Dhar, B. E. Conway, and K. M. Joshi, *Electrochim. Acta*, **11**, 789 (1973).
(23) G. J. Hills and R. Payne, *Trans. Faraday Soc.*, **61**, 326 (1965).
(24) J. A. Harrison, J. E. B. Randles, and D. J. Schiffrin, *J. Electroanal. Chem.*, **48**, 359 (1973).
(25) B. B. Damaskin, O. A. Petrii, and V. V. Batrakov, "Adsorption of Organic Compounds on Electrodes", Plenum Press, New York, N.Y., 1971.
(26) The mathematical form of the function $Z(\theta)$ is identical with that of the Bockris–Swinkels isotherm.[27]
(27) J. O'M. Bockris and D. A. Swinkels, *J. Electrochem. Soc.*, **111**, 736 (1964).
(28) A. N. Frumkin and B. B. Damaskin in "Modern Aspects of Electrochemistry", No. 3, J. O'M. Bockris and B. E. Conway, Ed., Butterworths, Washington, D.C., 1964, Chapter 3.

An Infrared Study of the Solvation of Halide Ions by Methanol and 2,2,2-Trifluoroethanol

Ralph R. Ryall, Howard A. Strobel,*

Paul M. Gross Chemical Laboratory, Duke University, Durham, North Carolina 27706

and Martyn C. R. Symons

Department of Chemistry, The University, Leicester, LE1 7RH, England *(Received June 3, 1976)*

Using infrared spectroscopy, we have measured the concentration of free and hydrogen bonded methanol in carbon tetrachloride solutions of tetraalkylammonium halides (Cl^-, Br^-, I^-) and calculated formation constants and free energies for the halide monosolvates. Formation constants have also been obtained for trifluoroethanol and these anions. Further, for the iodide–methanol solvate, enthalpy and entropy values of formation have also been determined. For both alcohols, frequency shifts from the $(O-H)_{free}$ absorption on solvation are proportional to the free energy of hydrogen-bond formation, and to the half-widths of the bands. Fluoride ion was included in this part of the study and, as expected, the order of shifts was $F^- > Cl^- > Br^- > I^-$. Formation constants for trifluoroethanol solvates were an order of magnitude larger, reflecting the greater acidity of this alcohol. The spectral shifts on complex formation were also proportionately enhanced.

Introduction

Although the O–H stretching region of the infrared spectra for hydroxylic solvents is of limited use for studying ionic solvation, because the breadth of the features involved is usually greater than the band shifts, valuable information can nevertheless be obtained by studying dilute solutions in relatively inert solvents.[1,2] Certain tetraalkylammonium salts dissolve in inert solvents such as carbon tetrachloride or methylene chloride as ion pairs or clusters, and added protic solvents selectively hydrogen bond to the anions. The O–H stretching frequencies of monomeric alcohol molecules appear as narrow bands whose oscillator strengths can be readily determined, and these can be fairly accurately monitored to provide the total concentration of unbound alcohol. The anion–alcohol complexes give broader bands at lower frequencies, the shift being a function of the hydrogen-bond strengths.

There have been several previous studies of methanol–halide ion complexes, but the results are not very consistent, and we have therefore carried out a careful study of these complexes in carbon tetrachloride in order to obtain accurate results for comparison with our results for the 2,2,2-trifluoroethanol systems.

In 1958, Lund[3] established the pattern of spectral changes when alcohols solvate tetraalkylammonium halides in chloroform solution. Bufalini and Stern[4] measured formation constants at various temperatures for the bromide salt and methanol using benzene as an inert solvent, and hence calculated $\Delta H°$ and $\Delta S°$ parameters. They were particularly concerned with the presence of ion–quadrupoles and higher clusters, and concluded that ion pairs were solvated in preference to clusters. Hyne and Levy,[5] on the other hand, using *tert*-butyl alcohol and the bromide salt in carbon tetrachloride discussed the spectral changes in terms of aggregation of the solvent rather than hydrogen bonding to the bromide ion. Allerhand and Schleyer[1] studied all four halide ions and concluded that the shifts ($\Delta\nu$) from the free O–H frequency followed the unexpected order $Cl^- > F^- > Br^- > I^-$. They explained this result in terms of a uniquely strong interaction between the tetraalkylammonium cations and fluoride anions. Blandamer et al.[6] studied the interaction between alkylammonium iodides and methanol and correlated the results with those from ultraviolet spectroscopic studies of the CTTS band for the iodide ions. Mohr et al.[2] extended these studies to water in carbon tetrachloride and found the expected trend in $\Delta\nu$ of $F^- > Cl^- > Br^- > I^-$.[1] Lipovskii and Dem'yanova[7] using tetradecylammonium halides in carbon tetrachloride also found that fluoride ion induced the greatest shift. They explained the previous results[1] in terms of the presence of water. It is extremely difficult to remove water from alkylammonium fluorides without inducing decomposition. One very interesting aspect of these studies[7] was the comparison between tetraalkylammonium and trialkylammonium salts. The $\Delta\nu$ and $\Delta G°$ values for the latter were considerably smaller than those for the former.

Experimental Section

Materials. Carbon Tetrachloride. Fisher ACS certified carbon tetrachloride was purified by fractional distillation, with only the middle fraction being collected. A Karl Fischer titration indicated not more than 0.01% water after distillation.

Methanol. Fisher ACS certified methanol was dried over magnesium. When there was no further evolution of hydrogen, the methanol was fractionally distilled and the middle portion collected. The purified methanol was found to contain no more than 0.03% water.

2,2,2-Trifluoromethanol. Eastman White Label 2,2,-2-trifluoroethanol was used without further purification. Gas chromatographic and infrared analysis gave no indication of the presence of water or other impurities.

Tetrahexylammonium Iodide and Tetrabutylammonium Bromide. Eastman Kodak salts were dried in vacuo at 75 °C for 4 days. A Karl Fischer titration on methanolic solutions indicated that not more than 0.02% water was present.

Tetrabutylammonium Chloride. Tetrabutylammonium chloride was prepared from silver chloride and tetrabutylammonium iodide. The product was dried in vacuo at 75 °C. Analysis revealed the absence of significant amounts of iodide or water.

Tetraalkylammonium Fluorides. We were unable to obtain dry samples of any tetraalkylammonium fluorides despite many attempts using a variety of procedures. However, we were able to obtain values for $\nu(OH)_b$ for MeOH---F adducts (ca. 3240 cm^{-1}) by dissolving the salts in dry methanol after removing as much water as possible, and drying the resulting solutions over molecular sieves

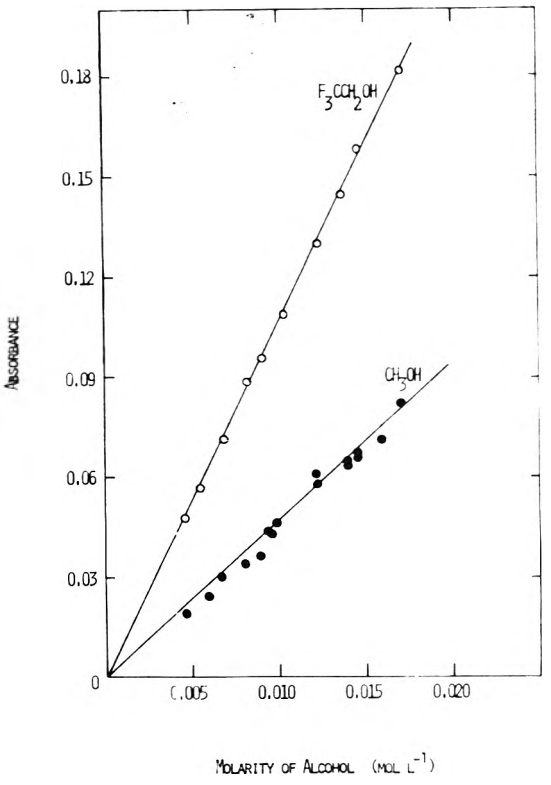

Figure 1. Absorbance of $\nu(OH)_{free}$ for methanol and 2,2,2-trifluoroethanol as a function of concentration in carbon tetrachloride at 29 °C.

for a prolonged period. These solutions were concentrated by vacuum distillation, and then added to carbon tetrachloride. The results were reproducible and the addition of traces of water resulted in the development of a new band at higher frequencies.

Spectrometry. Infrared spectrophotometric measurements were made using sealed, matched 1.00-mm sodium chloride cells supplied by Wilks Scientific Corp. By measuring the interference fringe patterns obtained on running spectra of the empty cells, the cells were found to be matched to within 3%. These were housed in a thermostatted cell chamber for studies at temperatures other than ambient (29 ± 1 °C).

All infrared measurements were performed on a Perkin-Elmer P-E 621 spectrometer. The ordinate spectral presentation was linear in percent transmittance. The spectral slit width was 3 cm^{-1} which corresponds to ca. 1/7 of the half-band width of the monomeric methanol peak.

Samples were prepared by weight, using a drybox when necessary. Peak heights of the ν(OH) free band were used to estimate concentrations after it was established that Beer's law was obeyed (Figure 1). The concentration of free methanol was determined directly and that of bound methanol found by difference on addition of the halide. Ordinate scale expansion of 5× was used as necessary. One major difficulty in measuring either the peak height or area was choosing the proper baseline. In this work the baseline was drawn as a straight line connecting the regions of constant transmission on either side of the absorption band. The true baseline was not strictly horizontal through the spectral region under investigation. As has been stressed by Potts,[8] uncertainties in the position of the baseline can result in larger errors for integrated absorbance measurements than for peak height measurements.

Results

Dilute alcohol solutions in carbon tetrachloride gave a sharp, apparently Gaussian peak slightly above 3600 cm^{-1}. When a quaternary ammonium salt was added, this peak decreased in intensity and a new band, which was much more broad and intense, appeared at a lower frequency.

The C–H stretch vibrations of the tetraalkylammonium cations gave rise to strong absorption bands, appearing around 3000 cm^{-1}, which overlapped the broad O–H stretching bands of the alcohol–halide complexes. Appropriate concentrations of the salt were added to the reference solution to compensate for these bands.

The equilibrium between the alcohol and the tetraalkylammonium salt can be represented by the equation:

$$ROH + (R_4N^+)X^- \rightleftharpoons ROH\cdots X^-(R_4N^+) \quad (1)$$

$$l(ROH)_p + n(R_4N^+X^-)_q = [(R_4N^+X^-)_k\cdots(HOR)_i]_m$$

where R is an alkyl group and X is a halide. It is assumed that $l = n = 1$; $i = k = 1$; and $p = q = m = 1$. Thus, the equilibrium constant, K, can be calculated from the following equation

$$K = [(R_4N^+)X^-\cdots HOR]/[ROH][(R_4N^+)X^-]$$

For the dilute solutions studied, activity coefficients are assumed to be equal to unity. All concentration terms were corrected when necessary for changes in density with temperature. Finally, values for the Gibbs free energy change in formation of the solvate, $\Delta G°$, were calculated using the mean value for the equilibrium constant at a specific temperature.

The enthalpy of formation of the hydrogen bond between Hex_4NI and methanol was estimated from the temperature dependence of the equilibrium constant as given by the van't Hoff equation:

$$\Delta H° = \frac{d \ln K}{d(1/T)} RT^2$$

An enthalpy value, $\Delta H°$, of −3.7 kcal/mol was determined by plotting $R \ln K$ against $1/T$. Further, using the relation, $\Delta G° = \Delta H° - T\Delta S°$, the entropy of hydrogen bond formation was found to be −6.7 eu for the complex at 29 °C.

The concentration plots establishing adherence to Beer's law are shown in Figure 1. The resulting molar absorptivities $\epsilon(OH)_{free}$ at 29 °C are given in Table I, together with those for methanol at 10 and 45 °C. Also included are approximate values for $\epsilon(OH)_b$, the molar absorptivities for the bound O–H group. The values of $\epsilon(OH)_b$ were calculated from the equilibrium concentration of the alcohol–halide adduct and the peak absorbance for the hydrogen bonded complex. For systems at 29 °C the calculated formation constants and $\Delta G°$ values are listed in Table II together with band frequencies $\nu(OH)_b$ and band shifts. The frequencies of band maxima were in agreement with those reported by Allerhand and Schleyer[1] and Lipovskii.[7] Calculated thermodynamic data for methanol iodide adducts are given in Table III. Formation constants are the mean of approximately ten determinations covering a range of *total* salt concentration between ca. 0.02 and 0.1 M for methanol and ca. 0.001 and 0.05 M for 2,2,2-trifluoroethanol. The total concentration

TABLE I: Molar Absorptivities, $\epsilon(OH)_{free}$, for Monomeric Methanol and 2,2,2-Trifluoroethanol in CCl_4, together with Approximate Values of $\epsilon(OH)_b$ for Methanol–Halide Adducts

	MeOH (10 °C)	MeOH (29 °C)	MeOH (45 °C)	CF_3CH_2OH (29 °C)
$\epsilon(OH)_{free}$, M^{-1} cm^{-1}	53.5 ± 4	43.9 ± 4	33.4 ± 3	103

	MeOH···Cl^-	MeOH···Br^-	MeOH···I^-
$\epsilon(OH)_b$ (29 °C)	185	174	122

TABLE II: Formation Constants, ΔG° Values, and Spectral Parameters for Alcohol-Halide Ion Complexes in Carbon Tetrachloride at 29 ± 1 °C

Alcohol	Salt	K	ΔG°, kcal/mol	$\nu(OH)_{free}$, cm^{-1}	$\nu(OH)_b$, cm^{-1}	$\Delta\nu$-$(OH)_b$,[a] cm^{-1}	$\nu(OH)_{free} - \nu(OH)_b$, cm^{-1}
MeOH	Bu_4NF			3643	(3240)		(403)
	Bu_4NCl	173 ± 16	−3.1	3643	3275	185	368
	Bu_4NBr	49 ± 6	−2.3	3643	3339	145	304
	Hex_4NI	16.8 ± 3	−1.7	3643	3390	120	253
CF_3CH_2OH[b]	Bu_4NCl	7660 ± 500	−5.4	3621	3140	230	481
	Bu_4NBr	920 ± 160	−4.1	3621	3220	207	401
	Hex_4NI	170 ± 10	−3.1	3621	3285	180	336

[a] Band width at half maximum. [b] Data applies to those cases where the ratio of initial concentration of Bu_4NBr or Hex_4NI to the concentration of alcohol was greater than 1.5; for Bu_4NCl the ratio was greater than unity.

TABLE III: Thermodynamic Data for Methanol-Iodide Solvates

Temp, °C	K	ΔG°, kcal/mol	ΔH°, kcal/mol	ΔS°, eu
10	27.1 ± 2.4	−1.86		
29	16.8 ± 2.5	−1.69	−3.7	−6.7
45	13.2 ± 1.2	−1.63		

of methanol or 2,2,2-trifluoroethanol was generally ca. 0.02 M. The magnitudes of the shifts from the $\nu(OH)_{free}$ maxima are shown as a function of the free energies, ΔG°, in Figure 2.

The values for $\nu(OH)_b$ were independent of concentration in the range covered except for the fluoroalcohol adducts where shifts to higher frequencies were detected when the [alcohol] > [salt]. These shifts are discussed below. Also $\nu(OH)_{free}$ for methanol and $\nu(OH)_b$ for MeOH---I^- adducts were independent of temperature between 10 and 45 °C. The K values showed no trends with concentration within the concentration ranges used.

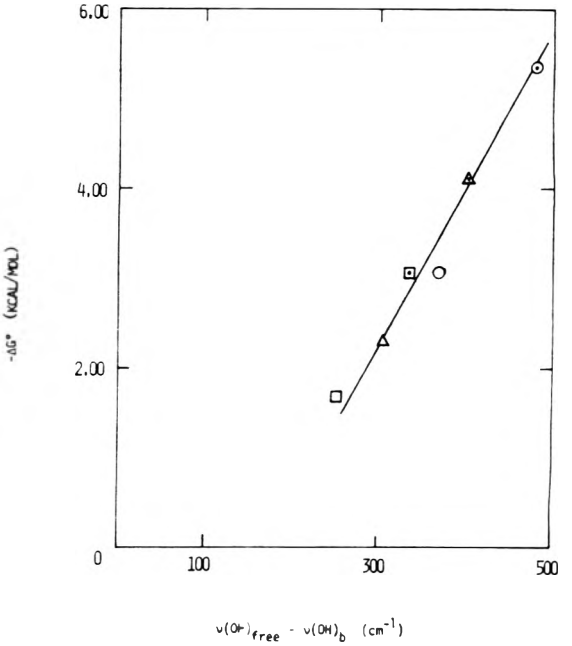

Figure 2. Free energy of formation of various hydrogen-bonded complexes at 29 °C vs. the shift, $\nu(OH)_{free} - \nu(OH)_b$: OH—$I^-$, methanol (□), F_3CCH_2OH (⊡); OH—Br^-, methanol (△), F_3CCH_2OH (▲); OH—Cl^-, methanol (○), F_3CCH_2OH (⊙).

Discussion

Our values for the molar absorptivity for methanol, $\epsilon(OH)_{free}$, agree reasonably with previous values.[9,10] However, it is clearly not temperature independent, as implied by Lipovskii and Dem'yanova.[7] Also, our values for $\epsilon(OH)_b$, given in Table I, do not agree well with those reported for their $C_9H_{19}OH$---hal$^-$ adducts.[7]

Our ΔH value of −3.7 kcal/mol for MeOH---I^- is smaller than that of −5.3 reported for $C_9H_{19}OH$---I^-.[7] This may be because of the difference in the alcohols, but since the latter was apparently based on the assumption of a temperature independent value for $\epsilon(OH)_{free}$, it is probably slightly large. On this basis, the difference in ΔS (−6.7 eu for MeOH---I^- and −10.5 for $C_9H_{19}OH$---I^-[7]) is also understandable.

The formation constant for MeOH---I^- reported by Blandamer et al.[6] of 13.7 is in fair agreement with the present value, but the Bufalini and Stern value for MeOH---Br^- in benzene[4] of 65.2 at 25 °C is higher than our value (49.0 at 29 °C). However, in this study, Bufalini and Stern used dielectric data to calculate equilibrium concentrations, and made allowance for the presence of quadrupoles on the assumption that only the ion pairs interacted with methanol. We see no reason why the alcohol molecules should discriminate between ion pairs and ion-quadrupoles, and this is supported by the self-consistency of the present results.

Our infrared results for fluoride, presented in Table II, confirm the findings of Lipovskii and Dem'yanova[7] that $\nu(OH)_b$ for MeOH---F^- is located at a lower frequency than the band maximum for MeOH---Cl^-. This order would be expected from the relative charge densities of the halide ions. It thus appears that the anomalous infrared results obtained by Allerhand and Schleyer[1] for MeOH---F^- may well be attributed to small amounts of water in their samples. They prepared the fluoride salt in an aqueous system. Because of the deliquescent nature of tetraalkylammonium fluorides we obtained only an estimate of K(MeOH---F^-), from which it appears that K(MeOH---F^-) > K(MeOH---Cl^-).

Results for the fluoroalcohol accord well with its increased acidity and indeed give a measure of this increase. It is of some interest that the results in Figure 2 for the two alcohols are nearly colinear. We do not think that the deviations from a single curve have any special significance. Though not shown, a similar, also essentially linear plot is obtained by graphing the half-widths $\Delta\nu(OH)_b$ of the solvate bands for the two alcohols against the frequency shifts for the solvates.

The shifts to high frequencies in $\nu(OH)_b$ as the [F_3C-CH_2OH] is increased above that for the salt is interpreted in terms of the addition of a second molecule:

$$ROH\cdots Hal^- + ROH \rightleftharpoons ROH\cdots Hal^-\cdots HOR \qquad (2)$$

The results suggest that this shift for chloride is greater than that for bromide which is in turn greater than that for iodide. The trend would follow the strengths of the bonds in the single solvates. We suggest that the extent of "neutralization" is greater for chloride and hence that the competition between the two solvent molecules is

greater. These shifts to high frequencies clearly stem from the same cause as that for the trialkylammonium ion shifts studied by Lipovskii and Dem'yanova.[7]

The alternative interaction that a second alcohol molecule might display is

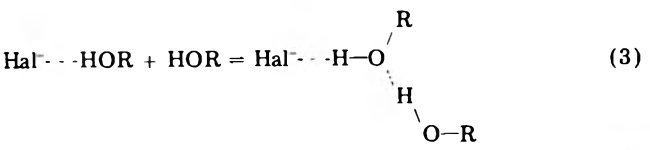

$$Hal^- \cdots HOR + HOR = Hal^- \cdots H{-}O(R)(H)(O{-}R) \quad (3)$$

We think that this is less likely to occur, especially for Cl^-. Also it would give rise to two new $(OH)_b$ bands, that for the primary solvent molecule being displaced to low rather than high frequency because of the increased strength of the hydrogen bond. No such *change* was detected.

Acknowledgment. We thank Mr. Scott A. Miller for early work in this field.

References and Notes

(1) A. Allerhand and P. v. R. Schleyer, *J. Am. Chem. Soc.*, **85**, 1233 (1963).
(2) S. C. Mohr, W. D. Wilk, and G. M. Barrow, *J. Am. Chem. Soc.*, **87**, 3048 (1965).
(3) H. Lund, *Acta Chem. Scand.*, **12**, 298 (1958).
(4) J. Bufalini and K. H. Stern, *J. Am. Chem. Soc.*, **83**, 4362 (1961).
(5) J. B. Hyne and R. M. Levy, *Can. J. Chem.*, **40**, 692 (1962).
(6) M. J. Blandamer, T. E. Gough, and M. C. R. Symons, *Trans. Faraday Soc.*, **60**, 488 (1964).
(7) A. A. Lipovskii and T. A. Dem'yanova, *Zh. Prikl. Spektrosk.*, 9, 239 (1968).
(8) W. J. Potts, "Chemical Infrared Spectroscopy", Vol. I, Techniques, Wiley, New York, N.Y., 1963.
(9) G. P. Hoover, E. A. Robinson, R. S. McQuate, H. D. Schreiber, and J. N. Spencer, *J. Phys. Chem.*, **73**, 4027 (1969).
(10) I. Motoyama and C. H. Jarboe, *J. Phys. Chem.*, **70**, 3226 (1966).

A Temperature Dependent Kinetics Study of the Reaction of OH with CH_2ClF, $CHCl_2F$, $CHClF_2$, CH_3CCl_3, CH_3CF_2Cl, and $CF_2ClCFCl_2$

R. T. Watson,† G. Machado, B. Conaway, S. Wagner, and D. D. Davis*

Georgia Institute of Technology, Atmospheric Sciences Division, Engineering Experiment Station, 339 Baker Building, Atlanta, Georgia 30332 *(Received March 26, 1976)*

Publication costs assisted by the Georgia Institute of Technology

The flash photolysis resonance fluorescence technique has been utilized to determine the Arrhenius parameters for several reactions between the hydroxyl radical and halogenated hydrocarbons. The reactions studied, and their corresponding Arrhenius expressions in units of cm^3 molecule^{-1} s^{-1} are shown: (1) $OH + CH_2ClF \rightarrow CHClF + H_2O$, $k_1 = (2.84 \pm 0.3) \times 10^{-12} \exp(-(1259 \pm 50)/T)$ (245–375) K; (2) $OH + CHCl_2F \rightarrow CCl_2F + H_2O$, $k_2 = (1.87 \pm 0.2) \times 10^{-12} \exp(-(1245 \pm 26)/T)$ (245–375) K; (3) $OH + CHClF_2 \rightarrow CClF_2 + H_2O$, $k_3 = (9.25 \pm 1.0) \times 10^{13} \exp(-(1575 \pm 71)/T)$ (250–350) K; (4) $OH + CH_3CCl_3 \rightarrow CH_2CCl_3 + H_2O$, $k_4 = (3.72 \pm 0.4) \times 10^{-12} \exp(-(1627 \pm 50)/T)$ (260–375) K; (5) $OH + CH_3CF_2Cl \rightarrow CH_2CF_2Cl + H_2O$, $k_5 = (1.15 \pm 0.15) \times 10^{-12} \exp(-(1748 \pm 30)/T)$ (273–375) K; (6) $OH + CF_2ClCFCl_2 \rightarrow$ products, $k_6 < 3 \times 10^{-16}$. Tropospheric lifetimes have been calculated for the above species by combining the rate constant data with global seasonally and diurnally averaged hydroxyl radical concentrations.

Introduction

It has been proposed that the injection of chlorinated compounds into the stratosphere will lead to a catalytic reduction in the integrated column density of ozone due to the interaction of odd oxygen (odd oxygen = $O(^3P) + O_3$) with ClO_x species ($ClO_x = Cl + ClO + ClOO$).[1] Numerous chlorinated compounds have already been shown to be present in the atmosphere and their concentrations determined by gas chromatographic detection.[2] These compounds can be classified into two separate groups: (a) fully halogenated, e.g., $CFCl_3$, CF_2Cl_2, and CCl_4; and (b) hydrogen containing, e.g., CH_3Cl, CHF_2Cl, etc. To date, no tropospheric sink mechanism has been identified for the fully halogenated compounds (i.e., the chemical lifetimes of these compounds in the troposphere far exceed the total atmospheric lifetimes that would be calculated based on stratospheric photodissociation alone). Consequently, for this type of compound, the principal atmospheric sink is believed to be vertical diffusion into the stratosphere, followed by photodissociation. However, some caution must be exercised here as there is still considerable scatter in the published results on the tropospheric concentrations of fluorocarbons. Within the range of this scatter, there could yet exist a significant unrecognized sink mechanism.[3] For those compounds reaching the lower and mid-stratosphere, photodissociation and, to a lesser extent, reaction with electronically excited atomic oxygen (O^1D), can result in the production of odd chlorine (Cl, ClO) which can directly participate in the destruction of odd oxygen:

$$Cl + O_3 \rightarrow ClO + O_2$$
$$O + ClO \rightarrow Cl + O_2$$
$$\overline{O + O_3 \rightarrow O_2 + O_2}$$

In contrast to the fully halogenated species, those compounds containing hydrogen atoms are expected to react with hydroxyl radicals, resulting in chemical lifetimes in the troposphere significantly shorter than would be expected from photolysis alone.[4] The relatively short lifetimes of these halocarbons (~1–20 years) would inhibit the buildup of large concentrations of these species in the troposphere, thus limiting the flux of chlorine into the stratosphere.

† Present Address: Physics Department, Jet Propulsion Laboratory, Pasadena, Calif.

This paper presents the results of a kinetic study of the behavior of hydroxyl radicals with several C_1 and C_2 halogenated compounds. The reactions were studied over a wide range of temperature and total pressure utilizing the technique of flash photolysis–resonance fluorescence. Recent measurements of tropospheric hydroxyl radical concentrations[5] have also permitted the calculation of tropospheric lifetimes for the various fluorocarbons studied. A comparison of our kinetic results with other recent data,[6-9] and a discussion of the atmospheric implications of our results is presented.

Experimental Section

The experimental details and operating principles of the flash photolysis-resonance fluorescence techniques have been fully described in the literature, and only a brief summary will therefore be presented in this text.[10]

The reaction vessel used in this work was a jacketed black anodized aluminum cell with an internal volume of ~850 cm^3. The cell temperature was controlled to within ±0.5 K by flowing methanol (240–325 K) or ethylene glycol (298–400 K) from a thermostated circulating bath through the outer jacket of the reaction vessel. An iron-constantan thermocouple was used to measure temperature, with a precision of better than 0.5 K.

As in earlier studies involving the kinetic behavior of the hydroxyl radical, photolysis of H_2O by a N_2 spark discharge lamp was used as the source of OH:[10]

$$H_2O + h\nu \rightarrow H + OH\ (X^2\Pi)$$

The spark discharge lamp was normally equipped with a quartz window in order to eliminate the transmittance of light at wavelengths shorter than 165 nm, thus minimizing the production of reactive intermediates from the photodecomposition of the added reagent. Based on the known absorption spectrum of H_2O, and previously conducted actinometry using ethylene as the actinic gas, it was determined that typical OH concentrations of ~3 × 10^{11} radical cm^{-3} were produced with an H_2O concentration of 6 × 10^{15} molecule cm^{-3}, and a flash energy of 88 J.

Excitation of OH was accomplished via the use of a discharge–flow hydroxyl resonance lamp which primarily produced the emission characteristic of the ($A^2\Sigma^+$: $v' = 0$) → ($X^2\Pi$: $v'' = 0$) transition of OH. A small fraction of the OH, produced by the photolysis of H_2O, was continuously excited by the resonance radiation emitted from the lamp. Fluorescence from excited OH was measured using a photomultiplier tube located at right angles to the lamp. As in previous studies, photon-counting electronics were used throughout this study. The intensity of the fluorescence was observed to be linearly proportional to the hydroxyl radical concentration in the reaction cell.

Each reaction was studied using pseudo-first-order kinetic conditions, $[\text{reagent}]_0 \gg [OH]_0$ ($[\text{reagent}]_0/[OH]_0 \simeq 1.5 \times 10^3$–$1.5 \times 10^5$), and as expected the hydroxyl radical concentration decayed exponentially with time. Because the initial hydroxyl radical concentration was kept low to prevent secondary reactions, multiple flashes on a single gas mixture were required to produce a smooth kinetic curve. However, the number of flashes per filling of the reaction cell was limited (i.e., less than 50) so as to minimize the possible accumulation of reactive photolysis or reaction products which might participate in secondary removal of hydroxyl radicals. For this reason, several fillings of an identical gas mixture were normally used to develop a single experimental decay curve. The hydroxyl radical decay was observed to be linear for at least two half-lives.

Gas pressures of 10–5000 mTorr were measured using a MKS Baratron which was frequently checked for accuracy. High pressure measurements (10–800 Torr) were made with a two-turn Bourdon gauge (Wallace and Tiernan Type FA-145). The precision to which gas mixtures could be made up, with the exception of H_2O, was estimated to be ~3% or better. The H_2O pressure could not be metered so precisely, due to absorption on the reaction vessel surfaces.

The purity of each of the halocarbons used in this study was as follows: CH_2FCl (Dupont, >99.92%); $CHCl_2F$ (Dupont, >99.8%); $CHClF_2$ (Dupont, >99.8%); CH_3CCl_3 (Dow Corning, >99.95%); CH_3CF_2Cl (Dupont, >99.8%); $CF_2ClCFCl_2$ (Dupont, >99.9%). The helium diluent gas was Matheson Gold Label Ultra-High Purity, and was used without further purification. Even though the CH_3CCl_3 provided by Dow was uninhibited (did not contain an antioxidant), it contained trace amounts (<0.1%) of a chlorinated olefin which was removed by fractional distillation before use. The nature of the trace impurities present in each of the gases was quantitatively known, and calculations verified that they were of no importance in the present study. Each of the halocarbons were subjected to a freeze and thaw purification process prior to use.

Results and Discussion

(a) *OH + C_1 and C_2 Halogenated Alkanes.* Since the kinetic behavior of hydroxyl radicals with CH_2ClF (1), $CHCl_2F$ (2), $CHClF_2$ (3); CH_3CCl_3 (4); CH_3CF_2Cl (5), and $CF_2ClCFCl_2$ (6) was studied using pseudo-first-order conditions, the hydroxyl radical decay rates could be analyzed using

$$OH + RH \xrightarrow{k_{bi}} R + H_2O;\ [RH]_0 \gg [OH]_0$$

$$\ln([OH]_0/[OH]_t) = K[RH]_0 t \qquad (I)$$

where $K = k_{bi}/[RH]_0$. A wide variation in experimental conditions was performed in order to verify that kinetic complications due to secondary processes were not affecting the observed OH decay rates. These variations were normally performed at 298 K and included: H_2O pressures of 50–400 mTorr; flash energies of 45–245 J; total pressures of 40–200 Torr; and the number of flashes per single filling of the reaction cell of 25–200 (not shown in the tables). The number of flashes per filling was varied to demonstrate that the formation of significant concentrations of reactive photolytic or reaction products was unimportant. In these experiments, the measured pseudo-first-order rate constants, K, were always observed to be invariant within the expected experimental uncertainty (~5%) of the measurements. Removal of hydroxyl radicals by processes such as a–c were also shown to be

$$OH + OH \rightarrow H_2O + O \qquad (a)$$

$$OH + OH + M \rightarrow H_2O_2 + M \qquad (b)$$

$$OH + H + M \rightarrow H_2O + M \qquad (c)$$

unimportant under typical operating conditions by examining the dependence of K upon flash energy, H_2O concentration, and total pressure. In these experiments, only when the flash energy was increased to 245 J were significantly higher K values (20%) measured over those obtained at lower flash energies, thus indicating some importance of radical–radical processes. Under these conditions, a ninefold increase in the radical concentration would have resulted. It should be noted, however, that no change was observed in the first-order rate constant when the flash energy was reduced from 88 to 45 J. In the calculation of K values for reactions 1–6, only data taken

TABLE I: $OH + CH_2ClF \rightarrow CHClF + H_2O$

Temp, K	[Reactant], mTorr	[Diluent], Torr	Flash energy, J	[Photolyte], mTorr	k', s^{-1}	k_{bimol}, cm^3 molecule^{-1} s^{-1}
245	0	40	88	100	24	
	50	40	88	100	61	
	97	40	88	100	91	
	100	40	88	100	85	
	125	40	88	100	119	
	150	40	88	100	120	
	200	40	88	100	155	
	250	40	88	100	192	$(1.65 \pm 0.36) \times 10^{-14}$
298	0	40	88	200	41	
	25	40	88	200	70	
	50	40	88	200	111	
	59	40	88	200	116	
	75	40	88	200	146	
	100	40	88	200	184	
	100	40	45	200	180	
	100	40	245	200	190	
	100	40	88	50	166	
	100	40	88	300	183	
	125	40	88	200	221	
	150	40	88	200	243	
	175	40	88	200	285	
	200	40	88	200	326	$(4.42 \pm 0.24) \times 10^{-14}$
	0	200	88	200	12.5	
	50	200	88	200	79	
	100	200	88	200	138	
	125	200	88	200	170	
	150	200	88	200	194	$(3.79 \pm 0.30) \times 10^{-14}$
375	25	100	88	200	95	
	40	100	88	200	135	
	50	100	88	200	154	
	75	100	88	200	219	
	100	100	88	200	280	
	125	100	88	200	350	$(9.80 \pm 0.34) \times 10^{-14}$

with flash energies of 88 J or less was used. The bimolecular rate constants for CH_2FCl, $CHCl_2F$, CHF_2Cl, CH_3CCl_3, CH_3CF_2Cl, and $CF_2ClCFCl_2$ were determined from a weighted least-squares treatment of the data shown in Tables I–VI. At 298 K, these k values are:

$$OH + CH_2ClF \rightarrow CHClF + H_2O \quad (1)$$
$$k_1 = (4.21 \pm 0.41) \times 10^{-14}$$

$$OH + CHCl_2F \rightarrow CCl_2F + H_2O \quad (2)$$
$$k_2 = (2.88 \pm 0.24) \times 10^{-14}$$

$$OH + CHClF_2 \rightarrow CClF_2 + H_2O \quad (3)$$
$$k_3 = (4.8 \pm 0.46) \times 10^{-15}$$

$$OH + CH_3CCl_3 \rightarrow CH_2CCl_3 + H_2O \quad (4)$$
$$k_4 = (1.59 \pm 0.16) \times 10^{-14}$$

$$OH + CH_3CF_2Cl \rightarrow CH_2CF_2Cl + H_2O \quad (5)$$
$$k_5 = (3.22 \pm 0.48) \times 10^{-15}$$

$$OH + CF_2ClCFCl_2 \rightarrow \text{products} \quad (6)$$
$$k_6 < 3 \times 10^{-16}$$

Units are cm^3 molecule^{-1} s^{-1}. For those reactions where several different total pressures were employed, a weighted averaged k value has been reported. The uncertainty limits shown for the above 298 K data, as well as those given in Tables I–VI for other temperatures, are the two σ values calculated from a weighted least-squares treatment of the data.

The temperature dependence of each reaction was studied over a nominal temperature range of ~100 deg. The limiting factors which determined the lowest temperature used in these measurements were: (a) the vapor pressure of H_2O at low temperatures; and (b) the magnitude of the rate constant. (The concentration of fluorocarbon was limited to 1500 mTorr due to electronic quenching of the $A^2\Sigma^+$ state of OH.) Figure 1 shows the

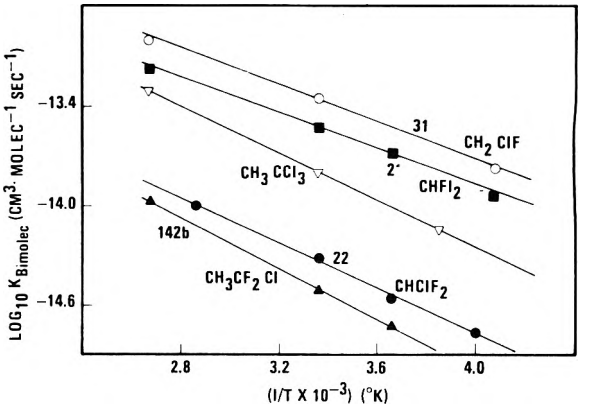

Figure 1.

Arrhenius plots for reactions 1–5. The resulting Arrhenius expressions are summarized as follows:

$$k_1 = (2.84 \pm 0.3) \times 10^{-12} \exp[-(1259 \pm 50/T)]$$
$$k_2 = (1.87 \pm 0.2) \times 10^{-12} \exp[-(1245 \pm 26/T)]$$
$$k_3 = (9.25 \pm 1.0) \times 10^{-13} \exp[-(1575 \pm 71/T)]$$
$$k_4 = (3.72 \pm 0.4) \times 10^{-12} \exp[-(1627 \pm 50/T)]$$
$$k_5 = (1.15 \pm 0.15) \times 10^{-12} \exp[-(1748 \pm 30/T)]$$

Units for the above k values are cm^3 molecule^{-1} s^{-1}. The activation energy has been expressed in terms of K^{-1}. The uncertainties quoted for k_1–k_5 apply only to the temperature range over which each system was studied and represent the 90% confidence limits.

Comparison and Discussion of Recent Work

A comparison of the results from this study with both published[6,8,9] as well as unpublished[7] rate data from other laboratories is shown in Table VII. It is readily seen that

TABLE II: OH + $CHFCl_2$ → $CFCl_2$ + H_2O

Temp, K	[Reactant], mTorr	[Diluent], Torr	Flash energy, J	[Photolyte], mTorr	k', s^{-1}	k_{bimol}, cm^3 $molecule^{-1}$ s^{-1}
245	50	40	88	100	51	
	100	40	88	100	81	
	150	40	88	100	103	
	200	40	88	100	119	
	250	40	88	100	143	
	300	40	88	100	158	
	350	40	88	100	186	
	400	40	88	100	229	$(1.12 \pm 0.12) \times 10^{-14}$
273	75	40	88	200	102	
	100	40	88	200	120	
	150	40	88	200	161	
	200	40	88	200	196	
	250	40	88	200	240	
	300	40	88	200	270	
	350	40	88	200	303	
	400	40	88	200	351	$(2.09 \pm 0.18) \times 10^{-14}$
298	0	40	88	200	38	
	50	40	88	200	75	
	75	40	88	200	108	
	100	40	88	200	123	
	125	40	88	200	161	
	150	40	88	200	180	
	150	40	45	200	175	
	150	40	245	200	217	
	150	40	88	50	174	
	150	40	88	400	204	
	175	40	88	200	206	
	200	40	88	200	210	
	200	40	45	200	222	
	250	40	88	200	263	
	275	40	88	200	302	
	300	40	88	200	340	$(2.99 \pm 0.24) \times 10^{-14}$
298	0	200	88	200	12	
	50	200	88	200	60	
	100	200	88	200	98	
	125	200	88	200	115	
	150	200	88	200	140	
	175	200	88	200	173	
	200	200	88	200	185	
	200	200	88	200	180	
	225	200	88	200	238	
	250	200	88	200	229	
	250	200	88	200	206	
	300	200	88	200	263	$(2.66 \pm 0.58) \times 10^{-14}$
375	0	100	88	200	70	
	15	100	88	200	104	
	25	100	88	200	116	
	40	100	88	200	135	
	50	100	88	200	157	
	65	100	88	200	175	
	75	100	88	200	206	
	90	100	88	200	217	
	100	100	88	200	232	
	110	100	88	200	263	
	125	100	88	200	298	$(6.68 \pm 0.82) \times 10^{-14}$

at 298 K virtually all results are in excellent agreement within the quoted experimental uncertainties. An exception to this is the compound $CHClF_2$ where the result quoted by Howard and Evenson is lower than that of the other two studies by ~25–30%. At present, no explanation can be forwarded for this apparent discrepancy. Howard and Evenson[6,7] used a low pressure discharge flow system with laser magnetic resonance detection of the hydroxyl radical to determine the rate constants for reactions 1–5 at 298 K. Pitts, Atkinson, et al.,[8,9] as in this investigation, utilized the technique of flash photolysis–resonance fluorescence to examine the kinetic behavior of reactions 2 and 3 between 298 and ~430 K. The results of the two high pressure flash photolysis studies are in excellent agreement for both reactions 2 and 3. This is especially encouraging in that the temperature ranges used in the two studies only partially overlapped, and yet the experimental data of one study were always within the stated experimental uncertainties of that predicted from the Arrhenius expression reported from the other study. A least-squares treatment of all the data points obtained in the two temperature dependence studies of k_2 and k_3 resulted in the following evaluated Arrhenius expressions:

$$k_2 = (1.59 \pm 0.2) \times 10^{-12} \exp[-(1204 \pm 50/T)] \text{ (245-423) K}$$

$$k_3 = (1.21 \pm 0.17) \times 10^{-12} \exp[-(1648 \pm 75/T)] \text{ (250-434) K}$$

Atmospheric Implications of Rate Data

The chemical degradation of halogenated alkanes via hydroxyl radical attack was discussed in the Introduction with particular reference to the tropospheric lifetimes of

TABLE III: $OH + CHF_2Cl \rightarrow CF_2Cl + H_2O$

Temp, K	[Reactant], mTorr	[Diluent], Torr	Flash energy, J	[Photolyte], mTorr	k', s^{-1}	k_{bimol}, cm^3 molecule^{-1} s^{-1}
250	300	40	88	200	47	
	500	40	88	200	60	
	700	40	88	200	70	
	900	40	88	200	87	
	1100	40	88	200	93	
	1300	40	88	200	116	$(1.70 \pm 0.40) \times 10^{-15}$
273	300	40	88	200	63	
	400	40	88	200	73	
	500	40	88	200	84	
	600	40	88	200	89	
	700	40	88	200	102	
	800	40	88	200	115	
	900	40	88	200	121	$(2.77 \pm 0.38) \times 10^{-15}$
298	0	40	88	200	25	
	100	40	88	200	53	
	300	40	88	200	87	
	400	40	88	200	99	
	500	40	88	200	117	
	500	40	45	200	111	
	500	40	245	200	123	
	500	40	88	500	120	
	600	40	88	200	131	
	700	40	88	200	141	
	800	40	88	200	166	
	900	40	88	200	178	
	960	40	88	200	190	$(4.84 \pm 0.46) \times 10^{-15}$
	0	200	88	200	15	
	400	200	88	200	66	
	600	200	88	200	90	
	700	200	88	200	114	
	800	200	88	200	128	
	900	200	88	200	151	$(4.69 \pm 1.06) \times 10^{-15}$
350	0	100	88	200	34	
	200	100	88	200	82	
	300	100	88	200	110	
	400	100	88	200	136	
	500	100	88	200	168	
	600	100	88	200	193	$(1.01 \pm 0.08) \times 10^{-14}$

TABLE IV: $OH + CH_3CCl_3 \rightarrow CH_2CCl_3 + H_2O$

Temp, K	[Reactant], mTorr	[Diluent], Torr	Flash energy, J	[Photolyte], mTorr	k', s^{-1}	k_{bimol}, cm^3 molecule^{-1} s^{-1}
260	0	40	88	200	25	
	100	40	88	200	54	
	200	40	88	200	65	
	250	40	88	200	68	
	300	40	88	200	110	
	400	40	88	200	115	
	500	40	88	200	155	
	700	40	88	200	204	
	750	40	88	200	210	
	1000	40	88	200	285	$(7.12 \pm 0.94) \times 10^{-15}$
298	0	40	88	200	38	
	100	40	88	200	87	
	150	40	88	200	117	
	200	40	88	200	140	
	250	40	88	200	150	
	300	40	88	200	205	
	400	40	88	50	280	
	400	40	88	200	255	
	400	40	88	400	273	
	405	40	88	200	249	
	500	40	88	200	285	
	800	40	88	200	450	$(1.59 \pm 0.16) \times 10^{-14}$
	200	40	245	200	171	
	400	40	245	200	270	
	600	40	245	200	373	$(1.56 \pm 0.04) \times 10^{-14}$
	200	40	31	200	120	
	400	40	31	200	~215	$\sim 1.5 \times 10^{-14}$
375	25	40	88	200	125	
	50	40	88	200	150	
	100	40	88	200	225	
	150	40	88	200	296	
	200	40	88	200	347	
	250	40	88	200	400	$(4.85 \pm 0.58) \times 10^{-14}$

TABLE V: $OH + CH_3CF_2Cl \rightarrow CH_2CF_2Cl + H_2O$

Temp, K	[Reactant], mTorr	[Diluent], Torr	Flash energy, J	[Photolyte], mTorr	k', s^{-1}	k_{bimol}, cm^3 molecule^{-1} s^{-1}
273	250	40	88	200	32	
	500	40	88	200	77	
	750	40	88	200	101	
	1000	40	88	200	117	
	1250	40	88	200	126	
	1500	40	88	200	139	$(1.92 \pm 0.48) \times 10^{-15}$
298	200	40	88	200	51	
	400	40	88	200	77	
	600	40	88	200	99	
	800	40	88	200	117	
	1000	40	88	200	147	
	1200	40	88	200	156	
	1200	40	45	200	167	
	1200	40	245	200	200	
	1200	40	88	400	161	
	1400	40	88	200	177	
	1500	40	88	200	181	
	1600	40	88	200	199	$(3.12 \pm 0.48) \times 10^{-15}$
	0	200	88	200	12.5	
	600	200	88	200	90	
	800	200	88	200	117	
	1000	200	88	200	116	
	1400	200	88	200	172	$(3.42 \pm 0.68) \times 10^{-15}$
375	75	100	88	200	65	
	150	100	88	200	86	
	200	100	88		111	
	300	100	88		123	
	400	100	88		147	
	500	100	88		178	
	600	100	88		216	
	800	100	88		273	$(1.09 \pm 0.14) \times 10^{-14}$

TABLE VI: $OH + CF_2ClCFCl_2 \rightarrow$ products

Temp, K	[Reagent], mTorr	[Diluent], Torr	Flash energy, J	[Photolyte], mTorr	k', s^{-1}	k_{bimol}, cm^3 molecule^{-1} s^{-1}
298	250	40	88	200	27	
	500	40	88	200	36	
	750	40	88	200	31	
	1250	40	88	200	39	$< 3 \times 10^{-16}$

TABLE VII: Comparison of Rate Data

Compd	k(298K) × 10^{15} cm^3 molecule^{-1} s^{-1}			Arrhenius expressions	
	This work	Ref 6,7	Ref 8,9	This work	Ref 8,9
CH_2ClF	42.1 ± 4	37 ± 6		$2.84 \times 10^{-12} \exp[-(1259/T)]$	
$CHCl_2F$	28.8 ± 3	26 ± 4	27 ± 3	$1.87 \times 10^{-12} \exp[-(1245/T)]$	$1.75 \times 10^{-12} \exp[-(1253/T)]$
$CHClF_2$	4.8 ± 0.3	3.4 ± 0.7	4.75 ± 0.48	$9.25 \times 10^{-13} \exp[-(1575/T)]$	$1.21 \times 10^{-12} \exp[-(1636/T)]$
CH_3CCl_3	15.9 ± 2	15 ± 3		$3.72 \times 10^{-12} \exp[-(1627/T)]$	
CH_3CF_2Cl	3.22 ± 0.3	2.8 ± 0.4		$1.15 \times 10^{-12} \exp[-(1748/T)]$	
$CF_2ClCFCl_2$	< 0.3				

these compounds. The most significant consequence of a short tropospheric lifetime for partially hydrogenated halocarbons is that of restricting the stratospheric burden of chlorine from these compounds. Table VIII, for example, shows the results of a calculation[11] which gives the fraction of a given halocarbon which would diffuse into the stratosphere and photolyze as a function of its tropospheric lifetime at steady state. It can readily be seen that a lifetime of 10 years or less drastically reduces the flux of these compounds into the stratosphere at steady state (see comments on ref 11). The destruction rate for a halocarbon containing hydrogen is given by

$$-d[RX]/dt = k[OH][RX]$$

and

$$\tau_e(\text{tropospheric lifetime}) = [k[OH]_{av}]^{-1}$$

Thus, the two parameters required to calculate tropo-

TABLE VIII

Lifetime, yr	$CFCl_3$	CF_2Cl_2
∞	1.0	1.0
50	0.66	0.4
40	0.53	0.32
20	0.27	0.16
10	0.13	0.08

TABLE IX: Calculated Tropospheric Lifetimes

Compd	k_{bimol}, (265 K)	Lifetime,[a] yr
CH_2ClF	2.45×10^{-14}	1.44
$CHCl_2F$	1.70×10^{-14}	2.07
$CHClF_2$	2.43×10^{-15}	14.50
CH_3CCl_3	8.02×10^{-15}	4.39
CH_3CF_2Cl	1.57×10^{-15}	22.44
$CF_2ClCFCl_2$	$< 3 \times 10^{-16}$	>117

[a] Lifetime: $\ln(A_0/A) = k[OH]_{av}t$, where $\ln(A_0/A) = 1$.

spheric lifetimes are (a) the value of the bimolecular rate constant for a given OH reaction and (b) the global seasonally and diurnally averaged OH steady state concentration. In Table IX, we have calculated the tropospheric lifetimes of all six compounds investigated in this study. These calculations have been based on a weighted average temperature for the troposphere of 265 K and a global seasonally and diurnally averaged OH concentration of 9×10^5 cm $^{-3}$. The latter value has been estimated using results from Crutzen's two-dimensional atmospheric model[12] and data from recent direct measurements of atmospheric OH at 32 and 21°N latitude at 7 and 11.5 km reported by Davis, McGee, and Heaps.[5]

From Table IX, it can be seen that the tropospheric lifetimes of CH_2ClF (fluorocarbon 31), $CHCl_2F$ (fluorocarbon 21), and CH_3CCl_3 are sufficiently short that their potential impact on stratospheric ozone should be minimal. However, the predicted lifetimes for $CHClF_2$ (fluorocarbon 22) and CH_3CF_2Cl (fluorocarbon 142) are sufficiently long that the sink for 10–20% of the anthropogenic production rate could be expected to be photodissociation in the stratosphere at steady state. Additional factors of importance, however, are that both these compounds contain only one chlorine atom per molecule in contrast to fluorocarbons 11 and 12 which contain three and two chlorine atoms, respectively. This fact combined with the predicted shorter tropospheric lifetime of fluorocarbons 22 and 142 would indicate that the potential impact of an equal source strength of these compounds compared to fluorocarbon 11 or 12 would be four to ten times less. As expected, no observable reaction was detected between OH and $CF_2ClCFCl_2$ (TF 13), suggesting a chemical lifetime in the troposphere comparable to that for fluorocarbons 11 and 12.

Acknowledgment. The author, Dr. D. D. Davis, wishes to express his appreciation to the National Aeronautics and Space Administration and the E. I. DuPont de Nemours Company for their support of this research. It is also acknowledged that part of this work was carried out by the authors at the University of Maryland, Chemistry Department.

References and Notes

(1) (a) F. S. Rowland and M. J. Molina, *Rev. Geophys. Space Phys.*, **13**, 1 (1975); (b) M. J. Molina and F. S. Rowland, *Nature (London)*, **249**, 810 (1974); *Geophys. Res. Lett.*, 309 (1974); (c) S. Wofsy, M. McElroy, and N. Sze, *Science*, **187**, 535 (1975); (d) S. Wofsy and M. McElroy, *Can. J. Chem.*, **52**, 1582 (1974); (e) P. J. Crutzen, *Geophys. Res. Lett.*, **1**, 205 (1974); (f) R. J. Cicerone, R. S. Stolarski, and S. Walters, *Science*, **185**, 1165 (1974); (g) R. J. Cicerone, D. H. Stedman, and R. S. Stolarski, *Geophys. Res. Lett.* **2**, 219 (1975); (h) P. J. Crutzen and L. S. A. Isakensen, *J. Geophys. Res.*, accepted for publication.

(2) (a) L. E. Heidt, R. Lueb, W. Pollock, and D. H. Ehhalt, *Geophys. Res. Lett.*, **2**, 445 (1975); (b) N. E. Hester, E. R. Stephens, and O. C. Taylor, *Environ. Sci. Technol.* **9**, 875 (1975); (c) P. W. Krey and R. J. Lagomarsino, ERDA Environment Quarterly Report HASL-294, 97 (1975); (d) J. E. Lovelock, *Nature (London)*, **252**, 292 (1974); (e) J. E. Lovelock, R. J. Maggs, and R. J. Wade, *ibid.*, **241**, 194 (1973); (f) A. L. Schmeltekopf, P. O. Golden, W. R. Henderson, W. J. Harrap, T. L. Thompson, R. S. Fehsenfeld, H. I. Schiff, P. J. Crutzen, I. S. A. Isaksen, and E. E. Ferguson, *Geophys. Res. Lett.*, **2**, 393 (1975); (g) W. J. Williams, J. J. Kosters, A. Goldman, D. G. Murcray, presented at AGU, Dec, 1975; (h) P. E. Wilkness, J. W. Swinnerton, D. J. Bresson, R. A. Lamontagne, and R. E. Larson, *J. Atm. Sci.*, **22**, 158 (1975); (i) P. E. Wilkness, J. W. Swinnerton, R. A. Lamontagne, and D. J. Bresson, *Science*, **187**, 832 (1975).

(3) N. D. Sze and M. F. Wu, *Atmos. Environ.*, submitted for publication.

(4) D. D. Davis, G. Machado, B. Conaway, Y. Oh, and R. T. Watson, *J. Chem. Phys.*, accepted for publication.

(5) D. D. Davis, T. McGee, and W. Heaps, *J. Geophys. Res. Lett.*, submitted for publication.

(6) C. J. Howard and K. M. Evenson, *J. Chem. Phys.*, **64**, 197 (1976).

(7) C. J. Howard and K. M. Evenson, *J. Chem. Phys.*, submitted for publication.

(8) R. A. Perry, R. Atkinson, and J. N. Pitts, Jr., *J. Chem. Phys.*, **64**, 1618 (1976).

(9) R. Atkinson, D. A. Hansen, and J. N. Pitts, Jr., *J. Chem. Phys.*, **63**, 1703 (1975).

(10) (a) D. D. Davis, R. Schiff, and S. Fischer, *J. Chem. Phys.*, **61**, 2213 (1974); (b) D. D. Davis, R. Huie, J. Herron, W. Braun, and M. Kurylo, *ibid.*, **56**, 4868 (1972); (c) D. D. Davis and R. B. Klemm, *Int. J. Chem. Kinet.*, **4**, 367 (1972).

(11) N. D. Sze, private communication. These calculations used the Hunten eddy diffusion coefficient. Use of any other K_z function would show a lesser dependence of flux upon lifetime. The magnitude of the effect is different for all gases and is governed by the destruction ratio (photolytic and chemical) in the stratosphere.

(12) P. Crutzen, "Results from a 2-D Atmospheric Model", paper presented at the 4th Climatic Impact Assessment Program, Cambridge, Mass., Feb, 1975.

Effect of Complexation of Zinc(II) on Zinc-67 Chemical Shifts

Gary E. Maciel,* Larry Simeral, and Joseph J. H. Ackerman

Department of Chemistry, Colorado State University, Fort Collins, Colorado 80523 *(Received August 2, 1976)*

Publication costs assisted by the National Science Foundation

Fourier transform ^{67}Zn NMR spectra were obtained on natural abundance samples. ^{67}Zn chemical shifts are reported for a variety of aqueous Zn(II) solutions. The dependence of the ^{67}Zn chemical shift of a $Zn(ClO_4)_2$ solution as a function of added Cl^- or Br^- is analyzed in terms of relevant complexation equilibria. Chemical shift values of ZnX^+, ZnX_2, ZnX_3^-, and ZnX_4^{2-} species (X = Cl^- or Br^-) are derived and discussed.

Introduction

The Zn^{2+} ion and its complexes are not only important in inorganic chemistry, but play a role in organic chemistry and are extremely important in biological chemistry. Yet, good physical probes, e.g., spectroscopic approaches, have not been available for delineating the role of Zn(II) species in chemical processes, including those relevant to biological systems. For example, Zn(II) does not exhibit convenient properties for uv–visible spectroscopy, and has no EPR spectrum. A priori, the ^{67}Zn nuclide, a spin 5/2 nuclide which is 4.1% naturally abundant, could provide a spectroscopic probe via its NMR spectra.

There have been few previous reports of ^{67}Zn NMR observations,[1-3] and they were largely oriented toward measurements of physical rather than chemical interests. The small magnetogyric ratio and low natural abundance of this nuclide, together with the expectation of wide lines because of quadrupolar relaxation, yield a relatively unfavorable case for NMR study, at least in comparison with commonly studied nuclei. Nevertheless, with the availability of modern multinuclide Fourier transform (FT) NMR techniques,[4-7] and considering the potential importance of having an attractive Zn(II) probe, a serious attempt to explore the characteristics of ^{67}Zn NMR and its possible scope of applicability is warranted, as the results of Epperlein et al. demonstrate.[3]

This paper presents some representative ^{67}Zn NMR results we have obtained on aqueous Zn(II) systems, and provides the first detailed information on the sensitivity of ^{67}Zn chemical shifts to systematic variation in the structure of Zn(II) species in solution. Together with the results published by Epperlein et al.,[3] this study provides some insight into the role that FT ^{67}Zn NMR can play in studies of Zn(II) solution chemistry.

Experimental Section

(a) *Measurements.* ^{67}Zn NMR measurements were made in natural abundance at 5.63 MHz on a Bruker HFX-90 spectrometer, interfaced to a Digilab FTS/NMR-3 data system, using a multinuclide configuration reported earlier.[6,7] Field/frequency lock was based on the ^{19}F signal of an external sample of C_6F_6 or C_4F_8 placed next to the ^{67}Zn receiver insert. Samples were run at 300 ± 0.3 K in 10-mm tubes. Typically, 20 000 to 60 000 free induction decays were collected for each spectrum, requiring 2000 to 6000 s. The loss of signal-to-noise ratio associated with the substantial line widths encountered because of quadrupole relaxation is to some extent offset by the increased pulse repetition rate that one can use because of the corresponding short spin–lattice relaxation times.

In earlier experiments, bulk susceptibility corrections were explored by measuring (on a JEOL MH-100 spectrometer) the apparent shift differences between the methyl-^{1}H resonances of 3-(trimethylsilyl)propanesulfonate (sodium salt) dissolved in the sample and the ^{1}H resonance of tetramethylsilane contained in a 1-mm capillary centered concentrically within the 5-mm NMR tube used for the measurements. All susceptibility corrections determined in this manner were found to fall within the experimental uncertainties of the ^{67}Zn chemical shifts (±0.5 ppm), and were not applied to the ^{67}Zn data. In later experiments the ^{1}H resonances of water were observed on the same samples immediately before or after the ^{67}Zn measurements were made. A total range of about 0.2 ppm was observed for the ^{1}H chemical shifts measured, supporting our neglect of bulk susceptibility effects in these systems.

TABLE I: ^{67}Zn Chemical Shifts for Various Solutions of Zinc Salts

Solution (in H_2O)	Chemical shift, ppm[a]	$\Delta\nu_{1/2}$[b]
1.0 M $Zn(NO_3)_2$ in 11.2 M NH_3	288.2	65 ± 5
1.0 M $Zn(CN)_2$ in 3 M NaCN	283.6	40 ± 5
1.0 M $ZnCl_2$ in 12 M HCl	256.6	37 ± 5
0.25 M $ZnCl_2$ in 12 M HCl	253.1	46 ± 5
1.0 M $ZnBr_2$ in 9 M HBr	168.9	46 ± 5
0.25 M $ZnBr_2$ in 9 M HBr	171.0	42 ± 5
2.0 M $ZnCl_2$	93 ± 3	200 ± 20
1.0 M $Zn(NO_3)_2$	0.0	47 ± 5
2.0 M $Zn(ClO_4)_2$	−1.4	37 ± 5
2.0 M $Zn(NO_3)_2$	−1.9	89 ± 10
1.0 M ZnI_2 in 12 M HI	−35.5	70 ± 5

[a] More positive values refer to lower shielding. Bulk susceptibility corrections were not applied, since they were found to be less than the experimental uncertainty. Experimental error ± 0.5 ppm unless noted otherwise. [b] Line width at half-height, Hz.

(b) *Materials.* All chemicals were obtained from commercial sources and used without further purification. Zinc chloride, sodium bromide, and zinc nitrate were Baker, reagent grade. Zinc bromide was obtained from Matheson Coleman and Bell, reagent grade. Zinc perchlorate was from Alfa/Ventron (98.9%). Sodium perchlorate was from G. Frederich Smith Chemical Co., reagent grade. Lithium chloride, sodium chloride, concentrated HCl, and concentrated HBr were Fisher, reagent grade. Lithium bromide was Fisher, purified.

Solutions of 0.5 M Zn(II) at constant ionic strength (4.5) were prepared volumetrically from solutions of zinc perchlorate (standardized by titration with EDTA), sodium perchlorate (standardized by evaporation to constant weight at 150 °C), and the sodium salt of whichever halide was being studied (Cl^- or Br^-).

Results and Discussion

Table I presents chemical shift and line width data for a number of ^{67}Zn(II) resonances in solution. The total

Scheme I

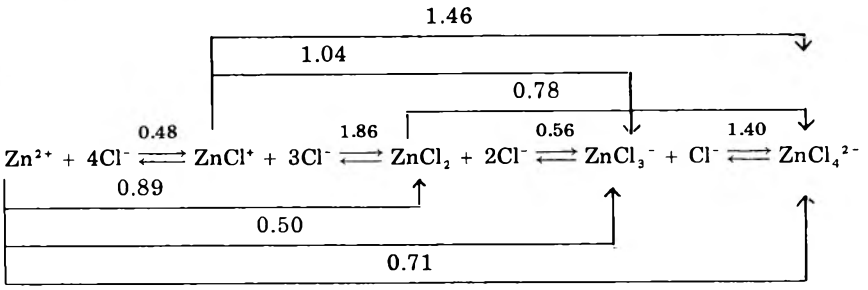

range of chemical shifts is in excess of 300 ppm. Such large variations in shielding are attributed to domination of the shielding constant by local paramagnetic contributions.[8,9]

The solutions whose chemical shifts are summarized in Table I were chosen so as to examine qualitatively the sensitivity of the ^{67}Zn chemical shift and line width of Zn^{2+} to common ligands known to coordinate with zinc(II). The high concentrations of zinc(II) were necessitated by the low natural abundance and low NMR sensitivity of ^{67}Zn. Concentrations of about 0.25–0.50 M solutions of zinc salts represent the lowest concentration for which a large number of spectra could conveniently be gathered in a reasonable amount of time with the instrumental configuration employed. With the use of ^{67}Zn enriched samples, higher magnetic fields, larger sample tubes, and available electronic improvements (e.g., crystal filter,[10] quadrature detection,[11] etc.) one should be able to extend such studies to much lower concentrations. For example, with enrichment to the 40% level, a factor of 10 in effective chemical sensitivity would be gained. A maximum improvement of between 2 and 3 orders of magnitude can be anticipated on the basis of current technology.

A set of experiments was carried out in which the ^{67}Zn resonances were observed on a series of aqueous 0.5 M $Zn(ClO_4)_2$ solutions containing varied concentrations of Cl^- and with the formal ionic strength maintained at 4.5 M with $NaClO_4$. The dependence of the ^{67}Zn chemical shift on added chloride is shown in Figure 1.

It must be kept in mind that the shifts of the systems reported in Table I and in Figure 1 represent weighted averages of the shifts for the various species in equilibrium in the solution. The formation constants for zinc(II)–chloride complexes are low enough that, even though the tetrahalo complex may predominate in very concentrated chloride solutions, the mono-, di-, and trihalo complexes may have appreciable concentrations for intermediate chloride concentrations. Considering zinc(II) as being in rapid equilibrium between a hydrated state and a state in which it is bound in various complexes to a coordinating ligand, L^{n-}, the following equations can be written:

$$Zn^{2+} + L^{n-} = ZnL^{2-n} \qquad K_1 \qquad (1)$$

$$ZnL^{2-n} + L^{n-} = ZnL_2^{2-2n} \qquad K_2 \qquad (2)$$

$$ZnL^{2-2n} + L^{n-} = ZnL_3^{2-2n} \qquad K_3 \qquad (3)$$

$$ZnL_3^{2-2n} + L^{n-} = ZnL_4^{2-4n} \qquad K_4 \qquad (4)$$

where n may be 0, 1, 2, etc. (the magnitude of the charge of the ligand), and K_n is the equilibrium constant for the indicated association reaction. Although transient species with higher coordination numbers of ligand L^{n-} (e.g., Cl^-) can be envisioned, current evidence indicates that the species indicated in eq 1–4 are the most important.[12-14] The extent to which water is involved in Zn(II) coordination is not known unequivocally for all species of the types represented in eq 1–4, and is not represented explicitly in the symbolism. In the rapid exchange limit, the

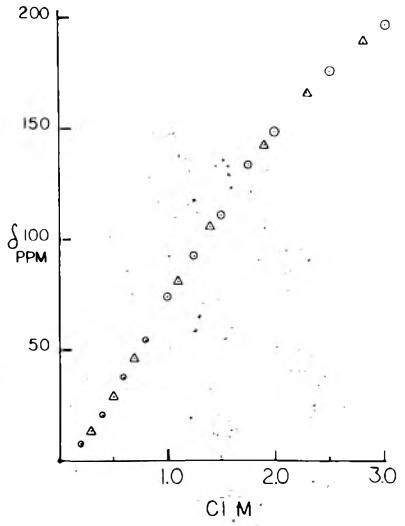

Figure 1. The dependence of the ^{67}Zn chemical shift of a 0.50 M $Zn(ClO_4)_2$ solution on added sodium chloride, with the total Zn(II) concentration maintained at 0.50 M and the ionic strength maintained at 4.5 M. Experimental data are represented by circles, while triangles represents values that were calculated using eq 5, and mole fractions of Zn(II)–chloride species calculated from known equilibrium constants.[12] The solvent is H_2O.

observed shift is given by the "weighted average" expression,

$$\delta_{obsd} = \delta_0 X_0 + \delta_1 X_1 + \delta_2 X_2 + \delta_3 X_3 + \delta_4 X_4 \qquad (5)$$

where X_0, X_1, etc., are the respective mole fractions (with respect to total Zn(II)) of hydrated and halide-bound zinc species as indicated in eq 1–4, and δ_0, δ_1, etc., are the respective chemical shifts of the species indicated in eq 1–4.

If, for a given total Zn(II) concentration, one knows the time-average ^{67}Zn chemical shift and the mole fractions of the individual zinc species in solution as functions of added ligand concentration, the corresponding set of linear, weighted-average shift equations based on eq 5 can be solved for the shifts of the individual species in solution. For ionic strength 4.5 M, the stepwise and overall formation constants shown in Scheme I have been reported for the Zn(II)–chloride system.[12] Based upon these constants and a computer program (HALTAFALL[15]) kindly provided by Dr. J. Christie, the curves shown in Figure 2 were generated, showing the values of X_0, X_1, X_2, X_3, and X_4 of eq 5 for the range of "total added Cl^- concentrations" employed in this study. From the curves of this figure, it is clear that appreciable concentrations of all five species exist in the added Cl^- concentration range of 1–3 M. Using X values taken from these calculations, a least-squares treatment was applied to eq 5 to determine values for δ_0, δ_1, δ_2, δ_3, and δ_4. The values obtained are: $\delta_0 = 0$ (arbitrary reference being Zn^{2+}), $\delta_1 = 30$ ppm (for $ZnCl^+$), $\delta_2 = 295$ ppm (for $ZnCl_2$), $\delta_3 = 119$ ppm (for $ZnCl_3^-$), and $\delta_4 = 253$

Scheme II

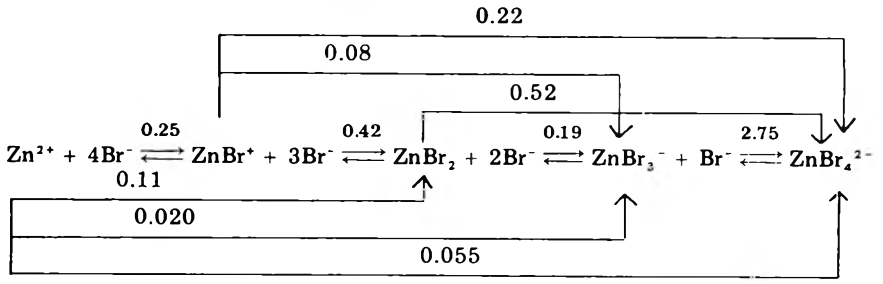

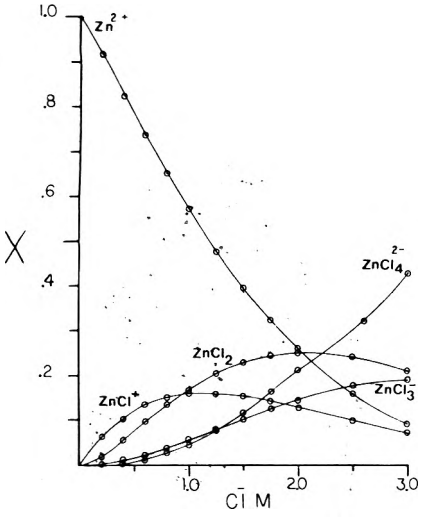

Figure 2. The calculated dependence of the fractions of Zn(II) present as various Zn(II) species upon the total added Cl^- concentration, with the total Zn(II) concentration maintained at 0.50 M. The solvent is H_2O.

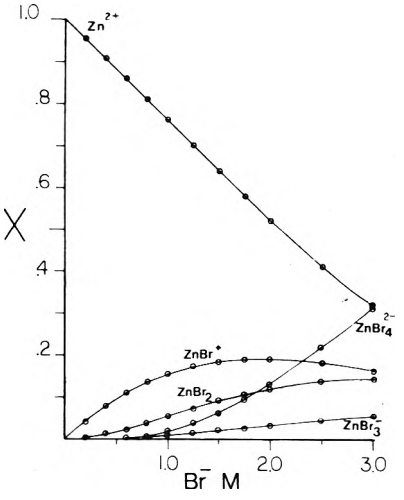

Figure 3. The calculated dependence of the fractions of Zn(II) present as the various Zn(II) species upon the total added Br^- concentration, with the total Zn(II) concentration maintained at 0.50 M. The solvent is H_2O.

ppm (for $ZnCl_4^{2-}$). From Table I it is seen that the ^{67}Zn chemical shift of a 0.25 M solution of $ZnCl_2$ in concentrated HCl (12 M), in which the dominant zinc species is believed to be $ZnCl_4^{2-}$, is also 253 ppm. Hence, the least-squares analysis appears to give reasonable results, in terms of consistency with the other data. The quality of the least-squares fit is shown in Figure 1, where both experimental points and points calculated by eq 5 are shown.

A similar set of experiments was carried out for the Zn(II)–bromide system, examining a series of solutions in which the total Zn(II) concentration was 0.5 M, the ionic strength was maintained at 4.5 M with $NaClO_4$, and the "total added Br^- concentration" was varied up to 3 M. For this system, the previously reported formation constants are[12] shown in Scheme II. Based upon these constants, the curves shown in Figure 3 were generated, showing the Zn(II) mole fractions of the five pertinent species as the "total added Br^- concentration" is varied. It is seen from these curves that, because of small formation constants of $ZnBr_3^-$ from Zn^{2+}, $ZnBr^+$, or $ZnBr_2$, and because of a relatively large equilibrium constant for the formation of $ZnBr_4^{2-}$ from $ZnBr_3^-$, the concentration of the later species is small over the entire range of the figure. Using the same kind of least-squares treatment employed for the Zn(II)–chloride case, the assumption of eq 5 led to the following results: $\delta_0 = 0$, $\delta_1 = 10$ ppm (for $ZnBr^+$), $\delta_2 = 511$ ppm (for $ZnBr_2$), $\delta_3 = -230$ ppm (for $ZnBr_3^-$), and $\delta_4 = 136$ ppm (for $ZnBr_4^{2-}$). The level of agreement between the experimental chemical shifts and those computed by eq 5 is shown in Figure 4. As the concentration of $ZnBr_3^-$ is so small throughout most of the range of these experiments, the quality of the fit is not sensitive to the value of δ_3. Hence, the value −230 ppm is probably not significant.

The ^{67}Zn chemical shift given in Table I for a 0.25 M solution of $ZnBr_2$ in concentrated HBr (9 M) is 171 ppm,

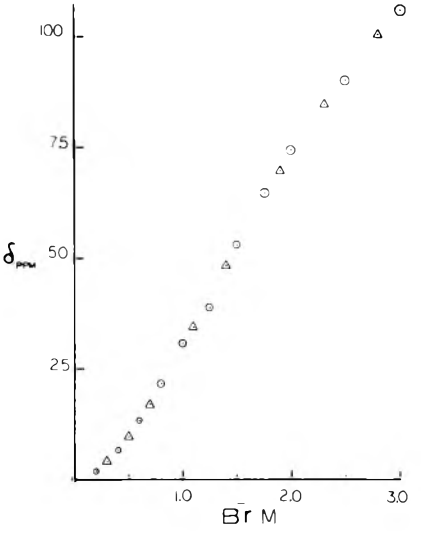

Figure 4. The dependence of the ^{67}Zn chemical shift of a 0.50 M $Zn(ClO_4)_2$ solution on added sodium bromide, with the total Zn(II) concentration maintained at 0.50 M and the ionic strength maintained at 4.5 M. Experimental data are represented by circles, while triangles represents values that were calculated using eq 5 and mole fractions of Zn(II)–bromide species calculated from known equilibrium constants.[12] The solvent is H_2O.

appreciably different from the value derived for $ZnBr_4^{2-}$ from the least-squares analysis based on eq 5. There are at least two reasons that could account for this difference. First, one could question the reliability of utilizing formation constants for the calculation of concentrations in solutions of such high electrolyte concentrations, even though the ionic strength of our solutions was the same as those upon which the experiments for determining the formation constants were based. Second, it is possible that

the time-average structure of Zn(II) in concentrated HBr, presumably a $ZnBr_4^{2-}$ species, is not precisely the same as that of a $ZnBr_4^{2-}$ species in aqueous solution without excess acid. The results described above for the Zn(II)–chloride system, however, provide no direct support for either of these rationalizations. If, for the sake of discussion, one assumes that the 171 ppm value obtained in the concentrated HBr system *should* apply to the data represented in Figure 4, a least-squares analysis based on eq 5 can be carried out with δ_4 *constrained* at the value 171 ppm. In this case, the following results are obtained: $\delta_0 = 0$, $\delta_1 = 0.03$ ppm, $\delta_2 = 585$ ppm, $\delta_3 = -590$ ppm (not meaningful, for the reasons discussed above) and, of course, $\delta_4 = 171$ ppm. Both this set of values and the ones obtained directly from an unconstrained least-squares analysis (neglecting the results for $ZnBr_3^-$) are qualitatively consistent with the shielding order derived for the Zn(II)–chloride system, i.e., $Zn^{2+} > ZnL^{2-n} > ZnL_3^{2-3n} > ZnL_4^{2-4n} > ZnL_2^{2-2n}$. Based upon previous studies of the coordination geometries of Zn(II)–halide species,[13,14] it would appear that this pattern reflects primarily differences in coordination geometry and/or coordination number. Raman studies have been interpreted in terms of an octahedral arrangement of water ligands about Zn^{2+} in aqueous solution, and tetrahedral structures for $ZnCl_4^{2-}$ and $ZnBr_4^{2-}$. It has been suggested, on the basis of analogy to X-ray studies of $[HgCl{\cdot}5H_2O]^+$, that the complexes $ZnCl^+$ and $ZnBr^+$ involve the replacement of one water molecule from octahedrally coordinated $[Zn(H_2O)_6]^{2+}$ by halide ion.[14] The Raman results on $ZnCl_2$ and $ZnBr_2$ have been interpreted in terms of linear Cl–Zn–Cl and Br–Zn–Br arrangements, with four Zn–OH_2 contacts for octahedral coordination.[14] For $ZnCl_3^-$ and $ZnBr_3^-$, based on Raman and solvent extraction data, trigonal bipyramidal structures with two apical water ligands and planar $ZnCl_3$ and $ZnBr_3$ systems have been proposed.[14] If these assessments of structure are correct, then the octahedral Zn(II) systems of this Zn(II)–halide study include both the most shielded, $[Zn{\cdot}6H_2O]^{2+}$, and least shielded, $[ZnCl_2{\cdot}4H_2O]$ and $[ZnBr_2{\cdot}4H_2O]$, cases, with the tetrahedral $ZnCl_4^{2-}$ and $ZnBr_4^{2-}$ species having intermediate shielding values.

The values of the chemical shifts derived for the halide complexes are, of course, only as good as the equilibrium constants from which they are derived by the least-squares fitting scheme described above. It is noteworthy that the agreement cited above for the $ZnCl_4^{2-}$ species is much better than that for the $ZnBr_4^{2-}$ species. This is consistent with the fact that the uncertainties reported for the pertinent K values for the Br^- complexes are generally much larger than those reported for the corresponding chloride complexes. As the equilibrium constant for the formation of $ZnBr_4^{2-}$ from the simple ions has the largest reported uncertainty of any of the eight formation constants,[12] the source of the $ZnBr_4^{2-}$ discrepancy may well be such uncertainties. When the formation constants for $ZnCl^+$, $ZnCl_2$, $ZnCl_3^-$, and $ZnCl_4^{2-}$ were individually increased arbitrarily by 10% (the general magnitude of the reported uncertainties for the chloride complexes[12]), the corresponding δ_1, δ_2, δ_3, and δ_4 values changed appreciably (up to 20% for δ_3), but not enough to alter the order of the shifts given above.

It is interesting to note that the shielding of the $ZnCl^+$ species is found to be lower than that of the $ZnBr^+$ species. This behavior, which can be viewed as manifestations of interactions of [Ar] $3d^{10}$ ions (Zn^{2+}), is opposite to what has been attributed to the effect of ion pairing between Cl^- or Br^- and $^{39}K^+$,[16] an ion with the [Ar] electronic configuration. While the bromide–chloride order is reversed for these two cases, for both Zn^{2+} and K^+ the interaction with Cl^- or Br^- reduces the shielding of the metal nucleus, relative to its value in octahedrally hydrated Zn^{2+}. It is also interesting that, just as the shielding of ^{13}C in CCl_4 is lower than that in CBr_4,[17] the ^{67}Zn shielding of $ZnCl_4^{2-}$ is lower than that of $ZnBr_4^{2-}$. While this correspondence may not be especially significant, it should be noted that all four of the species being compared have tetrahedral geometries.

It was not possible to study the ^{67}Zn shift of $Zn(NO_3)_2$ as a function of added cyanide or ammonia due to the low solubilities of zinc cyanide and zinc hydroxide. Zinc (at 1 M) is soluble in cyanide or ammonia only in large excess of these ligands, in which cases primarily tetracoordinate species are present.[12] At the concentrations employed in the solutions shown in Table I, the Zn(II) exists nearly quantitatively as the tetracoordinate, tetrahedral,[18] cyanide, and ammonia species. Thus, the data given in Table I show that, as was the case with the tetrahedral tetrachloride and tetrabromide complexes, the tetracyano and tetraammine complexes have lower shieldings than the octahedral Zn^{2+} species.

Line widths were also measured for the species on which chemical shift data are given in Table I and Figures 1 and 4. Large experimental uncertainties in much of the data preclude attempting a detailed interpretation. Because the ^{67}Zn line width of an individual Zn(II) species is expected to be dominated by the quadrupolar relaxation mechanism, which in turn depends upon the symmetry of the electric field gradient at the nucleus (as well as the correlation time for reorientation of the species),[19] one expects the narrowest lines to be associated with species that approach cubic symmetry most closely. In the rapid exchange limit, the line width of the single signal observed is a weighted average of the line widths of all the species involved in the exchange. Assuming this limit is valid for the systems for which data are summarized in Figures 1 and 4, one might expect increasing ^{67}Zn line widths as the halide ion concentration is increased, driving the Zn(II) distribution from Zn^{2+}(aq) to include contributions from species of lower symmetry (such as ZnX^+, ZnX_2, and ZnX_3^-). A rough trend of this type was observed (data not shown here) most definitively for the chloride case. The fact that the ^{67}Zn line width of a 2 M $Zn(NO_3)_2$ solution is roughly twice that of a 2 M $Zn(ClO_4)_2$ solution or a 1 M $Zn(NO_3)_2$ solution may indicate interactions, *albeit* transient and weak, between Zn^{2+} and nitrate ion.

Summary and Conclusions

The ^{67}Zn experiments reported here demonstrate the potential utility of ^{67}Zn NMR for studying the nature of Zn(II) species in solution. Both the chemical shift and line width are sensitive to details of the environment of the ^{67}Zn nucleus. Using available equilibrium constants for complexation, and the assumption of a weighted-average shift for a rapidly exchanging system, approximate values of the shifts of individual Zn(II) species have been obtained, reflecting differences in coordination number and geometry. When a large number of studies of this general type on a variety of metal nuclides are described in the literature (hopefully during the next couple of years), it should be possible to develop empirical relationships that will be useful for structural studies of dynamic systems in solution and to develop theoretical guidelines to account for them.

Acknowledgment. The authors are grateful to the National Science Foundation for support of this work

under Grant No. MPS74-23980 and for grants contributing to the purchase of the spectrometer and data system. They also wish to thank Dr. Christie for his assistance with the equilibrium calculations and Dr. V. J. Bartuska for helpful discussions.

References and Notes

(1) P. W. Spence and M. N. McDermott, *Phys. Lett.*, **24A**, 430 (1967).
(2) B. W. Epperlein, H. Kruger, O. Lutz, and A. Schwenk, *Phys. Lett.*, **45A**, 255 (1973).
(3) B. W. Epperlein, H. Kruger, O. Lutz, and A. Schwenk, *Z. Naturforsch., A*, **29**, 660, 1553 (1974).
(4) D. D. Traficante, J. A. Simms, and M. Mulcay, *J. Magn. Reson.*, **15**, 484 (1974).
(5) P. D. Ellis, H. C. Walsh, and C. S. Peters, *J. Magn. Reson.*, **11**, 426 (1973).
(6) H. C. Dorn, L. Simeral, J. J. Natterstad, and G. E. Maciel, *J. Magn. Reson.*, **18**, 1 (1975).
(7) G. E. Maciel and J. J. H. Ackerman, *J. Magn. Reson.*, **23**, 67 (1976).
(8) C. J. Jameson and H. S. Gutowsky, *J. Chem. Phys.*, **40**, 1714 (1964)
(9) J. H. Letcher and J. R. Van Wazer, *J. Chem. Phys.*, **44**, 815 (1966).
(10) A. Allerhand, R. F. Childers, and E. Oldfield, *J. Magn. Reson.*, **11**, 272 (1973).
(11) E. O. Stejskal and J. Schaefer, *J. Magn. Reson.*, **14**, 160 (1974).
(12) (a) L. G. Sillen and A. E. Martell, *Chem. Soc., Spec. Publ.*, **No. 17** (1964); (b) S. A. Shchukarev, L. S. Lilich, and V. A. Latysheve, *J. Inorg. Chem.* (USSR), **1**, 36 (1956).
(13) C. O. Quicksall and T. G. Spiro, *Inorg. Chem.*, **5**, 2233 (1966).
(14) D. F. C. Morris, E. L. Short, and D. N. Waters, *J. Inorg. Nucl. Chem.*, **25**, 975 (1963).
(15) N. Ingri, W. Kakolowicz, L. G. Sillen, and B. Narnqvist, *Talanta*, **14**, 1261 (1967).
(16) (a) C. Deverell and R. E. Richards, *Mol. Phys.*, **10**, 551 (1966); (b) E. G. Bloor and R. G. Kidd, *Can. J. Chem.*, **50**, 3926 (1972).
(17) J. B. Stothers, "Carbon-13 NMR Spectroscopy", Academic Press, New York, N.Y., 1972, Chapter 5.
(18) F. A. Cotton and G. Wilkinson, "Advanced Inorganic Chemistry", 2d ed, Interscience, New York, N.Y., 1966, p 610.
(19) A. Abraham, "The Principles of Nuclear Magnetism", Clarendon Press, Oxford, 1961, Chapter 8.

Phenomenology of Excess Electron Reactions in Liquid Hydrocarbons

Robert Schiller* and Lajos Nyikos

Central Research Institute for Physics, H-1525 Budapest, Hungary *(Received December 18, 1975)*

Publication costs assisted by the Central Research Institute for Physics

The aim of the present calculation is to give a phenomenological description of the reactions between excess electrons and solutes in liquid hydrocarbons. Reaction rates and their temperature dependence are quantitatively described in terms of the Noyes theory of diffusion-controlled reactions by making use of the theory of partial electron localization and by adding a conjecture to the established picture, i.e., that the reactivity of the electrons depends on their states.

Introduction

Excess electrons in liquid hydrocarbons are highly reactive upon a number of solutes. The second-order rate constants were measured as falling between 10^{11} and several times 10^{14} M^{-1} s^{-1}, values which were much higher than those usually observed in liquids and for ionic or atomic reactants. This seems to harmonize well with the fact that electrons in saturated hydrocarbons move much faster than do heavy ions.

A closer investigation, however, reveals that the electrons behave paradoxically. Apparent chemical rate constants, k_a, are usually found to be either independent of reactant mobility, μ, or to change monotonically (most often proportionally) with it. The independence of k_a and μ corresponds to a rate of chemical transformation much slower than that of diffusion, while their proportionality indicates diffusion to be much slower than chemical transformation. This latter is the limiting case of diffusion-controlled chemical reactions. The apparent diffusion-controlled rate constant is given by the general expression of Noyes[1] as

$$k_a = \frac{k}{1 + \frac{ek}{4\pi \mathbf{k} T R \mu}} \qquad (1)$$

Here k is the "genuine" rate constant, i.e., the value one would observe if the reactants moved extremely fast; e the elementary charge; $\mathbf{k}$ the Boltzmann constant, T the temperature, and R the reaction radius. The diffusivity, D, has been replaced by the mobility by virtue of the relationship $D = \mathbf{k}T\mu/e$, μ denoting the sum of the reactant mobilities.

Electron reactions, in spite of their high rate, do not seem to obey eq 1, neither in its general form nor as an approximate proportionality between k_a and μ. In these cases μ is equal, to a fair degree of accuracy, to electron mobility since the heavy electron-acceptor molecules move with a velocity negligible in comparison to that of the electrons. Beck and Thomas[2] and Allen, Gangwer, and Holroyd[3] measured the rates in different hydrocarbons. The rate constant with a given solute was found to vary proportionally to a noninteger power of electron mobility measured in the liquids, e.g., k_a appeared to be proportional to $\mu^{0.8}$ or $\mu^{0.5}$ depending on the solute. In several cases the k_a vs. μ function[2] exhibited a maximum at a certain mobility, μ_m. The activation energy of a given reaction was observed to be positive in solvents of low electron mobility, i.e., where μ was lower than μ_m, and to be negative in the opposite case.

The aim of the present work is to attempt a rationalization of these phenomena unexpected of conventional reactants and reactions. We intend to demonstrate the Noyes expression as holding for the electron reactions if one only considers the electrons to be in different states in different liquids. The real nature of interaction between electron and solute will not be tackled here, the treatment being given in terms of phenomenological reaction kinetics.

Electrons in liquids are now generally acknowledged to be either in the quasi-free or in the localized state. The first of these two is described as a plane-wave scattered by the molecules, hence in this state the electron exhibits high mobility and does not distort the medium. The

formation of a localized state, however, involves the rearrangement of the liquid structure and the localized electron becomes a slow moving entity.

Several explanations of electron reaction kinetics have been based on the assumption that electrons react in the quasi-free state. Baxendale and his co-workers[8] propose the following kinetic scheme:

$$e_L^- \rightleftharpoons e_F^- \tag{2a}$$

$$e_F^- + S \rightarrow S^- \tag{2b}$$

(Here and throughout the text the subscripts L and F refer to the localized and to the quasi-free state, respectively.) According to this the observed rate constant always increases by increasing delocalization (or mobility) and so cannot describe, without further assumptions, the observed behavior of the rate constant in the entire mobility region.

Allen, Gangwer, and Holroyd[3b] assume the reaction to take place when the electron is in the quasi-free state of mobility μ_F. The apparent rate constant is smaller than the true one by a factor of $P(T) = \mu/\mu_F$, which is the fraction of time the electrons spend in the mobile reactive state. In this model μ_F is much smaller (around 10 cm V^{-1} s^{-1}) than was hitherto accepted, and varies from liquid to liquid.

In a recent paper Henglein[9] estimates the distribution functions of occupied and unoccupied electronic levels with regard to the oxidation–reduction system solute/anion and unoccupied trap/trapped electron. On this basis he can account in qualitative terms for all the observed phenomena.

Funabashi and Magee[10] propose an electron capture process completely analogous to the gas phase process—the role of the solvent being simply to shift the energy level of the initial free electron state by V_0, the conduction state or quasi-free state energy. The model holds only for solvents of high electron mobility and scavenging is thought to occur with the electron in the quasi-free state. The expression based on this picture has two adjustable parameters and quantitatively describes the reaction rates in the high mobility region. The temperature dependence of the scavenging rates is qualitatively consistent with the proposed model, too.

Several years ago we proposed[5a] the localized electron to be the reactive form. This was based on an observation made by Rzad and Warman[11] who had found the ions to be more difficult to scavenge in liquids of high free ion yield. Beck and Thomas[2] also regard the localized electron to be reactive. Yakovlev and his co-workers[12] arrive at similar conclusion. Analyzing their experimental data as in ref 3b the obtained μ_F values appeared to them to be too low for quasi-free electrons.

The partial localization theory[5b-d] regards the electrons as changing their states perpetually and uninterruptedly between localization and delocalization. The fraction of localized electrons, P, equals

$$P = \frac{c_{L\infty}}{c_{L\infty} + c_{F\infty}} \tag{3}$$

where $c_{L\infty}$ and $c_{F\infty}$ are the bulk equilibrium concentrations of localized and free electrons, respectively. Statistical mechanical considerations render P to be a function of the quasi-free state (conduction band) energy, V_0, of the localized state energy, E_t, and of a parameter characteristic to energy fluctuations, σ. The expression is of the form

$$P = (2\pi)^{-1/2} \int_{-\infty}^{(V_0 - E_t)/\sigma} \exp(-t^2/2)\, dt \tag{4}$$

Neglecting the contribution of the localized state to electron mobility, μ can be expressed by P as

$$\mu = \mu_F(1 - P) \tag{5}$$

with μ_F denoting the mobility of the quasi-free state. These expressions were successful in describing mobility as a function of V_0 and temperature. Similar considerations[5e] were made for the interrelation of free ion yield with μ and V_0. In the following section the combination of the partial localization model with diffusion-controlled kinetics will be discussed as a possible clue to the problem of electron reactions.

Partial Localization and Apparent Rate Constants

The basic idea of the Noyes theory[1] is that in the case of very fast reactions there exists a concentration gradient of one reactant in the neighborhood of any molecule of the other reactant. The concentration of the first reactant at a distance R measured from the center of a molecule of the other is given by the expression

$$c_R = \frac{c_\infty}{1 + \dfrac{ek}{4\pi \mathbf{k} T R \mu}} \tag{6}$$

where c_R and c_∞ are the concentrations at distances R and infinity, respectively; the other symbols having been explained in connection with eq 1. If R equals the reaction radius, the apparent rate constant k_a and the "genuine" rate constant k are interrelated by the expression

$$k_a c_\infty = k c_R \tag{7}$$

A simple rearrangement of this expression leads to eq 1.

For the case of electron reactions eq 7 must be reconsidered since the partial localization theory regards the electrons to be present both in localized and in quasi-free states. If the rate coefficients for the two states are equal, localized and quasi-free electrons are kinetically indistinguishable and the apparent, diffusion-controlled rate coefficients of the electron reactions are given by eq 1.

If, however, the rate coefficients for the two states are different, an effective rate coefficient must be defined in the form of a weighted sum

$$k = Pk_L + (1 - P)k_F \tag{8}$$

where k_L and k_F are the "genuine" rate constants of localized and free electrons, respectively. Introducing k of eq 8 into eq 6 and 7 and expressing k_a one finds for the apparent rate constant

$$k_a = \frac{Pk_L + (1 - P)k_F}{1 + \dfrac{e[Pk_L + (1 - P)k_F]}{4\pi \mathbf{k} T R \mu}} \tag{9}$$

The diffusion of the scavenger molecule has been ignored, since it is several orders of magnitude slower than that of the electron. The diffusive motion of the electron can be characterized by the resultant experimental mobility, instead of using μ_L in the first and μ_F in the second term, since the relaxation of the electron between its two states occurs with a frequency of about 10^{13} s^{-1} whereas the reaction half-lives are of the order of 10^{-9} to 10^{-6} s. (For a more rigorous demonstration see Appendix I.)

The combination of the Noyes theory with the model of partial electron localization is expressed by eq 9. Since P, V_0, and μ are interrelated by eq 4 and 5 in agreement with the observations, one can consider k_a as a single-varied function of either V_0 or μ. The $k_a(\mu)$ function takes different shapes according to eq 9 when making different assumptions regarding the reactivity of e_L^- and e_F^-. If $k_L = k_F$ and $R_L = R_F$ eq 9 reduces to eq 1 as it has already

been indicated, resulting in a monotonous $k_a(\mu)$ curve. With $k_L \neq k_F$, however, the $k_a(\mu)$ or $k_a(V_0)$ function might exhibit a maximum as is found experimentally for a number of cases. Investigating two limiting cases the inequality $k_L \gg k_F$ brings about a maximum in the $k_a(\mu)$ curve whereas the opposite of this, $k_L \ll k_F$, renders a monotonous function.

A search for a numerical agreement between eq 9 and experiment would be of somewhat dubious value in view of three unknown parameters in this expression, viz. k_L, k_F, and R.

Some previous knowledge is needed about their magnitude. There are experimental indications, mentioned in the Introduction, that localized electrons are in the more reactive state toward several solutes. This, however, does not seem to be a general rule.

We propose to make simple energetic considerations in order to predict the reactivity of different electron states toward different solutes.

The energy of the localized state, E_t, is the sum of the electronic energy, E_e, and the medium reorganization energy, E_M, they being of opposite sign. E_e is always positive and of the order of several tenths of electron volts. The energy of the quasi-free state, V_0, is lower than E_e for all the hydrocarbons in question; the difference being of the order of but usually greater than E_e. Since the electron transfer is most probably fast it must be regarded as a vertical transition which renders E_M to be inaccessible. Hence localized electrons have an initial energy E_e for chemical reactions to be brought about in constrast to the quasi-free ones which start their reaction from the V_0 level. Thus for all the reactions which require some threshold energy the localized electrons are in a much more favorable energy state. This makes the conjecture $k_L \gg k_F$ reasonable for such reactions. Solutes reacting without any threshold energy do not prefer higher energy states hence for them the approximate equality $k_L \approx k_F$ will hold. Assuming $k_L \gg k_F$ eq 9 takes the simpler form

$$k_a = \frac{Pk_L}{1 + \dfrac{ePk_L}{4\pi \mathbf{k}TR\mu}} \tag{10}$$

The present form of eq 10 has been suggested by Allen with him pointing out some inconsistencies in the first version of the paper.

This final expression is amenable to an experimental check. Again k_a is a function of V_0 or μ. These two quantities vary from hydrocarbon to hydrocarbon in strong parallelism and while characteristic to the solvent they are independent of the nature of the solute. This latter determines only k_L and R though these do not depend on the nature of the solvent. Hence if the electron rate contants with one and the same scavenger have been measured in different solvents, one can check the validity of the model. Having adjusted the values of k_L and R, the observed $k_a(V_0)$ or $k_a(\mu)$ functions must obey eq 10. Different solutes require, of course, different k_L and R values, though the same pair of parameters must be used for a given solute in each of the solvents.

The temperature coefficient can be computed by virtue of the definition $E_A = \mathbf{k}T^2\ \mathrm{d}\ \ln k_a/\mathrm{d}T$. Applying this expression to eq 10 one obtains for the apparent activation energy of electron reactions with $k_L \gg k_F$

$$E_{AL} = \frac{ek_a}{4\pi \mathbf{k}R\mu T}\left(E_\mu \frac{\mu_F}{\mu_F - \mu} + \mathbf{k}T\right) - E_\mu \frac{\mu}{\mu_F - \mu} \tag{11}$$

where E_μ is the activation energy of mobility. The eventual

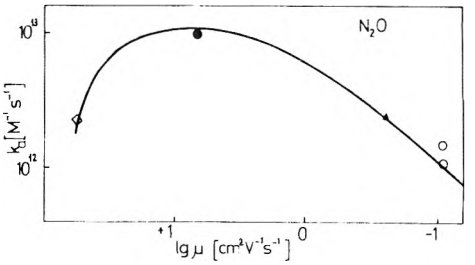

Figure 1. Electron rate constants at room temperature as a function of μ for reaction with N_2O (positive onset energy, eq 10). Data taken from ref 3b and 8c. Parameters used were $k_L = 1.38 \times 10^{13}\ M^{-1}\ s^{-1}$ and $R = 7.3$ Å: (◑) methylcyclohexane, (○) *n*-hexane, (♦) *n*-pentane, (△) cyclohexane, (▲) cyclopentane, (●) isooctane, (◇) neopentane.

TABLE I: Activation Energies for Electron Reactions[h]

	Solvent			
	n-Hexane[f]		Isooctane[f]	
Reactant	Measd	Calcd	Measd	Calcd
N_2O	5.3[a]	4.5[d]	0.05[a]	0.19[a]
Biphenyl	4.4[c]	4.6[d]	0.51[b]	0.24[d]
	6.4[b]	4.6[e]		0.27[e]
C_2HCl_3[g]	5.3[a]	5.0[d]	1.4[a]	1.2[d]
		4.7[e]		0.33[e]
SF_6	4.6[a]	4.6[e]	1.3[a]	1.3[e]

[a] Reference 3. [b] Reference 12. [c] Reference 2. [d] Equation 11. [e] Equation 12. [f] E_μ taken from ref 12b and 12c. [g] Applying eq 11: $k_L = 3.01 \times 10^{14}\ M^{-1}\ s^{-1}$ and $R = 8.8$ Å, applying eq 12: $k = 5.18 \times 10^{13}\ M^{-1}\ s^{-1}$ and $R = 15.3$ Å. [h] All data in units of kcal mol^{-1}.

temperature dependence of k_L and R has been ignored. (The temperature dependence of R can be approximated in terms of the ideas put forward in Appendix II.)

For the case $k_L \approx k_F$ the apparent activation energy can be evaluated from eq 1 as

$$E_A = \frac{ek_a}{4\pi \mathbf{k}R\mu T}(E_\mu + \mathbf{k}T) \tag{12}$$

E_{AL} can be seen to change sign in the vicinity of the mobility μ_m where the reaction rate is maximum; E_{AL} is positive in liquids where $\mu < \mu_m$ (V_0 is high) and negative where $\mu > \mu_m$ (V_0 is low). Both the existence of a maximum in k_a and the change of the sign of E_{AL} around this maximum are in complete agreement with the experimental findings of Allen, Gangwer, and Holroyd.[3]

Detailed calculations were made for a number of solutes and solvents in order to check eq 10.

The solutes had to be investigated individually if their electron attachment required some threshold energy. To this end recourse was taken to electron attachment kinetics in the gas phase. The experimentally determined attachment is negligible. Among the scavengers already investigated in hydrocarbons there were three substances which fell into this class they being N_2O, ethyl bromide,[13a] and most probably pyrene.[13c] Electron reactions with these solutes were expected to obey eq 10. The parameters k_L and R were found by curve fitting. The computation of E_{AL} did not involve any further free parameters. Figures 1–3 and Table I summarize our results. The calculated curves in Figures 1–3 seem to coincide reasonably with the experiments.

Two further solutes, SF_6 and CCl_4, do not exhibit any measurable onset energy in the gas phase. Thus the higher potential energy of e_L^- does not render a rate coefficient higher than that of e_F^- toward these two solutes. Hence the approximate equality of k_L and k_F and the prevalence of eq 1 is to be expected. The curves in Figures 4 and 5

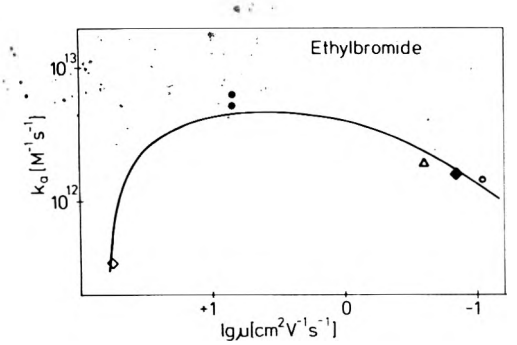

Figure 2. Electron rate constants for reaction with ethyl bromide (positive onset energy, eq 10). Data taken from ref 3. Parameters used were $k_L = 5.12 \times 10^{12}$ M^{-1} s^{-1} and $R = 10.2$ Å. Symbols as in Figure 1.

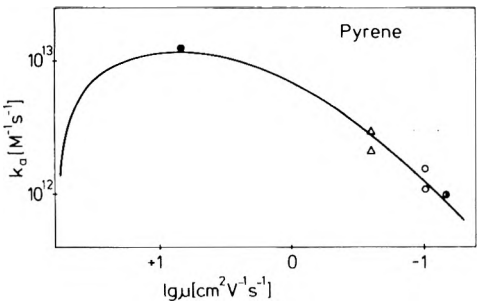

Figure 3. Electron rate constants for reaction with pyrene (positive onset energy, eq 10). Data taken from ref 8a, 8b, and 12. Parameters used were $k_L = 1.47 \times 10^{13}$ M^{-1} s^{-1} and $R = 7.4$ Å. Symbols as in Figure 1.

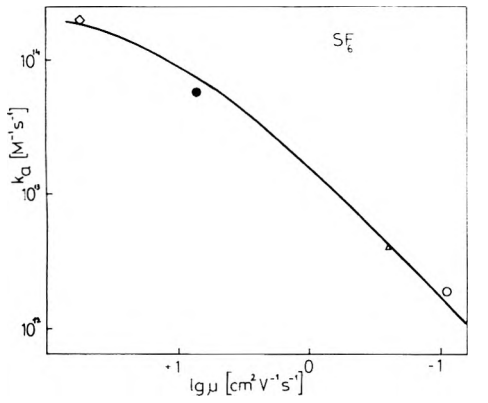

Figure 4. Electron rate constants for reaction with SF_6 (no onset energy, eq 1). Data taken from ref 3b. Parameters used were $k_L = k_F = 2.10 \times 10^{15}$ M^{-1} s^{-1} and $R = 8.9$ Å. Symbols as in Figure 1.

fitted to the experimental points apparently obey this expression with reasonable parameter values. The inequality $k_L \ll k_F$ would yield monotonous curves similar to those in Figures 4 and 5. However, apart from the difficulty to understand such an assumption, unrealistic parameter values would be found by curve fitting, viz. $R \approx 10^3$–10^4 Å would appear.

No information regarding the gas-phase onset energy of biphenyl was found, hence the relative magnitude of k_L and k_F was impossible to predict. So we fitted both eq 1 and eq 10 to the experimental points (Figure 6) finding both curves to coincide reasonably with the experiment. Only kinetic measurements performed in high-mobility liquids such as neopentane could tell which curve is the true one. Activation energy values are summarized in Table I. The activation energy of N_2O was calculated via eq 11, that of SF_6 via eq 12.

Both expressions, eq 11 and 12, were used for the biphenyl and C_2HCl_3 case with eq 11 yielding a better value for the latter compound. This may indicate that for

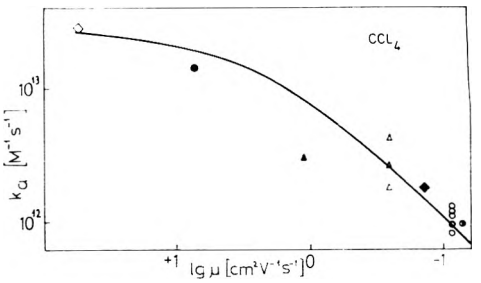

Figure 5. Electron rate constants for reaction with CCl_4 (no onset energy, eq 1). Data taken from ref 2a, 3, and 8. Parameters used were $k = 1.26 \times 10^{14}$ M^{-1} s^{-1} and $R = 4.5$ Å.

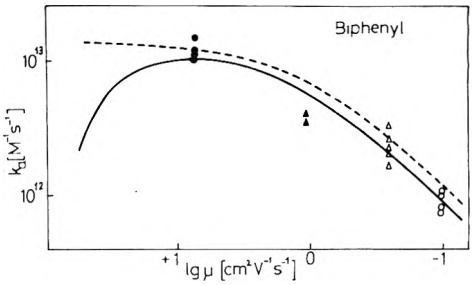

Figure 6. Electron rate constants for reaction with biphenyl (onset energy unknown, eq 1 and 10). Data taken from ref 2, 8a, 8d, 12a, 12c, 21, and 22. Parameters used were (continuous line) $k_L \gg k_F$, $k_L = 1.35 \times 10^{13}$ M^{-1} s^{-1} and $R = 5.7$ Å; (dotted line) $k_L = k_F = 1.38 \times 10^{13}$ M^{-1} s^{-1} and $R = 6.4$ Å. Symbols as in Figure 1.

C_2HCl_3 the inequality $k_L \gg k_F$ holds. The overall agreement of calculated and measured activation energies seems to be reasonable particularly if one considers that here no further adjustable parameter was used.

Discussion

The partial localization theory originally developed for the understanding of the interrelation of μ and V_0, and developed further for the description of the free ion yields, has now been extended to rationalize the kinetics of electron reactions. Although the functional forms and the numerical values of the results are mostly in accordance with the observations the approximations involved certainly need some consideration.

While experiment has shown V_0 to change from liquid to liquid, E_t and μ_F were regarded, both in previous calculations[5] and in the present one, to be constant. Although this is certainly an oversimplification which has duly been criticized by Allen[14] it should be stressed that it has nothing to do with the essence of the model being only a practical implement used for computational purposes. A knowledge of the parameters for different liquids would remove this assumption at once. We are convinced, nevertheless, that the main difference between liquids lies with V_0. The relative constancy of E_t is indicated by positronium annihilation, that of μ_F by the calculation of Davis, Schmidt, and Minday[15] and Fueki, Feng, and Kevan[16] although the latter results have been challenged by Funabashi's computations.[17] The measurement of the Hall coefficient might settle this issue.[18] It is certainly rewarding that the same parameter value, $\mu_F = 65$ cm^2 V^{-1} s^{-1}, can be used throughout our calculations.

Recent measurements lend some support to our assumption regarding the qualitative interrelation between rate constants and gas-phase onset energies. Very high rate constants were measured for the $SF_6 + e^-$ reaction (no onset energy) in liquid Ar or Xe[19] where the electron is in the quasi-free state. In contrast to this Bakale[20] observed a very low rate constant for the $N_2O + e^-$ process (positive onset energy) in liquid Xe.

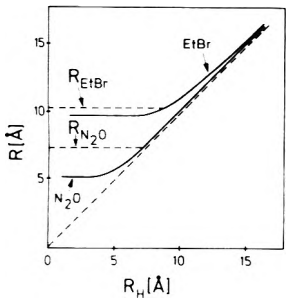

Figure 7. Effective and "hard-core" reaction radii for electron-scavenger reactions. (See Appendix II.)

The neglect of k_F makes our curves "break down" at $\mu = \mu_F$. This reflects on the one hand the obvious fact that k_F is not equal to zero even if it is much lower than k_L and on the other hand the strict constancy of μ_F to be arguable as has already been indicated.

The neglect of k_F in comparison to k_L does not necessarily mean k_F to be low also in absolute terms. The fitted k_L values are on the order of magnitude of 10^{12}–10^{13} M^{-1} s^{-1} which can make k_F negligible even if it is not lower than 10^{10}. This is, however, around the diffusion-controlled rate constants in water, a value which was always regarded to be very high. This, together with our ignorance of the onset energy of the contaminants, explains the experimental difficulties one has to face when one tries to purify liquid Ar in order to produce quasi-free electrons in it.

Tetramethylsilane has been excluded from our present considerations as in the case of the mobility and free-ion yield calculations since this substance apparently cannot be described with parameter values appropriate for the hydrocarbons.

Nothing has been said about the reaction radius R and rate constant k_L, these having been used only as adjustable parameters. (For the long-range interaction correction of R see Appendix II.) The parameters could be predicted only from a theory similar to those developed by Henglein[9] or Funabashi and Magee,[10] which describes the dynamic details of the electron–solute interaction. This is, however, much beyond the scope of our present treatment.

Conclusions

The combination of the Noyes theory of diffusion-controlled reactions with the model of partial electron localization offers a possibility for the adequate description of electron–solute reactions in saturated hydrocarbons. It needs only be assumed that a difference might exist between the reactivities of the localized and the quasi-free electrons, k_L and k_F, respectively.

Apparent rate constants and temperature coefficients can easily be evaluated if the inequality $k_L \gg k_F$ or the equality $k_L \approx k_F$ hold. Both energetic considerations and the results of curve fitting show the inequality to be true in cases where the electron attachment in the gas phase requires a positive onset energy, whereas the equality is found to be valid by similar reasoning if no onset energy can be observed.

The interdependence of conductivity band energy, mobility, free ion yield, and electron reactivity can be understood in terms of the model of partial electron localization.

Acknowledgment. The authors are indebted to Professor A. Henglein for stimulating criticism, to Dr. G. Bakale for measuring the $N_2O + e^-$ reaction in liquid xenon, and to Professor L. G. Christophorou for making available ref 13b to us. The helpful comments of Dr. A. O. Allen and of an unknown referee upon the first version of the manuscript are gratefully acknowledged.

Appendix I. Time Scale of Electron Diffusion

The aim of the following calculation is to estimate the average period of time that it takes for an electron to reach the reaction radius of the solute. The problem is treated in terms of the Noyes[1] theory.

The velocity, v, of a particle performing diffusive motion in a field of inhomogeneous concentration, $c(r)$, is given as

$$v = \frac{\mathbf{k}T\mu}{e} \text{ grad ln } c \tag{A1}$$

The time of motion from r_α to R if the concentration distribution is in a steady state can be computed by the integral

$$t = -\int_{r_\infty}^{R} \frac{dr}{v} \tag{A2}$$

According to Noyes grad $c = ek_a c_\infty / 4\pi \mathbf{k}T\mu r^2$ and $c = c_\infty - ek_a c_\infty / 4\pi \mathbf{k}T\mu r$. Introducing these expressions into eq A1 and then carrying out integral A2 one finds

$$t = \frac{4\pi}{3k_a}(r_\infty^3 - R^3) - \frac{e}{2\mathbf{k}T\mu}(r_\infty^2 - R^2) \approx \frac{4\pi r_\infty^3}{3k_a} \tag{A3}$$

In the actual case r_∞ is the average distance between the center of a solute molecule and the site of the birth of an electron. This depends on the solute concentration being approximately equal to $c_S^{-1/3}$ with c_S expressed as number density. The concentrations characteristic to the measurements in question are in the order of 10^{-5} M resulting in $r_\infty^3 \approx 2 \times 10^{-16}$ cm^3. Inserting this value into eq A3 together with $k_a \approx 10^{13}$ M^{-1} s^{-1} one obtains $t \approx 40$ ns.

The time of diffusive motion exceeds the period of electron localization–delocalization by several orders of magnitude the latter being in the 0.1–1-ps range. Thus so far the solution is not much more concentrated than 10^{-5} M the use of the average electron mobility seems to be justified.

Appendix II. Coulomb Interaction between Electron and Solute

The electron "current" flowing toward the acceptor molecules was seen to be the consequence of a steady-state concentration gradient. This picture can be somewhat modified taking into consideration the long-range electron–molecule interactions. These long-range forces are supposed to have no effect on the rate constant of the "genuine" chemical transformation k_L or k_F. What they might change is the reactions radius, formally the distance at which the reaction occurs. According to Noyes[1] the reaction radius as corrected for long-range interactions is given as

$$R^{-1} = \int_{R_H}^{\infty} r^{-2} \exp[U(r)/\mathbf{k}T]\, dr \tag{A4}$$

$U(r)$ denoting the interaction energy between the two reactants and R_H the sum of their hard-core radii.

Supposing electron-induced dipole and electron-permanent dipole interactions (the latter being thermally averaged) the interaction energy is given as

$$U(r) = \frac{\left(\bar{\alpha} + \frac{\mu^2}{3\mathbf{k}T}\right)e^2}{2\epsilon \mathbf{k}T r^4} \tag{A5}$$

where $\bar{\alpha}$ is the average polarizability, μ the dipole moment of the solute, and ϵ the dielectric constant of the solvent.

The computed effective R values are plotted in Figure 7 as a function of R_H for the solutes N_2O and ethyl bromide. The effective reaction radius always exceeds the hard-core one since the interaction is attractive. R tends to R_H if $U(r)$ tends to zero. At low R_H values R becomes independent of R_H indicating that the attraction gives a lower limit to reaction radius. The parameter values rendered by curve fitting in the previous sections are above these limits (cf. Figure 7). Furthermore it can be seen that, for reaction radii as high as the fitted values, the effective and "hard-core" reaction radii practically coincide. Hence one can conclude that the long-range forces which act between electrons and *solute molecules* play no important role in the reactions investigated.

References and Notes

(1) R. M. Noyes, "Progress in Reaction Kinetics", G. Porter, Ed., Pergamon Press, London, 1961.
(2) (a) G. Beck and J. K. Thomas, *J. Chem. Phys.*, **57**, 3649 (1972); (b) *ibid.*, **60**, 1705 (1974).
(3) (a) A. O. Allen and R. A. Holroyd, *J. Phys. Chem.*, **78**, 796 (1974); (b) A. O. Allen, T. E. Gangwer, and R. A. Holroyd, *J. Phys. Chem.*, **79**, 25 (1975).
(4) Allen, Gangwer, and Holroyd plotted their rate constant data as a function of V_0, the conduction state energy. As there is a close relationship between V_0 and μ (cf. ref 5–7) our presentation is equivalent to theirs.
(5) (a) R. Schiller in "Progress and Problems in Contemporary Radiation Chemistry", Academia, Prague, 1971, p 221; (b) *J. Chem. Phys.*, **57**, 2222 (1972); (c) R. Schiller, Sz. Vass, and J. Mandics, *Int. J. Radiat. Phys. Chem.*, **5**, 491 (1973); (d) L. Nyikos and R. Schiller, *Chem. Phys. Lett.*, **34**, 128 (1975); (e) R. Schiller and Sz. Vass, *Int. J. Radiat. Phys. Chem.*, **7**, 193 (1975).
(6) N. R. Kestner and J. Jortner, *J. Chem. Phys.*, **59**, 26 (1973).
(7) (a) R. A. Holroyd and M. Allen, *J. Chem. Phys.*, **54**, 5014 (1971); (b) R. A. Holroyd and W. Tauchert, *J. Chem. Phys.*, **60**, 3715 (1974).
(8) (a) J. H. Baxendale, C. Bell, and P. Wardman, *Chem. Phys. Lett.*, **12**, 347 (1971); (b) *J. Chem. Soc., Faraday Trans. 1*, **69**, 776 (1973); (c) J. H. Baxendale and E. J. Rasburn, *ibid.*, **70**, 705 (1973); (d) J. H. Baxendale, J. P. Keene, and E. J. Rasburn, *ibid.*, **70**, 718 (1973).
(9) A. Henglein, *Ber. Bunsenges. Phys. Chem.*, **79**, 129 (1975).
(10) K. Funabashi and J. L. Magee, *J. Chem. Phys.*, **62**, 4428 (1975).
(11) (a) S. J. Rzad and J. M. Warman, *J. Chem. Phys.*, **49**, 2861 (1968); (b) J. M. Warman and S. J. Rzad, *ibid.*, **52**, 485 (1970).
(12) (a) B. S. Yakovlev, Y. A. Boriev, L. T. Novikova, and E. L. Frankievich, *Int. J. Radiat. Phys. Chem.*, **4**, 395 (1972); (b) B. S. Yakovlev, Y. A. Boriev, and A. A. Balakin, *ibid.*, **6**, 23 (1974); (c) Y. A. Boriev and B. S. Yakovlev, *ibid.*, **7**, 15 (1975).
(13) (a) L. G. Christophorou, "Atomic and Molecular Radiation Physics", Wiley-Interscience, New York, N.Y., 1971; (b) *Chem. Rev.*, **76**, 409 (1976); (c) H. Venghaus and H-J. Hinz, *J. Chem. Phys.*, **64**, 30 (1976).
(14) A. O. Allen, personal communication, 5th International Congress on Radiation Research, Seattle, Wash., 1974.
(15) H. T. Davis, L. D. Schmidt, and R. M. Minday, *Chem. Phys. Lett.*, **13**, 413 (1972).
(16) K. Fueki, D.-F. Feng, and L. Kevan, *Chem. Phys. Lett.*, **13**, 616 (1972).
(17) K. Funabashi and I. Cheng, *Int. J. Radiat. Phys. Chem.*, **6**, 497 (1972).
(18) L. Kevan, *J. Phys. Chem.*, **76**, 3830 (1972).
(19) U. Sowada, G. Bakale, K. Yoshino, and W. F. Schmidt, *Chem. Phys. Lett.*, **34**, 466 (1975).
(20) G. Bakale, private communication.
(21) G. Bakale, E. C. Gregg, and R. D. McCreary, *J. Chem. Phys.*, **72**, 4246 (1972).
(22) J. M. Warman, M. P. Deltaas, and A. Hummel, *Chem. Phys. Lett.*, **22**, 480 (1973).

The Raman Spectra of Carbon Dioxide in Liquid H_2O and D_2O

George R. Anderson*

Department of Chemistry, University of Minnesota, Minneapolis, Minnesota 55455 and Department of Chemistry, Bowdoin College, Brunswick, Maine 04011 *(Received September 28, 1976)*

Publication costs assisted by The Pillsbury Company

The Raman spectra of dissolved carbon dioxide at ca. 10 °C and 45 atm pressure are reported for the two solvents H_2O and D_2O. Comparisons are made with spectra of the gas and liquid phases of CO_2. Results indicate that only one species, $CO_2(aq)$, is detected in solution by the experimental technique employed, and that H_2CO_3 and other carbonates have insufficient concentrations in pure water for us to observe them directly. Attention is given to the significant spectral changes in $CO_2(aq)$ upon change in solvents, H_2O to D_2O.

Introduction

The vibrational spectra of gaseous carbon dioxide have been studied in great detail. Owing to the high symmetry of the molecule ($D_{\infty h}$), the infrared and Raman spectra are mutually exclusive and involve separate transitions between vibrational states, ν_1 (Σ_g^+), $\nu_2(\pi_u)$, and ν_3 (Σ_u^+), and their overtones.[1] One of the overtones, $2\nu_2$, is of particular importance to the Raman spectrum of CO_2[2] as it is well known that a component of this state, $2\nu_2(\Sigma_g^+)$, is in resonance with the $\nu_1(\Sigma_g^+)$ fundamental giving rise to a pair of bands of nearly equal intensity. Known as Fermi resonance, these two vibrational states are neither pure CO stretch (ν_1) nor pure OCO bend ($2\nu_2$). They are mixtures, often referred to ambiguously as the $\nu_1 + 2\nu_2$ diad. The Raman spectra of the Fermi diad thus is the experimental probe used in this study by which we can observe structural and vibrational changes in the CO_2 molecule in response to the aqueous environment.

Although the Raman spectrum of $CO_2(aq)$ has not been reported to our knowledge, spectra have been reported going back over 4 decades for the gas,[3] liquid, and solid[4] phases (by Langseth and Nielson[3] and by McLennan and Smith[4]) as well as recent gas phase results at high resolution by Stoicheff.[2] These and other results have led to a general anharmonic force constant calculation for CO_2 by Suzuki[5] along with further considerations on the relation of force constants by Machida and Overend.[6] Amat and Pimbert[7] have proposed a method to obtain a set of more consistent force constants for CO_2. However, this is achieved at the expense of reversing the traditional assignment of the $\nu_1 + 2\nu_2$ diad given by Herzberg[1] and Stoicheff.[2] We have followed in this paper the traditional nomenclature of the later calling ν_1 and $2\nu_2$ the higher and lower energy states, respectively.

A phase diagram for the two-component system CO_2–H_2O is reported by Larson.[8] Above 10 °C and 45 atm pressure and below the critical point of CO_2 (T_c = 31.0 °C, P_c = 72.8 atm), he finds that two and only two liquid phases are maintained in equilibrium. Very little water is dissolved in the less dense CO_2(liq) phase while the (bottom) aqueous phase contains appreciable amounts of CO_2. From solubility tables at 10 °C, $[CO_2(\text{total})] \simeq 1$ M in H_2O at 45 atm, the pressure at which these phases (gas and two liquid) are in equilibrium.

The aqueous phase contains carbon dioxide in an equilibrium mixture of several components, the largest being the two species

$$CO_2(aq) \overset{H_2O}{\rightleftharpoons} H_2CO_3(aq) \quad (1)$$

It has been shown and discussed by numerous authors, recently reviewed by Kern[9] and Edsall,[10] that aqueous carbon dioxide and carbonic acid are chemically distinct. The equilibrium is slow in pure water ($k \sim 1$ min^{-1}), and estimates of the equilibrium constant[1] are clearly quite small at 25 °C.

$$K = [H_2CO_3(aq)]/[CO_2(aq)] = 0.0026 \quad (2)$$

The related thermodynamic state functions governing eq 1 are $\Delta H° = 1.13$ kcal mol^{-1}, $\Delta S° = -8$ cal mol^{-1} deg^{-1}, and $\Delta G° = 3.53$ kcal mol^{-1}. Thus it can be seen that the Raman spectrum of dissolved CO_2 will be largely that of the spectrum of $CO_2(aq)$. In fact, we have yet to detect the presence of $H_2CO_3(aq)$ using the Raman technique.

Experimental Section

The spectroscopic measurements were carried out on a JEOL laser Raman spectrometer JRS-S1 with an argon ion laser source (Model 52 coherent Radiation Laboratories) operating at approximately 300-mW power in the 4880-Å wavelength mode. Using the double grating monochrometer (0.5 M focal length, $f/6.7$) and a cooled ITT photomultiplier photon counting system, the spectral slit width was set at a rated value of 3.6 cm^{-1}. This resulted in an observed half-width of the laser exciting lines of $\Delta\nu_{1/2}$ = 2.2 cm^{-1}.

Samples were prepared and sealed off in long pyrex heavy-wall tubing (8 mm o.d. and approximately 25 cm in length). The procedure found to be most satisfactory produced sample tubes usually containing three visible phases (at room temperature): the aqueous phase, the liquid CO_2 phase, and on top the vapor phase (largely CO_2(g)). The sample tubes were produced without much difficulty. (1) An end seal was blown on a 30–35 cm length of 8 mm tubing. (2) After careful cleaning, a small sample (~0.5 ml) of water was added to the tube. (3) The water was next frozen by inserting the tube in crushed dry ice. (4) A quantity of crushed dry ice was next added to the tube making a column of loosely packed solid CO_2 of approximately 5–6 cm. An amount of CO_2 sublimation took place during this operation flushing the tube with gaseous CO_2. (5) Finally after the tube was submerged in sufficient dry ice to cover the bottom half of the tube (bringing the solid H_2O and CO_2 into thermal equilibrium), the top portion of the tube was heated, sealed off, and annealed. When allowed to warm up (slowly inside a steel safety tube), we had no difficulty with breakage or explosions from the pressures generated by the CO_2 (~60 atm).

* Present address: The Pillsbury Company, 311 Second St. S.E., Minneapolis, Minn. 55414.

TABLE I: The $\nu_1 + 2\nu_2$ Fermi Diad of CO_2 Observed under Various Equilibrium Conditions[e]

Phase	T, °C	ν_1	$\Delta\nu_{1/2}$	ρ	$2\nu_2$	$\Delta\nu_{1/2}$	ρ	$I_{2\nu_2}/I_{\nu_1}$
Gas[a]	20	1388.15		0.14[b]	1285.51		0.18[b]	0.67[c]
Gas[d]	10	1388	2.2	0.01	1285	2.2	0.01	0.53 ± 0.06
Liquid[c]	−56	1387.5			1285.5			0.33[c]
Liquid[d]	10	1386	2.5	0.01	1282	2.5	0.01	0.47 ± 0.07
D_2O	10	1384	3.5	0.02	1280	9	0.06	0.33 ± 0.03
HDO	10	1384	7.5		1277	14		0.31 ± 0.03
H_2O	10	1383	10	0.03	1274	18	0.07	0.29 ± 0.30

[a] Reference 2. [b] Reference 3. [c] Reference 4. [d] This work. Uncertainties in ρ values are large because the intensities of the CO_2(aq) depolarized bands are broad and weak and of the same magnitude as the background radiation scattered from the solvent. The numbers listed as the depolarization ratio are the approximate lower limits to ρ since attempts were made to draw a suitable baseline and substract off the weak solvent continuum in each case. [e] Ca. 10 °C, 45 atm pressure. Frequencies in cm^{-1}, depolarization ratio range $0 < \rho < 3/4$.

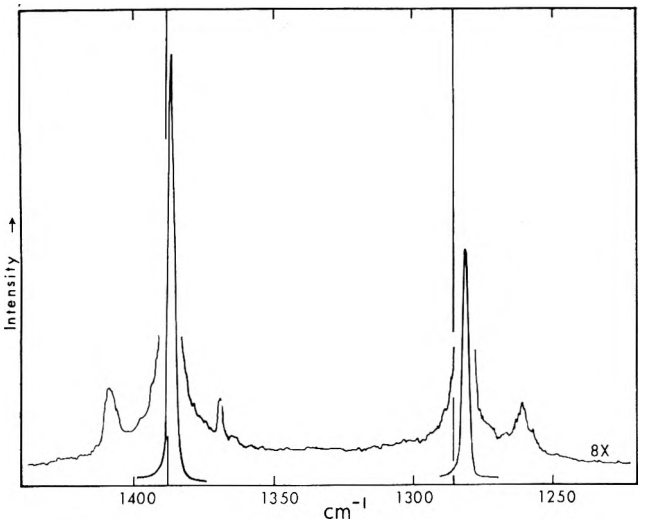

Figure 1. Liquid carbon dioxide Raman spectrum at ca. 10 °C, 45 atm pressure. Displayed at two different signal gain settings (8× factor apart), the two main bands in Fermi resonance (ν_1, $2\nu_2$) are observed as sharp peaks slightly displaced from the gas phase band centers shown as separate vertical lines; the three observed weaker bands are discussed in the text.

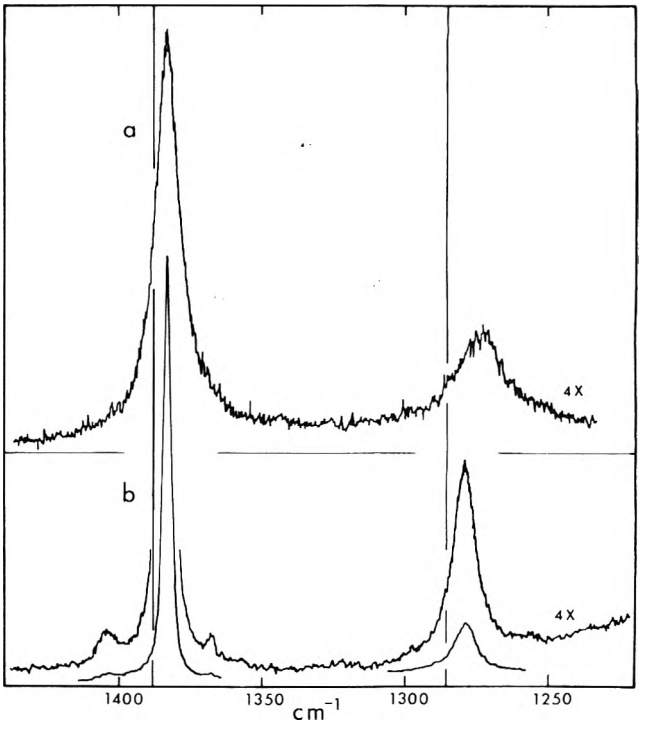

Figure 2. Dissolved carbon dioxide Raman spectra in solvents (a) H_2O and (b) D_2O. At equilibium with CO_2(liq) ⇌ CO_2(g) at ca. 10 °C and 45 atm pressure, the concentration of CO_2(aq) is calculated to be ~1 M. Again as in Figure 1, the separate vertical lines indicate the band centers of the CO_2 spectrum in the gas phase. Two different gain settings are indicated as before.

The sample compartment in the JEOL spectrometer was altered in order to accommodate the sample tubes and to maintain temperature control. Using the standard 90° scattering configuration and the 40-mm $f/1.0$ objective lens provided with the instrument, the sample positioner was replaced with a water jacked 8.1 mm i.d. copper tube mounted vertically on a heavy-duty three-way micrometer positioner. In the middle of the copper tube were three holes (7 mm diameter), two at 180° for the laser beam, and one at 90° for observing Raman scattering. In addition, there was a small hole on the back side of the copper tube into which a thermistor was inserted. Thus when the circulating water was maintained at a temperature of 6 °C, the thermistor temperature corresponded to a temperature of 10 °C. Observing no noticeable effects of temperature on Raman band positions, we made no further efforts to establish the precise temperature inside the sample tube.

Results and Discussion

Raman spectra were taken of all three phases (gas, CO_2(liq), aqueous) of several high pressure sample tubes (prepared as described) using three different water mixtures, pure H_2O, pure D_2O, and HDO, a 50–50 mixture of each. Several of these spectra are shown in Figures 1 and 2. Over a temperature range 3–30 °C, we found experimental difficulties with the aqueous phase below 10 °C and with the CO_2(liq) phase above 20 °C. (The H_2O–CO_2 system is reported[8] to form a solid (clathrate) phase below 9.5 °C; the CO_2(liq) phase becomes unstable in the intense laser beam above 20 °C causing profuse bubbling action and complete scattering of the Raman excitation light.) Aside from concentration effects on the Raman spectra, we saw no significant changes with temperature on band positions or band shapes. We would have been able to see a 2–3-cm^{-1} spectral shift with a signal/noise ratio ~50 taking (as it did) approximately 4 h to run a 250-cm^{-1} spectrum.

Figure 1 presents the $\nu_1 + 2\nu_2$ spectrum of liquid carbon dioxide at two different gain settings. The two vertical lines represent the position of the ν_1 and $2\nu_2$ bands of the gas phase CO_2(g) for comparison, the frequencies given in Table I. Under our experimental conditions, we observe a 2- and 3-cm^{-1} red shift, respectively, in going from gas to liquid. These changes were not reported in earlier work.[4] The remainder of the 100–4000-cm^{-1} spectral region showed no additional Raman lines, confirming the earlier findings[4] on the CO_2(liq) spectrum and confirming Larson's conclusions[4] that H_2O is very insoluble in CO_2(liq).

The spectral details of Figure 1 are also worth noting. At 1261 and 1408 cm^{-1} in CO_2(liq), two weaker bands directly correspond to the gas phase "hot" bands at 1265.17 and 1409.44 cm^{-1} reported by Stoicheff.[2] Figure 3 presents a vibrational energy level diagram of the CO_2 molecule, and

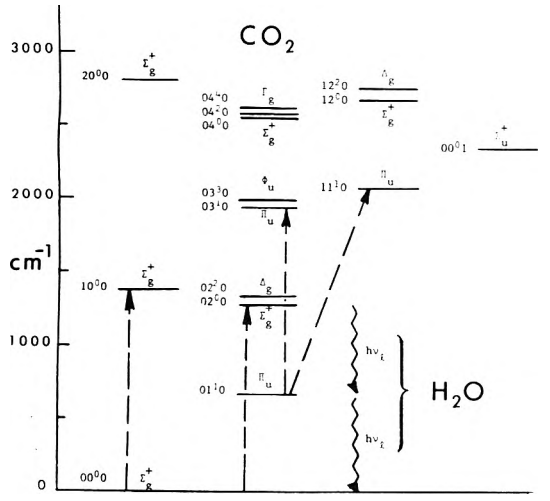

Figure 3. A vibrational energy level diagram of the CO_2 molecule. The horizontal lines are at energies observed for the gaseous molecule[1,2,5] and the vertical (broken-line) arrows represent Raman transitions observed in this study. The zig-zag arrows labeled with $h\nu_l$'s represent possible vibrational relaxation modes of CO_2 in the 02^00 and 01^10 states when solvated in the aqueous phase and coupled to the intermolecular libration mode, ν_l, of liquid water.

on it the Raman transitions are shown by the dashed line arrows. The "hot" bands originate from the 667-cm^{-1} ν_2 state of CO_2, (01^10), being thermally populated at 283 K by a Boltzmann factor of $e^{-3.4} = 0.033$. The isotopic molecule $^{13}CO_2$ (~1% abundance) gives rise to two Raman lines displaced to lower frequencies. One stands by itself at 1369 cm^{-1}, and the other apparently is not resolved from the (03^10) ← (01^10) "hot" band. In the gas phase, they are reported[2] at 1369.90 and 1266.03 cm^{-1}.

Aqueous Carbon Dioxide

Figure 2 gives the $\nu_1 + 2\nu_2$ spectra of CO_2 in (a) H_2O and (b) D_2O at ca. 10 °C and 45 atm pressure. No other carbon dioxide or carbonic acid bands could be observed over the background. This puts our limit of detectability (based on the CO_2 Raman scattering crosssection) at ~0.005 M. For instance, the ^{13}C isotope peak (at 1% abundance) for CO_2 in D_2O (Figure 2b) at 1367 cm^{-1} corresponds to a concentration of ~0.01 M. Depending upon bandwidth, a Raman line of half the intensity shown may be about the lower limit we could identify with reasonable confidence.

Comparing Figures 1 and 2, the vibrational "fingerprint" of CO_2 does not seem to change from one phase to another, i.e., gas → liquid → aqueous solutions. In addition we can conclude from this fact that the average structure of the molecule does not change from linear and symmetric either. The question of how the CO_2 molecule is bound to the solvent (or into the solvent cage) remains an open question. In a way, it is dependent upon the model by which we attempt to describe the solvent. Since the H_2O and D_2O solvents produce noticeably different spectra, the CO_2 molecule may be useful as a probe to help understand the important differences of these two solvent systems. Several details of these spectra thus need mentioning.

The band positions of ν_1 and $2\nu_2$, given in Table I, shift in a progression, CO_2(liq) to $CO_2(D_2O)$ to $CO_2(HDO)$ to $CO_2(H_2O)$. Other spectral parameters listed, the band half-widths, the depolarization ratio (perhaps), and the integrated intensity ratio of $2\nu_2/\nu_1$, all seem to follow the same trend. The origin of these effects is not clear.

The band shapes and the resulting band half-widths, $\Delta\nu_{1/2}$, have great potential importance in providing clues to the kinds of interactions taking place in the CO_2–water mixture. Taking note of the very fine work currently being done on line shape analysis[11] and vibrational energy transfer,[12] one hesitates in proceeding any further without more detailed analysis. However, this would exceed the scope of our current investigation so that we will close with some preliminary speculative remarks regarding observed half-widths.

The source of line broadening for ν_1 and $2\nu_2$ are not identical since the latter bands (given in Table I) are 2–3 times as broad as the former. Remembering that ν_1 and $2\nu_2$ are a resonant mixture of two vibrational base states, ν_1^0 and $2\nu_2^0$, we may be seeing an effect of selective line broadening on one of the two base states (say $2\nu_2^0$) which gives rise to the more complex resonance effects.

There are in fact numerous mechanisms that one could invoke for vibrational line broadening: structural inhomogeneity of the solvent, fast chemical equilibrium, collisional broadening (V → T energy transfer), hindered rotation (V → R energy transfer), and vibration exchange (V → V energy transfer) among others. The latter three mechanisms imply the uncertainty relationship between the lifetime of the excited vibrational state (τ) and line width (ΔE) vis-a-vis $\tau\,\Delta E \simeq \hbar$.

Of these mechanisms, one looks particularly interesting to consider. Liquid water has an intermolecular vibration (libration) at 685 cm^{-1} for H_2O and 505 cm^{-1} for D_2O.[13] It is observed as a strong broad band in the infrared spectrum of water; its Boltzmann factor is (again) about $e^{-3.4} \approx 0.03$ for H_2O at room temperature. It is possible that this mode can couple strongly with CO_2 (particularly for H_2O) and act as a reservoir for vibrational energy from the excited CO_2 molecule. A strong coupling mechanism implies a short lifetime (τ) of the vibrational excited state and a large line width (ΔE).

The coupling mechanism between the CO_2 molecule and the water surrounding it cannot be directly identified from what we have measured and reported. However, energy transfer of the dipole–dipole (or Förster) type has been well known for many years in (electronic) fluorescence spectroscopy.[14] The CO_2 molecule in the $2\nu_2^0(\Sigma_g^+)$ state is coupled to $\nu_2(\pi_u)$ state by the dipole operator (er) and could swiftly relax down the vibrational "ladder" to the ground state (Σ_g^+) provided liquid water was close by to absorb the energy. The coincidences in vibrational energy states in CO_2 ($2\nu_2^0 \rightarrow \nu_2 = 673$ cm^{-1}, $\nu_2 \rightarrow$ ground state = 667 cm^{-1})[5] and H_2O ($\nu_l \approx 685$ cm^{-1}) are good. But for D_2O, $\nu_l \approx 505$ cm^{-1}, the overlap of vibrational energy levels is down significantly (factor of ca. 1/3), and thus the dipole–dipole coupling mechanism is less efficient.

Finally, we may notice that the spectra of CO_2 in H_2O and D_2O (Figure 2a and b) have different integrated intensities of the $\nu_1 + 2\nu_2$ diad. Although differing in band shapes, we have compared enough spectra obtained under identical conditions to be confident that the *total* intensity of the diad in D_2O is 35(±5)% greater than it is in H_2O. This difference we feel is largely due to a difference in solubility of CO_2 in ordinary and heavy water. Ben-Naim[15] has reported a ~10% enhanced solubility of argon gas in D_2O relative to H_2O. Although one may attribute this difference to the "higher degree of crystallinity" of the D_2O solvent,[15] the origin of solubility effect is not clearly understood.

Experimental tests to better understand the vibrational relaxational mechanism(s) are being considered.

Acknowledgment. The author wishes to acknowledge helpful discussions with several individuals without whom this study would have been seriously prolonged. They are Professors Crawford, Fenton, Hexter, Kreevoy, and Overend. The generous use of the spectroscopic facilities at

the University of Minnesota are greatly appreciated.

References and Notes

(1) G. Herzberg, "Infrared and Raman Spectra", Van Nostrand-Reinhold, New York, N.Y., 1945, p 272 *ff.*
(2) B. P. Stoicheff, *Can. J. Phys.*, **36**, 218 (1958).
(3) A. Langseth and J. R. Nielson, *Phys. Rev.*, **46**, 1057 (1934).
(4) J. C. McLennan and H. D. Smith, *Can. J. Res.*, **7**, 551 (1932).
(5) I. Suzuki, *J. Mol. Spectrosc.*, **25**, 479 (1968).
(6) K. Machida and J. Overend, *J. Chem. Phys.*, **50**, 4429 (1969).
(7) G. Amat and M. Pimbert, *J. Mol. Spectrosc.*, **16**, 278 (1965).
(8) S. D. Larson, Ph.D. Thesis, 1955, University of Illinois.
(9) D. M. Kern, *J. Chem. Educ.*, **37**, 14 (1960).
(10) J. T. Edsall, *NASA Spec. Publ.*, NASA SP-188, 15 (1969).
(11) R. G. Gordon, *J. Chem. Phys.*, **43**, 1307 (1965); G. E. Ewing, *Acc. Chem. Res.*, **2**, 168 (1969).
(12) A. Laubereau, D. Von der Linde, and W. Kaiser, *Phys. Rev. Lett.*, **28**, 1162 (1972).
(13) D. Eisenberg and W. Kauzmann, "The Structure and Properties of Water", Oxford University Press, London, 1969.
(14) A. J. Pesce, C. G. Rosen, and T. L. Pasby, "Fluorescence Spectroscopy", Marcel Dekker, New York, N.Y., 1971.
(15) A. Ben-Naim, *J. Chem. Phys.*, **42**, 1512 (1965).

COMMUNICATIONS TO THE EDITOR

Transient Intermolecular Spin Coupling of $CHCl_3$ with Di-*tert*-butyl Nitroxide Free Radical

Publication costs assisted by the U.S. Army Research Office

Sir: Recent studies of the interaction of nitroxide free radicals with protons on solvent molecules have demonstrated (1) a shift of the proton NMR line induced by the paramagnetic species,[1-9] and (2) a broadening of the solvent proton NMR line.[2,4,5] Alternatively, the ESR line of the radical may be examined to determine the role that such intermolecular associations may play in solvent–solute interaction.[2,10-13] Yet, in examining either the ESR signal or the NMR signal, when the duration of the interaction is very short, the primary manifestation of the effect of the interaction is a small shift in the basic property or an averaged value with the basic property. These techniques respond to the contributions of both the interacting species and the noninteracting species.

The association of the proton-containing solvent with the paramagnetic molecule can be examined directly by observing the intermolecular coupling of the two spins. Dynamic nuclear polarization (DNP) is a double resonance technique that probes the intermolecular interaction of two such molecules in a liquid by monitoring the NMR signal amplitude while the ESR line is saturated by applying radiofrequency power of the correct frequency to the system. The interaction to which DNP is sensitive may occur in the 10^{-8} to 10^{-11} s range. However, the effect of the interaction on the nuclear spin state populations persists in solution on the time scale of the nuclear relaxation time, which is on the order of 10^{-2} to 10 s in such systems. Thus the signals can be examined by conventional signal processing techniques.

Recent work has clearly demonstrated the value of simultaneous examination of the dynamic polarization in conjunction with the paramagnetic species-induced nuclear relaxation time.[14,15] These measurements provide far greater information than a single measurement and can give a much clearer picture of the nature, strength, and duration of the interaction.

Until recently, DNP of solvent protons has been regarded to be of limited interest.[16] The dynamic polarization of protons on common organic solvent molecules by free radical electrons had generally given enhancements at low magnetic field strengths that extrapolate to the dipolar limit of −329. From a chemical viewpoint, dipolar coupling, which corresponds to the direct through-space coupling of the nuclear spin with the unpaired electron spin as modulated by the relative diffusional motion of these spins, is much less interesting than the scalar coupling of these spins, though it has proved to be useful in biochemical studies using spin labels. This scalar or contact coupling indicates the generation of unpaired electron spin density at the nucleus, and thus reflects orbital disposition, bonding tendency, and related chemical features.

TABLE I: Observed Enhancements at 20- and 40-W Applied Radio-Frequency Power for $CHCl_3$:C_6D_6 and $CDCl_3$:C_6H_6 Solutions with DTBN Free Radical

Radical concn	0.038 M	0.019 M	0.0076 M
G_H (20 W) for C_6H_6	−42.3	−47.0	−40.7
G_H (20 W) for $CHCl_3$	−35.1	−38.0	−32.4
G_H (40 W) for C_6H_6	−77.5	−84.9	−70.8
G_H (40 W) for $CHCl_3$	−62.6	−69.9	−56.4
G_D (20 W) for C_6D_6	−32.7	−22.4	−8.2
G_D (20 W) for $CDCl_3$	−139.4	−99.0	−23.7
G_D (40 W) for C_6D_6	−62.7	−43.7	−14.7
G_D (40 W) for $CDCl_3$	−258.7	−178.6	−46.6

The unfilled orbitals associated with protons are generally of such high energy that scalar-transmitted polarization is very weak and, except for a limited number of special cases, enhancements other than those determined solely by dipolar coupling are rarely observed.[17-23] Previous work on transient complexation of solvent molecules with nitroxide radicals encourages the continued search for direct observation of this chemically important scalar coupling of the solvent protons with the unpaired electron spin.[1,9,20,21,24] The $CHCl_3$–di-*tert*-butyl nitroxide radical (DTBN) system is especially favored for such a study as the propensity for hydrogen bond formation by $CHCl_3$ is well documented,[25] and the apparent high polarizability of the chlorine electron could suggest the possible enhanced scalar coupling for adjacent protons.[22,23,26] This paper reports the study, using DNP and solvent relaxation times, of the intermolecular coupling of DTBN with

solvent molecules in solutions of this radical in benzene and chloroform and their deuterated analogues.

Theory. The enhancement ($G^N(P)$) of the observed NMR signal is related (1) to the observed signal amplitude at applied power P [$A(P)$], and (2) to the NMR signal amplitude for the same sample and under the same conditions but with no power applied [$A(0)$] by:[14-16]

$$G^N(P) = \{A(P) - A(0)\}/\{A(0)\} = U_\infty^N f^N S_e(P) \quad (1)$$

$$U_\infty^N = \frac{\gamma_e}{\gamma_N} \frac{\bar{r} - \bar{s} + \bar{c}}{2\bar{q} + \bar{r} + \bar{s} + \bar{c}} \quad (2)$$

$$f^N = (2\bar{q} + \bar{r} + \bar{s} + \bar{c})/(2\bar{q} + \bar{r} + \bar{s} + \bar{c} + 2\bar{q}_B) \quad (3)$$

$$S_e(P) = 1/\{1 + \bar{p}_B/F(P)\} \quad (4)$$

$$\bar{q} = \frac{\pi \gamma_N^2 \gamma_e^2 \hbar^2 \tau_d N_e}{5d^3} J(\omega_I) \quad (5)$$

$$J(\omega_I) = \frac{1}{(1 + \tau_d^2 \omega_I^2)} \quad (6)$$

The term $S_e(P)$ is a measure of the effectiveness of the saturation of the ESR line. The inverse of the function $S_e(P)$ goes linearly to one as $1/P$ goes to zero. The term f^N is a measure of the degree to which the coupled relaxation transitions dominate the observed relaxation of the nuclear spin, and is called the leakage factor. The term f^N goes to one linearly as $1/N_e$, the inverse of the radical concentration, goes to zero. $J(\omega)$ is the spectral density function, and the form shown in eq 6 is that for a rotational diffusion or sticking model. The dipolar coupling terms, $\bar{q}$, $\bar{r}$, and $\bar{s}$, and the scalar coupling term, $\bar{c}$, have been discussed in detail previously.[14] The term U_∞^N is that which is most revealing about the system. It determines the relative amounts of dipolar vs. scalar coupling of the two spins, and thus serves to categorize the mechanism and nature of the transient interactions.

A widely applied data-collection technique has relied on the observation that the proton enhancements, except for one or two well-documented exceptions,[17-19] give values of U_∞^H of −329, the dipolar limit. This is the result of the scalar term being zero in comparison with the dipolar. Thus previous samples have commonly been prepared with two nuclei that can be studied, one on which information is to be obtained, the other ^1H for reference. In that case, the ratio of the enhancements for the two nuclei is

$$\frac{G_N(P)}{G_H(P)} = \frac{U_\infty^N f^N}{U_\infty^H f^H} \quad (7)$$

The term $S_e(P)$ is identical in the numerator and denominator, and any peculiarities in the way the radical saturates are removed. For concentrated solutions where both f^N and f^H go to one, eq 7 gives values for U_∞^N very simply, and the results can be averaged for several applied powers. Alternatively some systems can be studied by extrapolating to obtain U_∞^N.

$$U_\infty^N = \lim_{N_e \to \infty} \lim_{P \to \infty} G(P) \quad (8)$$

This method is much more difficult to employ when the radical ESR spectrum consists of more than one line.[20-21,27,28]

The other important piece of information to be obtained is the nuclear relaxation rate $1/T_1^N$.

$$1/T_1^N = 2\bar{q} + \bar{r} + \bar{s} + \bar{c} + 2\bar{q}_B = \Gamma_e N_e + (1/T_1)_B \quad (9)$$

This term is the sum of the radical-induced terms and the bulk relaxation of the nucleus, $2\bar{q}_B$. Γ_e is thus a measure of the total strength of the coupling, while U_∞^N gives the relative contribution of the scalar and dipolar mechanisms.

Experimental Section. A difficulty arises in planning the preparation of samples for this work due to the expected subtlety of the scalar coupling to be detected. A suitable scheme for meaningful comparison of small variations in signal enhancement is required. The use of the ratio method (eq 7) requires the simultaneous presence of the nucleus to be studied ($CHCl_3$ proton) and the reference nucleus (C_6H_6 proton). However, the chemical shifts at 75 G are too small to resolve the signals from the two chemically different nuclei if they are in the same sample vial. In order to investigate unambiguously the subtle effect on the ^1H of interest and maintain the chemical character of the radical interaction with both ^1H on C_6H_6 and ^1H on $CHCl_3$ such that $S_e(P)$ (eq 4) is consistent, a special technique of sample preparation must be used.

Samples were prepared by successive dilution of a known volume of the liquid free radical with the selected solvent mixture. Complementary samples were prepared by using two solvent mixtures, the first containing one part by volume benzene to five parts deuteriochloroform, the second one part perdeuteriobenzene to five parts chloroform. Pairs of samples were prepared, each pair consisting of the same radical concentration first in solvent mixture one, second in solvent mixture two. This pairwise preparation of samples ensures that both the C_6H_6 protons and the $CHCl_3$ protons see the same free-radical environment, giving rise to the same saturation of the ESR line and the same solvation processes.

Samples were deoxygenated by several freeze–pump–thaw cycles, then sealed. The apparatus for examining low-field DNP signals has been described previously.[16] Experiments were performed at a magnetic field strength of 75 G, for which proton and deuteron magnetic resonance frequencies are 319.7 and 49.1 kHz, respectively. Details of the technique for obtaining usable deuterium signals have been presented.[14] Nuclear relaxation rates were determined by observing the rate of recovery of the nuclear magnetism following inversion by rapid passage techniques.

Results. Observed polarizations at two different applied powers are shown in Table I for chloroform and benzene and the deuterated analogues. Table II gives results for the ratio method comparison of selected pairs of observed polarizations for three different DTBN concentrations. The row labeled $G_{CHCl_3}/G_{C_6H_6}$ shows the ratio of the observed proton enhancements for these species averaged over all rf powers used. The other columns are shown for comparison and to establish trends in the data for the deuterium nuclei.

Table III shows the relaxation rates for the protons in the two complementary sets of samples: $CHCl_3$ proton relaxation rates in 5:1 $CHCl_3$:C_6D_6 mixtures with DTBN, and C_6H_6 proton relaxation rates in 5:1 $CDCl_3$:C_6H_6 mixtures with DTBN. Also given for comparison is the relaxation rate for benzene protons with DTBN in the absence of either of the chloroform species.

Discussion. The DNP results show a small scalar component contribution to the coupling between $CHCl_3$ protons and the unpaired electron spin of the nitroxide radical. The results of the ratio method in Table II give a value of 0.81 ± 0.07 for $G_{CHCl_3}/G_{C_6H_6}$ when averaged over all samples and applied powers. This corresponds to 8% scalar coupling, or a scalar component of 1.7 ($\bar{q}:\bar{r}:\bar{s}$ = 3:12:2

TABLE II: Ratios of Polarizations for the Same Radical Concentration Averaged over All Powers Applied to Saturate ESR Line

Radical concn	0.038 M	0.019 M	0.0076 M
G_H for $CHCl_3/G_H$ for C_6H_6[b]	0.83 ± 0.04[a]	0.79 ± 0.08	0.81 ± 0.02
G_D for C_6D_6/G_H for C_6H_6[c]	0.78 ± 0.04	0.49 ± 0.05	0.20 ± 0.03
G_D for $CDCl_3/G_H$ for C_6H_6[d]	3.39 ± 0.22	2.10 ± 0.09	0.61 ± 0.08

[a] ± values are 2σ values. [b] This value for each radical concentration is calculated by averaging the ratio of observed enhancements at several applied powers for $CHCl_3$ protons in the $CHCl_3$:C_6D_6 sample to those for C_6H_6 protons in the $CDCl_3$:C_6H_6 sample. [c] This value for each radical concentration is calculated by averaging the ratio of observed enhancements at several applied powers for C_6D_6 deuterons in the $CHCl_3$:C_6D_6 sample to those for C_6H_6 protons in the $CDCl_3$:C_6H_6 sample. [d] This value for each radical concentration is calculated by averaging the ratio of observed enhancements at several applied powers for $CDCl_3$ deuterons and C_6H_6 protons in the same samples.

TABLE III: Proton Relaxation Rates as a Function of DTBN Free Radical Concentrations for Chloroform: Benzene Solvent Systems

Solvent system[a]	DTBN concn, M	^1H relaxation rate, s^{-1}
$CHCl_3$:C_6D_6	0.0019	2.2
$CHCl_3$:C_6D_6	0.0038	3.8
$CHCl_3$:C_6D_6	0.0076	8.1
$CHCl_3$:C_6D_6	0.019	14.2
$CDCl_3$:C_6H_6	0.0019	0.13
$CDCl_3$:C_6H_6	0.0038	0.56
$CDCl_3$:C_6H_6	0.0076	0.61
$CDCl_3$:C_6H_6	0.019	2.7
C_6H_6:C_6D_6	0.019	4.5

[a] All mixed solvent systems were 5 parts chloroform to 1 part benzene. The accuracy of measured relaxation rates is no better than 20%.

on this scale) if C_6H_6 is assumed to have $\bar{c} = 0$. Based on this result, one would expect that $CHCl_3$ protons would give a value of U_m^H of −279 ± 24. For comparison, the extrapolation method using eq 8 gives directly a value of U_r^H of −259 for $CHCl_3$, though this technique is less reliable for multiline radicals. This decrease in the value of U_m^H from the dipolar limit could possibly be the result of a long correlation time causing a decrease in the value of $J(\omega)$ shown in eq 6 for the terms $\bar{r}$ and $\bar{s}$. A simple calculation based on a rotational diffusion model reveals that the dipolar correlation time, τ_d, would then have to be between 10^{-8} and 10^{-9} s, far longer than experience indicates is feasible for the dipolar component of such interactions in nonionic liquids. In addition, the observation of normal behavior for C_6H_6 protons in the complementary samples serves to preclude the effect of the viscosity of the medium in increasing the dipolar correlation time. The observation of a small scalar component is consistent with the high-field measurements of Morishima and co-workers and of Buchachenko and co-workers who have observed concentration-dependent contact shifts for several nitroxide radicals with selected solvents.[1-9]

The observation of a scalar component for protons is unusual in itself as the ^1H have generally given ultimate enhancements at the dipolar limit.[16] The presence of the scalar component indicates the direct interaction of the unpaired electron on the radical with the nucleus, either through exchange polarization or direct delocalization of the unpaired electron. The latter method is favored by the recent evidence of electron delocalization from the free radical when hydrogen-bonded complexes with solvent molecules are formed.[1-9] Earlier studies using DNP have shown evidence for a weak scalar component in the interaction of acetic acid with nitroxide radicals when the possible formation of hydrogen bonds exists.[21] A more recent report indicates the possibility of a scalar component in the interaction of three nitroxide radicals with H_2O as solvent.[29]

Perhaps of greater interest than a very small scalar component is the overall enhanced interaction with the radical of $CHCl_3$ when compared with C_6H_6. The relaxation data provided in Table III show very clearly that the protons on $CHCl_3$ relax much more quickly than do those on C_6H_6 for the same DTBN concentration. The relaxation term Γ_e corresponding to the coupling of the proton and free radical spins is greater in the $CHCl_3$ case, being 1030 ± 340 for $CHCl_3$ but only 95 ± 90 for C_6H_6. A contribution of only 8% to this relaxation can be attributed to the scalar coupling component present with $CHCl_3$ but not with C_6H_6. Thus, in addition to the presence of a small scalar component, the $CHCl_3$–DTBN interaction is characterized by an enhanced dipolar coupling strength. Examination of the expression for the dipolar coupling strength indicates that this increased dipolar component could arise in any of three places. The term d can be smaller, indicating a real or apparent closer interaction of the proton and unpaired electron spins. The effective number of free radical molecules per cm^3 available for polarization, N_e, may change due to clustering and occlusion. Finally, τ_d could be larger, indicating that the correlation of the two interacting spins may occur over a longer time, perhaps due to the slower tumbling of the coupled species. The dipolar coupling with the $CHCl_3$ most likely includes both a translationally modulated and a rotationally modulated dipolar contribution because of weak complexation, though for the benzene, the rotational term is probably absent. If the dipolar correlation times get too long, the contribution of the coupling to the relaxation rate will decrease because $J(\omega)$ becomes less than one due to the τ_d^2 term in the denominator. In all likelihood, all three of these do contribute to the overall behavior, but clear differentiation among these causes requires very accurate measurement of the relaxation rates as a function of magnetic field strength, a capability not presently available.

The possible enhanced dipolar coupling strength that accompanies the increased scalar coupling in the $CHCl_3$–DTBN system agrees with previous observations of polarization of fluorine nuclei, which typically show substantial scalar components, and with later observations for lithium nuclei.[30,31] The augmented magnitudes of both components may arise from an indirect coupling via polarized chlorine orbitals, a route that has appeared to be effective in several previous studies.[26,32,33] The role of chlorine atoms in enhancing similar intermolecular interactions has been considered by more classical techniques, but the conclusions are still uncertain. Moreover, the observed decrease in the benzene ^1H relaxation rate when $CDCl_3$ is present vs. that for C_6D_6:C_6H_6 solutions alone indicates that the enhanced $CHCl_3$ interaction is at the expense of the benzene in the same solution, presumably because the benzene is denied access to the polarizing site by transient complexation between $CHCl_3$ and radical.

Our results can be compared with those obtained by other methods for solvent–solute dynamics using nitroxide radicals. Morishima and co-workers have examined in detail ^1H and ^{13}C contact shifts of solvent molecules, and

have correlated this experimental work with theoretical calculations on the same systems.[6,7] They estimate the dipolar correlation time to be approximately 10^{-10} s, and the lifetime of the hydrogen-bonded $CHCl_3$–DTBN complex to be 3.6×10^{-8} s.[9] Buchachenko and co-workers have also investigated the paramagnetic shifts and the broadening of ^1H and ^{13}C lines induced by free radicals,[1-3] and find complex lifetimes on the order of 3 to 8×10^{-11} s.[5] If 3.6×10^{-8} s is in fact the scalar correlation time, the 8% scalar component for the total coupling observed in this study at 75 G would decrease by over 3 orders of magnitude in going to 3000 G due to the transition-frequency dependence in the spectral density of the type given in eq 6, but the dipolar component would change imperceptibly. A complex lifetime on the order of 10^{-10} s would be more consistent with these results, but actual determination of the dipolar and scalar correlation times can best be obtained from the frequency dependence of the dipolar and scalar coupling components. However, this capability is not widely available.

The results in the present study with deuterated analogues of the two molecules also prove to be very revealing. For protons, even with the fairly dilute solutions of DTBN used, the coupling with the free radicals is very strong. Thus the leakage factor f, which indicates the degree to which the radical dominates the relaxation of the nucleus, is nearly one. Even in the most dilute solutions, the value of f is 0.9 or greater for benzene, and even closer to one for $CHCl_3$. With the deuterium, a much different situation is encountered. A previous study has demonstrated the much weaker coupling of the free radical electron to ^2H than to ^1H by a factor of 42, because of the smaller γ_N^2 as shown in eq 5.[14] Thus the radical is far less efficient in dominating the coupling. As a result the coupling is much diminished, and observed enhancements are far below the dipolar limit of −2145, as indicated in Table I. However as the radical concentration increases, the observed enhancements increase sharply, indicating the radical is becoming more efficient in polarizing the ^2H nuclei. However, the $CDCl_3$ results show far greater observed enhancements than do the C_6D_6. This is due to the stronger coupling. In this case the weaker coupling to ^2H than to ^1H precludes employing ^2H relaxation measurements as a probe of the coupling, as these rates are much the same as the relaxation rate in the absence of the radical, within experimental error.

Conclusions. (1) The presence of a contact component in the intermolecular coupling of $CHCl_3$ with DTBN has been demonstrated by DNP. This scalar component arises from the coupling of the $CHCl_3$ proton with the radical's unpaired electron either by partial delocalization of the electron during transient complex formation, or by exchange polarization involving electron clouds near the proton.

(2) The scalar component in this system is overwhelmed by an enhanced dipolar coupling, indicating an effectively increased intimacy of the $CHCl_3$–DTBN interaction that accompanies the scalar coupling.

(3) The increased $CHCl_3$–DTBN interaction is accompanied by a decrease in the coupling of the cosolvent benzene with the DTBN, implying that access of C_6H_6 to the radical electron is inhibited by the transient complex formed between $CHCl_3$ and DTBN.

Acknowledgments. The authors gratefully acknowledge useful discussions with John Helbert and Philip Caplan, and thank Anthony Montedoro for help in sample preparation and data collection and Ruthann Bates for critically reading the manuscript. One author (Richard D. Bates, Jr.) gratefully acknowledges partial support of this work by the Donors of the Petroleum Research Fund, administered by the American Chemical Society; U.S. Army Research Office, under Grants DAHC04-75-G-0042 and DAAG29-76-G-0132; and a Summer Research Grant from Georgetown University.

References and Notes

(1) N. A. Sysoeva and A. L. Buchachenko, *Zh. Strukt. Khim.*, **13**, 42 (1972).
(2) N. S. Sysoeva and A. L. Buchachenko, *Zh. Strukt. Khim.*, **13**, 221 (1972).
(3) A. S. Kabankin, G. M. Zhidomirov, and A. L. Buchachenko, *Zh. Struckt. Khim.*, **13**, 423 (1972).
(4) A. S. Kabankin, G. M. Zhidomirov, and A. L. Buchachenko, *J. Magn. Reson.*, **9**, 199 (1973).
(5) N. A. Sysoeva, A. Y. Karmilov, and A. L. Buchachenko, *Chem. Phys.*, **7**, 123 (1975).
(6) I. Morishima, K. Endo, and T. Yonezawa, *Chem. Phys. Lett.*, **9**, 203 (1971).
(7) I. Morishima, K. Endo, and T. Yonezawa, *J. Am. Chem. Soc.*, **93**, 2048 (1971).
(8) I. Morishima, K. Endo, and T. Yonezawa, *J. Chem. Phys.*, **58**, 3146 (1973).
(9) K. Endo, B. Knuettel, I. Morishima, T. Inubushi, and T. Yonezawa, *Chem. Phys. Lett.*, **31**, 387 (1975).
(10) B. E. Wagner, J. N. Helbert, R. D. Bates, Jr., and E. H. Poindexter, *J. Chem. Soc., Chem. Commun.*, 748 (1973).
(11) A. H. Cohen and B. M. Hoffman, *Inorg. Chem.*, **13**, 1484 (1974).
(12) C. Mailer and B. M. Hoffman, *J. Phys. Chem.*, **80**, 842 (1976).
(13) Y. Murata and N. Mataga, *Bull. Chem. Soc. Jpn.*, **44**, 354 (1971).
(14) R. D. Bates, Jr., E. H. Poindexter, and B. E. Wagner, *J. Chem. Phys.*, **59**, 3031 (1973).
(15) J. A. Potenza, J. W. Linowski, E. H. Poindexter, B. E. Wagner, and R. D. Bates, Jr., *Mol. Phys.*, **29**, 1597 (1975).
(16) J. Potenza *Adv. Mol. Relaxation Processes*, **4**, 229 (1972).
(17) R. S. Codrington and N. Bloembergen, *J. Chem. Phys.*, **29**, 600 (1958).
(18) R. A. Dwek, J. G. Kenworthy, and R. E. Richards, *Mol. Phys.*, **10**, 529 (1966).
(19) J. C. Collingwood and J. W. White, *Mol. Phys.*, **25**, 1241 (1973).
(20) W. Muller-Warmuth and E. Oztekin, *Mol. Phys.*, **17**, 105 (1969).
(21) W. Muller-Warmuth, E. Oztekin, R. Vilhjalmsson, and A. Yalciner, *Z. Naturforsch. A*, **25**, 1696 (1970).
(22) R. A. Dwek, H. D. W. Hill, J. G. Kenworthy, D. F. S. Natusch, and R. E. Richards, *Mol. Phys.*, **13**, 27 (1967).
(23) R. A. Dwek, O. W. Howarth, D. F. S. Natusch, and R. E. Richards, *Mol. Phys.*, **13**, 457 (1967).
(24) M. S. Davis, C. Mao, and R. W. Kreilick, *Mol. Phys.*, **29**, 665 (1975), and earlier papers.
(25) R. D. Green, "Hydrogen Bonding by C–H Groups", Wiley, New York, N.Y., 1974.
(26) R. D. Bates, Jr., B. E. Wagner, and E. H. Poindexter, *Chem. Phys. Lett.*, **17**, 328 (1972).
(27) A. Landesman, *J. Phys. Radium*, **20**, 937 (1957).
(28) A. Abragam, "The Principles of Nuclear Magnetism", Clarendon Press, Oxford, 1961.
(29) K. Meise, W. Muller-Warmuth, and H. W. Nientiedt, *Z. Naturforsch.*, in press.
(30) E. H. Poindexter, P. J. Caplan, B. E. Wagner, and R. D. Bates, Jr., *J. Chem. Phys.*, **61**, 3821 (1974).
(31) B. E. Wagner, J. W. Linowski, J. A. Potenza, R. D. Bates, Jr., J. N. Helbert, and E. H. Poindexter, *J. Am. Chem. Soc.*, **98**, 4405 (1976).
(32) R. D. Bates, Jr., B. E. Wagner, and E. H. Poindexter, *J. Phys. Chem.*, **80**, 320 (1976).
(33) E. H. Poindexter, R. D. Bates, Jr., N. L. Paddock, and J. A. Potenza, *J. Am. Chem. Soc.*, **95**, 1714 (1973); R. A. Dwek, N. L. Paddock, J. A. Potenza, and E. H. Poindexter, *J. Am. Chem. Soc.*, **91**, 5436 (1969).
(34) D. E. Martire, J. P. Sheridan, J. W. King, and S. E. O'Donnell, *J. Am. Chem. Soc.*, **98**, 3101 (1976).

Department of Chemistry **Richard D. Bates, Jr.***
Georgetown University
Washington, D.C. 20057
U.S. Army Electronics Command **Burkhard E. Wagner**
Ft. Monmouth, New Jersey 07703 **Edward H. Poindexter**

Received September 22, 1976

ADDITIONS AND CORRECTIONS

1976, Volume 80

D. W. Beistel and W. Dan Edwards: The Internal Chemical Shift—A Key to Bonding in Aromatic Molecules. 2. Substituent Effects on Carbon-13 Magnetic Resonance Spectra of the 1,4-Disubstituted Benzenes.

Page 2024. The column heads in Table II are incorrectly placed. The corrected table is given below.

TABLE II: ^{13}C Shifts of the 4-Z-Substituted Benzonitriles (in ppm) Relative to TMS

Z	C≡N	C_1(Z)	C_2(Z)	C_3(CN)	C_4(CN)	$\Delta_{C_{23}}$
NMe_2	120.48	150.34	111.31	133.14	97.22	−21.83
NH_2	120.04	150.44	114.29	133.57	99.76	−19.28
OMe	119.01	162.7	114.68	133.77	103.85	−19.09
OH	119.0	160.12	116.39	134.17	102.98	−17.78
Me	118.93	143.49	129.64	131.83	109.29	−2.19
H	118.65	132.58	128.97	131.98	112.46	−3.01
Cl	117.70	139.40	129.52	133.17	110.75	−3.65
Br	117.78	127.78	133.17	132.46	111.27	0.71
I	117.86	100.00	138.29	132.94	111.71	5.35
COMe	117.70	139.84	128.53	132.30	116.23	13.77
NO_2	116.67	150.0	124.17	133.33	118.29	19.16

—D. W. Beistel

Corrected
V.Ph.
21 July 1977

BETTER BET ON THE RABBIT

In the fable, the tortoise wins.
Of course, everybody knows it didn't really happen that way.
That's why they call it a fable.
No two ways about it. . .
THE RACE IS TO THE SWIFT.

To keep current on developments in the fast-moving discipline of physical chemistry, you need a journal that publishes up-to-date articles, communications, and symposia. Biweekly—now *that's* up to date. And you'll get biweekly information in. . .

THE JOURNAL OF PHYSICAL CHEMISTRY.

Swift is fine, but it's not nearly enough for an authoritative publication of ACS. You'll find more than 20 papers in every issue, covering spectroscopy, thermodynamics, reaction kinetics, and other areas of experimental and theoretical physical chemistry.

Would you like to be a little bit ahead of the rest of your field—the people who don't use the Journal? Then, just . . . *Complete, clip, and mail the coupon below.* Now?

- **new concepts**
- **new techniques**
- **new interpretations . . . plus reports on classical areas**

The editors of the Journal of Physical Chemistry strive to select material that is useful in the classical areas of chemistry as well as in modern structural quantum mechanical areas. Start your subscription now. We'll do the rest.

Another service of ACS

The Journal of Physical Chemistry
American Chemical Society **1977**
1155 Sixteenth Street, N.W.
Washington, D.C. 20036

Yes, I would like to receive the JOURNAL OF PHYSICAL CHEMISTRY at the one-year rate checked below:

	U.S.	Foreign and Canada	Latin America
ACS Member *	☐ $24.00	☐ $ 34.00	☐ $ 33.00
Nonmember	☐ $96.00	☐ $106.00	☐ $105.00

Bill me ☐ Bill company ☐ Payment enclosed ☐

Air freight rates are available on request.

Name _____

Street _____ Home ☐ Business ☐

City _____ State _____ Zip _____

Journal subscriptions start in January '77.
Allow 60 days for your first copy to be mailed.
* NOTE: Subscriptions at ACS member rates are for personal use only.

Outstanding texts in physical chemistry

NEW

PHYSICAL CHEMISTRY WITH APPLICATIONS TO BIOLOGICAL SYSTEMS

Raymond Chang, Williams College

This outstanding new text presents the principles of physical chemistry in light of their application to chemical and biological problems. It is designed primarily for students interested in the biological sciences and premedical studies, however, some examples of environmental concern are also presented. The text's flexible format permits instructors to alter its length to suit one-semester, three-quarter, or two-semester courses.

These excellent features set this text apart from others in the field:

- an emphasis on principles rather than mathematical detail
- coverage of topics of current interest such as photobiology, photochemistry, and intermolecular interactions
- presentation of physical quantities in *both* SI and CGS units
- a large number of references to easily accessible journals
- approximately 250 problems in all, plus many worked examples
- an attractive two-color format.

An **Instructor's Manual** with valuable teaching suggestions, lecture demonstrations and worked-out solutions to all of the problems in the text is provided, *gratis*.

1977 576 pages (approx.)

NEW

PHYSICAL CHEMISTRY

Vojtech Fried, Brooklyn College of The City University of New York; **Hendrik F. Hameka,** University of Pennsylvania; and **Uldis Blukis,** Brooklyn College of The City University of New York

This *thoroughly modern* text presents the fundamental principles of classical thermodynamics, quantum mechanics, and statistical thermodynamics and their applications to chemical kinetics and electrochemistry. Numerous worked-out examples illustrate basic principles and all proofs are completely derived.

Physical Chemistry contains in-depth treatments of selected topics, rather than encyclopedic coverage. Special treatment is given to the presentation of reaction kinetics which incorporates the latest research findings in this area. Mathematical appendices provide the student with the tools necessary for the study of physical chemistry. Answers for eighty per cent of the text's end-of-chapter exercises are provided.

1977 992 pages (approx.)

FUNDAMENTALS OF PHYSICAL CHEMISTRY

Samuel H. Maron and **Jerome B. Lando,** both, Case Western Reserve University

This balanced, modern treatment of the fundamentals of physical chemistry stresses realistic applications of concepts. Thermodynamics, kinetics, atomic and molecular structure, crystal structure, spectroscopy—these are some of the basic topics covered in this general introduction to all major areas of the field.

An **Answer Manual** to the text's extensive selection of carefully constructed problems is available, gratis.

1974 853 pages

For further information, write to:

Macmillan Publishing Co., Inc., 100A Brown Street, Riverside, N.J. 08075

Macmillan